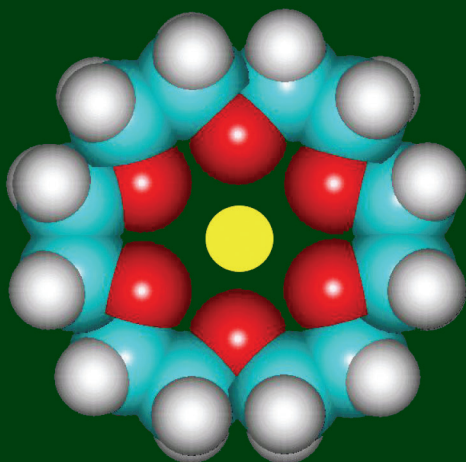


**Functionalized
molecules
- synthesis, properties
and application**

Edited by

Volodymyr I. Rybachenko



**Functionalized
molecules
- synthesis, properties
and application**

Edited by

Volodymyr I. Rybachenko

Donetsk 2010

**Видавниче підприємство “Східний видавничий дім”
Державне свідоцтво № ДК 697 від 30.11.2001
83086, м. Донецьк, вул. Артема, 45
тел./факс (062) 338-06-97, 337-04-80
e-mail: svd@stels.net**

Publishing house „Schidnyj wydawnyczyj dim”

ISBN 978-966-317-076

Contents

List of Contributors	5
The structure and physicochemical properties of gossypol and its imine derivatives	9
<i>N.S. Ilkevych, B. Brzezinski, G. Schroeder, V.I. Rybachenko V.I., C.Ju. Chotiy, R.A. Makarova and A.F. Dmitruk</i>	
Synthesis methods of silica-gold (silver) matrices	45
<i>Joanna Kurczewska and Grzegorz Schroeder</i>	
Synthesis, application and stability of phenylboronic esters	59
<i>Agnieszka Adamczyk-Woźniak</i>	
Molecular Complexation of Ivy Saponins with Some Drugs and Biologically Active Substances	85
<i>L.A. Yakovishin, V.I. Grishkovets, G. Schroeder and N.I. Borisenko</i>	
Dye-sensitized solar cells	105
<i>Maciej Zalas</i>	
Application of noble gases NMR in supramolecular and material chemistry. Complexes with supramolecular ligands	119
<i>Błażej Gierczyk</i>	
Applications of matrix-assisted laser desorption ionization mass spectrometry to synthetic polymers	159
<i>Grażyna Bartkowiak and Grzegorz Schroeder</i>	
Nano-systems and soft materials for anion complexation	189
<i>Bogusława Łęska and Radosław Pankiewicz</i>	
Selective fluorescent chemosensors	207
<i>Radosław Pankiewicz, Grzegorz Schroeder and Bogusława Łęska</i>	

List of Contributors

Agnieszka Adamczyk-Woźniak
Warsaw University of Technology
Faculty of Chemistry
Noakowskiego 3
00-664 Warsaw, Poland

Grażyna Bartkowiak
Adam Mickiewicz University
Faculty of Chemistry
Grunwaldzka 6
60-780 Poznań, Poland

N.I. Borisenko
Southern Federal University
Ecological and Analytical Center
Zorge Str., 7
Rostov-on-Don, 344090, Russia

Bogumił Brzezinski
Adam Mickiewicz University
Faculty of Chemistry
Grunwaldzka 6
60-780 Poznań, Poland

C.Ju. Chotiy
L.M. Litvinenko Institute of Physical Organic and Coal Chemistry NAS
of Ukraine
R. Luxemburg 70
83-114 Donetsk, Ukraine

A.F. Dmitruk

L.M. Litvinenko Institute of Physical Organic and Coal Chemistry NAS
of Ukraine
R. Luxemburg 70
83-114 Donetsk, Ukraine

Błażej Gierczyk

Adam Mickiewicz University
Faculty of Chemistry
Grunwaldzka 6
60-780 Poznań, Poland

V.I. Grishkovets

V.I. Vernadsky Taurida National University
Vernadsky Ave., 4
Simferopol, 95007, Crimea, Ukraine

N.S. Ilkevych

L.M. Litvinenko Institute of Physical Organic and Coal Chemistry NAS
of Ukraine
R. Luxemburg 70
83-114 Donetsk, Ukraine

Joanna Kurczewska

Adam Mickiewicz University
Faculty of Chemistry
Grunwaldzka 6
60-780 Poznań, Poland

Bogusława Łęska

Adam Mickiewicz University
Faculty of Chemistry
Grunwaldzka 6
60-780 Poznań, Poland

R.A. Makarova

L.M. Litvinenko Institute of Physical Organic and Coal Chemistry NAS
of Ukraine
R. Luxemburg 70
83-114 Donetsk, Ukraine

Radosław Pankiewicz

Adam Mickiewicz University
Faculty of Chemistry
Grunwaldzka 6
60-780 Poznań, Poland

Volodymyr I. Rybachenko

L.M. Litvinenko Institute of Physical Organic and Coal Chemistry NAS
of Ukraine
R. Luxemburg 70
83-114 Donetsk, Ukraine

Grzegorz Schroeder

Adam Mickiewicz University
Faculty of Chemistry
Grunwaldzka 6
60-780 Poznań, Poland

L.A. Yakovishin

Sevastopol National Technical University
Universitetskaya Str., 33
Sevastopol, 99053, Crimea, Ukraine

Maciej Zalas

Adam Mickiewicz University
Faculty of Chemistry
Grunwaldzka 6
60-780 Poznań, Poland

Chapter 1

The structure and physicochemical properties of gossypol and its imine derivatives

N.S. Ilkevych¹, B. Brzezinski², G. Schroeder², V.I. Rybachenko V.I.¹,
C.Ju. Chotiy¹, R.A. Makarova¹ and A.F. Dmitruk¹

¹*L.M. Litvinenko Institute of Physical Organic and Coal Chemistry NAS
of Ukraine, R. Luxemburg 70; 83-114 Donetsk, Ukraine*

²*Adam Mickiewicz University, Faculty of Chemistry; Grunwaldzka 6,
60-780 Poznań, Poland*

Gossypol and its imine derivatives

Gossypol, 2,2'-bis(8-formyl-1,6,7-trihydroxy-5-isopropyl-3-methyl naphthalene) is a yellow colored, polyphenolic binaphthalene compound isolated from cotton plants (fig. 1) The biological importance of gossypol and various aspects of its physiological and biochemical effects have been the subject of many works [1-4]. This compound is clinically used to reduce plasma cholesterol, resist tumor, and fungal pathogens [1]. It has also been demonstrated that polyphenol shows antiviral activity against enveloped viruses, such as HIV, by inhibiting their replication [5]. This bis-sesquiterpene is also capable of breaking supercoiled DNA, and its activity in this process strongly increases after the addition of Cu²⁺ and Fe³⁺ cations [6].

However, as a drug, it has restrained use due to its toxicity and side effect to human body. Its toxicity is directly related to the presence of two aldehyde groups that are blocked during the formation of imine derivatives [1]. Therefore, different reactions between gossypol and primary amines and hydrazines were studied. This condensation reaction is undoubtedly the reaction most often applied to the gossypol molecule [4].

Schiff bases and hydrazones of gossypol exhibit lower toxicity and still are biology active so they could be used instead of gossypol as therapeutic agents. Some gossypol Schiff bases show antimalarial activity [7]. Others are more efficient than gossypol in inhibiting the replication of HIV in vitro and show cytotoxic effect toward human cancer cells [8-10]. Chemical, physical, and organoleptic properties of gossypol and some of its derivatives are similar

to those of flavonoids such as quercetin and gossepetin, powerful antioxidants whose importance in modern medicine cannot be ignored [11, 12]. Gossypol is used in industry principally as an antioxidant. As other polyphenols, gossypol is multifunctional, and its antioxidant activity may be due to its capability to act as reducing agent by donating hydrogen or by quenching singlet oxygen, or by chelating.

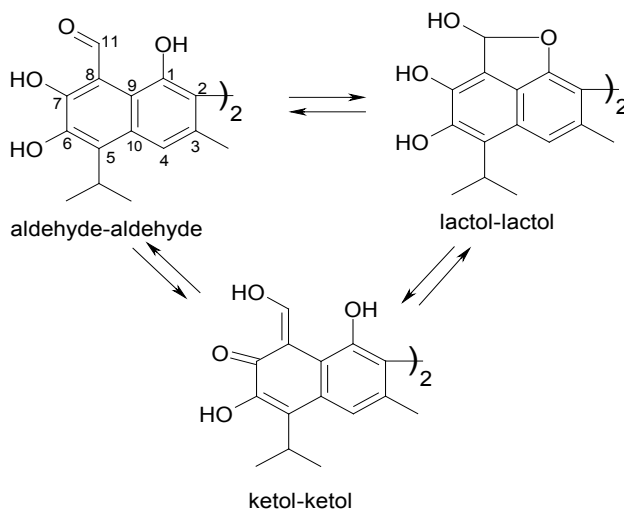


Figure 1. The structure and atoms numeration of tautomeric forms of gossypol

The first synthesized imine derivatives of gossypol were dianilnogossypol – condensation product of the reaction of gossypol molecule with two molecules of a primary aromatic amine, aniline [13]. In 1918 Carruth [14] was shown that aniline and gossypol react with a formation of stable crystalline compound and two water molecules. This reaction has been used to remove and quantify gossypol contained in cottonseed meal. It was found that this reaction is a typical for ammonia, primary amines and lysine amino groups contained in proteins [15].

The mechanism of this reaction is outlined in Fig. 2. The reaction between the primary amine's nitrogen and gossypol's aldehyde groups gives intermediate carbinol. Subsequent dehydration leads directly to Schiff's base [4]. Gossypol Schiff bases can occur in imine-imine and enamine-enamine tautomeric forms (Fig. 2), being analogues to the aldehyde-aldehyde and ketol-ketol tautomers of

gossypol, respectively.

The equilibrium between various tautomeric Schiff base structures has been extensively investigated by IR, NMR, and molecular modeling [9, 16–21]. For example, NMR experiments by Matlin and colleagues [19] on dianilinogossypol showed this compound exists as the enamine-enamine tautomer based on the signal observed at 174 ppm in the ^{13}C NMR spectrum, which is characteristic of a carbonyl carbon. The molecular crystal structures for dianilinogossypol crystals grown from ethyl acetate or dichloromethane indicate that dianilinogossypol exists as the enamine-enamine tautomer regardless of the solvent used to grow the crystals [21].

Haitbajev and colleagues investigated the Schiff bases tautomeric equilibrium by NMR and IR spectroscopy in CDCl_3 and Py-d_5 solutions. The data obtained indicate that for the alkylimines enamine-enamine form is predominant and for arylimines – imine-imine form [22]. Quang [23] has studied tautomeric equilibrium of some gossypol Schiff bases in different solvents by NMR spectroscopy and DFT method. Analysis of ^1H and ^{13}C NMR spectra showed that all this compounds exist only in enamine-enamine form.

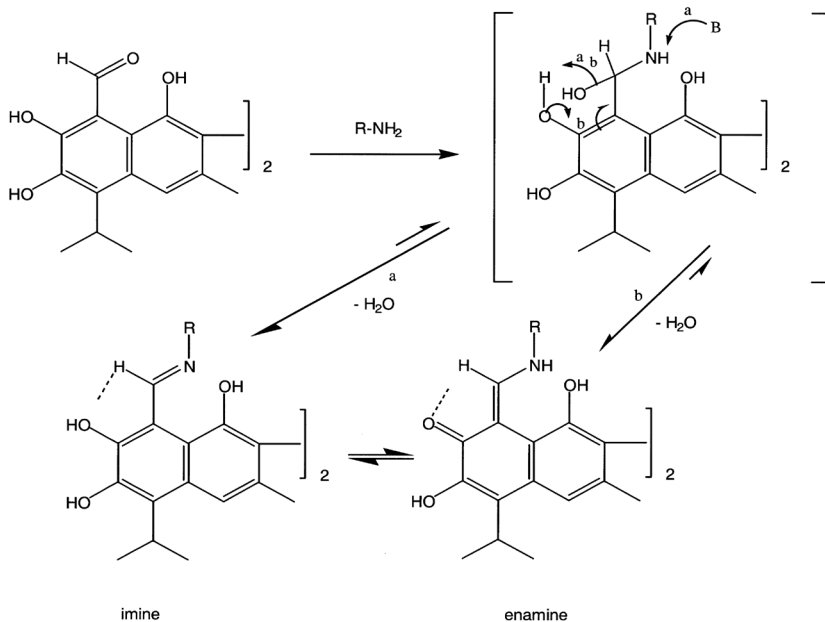


Figure 2. Tautomeric forms of gossypol Schiff bases.

Baram [18] and colleagues also have studied some aryl imines of gossypol by UV and NMR spectroscopy and showed these compounds in different solutions exist generally in enamine form. Dodou [9] have studied tautomeric equilibrium of alkyl and aryl imines and also has indicated that in solutions only enamine-enamine tautomer exists. Brzezinski and coworkers [24-27] have examined the equilibrium of some unique gossypol Schiff's bases and studied the influence of metals complexation on the gossypol Schiff's base equilibrium distribution. As a result of their study revealed that the protonation of nitrogen atoms of the gossypol imine derivative causes a complete shift of equilibrium from enamine-enamine to imine-imine form. In the case of complexes with metal cations complexation does not affect the tautomeric equilibrium and in solution is found only enamine-enamine form.

Much less information in the literature is about the hydrazone of gossypol (the condensation product of gossypol molecule with two molecules of hydrazines). For these derivatives the tautomeric equilibrium shifted from the enamine-enamine structure, observed for Schiff's bases in solution, to the imine-imine structure [17]. Brzezinski et al. [28, 29] have examined the equilibrium of some gossypol hydrazones and come to the conclusion that all this compounds exist in solution only in imine-imine form. This tautomeric form is stabilized by intramolecular H-bonds, the most strong of them is $O_7H \cdots N$. No reason for such equilibrium shift was given, although presumably the additional nitrogen atom reduces the nucleophilicity of the corresponding imine nitrogen, making it less likely to accept a proton needed to tautomerize into the enamine-enamine form [17].

Biological action of gossypol imine derivatives

Biological activity of these compounds is caused not only by the presence in their molecules gossypol fragment, but by the nature of imine group. Razakantoanina et al. [30] studied the effect of the structure of imine component on the activity against *Plazmodium falciparum*. Apparent antiviral effect gossypol Schiff bases exhibit at concentrations 3 - 4 times smaller than gossypol. Schiff base of (-)-gossypol with L-phenylalanine methyl ether was more effective than the (-)-gossypol against melanoma and leukemia.

Recent studies have shown that biological activity of gossypol and its imine derivatives, as well as other natural polyphenols, largely due to their antioxidant activity [31, 32].

Gossypol protects the rat heart phospholipids from free radicals generated in Fenton reaction [33]. It also effectively inhibits oxidation in rat liver microsomes induced by Fe^{3+} /ascorbic acid [11]. Dodou et al. [9] investigated the antioxidant

effect of gossypol, gossypolon and two gossypol Schiff bases on the peroxidation of liposomes initiated by Fe^{3+} /ascorbic acid using the thiobarbituric acid. It is interesting that gossypol itself and all its studied derivatives are more active than the standard compound - propyl gallate.

Mukhamedzhanova and coworkers [34] investigated the antioxidant activity of bis-diethylaniliniminogossypols, studied the action of these compounds on lipid peroxidation and found that the antioxidant activity of gossypol derivatives can be strengthened or weakened by functional groups. Jo [35] studied the effects of radiation on toxicity and antioxidant properties of gossypol, using thiobarbituric acid and stable free radical 2,2-diphenyl-1-picrylhydrazyl. It was found that irradiation of methanol solutions of gossypol significantly reduces its antioxidant activity. Wang [36] and co-workers, studying the biological activity of gossypol and some of its derivatives, have also shown the possibility of their interaction with free radicals. Kovacic [31] reviewed the various mechanisms of antioxidant action of gossypol and its derivatives in vivo and identified the following possible mechanism of their action:

1. quenching free radicals;
2. complex formation with metal ions;
3. formation of derivatives, possessing an antioxidant effect (enzymatic oxidation to gossypolon, Schiff bases formation with the molecules of proteins and peptides).

The structure of gossypol and its imine derivatives

We have synthesised five gossypol imine derivatives (Fig. 3).

In FT-IR spectra of gossypol and GDA (Table 1) intensive carbonyl absorption and C=C stretching vibrations are observed.

Table 1. Frequencies of characteristic vibrations of gossypol and its derivatives

Compound	ν , cm^{-1} (KBr)		
	C=O	C=N	C=C
G	1619	-	1573
GDA	1615	-	1541
GAPP	1611	-	1554
GGCP	1694	1569	1635, 1569
GGCPP	1606	1565	1570
GTDA	1624	-	1525

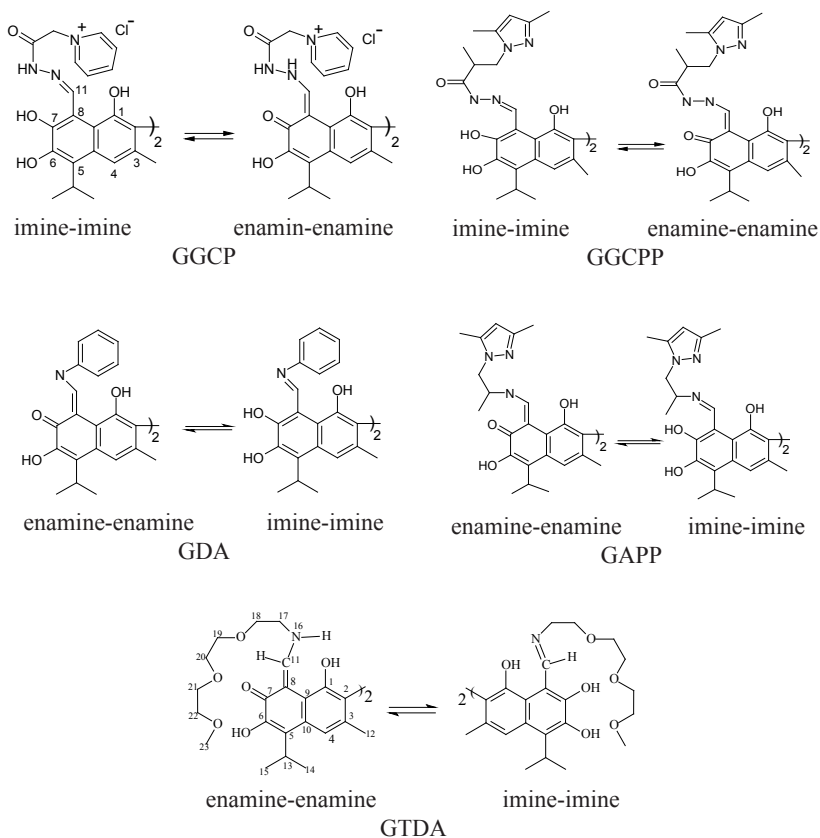


Figure 3. The structure of tautomeric forms and atom numeration of gossypol derivatives - hydrazone with 1-hydrazinocarboxymethylpyridinium chloride (GGCP), hydrazone with 1-(2-hydrazinocarboxylpropyl)-3,5-dimethyl-1H-pyrazole (GGCPP), dianilinogossypol (GDA), Schiff base with 1-(2-aminopropyl)-3,5-dimethylpyrazole (GAPP), Schiff base with c 3,6,9-trioxadecylamine (GTDA)

Similar situation is in the case of other gossypol Schiff bases (GAPP, GTDA). In FT-IR spectra broad band of medium intensity vibrations of C=C and intensive absorption of C=O are observed. This indicates that the Schiff bases of gossypol exist in enamine-enamine tautomeric form. In the spectra of hydrazones (GGCP and GGCPP) the $\nu(\text{C}=\text{O})$ vibration of hydrazone moiety and

the azomethine C=N-bond are observed. All this indicates that the hydrazones of gossypol, in contrast to the Schiff bases exist in imine-imine tautomeric form.

The $^1\text{H-NMR}$ data of gossypol and its imine derivatives are given in Table 2. In NMR spectrum of gossypol in DMSO is observed more intensive (~ 3 times) value of signals $\text{C}_{11}\text{-H}$ protons than O_1H . In solutions gossypol preferably occurs in aldehyde-aldehyde and lactol-lactol tautomeric forms (the ratio between tautomers in DMSO is $\sim 1/4$, respectively [37, 38]). In GDA spectra signals of $\text{C}_{11}\text{-H}$ and $\text{N}_{16}\text{-H}$ protons are observed.

Table 2. $^1\text{H NMR}$ chemical shifts (ppm) of gossypol and its derivatives in $\text{DMSO-}d_6$

Compound	Chemical shift, ppm						
	O_1H	O_6H	O_7H	C_{11}H	N_{16}H	N_{17}H	C_4H
G	5.60	8.40	9.95	11.20	-	-	7.60; 7.25
GDA	5.63	8.62	-	10.42	14.90	-	7.45
GAPP	5.69	8.33	-	9.20	13.25	-	7.48
GGCP	5.76	6.78	14.12	10.18	-	6.18	7.62
GGCPP	5.80	6.89	14.22	9.90	-	6.22	7.58
GTDA*	6.42	8.13	-	9.76	13.32	-	7.60

*- $^1\text{H NMR}$ spectrum is obtained in acetonitrile

Similar situation is in the case of other azomethine derivatives (GAPP, GTDA): in the NMR spectra are well visible signals of O_1H , O_6H , C_{11}H and N_{16}H protons, confirming the existence of these compounds in enamine-enamine tautomeric form, which is in agreement with the FT-IR observations and the results of quantum-chemical calculations.

PM3 method is used to calculate the normal vibrations of gossypol and its derivatives. To correct the calculated vibrational frequencies the small set of scaling factors have been used [39]: $\nu(\text{OH}) = 0.898 - 0.924$; $\nu(\text{CH}) = 0.963 - 1.0$; $\nu(\text{C} = \text{O}) = 0.843 - 0.900$. Figs. 4, 5 and 6 show the experimental and calculated IR spectra of gossypol and some of its imine derivatives.

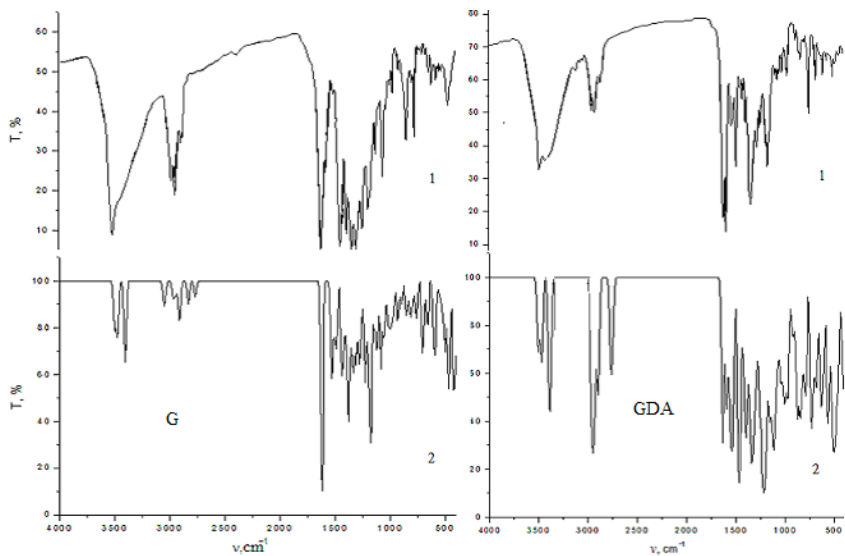


Figure 4. IR spectra of gossypol (G) and GDA (1 – experimental, 2 – calculated)

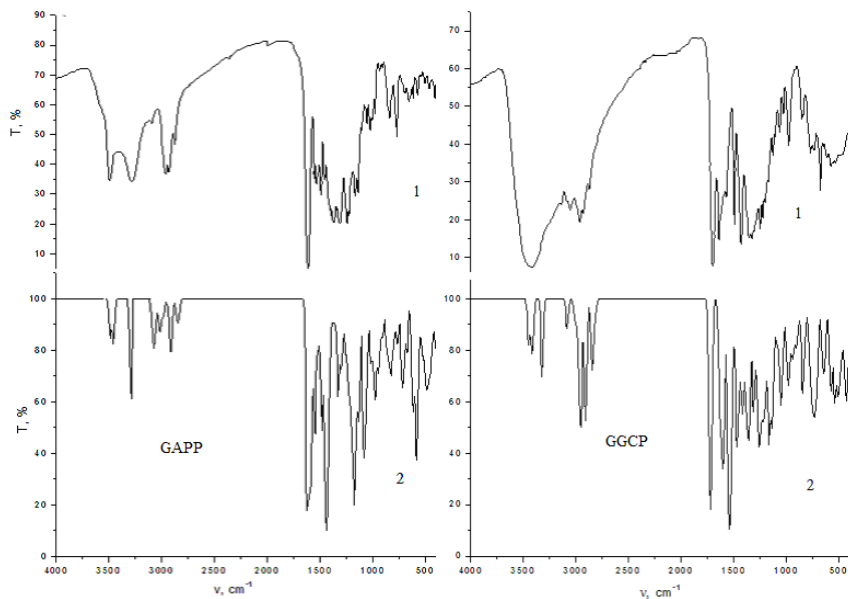


Figure 5. IR spectra GAPP and GGCP (1 – experimental, 2 – calculated)

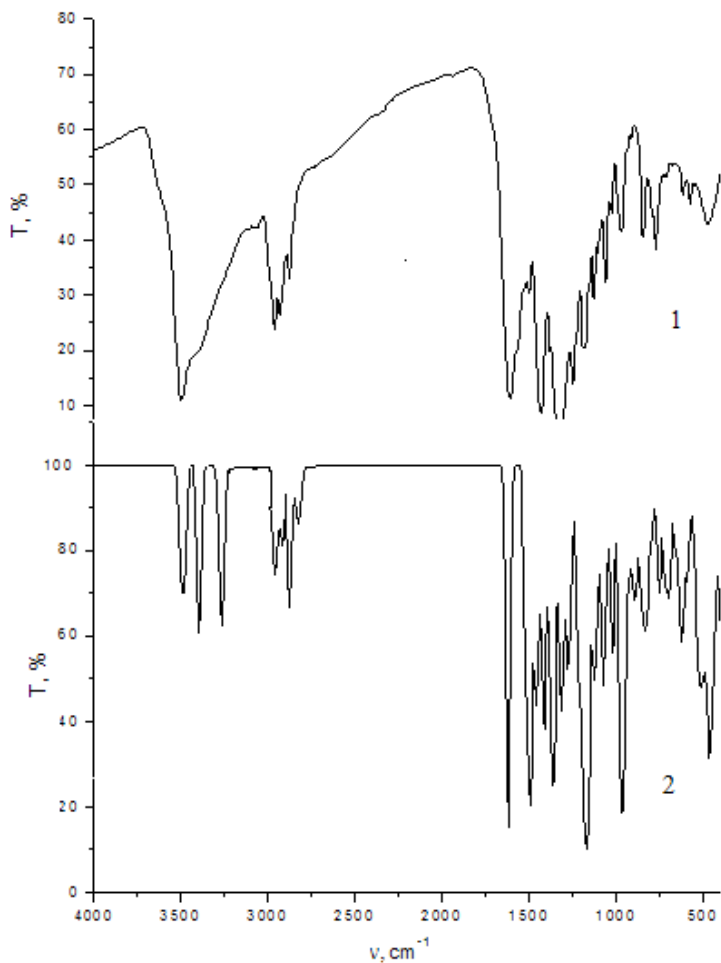


Figure 6. IR spectra of GGCPP (1 – experimental, 2 – calculated)

The results of quantum chemical calculation of tautomeric composition of gossypol at 298 K are given in Table 3. *Ab initio* calculations were carried out in 6-31G basic set using program GAMESS [40]. Effect of solvent was taken into account with the help of continual model PCM.

Table 3. Ratio (%) of aldehyde (I), lactol (II) and ketol (III) forms in tautomeric equilibrium of gossypol

Analysis		Tautomer		
		I	II	III
PM3, vacuum		5	95	~ 0
ab initio	vacuum	100	~ 0	~ 0
	DMSO	11 (17)*	89 (83)*	~ 0 (0)*
	chloroform	96 (100)*	4 (0)*	~ 0 (0)*

*- estimation according to experimental data [41]

According to PM3 semiempirical approximation in all tautomers naphthalene rings are practically orthogonal (dihedral angle 322.3 for I and III is close to 90°, while for II it is about 80°). *Ab initio* calculations give the value of this angle somewhat smaller. Thus, this angle for I и III is about 80°, while for II - 60°. In the *ab initio* calculations bond length C₂-C₂ is 0.02Å longer than finding in PM3 approximation and equals 1.50Å for I and III, while for II – 1.49Å. It is necessary to note, that in PM3 the most stable tautomer is II (it is more stable by 3.1 kcal than I and by 23 kcal than III). The *Ab initio* calculations give somewhat different values, the most stable tautomer is I, which is 7.1 kcal more stable than II and 31.0 kcal than III.

The calculations confirm considerable effect of solvent nature on the tautomeric equilibrium of gossypol. In polar solvent DMSO lactol form of gossypol dominates, whereas in nonpolar – aldehyde form and this fact have been completely confirmed with known experimental estimates. According to literary data, ketol form presents only in aqueous alkaline medium [37, 38].

Calculated total energies (E_{tot}) of tautomeric forms G and GDA (enamine-enamine GDA-1, imine-imine GDA-2, G-1 – aldehyde-aldehyde, G-2 – lactol-lactol, G – ketol-ketol) are shown in Table 4.

As can be seen in the case of gossypol the most preferable are two tautomeric forms – aldehyde-aldehyde and lactol-lactol. For dianilinogossypol energy of enamine-enamine form is less than imine-imine. Such difference exists in various solvents. Energetically the most stable tautomer of gossypol in a vacuum and non-polar solvent CHCl₃ is G-1, in polar solvents (CH₃OH and DMSO) – the most stable form is G-2. The thermodynamic evaluation of the tautomeric composition of gossypol gives the following results: in CHCl₃ solvent 96% G-1 and 4% G-2 (according to NMR data [41] 100% and 0%, respectively), while in

DMSO - 11% G-1 and 89% G-2 (according to [41] 17% and 83%, respectively). That is, the calculation agrees fairly well with the experimental data. For GDA in all cases is the most stable form is GDA-1, i.e. nature of the solvent has no significant effect on the tautomeric composition.

Table 4. Total energy ($-E_{tot}$, at. un.) for tautomeric structure of gossypol and GDA in different solvents

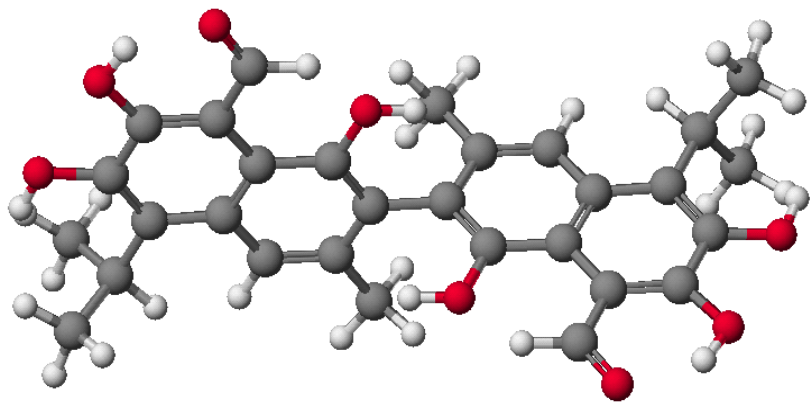
Tautomeric form	Solvent				
	vacuum	C ₆ H ₆	CHCl ₃	CH ₃ OH	DMSO
G-1	1751.70936	1751.72476	1751.73582	1751.74968	1751.74733
G-2	1751.69806	1751.71820	1751.73307	1751.75159	1751.74930
G-3	1751.66001	1751.68530	1751.70297	1751.72267	1751.72140
GDA-1	2170.98635	2171.00508	2171.01845	2171.03663	2171.03548
GDA-2	2170.97347	2170.98886	2171.00082	2171.01695	2171.01409

Table 5 shows the calculated values of dihedral angles between the naphthenic rings and the length of the central bond C₂-C₂. It should be noted that similar values of these parameters is obtained in [42] by molecular mechanics for the tautomers of gossypol G-1 and G-3. Significant difference was observed only for lactol-lactol form.

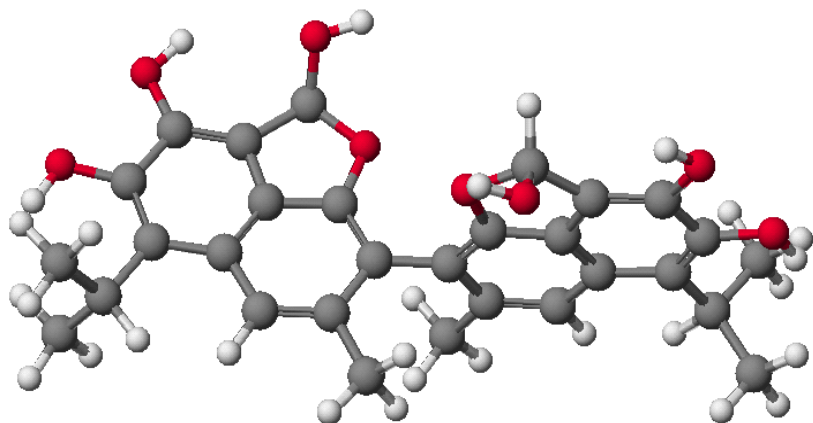
Table 5. Geometric characteristics of the tautomeric forms of G and GDA: dihedral angles 322'3' (°) and the length of the central bond C₂-C₂, R (Å) according to the RHF/6-31G and MM3 data [42]

	G-1		G-2		G-3		GDA-1	GDA-2
	6-31G	MM3	6-31G	MM3	6-31G	MM3	6-31G	MM3
R	1.499	1.520	1.489	1.501	1.501	1.521	1.498	1.506
322'3'	81.0	85.8	72.7	82.3	88.1	88.5	80.4	82.0

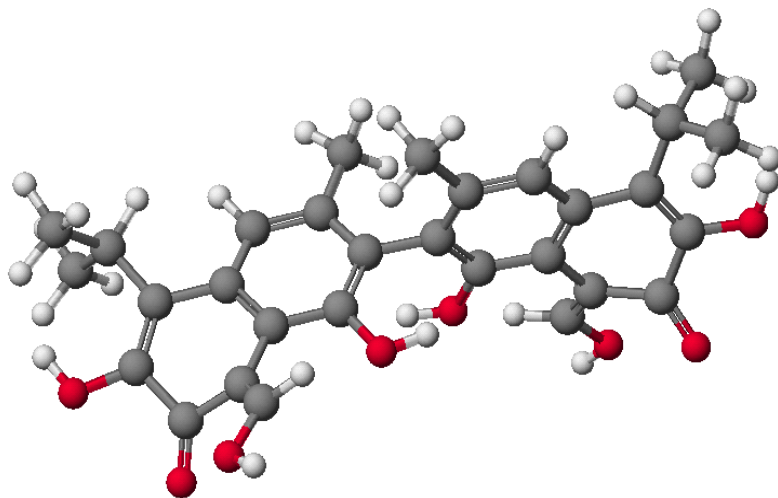
Fig. 7 shows calculated 3D-structures of the G and GDA tautomers.



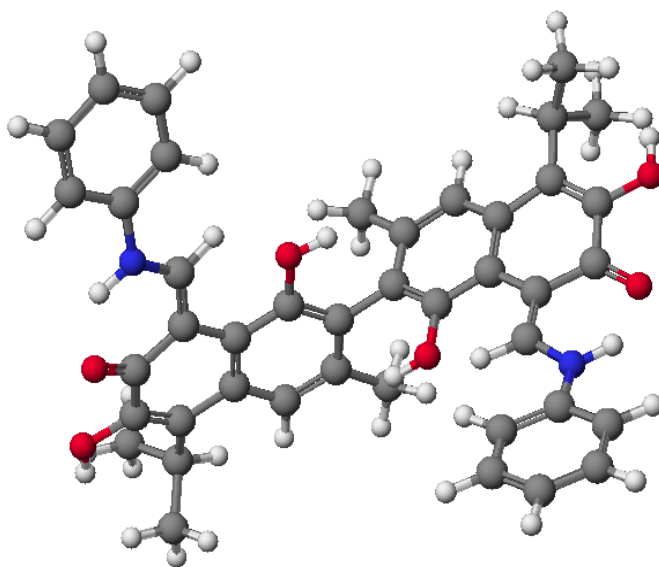
G-1



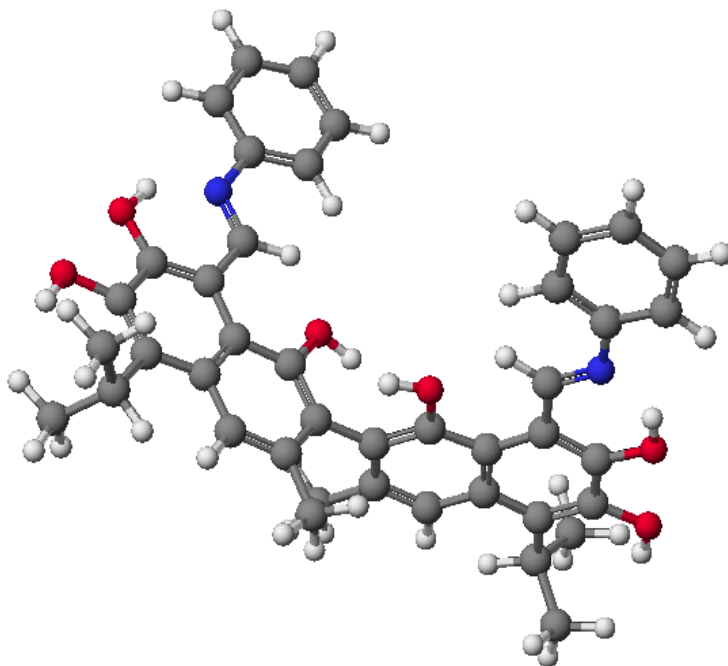
G-2



G-3



GDA-1



GDA-2

Figure 7. The calculated 3D-structures of gossypol and dianilinogossypol tautomers

Tables 6 and 7 present the formation energies and the characteristics of hydrogen bonds of gossypol derivatives tautomers calculated by the PM3 method using the program MOPAC 2002.

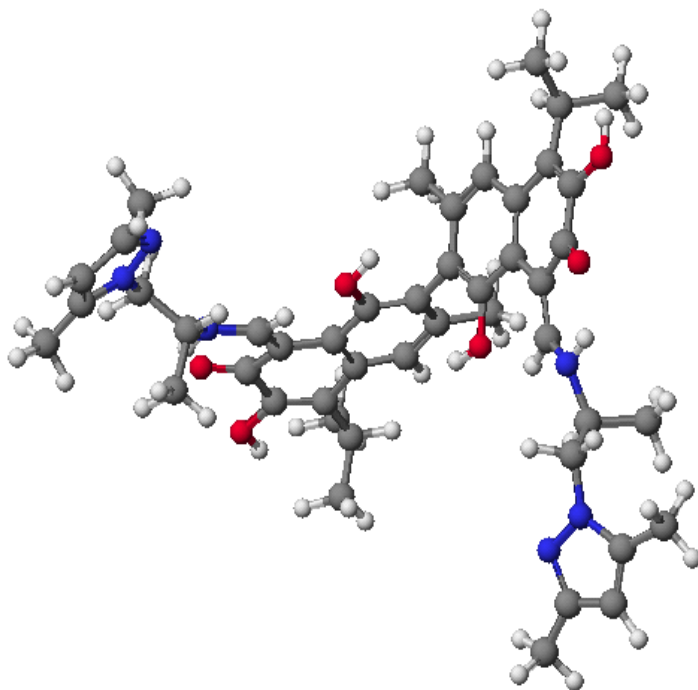
Table 6. Formation energies of the tautomers of gossypol derivatives

Compound	Formation energy, kcal/mol
GAPP(imine-imine)	-124.671
GAPP(enamine-enamine)	-130.382
GGCP(enamine-enamine)	-169.889
GGCP(imine-imine)	-151.120
GGCPP(imine-imine)	-146.812
GGCPP(enamine-enamine)	-161.479
GDA(imine-imine)	-128.027
GDA(enamine-enamine)	-130.520

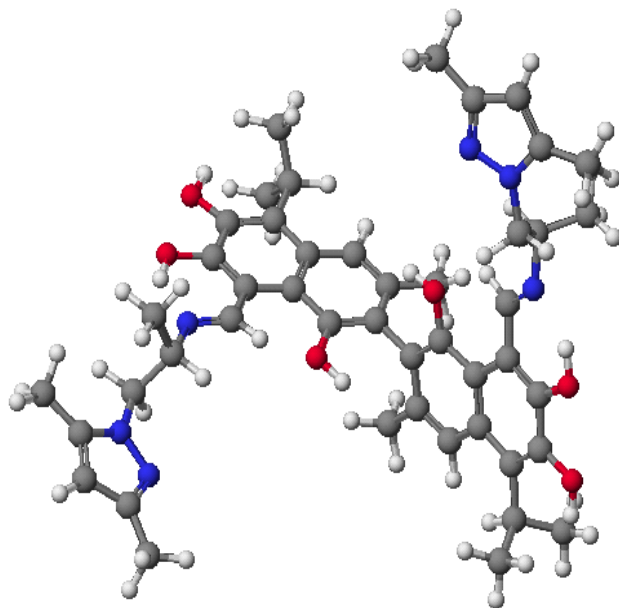
Table 7. Characteristics of hydrogen bonds of gossypol and its derivatives

Compound	H bond		
		length, Å	angle, °
G (aldehyde-aldehyde)	$O_{7,7'} \cdots O_{11,11'}$	1.782	141.5
GDA (enamine-enamine)	$O_7 \cdots H-N_{13}$	1.835	129.2
	$O_{7'} \cdots H-N_{13'}$	1.836	129.3
GAPP (enamine-enamine)	$O_{7,7'} \cdots H-N_{13,13'}$	1.837	130.1
GGCP (imine-imine)	$O_7 H \cdots N_{13}$	1.802	141.5
	$O_7 H \cdots N_{13'}$	1.836	141.9
GGCPP (imine-imine)	$O_7 H \cdots N_{13}$	1.811	141.2
	$O_7 H \cdots N_{13'}$	1.810	141.2

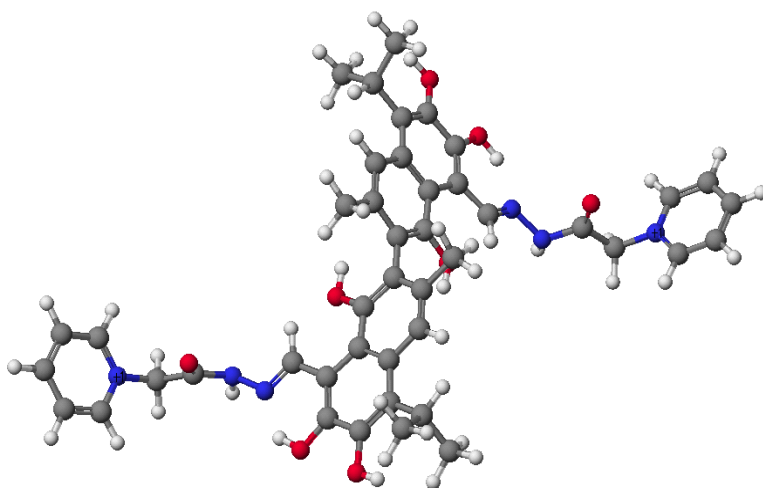
Fig. 8 presents the calculated 3-D structures of gossypol imine derivatives.



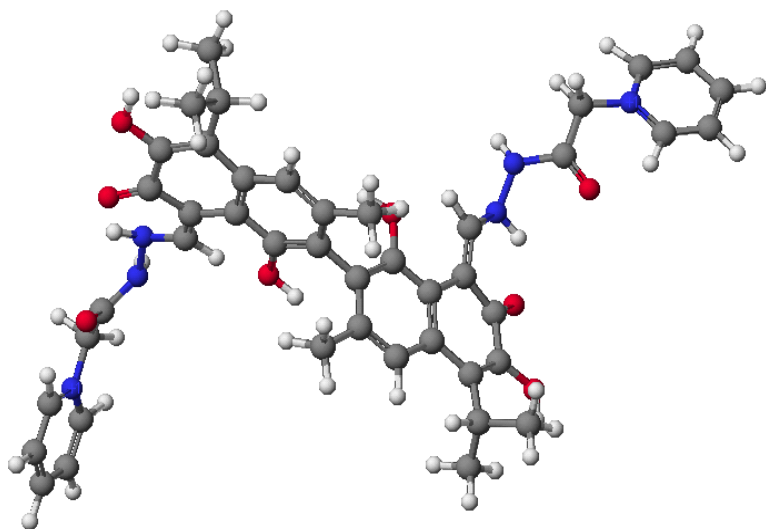
GAPP (en)



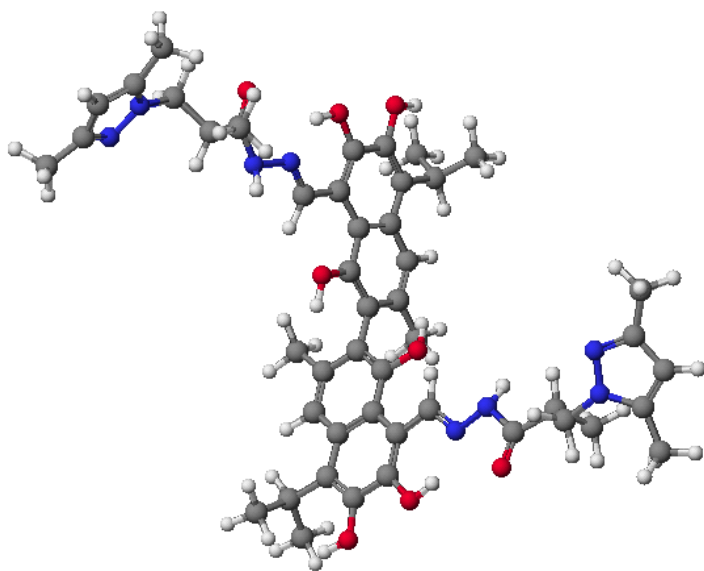
GAPP (im)



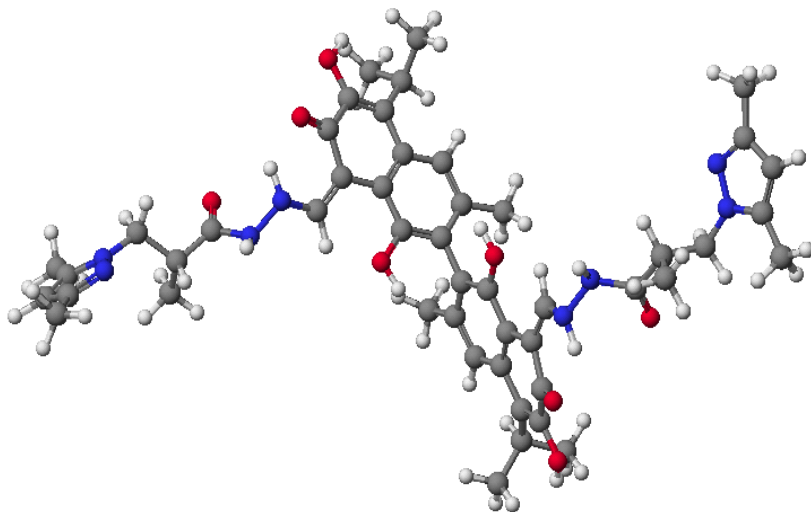
GGCP (im)



GGCP (en)



GGCPP (im)



GGCPP (en)

Figure 8. The calculated 3-D structures of gossypol imine derivatives (*im* – imine-imine, *en* – enamine-enamine)

Oxidation of G and GDA by molecular oxygen in DMSO

Kinetics of oxygen uptake by solutions of G and GDA was studied by volumetric analysis. Preliminary experiments showed that the rate of gossypol oxidation in DMSO in the presence of KOH is very small - less than 10^{-7} mol/l \times c, so further experiments were carried out in the system gossypol/radical initiator AIBN (α,α' -azobisisobutyronitrile).

Ratio of the maximum amount of absorbed oxygen and gossypol in general is equal to: - $(2.0 \pm 0.3):1,0$ mol. In the case of GDA, this ratio was $(1.0 \pm 0.2):1.0$ mol.

In contrast to the GDA gossypol in DMSO is oxidized by molecular oxygen much easier, and the reaction rate increases in the presence of solid alkali, but remains unchanged in the presence of radical initiator. This suggests that gossypol and GDA react with oxygen by two fundamentally different mechanisms: radical-chain and ion, respectively.

Using IR and NMR spectroscopy, we have established the probable oxidation

products of gossypol and proposed scheme of its degradation. Analysis of the ^1H NMR spectrum of gossypol (Fig. 9 (1), in DMSO), confirmed that in DMSO gossypol exists in two tautomeric forms: aldehyde-aldehyde and lactol-lactol.

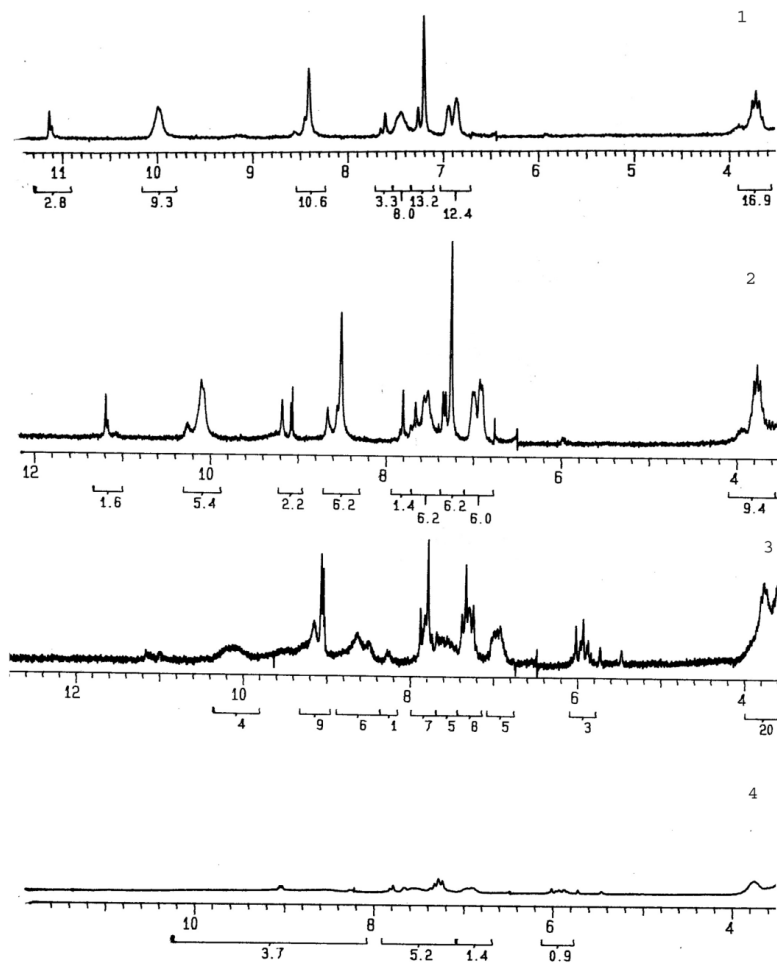


Figure 9. ^1H NMR spectra obtained during gossypol oxidation in DMSO (1 – gossypol before oxidation; 2 – NMR-ampoule held a week without heating; 3 – NMR-ampoule held 50 min at 80°C ; 4 – NMR-ampoule is held 100 min at 80°C)

In the ^1H NMR spectrum of gossypol in DMSO with the initiator (Fig. 9 (2), NMR-ampoule held a week without heating) is observed the appearance of several new signals (9.1, 9.2 and 7.8 ppm), which we assign, respectively, to O_6H , C_{11}H and H_4 protons of dianhydrogossypol (Fig. 10), one of the intermediate products of gossypol oxidation. It is known [43] that this compound is formed in gossypol solutions in contact with air.

In the spectrum of sample from the NMR-ampoule (held 50 min at 80°C) shown in Fig. 9 (3)), the significant decrease of intensity of the proton signals of aldehyde and O_1H groups of gossypol is observed, as well as the growth of signal intensity at 9.1, 9.2 and 7.8 ppm.

Additional NMR-ampoule thermostating at 80°C for 50 minutes shows (Fig. 9 (4)), that signals of aldehyde groups are completely eliminated as well as signals of all OH groups and dianhydrogossypol (9.1, 9.2 and 7.8 ppm).

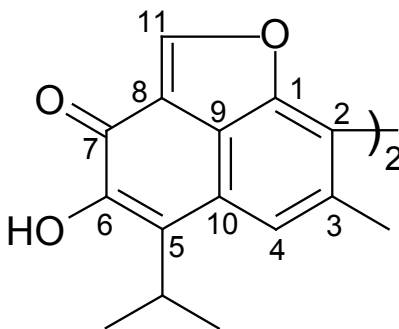


Figure 10. The structure and atom numeration of dianhydrogossypol

Fig. 11 shows the most interesting ranges of IR spectra of gossypol and its oxidation products in DMSO. In the spectrum of oxidized gossypol band $\nu(\text{C}=\text{C})$ shifts to 1628 cm^{-1} , which indicates a significant change in the π -system of the naphthalene rings. This is also confirmed by the appearance of two new bands at 1563 cm^{-1} and 1526 cm^{-1} . The band $\nu(\text{C}_{11}=\text{O})$ disappears, but instead three new bands $\nu(\text{C}=\text{O})$ at 1772 cm^{-1} , 1735 cm^{-1} and 1671 cm^{-1} are observed. The new band observed at 1735 cm^{-1} can be assigned to the $\nu(\text{C}_7=\text{O})$ stretching vibrations. Then, according to the spectra of diketones with six-membered ring in cis-form [44] band at 1772 cm^{-1} corresponds to $\nu(\text{C}_6=\text{O})$. The band 1671 cm^{-1} corresponds to $\nu(\text{C}_4=\text{O})$.

Analysis of ^1H NMR and IR spectra suggests the following scheme of the gossypol oxidation, Fig. 12 [45].

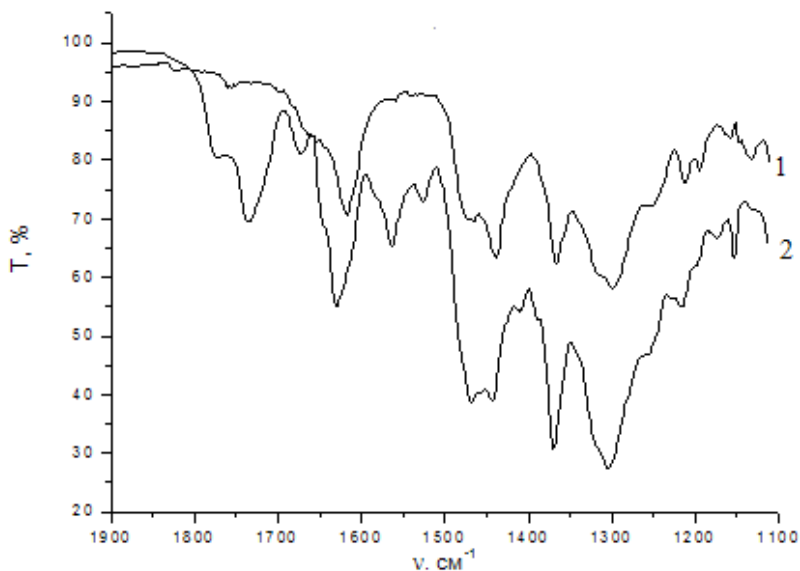


Figure 11. IR spectra of gossypol (1) and its oxidation products (2) in DMSO

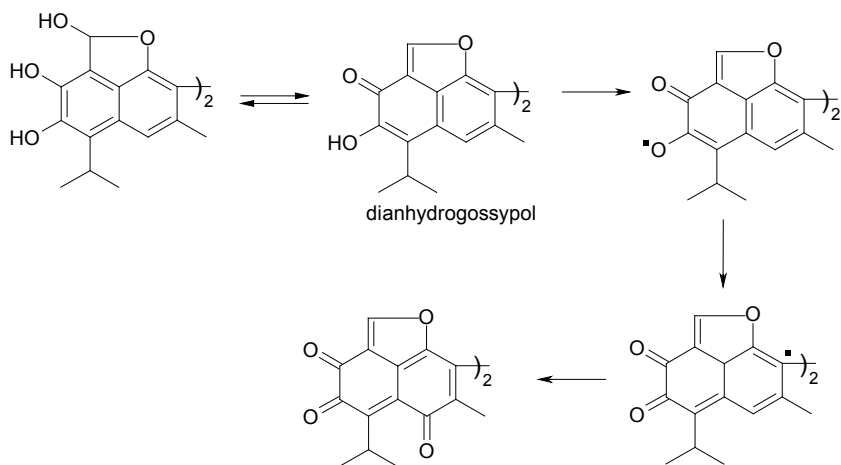


Figure 12. Scheme oxidation reaction of gossypol by atmospheric oxygen

Thus, we have experimentally confirmed the scheme of gossypol oxidation by atmospheric oxygen and suggested the probable oxidation products.

Antiradical activity of gossypol and its imine derivatives

It is known that gossypol is one of the most effective natural antioxidants. Antioxidative activity as well as many other aspects of polyphenols biological activity is determined by its ability to trap free radicals (antiradical activity). Gossypol itself can interact with DPPH [35, 36], but for its imine derivatives, such data are not available.

We investigated the reaction of G and four of its derivatives, of which three (GAPP, GGCP, GGCPP) were synthesized for the first time, with a stable free radical - 2,2-diphenyl-1-picrylhydrazyl (DPPH) in ethanol. Fig. 13 shows the kinetic curves of the reactions studied, and Table 8 shows calculated characteristics of antiradical activity of gossypol and its derivatives [46-49].

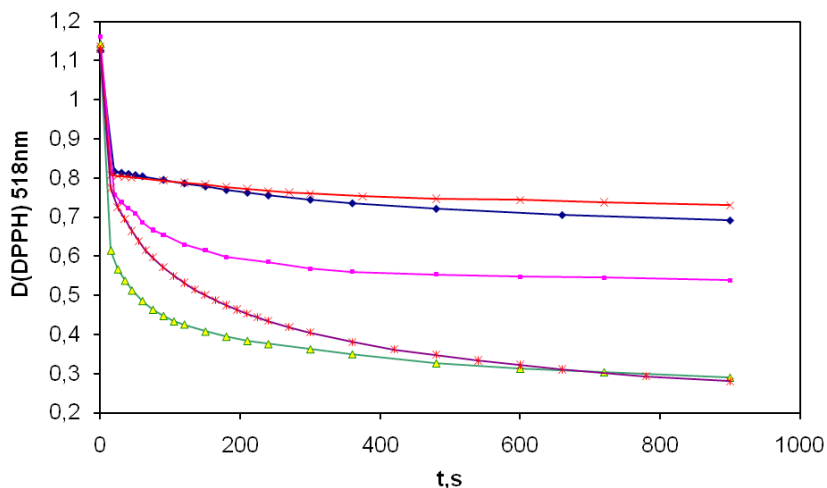


Figure 13. Decay of the visible absorbance at 518 nm of 0,18 mM DPPH solution in EtOH after phenol addition (××× - GDA, ♦♦♦ - GAPP, ■■■ - G, *** - GGCP, ΔΔΔ - GGCPP, ratio phenol/DPPH 0,130±0,005)

One parameter that has been introduced recently for the interpretation of the results from DPPH method is the “efficient concentration” or EC_{50} value. This parameter is often defined as the quantity of antioxidant (μg) in 1ml of standard DPPH solution ($\sim 10^{-4}$ M) that causes 50% loss of the DPPH activity (color).

We have obtained the EC_{50} values of the compounds according to [50] (Table 8) which are characteristic for effective natural antioxidants. For the compounds with estimated structure EC_{50} parameter is preferably defined as

the concentration of antioxidant needed to decrease by 50% the initial DPPH concentration. Table 3 presents EC_{50} values, which were calculated graphically.

Comparison of EC_{50} values obtained for gossypol with EC_{50} values of known natural and synthetic antioxidants [51] shows that gossypol is almost as active as quercetin and rutin (1.77×10^{-5} mol/l and 1.70×10^{-5} mol/l, respectively) and considerably more active than trolox and ascorbic acid (4.53×10^{-5} mol/l and 3.79×10^{-5} mol/l, respectively). Hydrazones of gossypol are as active as gallic acid ($EC_{50} = 1.53 \times 10^{-5}$ mol/l). Schiff bases are more active than caffeic and ferrulic acid ($EC_{50} = 3.88 \times 10^{-5}$ mol/l and 7.93×10^{-5} mol/l, respectively).

Table 8. Characteristics of antioxidant activity of gossypol and its imine derivatives

Compound	EC_{50}^1 , $\mu\text{g/ml}$	$EC_{50}^2(\times 10^5)$, mol/l	n_{300}^3	n_{tot}^4	n_{str}^5	$T_{1/2}^{DPPH}$, sec	$AE(\times 10^{-3})$, l/mol \times sec
G	4.1	1.92	3.95	4.80	6	20	2.60
GDA	10.0	3.07	2.51	3.10	6	90	0.36
GAPP	15.26	3.11	2.47	3.00	6	130	0.25
GGCPP	8.1	1.57	4.94	5.80	8	5-7	~ 12.0
GGCP	8.5	1.43	5.17	6.10	8	≥ 5	≤ 14.0

¹ the quantity of antioxidant (μg) in 1ml of standard DPPH solution ($\sim 10^{-4}$ M) that causes 50% decrease of the DPPH concentration;

² the concentration of antioxidant needed to decrease by 50% the initial DPPH concentration;

³ stoichiometric coefficient for the fast step 0 - 300 sec;

⁴ total stoichiometry of the antioxidant

⁵ possible number of OH and (or) NH groups in the molecule of antioxidant.

It is interesting and important to estimate the stoichiometry of the reaction between polyfunctional antioxidant and DPPH. Stoichiometric coefficient n is defined as a number of radicals trapped per antioxidant molecule and determined from the following equation:

$$n = (A_0 - A_t) / \epsilon c_0 l,$$

where A_0 and A_t – absorbance of DPPH solution at 518 nm at $t = 0$ and at $t = t$, ϵ – molar absorption coefficient of DPPH at 518 nm, c – initial concentration of antioxidant, l – layer thickness.

In Table 8 the values of n_{str} (highest possible number of OH and NH groups in molecule), n_{300} and n_{tot} which characterized stoichiometry of the reaction of polyphenol with DPPH during the fast step (monitored over 300 sec) and after

15-20 min are presented. The comparison of n values shows that during 300 sec the conversion of DPPH amounts 80-85%. Evidently, this is concerned with structural features of studied compounds. In ethanol solutions gossypol exists mainly as lactol-lactol tautomer. Oxidation of this form can stabilize lactol-lactol form in products and, as a result, lead to accumulation of compounds with weakly oxidizing C_{11} -OH group.

Interesting results were obtained by Wang and colleagues [36], which investigated the antiradical activity of gossypol, 6-methoxygossypol and 6,6'-dimethoxygossypol using DPPH assay in acetone. They turned out that the replacement of one hydroxyl group O_6 -H significantly reduced antiradical activity of 6-methoxygossypol. At the same time, 6,6'-dimethoxygossypol was almost the same active, as 6-methoxygossypol. It is interesting that gossypol itself and its derivatives were much more active than synthetic antioxidant butylated hydroxytoluene. Our results also suggest that not all the O-H groups of gossypol are involved in the reaction with DPPH ($n_{str} = 6$, $n_{300} = 3.95$ and $n_{tot} = 4.8$). Obviously, the six OH groups four quickly react with DPPH (within 300 seconds), while from the remaining two (probable O_6 -H and O_6' -H groups), one interacts slowly, and the second is inactive.

The data in Table 8 also show that in all cases values of n_{300} and n_{tot} Schiff bases of gossypol, regardless of the structure of the molecules imine component, significantly lower than that of gossypol, and, in particular, its hydrazones. The reason for this is changes in the naphthalene system of Schiff bases, involving the transfer of these compounds in enamine-enamine form. Consequently, the hydroxyl group O_7 -H and O_7' -H transformed into the keto group and lose the opportunity to interact with DPPH. This leads to a decrease of values n_{tot} GDA and GAPP approximately upon two units compared to gossypol. The values n_{tot} for all Schiff bases are close to three and indicate that from the remaining four O-H groups, as in the case of gossypol, one O-H group is not able to react with DPPH.

On the other hand, it is known, that the reactivity of amino groups in the reaction with DPPH, in comparison with phenolic, are much lower. Therefore, the proximity of the stoichiometric coefficients n_{tot} for the studied gossypol Schiff bases and hydrazones to the total number of OH groups can be regarded as an evidence of the fact that the antioxidant properties of these substances are associated with the transfer of H only from the phenolic O-H groups. It is known that hydrazones of gossypol, in contrast to Schiff bases, exist in solutions in imine-imine tautomeric form. Consequently, all 6 O-H groups remain unchanged in gossypolic part of their moleculars. The values of n_{300} and n_{tot} of these compounds is higher than gossypol and suggests that, in contrast with

gossypol and gossypol Schiff bases, all of their O-H groups are able to react with DPPH. Five of the six available OH groups react with DPPH during 300 seconds, while the latter reacts much more slowly.

We investigated the interaction of the complex GAPP: 2HClO_4 with DPPH. By analogy with [52 - 54] can be assumed that protonation of the nitrogen atoms of the molecule leads to the formation of imine-imine tautomeric form (instead of enamine-enamine in GAPP molecule). This leads to an increase of the number of reactive OH groups and, consequently, to a significant increase of antioxidant activity: $\text{EC}_{50} = 2.12 \times 10^{-5} \text{ mol/l}$; $n_{300} = 3.82$; $n_{\text{tot}} = 4.56$; $T_{1/2}^{\text{DPPH}} = 25 \text{ s}$, $\text{AE} = 1.89 \times 10^3 \text{ l/mol}\times\text{s}$. Therefore, changing tautomeric forms of gossypol Schiff bases from enamine-enamine to imine-imine increases the value of AE more than 7 times.

The disadvantage of EC_{50} parameter, as the test of antioxidant activity, is obvious - there is no connection between EC_{50} and the time of reaction. In a number of cases [50, 51] to describe such reactions is proposed to use the time required to reach equilibrium with the initial concentration of antioxidants equal to EC_{50} ($T_{\text{EC}_{50}}$). However, due to the obvious large errors in determination of these values $T_{\text{EC}_{50}}$ are not very suitable for the analysis of antioxidant activity. Preferable, in our view, is used as a parameter the half-time of reaction ($T_{1/2}^{\text{DPPH}}$). EC_{50} values and $T_{1/2}^{\text{DPPH}}$ can be combined by taking the product of their values. But for characterizing the properties of the reaction is better to use the reciprocal, because their values a priori antisymbatic to the antioxidant activity. By analogy with [50], we identified proposed characteristic of the reaction with “antioxidant effectiveness” AE [55]:

$$\text{AE} = 1/\text{EC}_{50} \times T_{1/2}^{\text{DPPH}}$$

In general, the reaction of polyphenols with DPPH in ethanol solution may proceeds by three mechanisms [56]: hydrogen atom transfer (HAT), electron transfer with subsequent proton loss (ET-PT) and dissociation of O-H groups, followed by electron transfer (SPLET) .

Ionization potentials (IP) and dissociation enthalpy (BDE) of the weakest bonds (O-H or N-H) in each molecule was calculated by PM3 method (Table 9).

If mechanism ET-PT is realised, with a decreasing of IP polyphenols should increase their antiradical activity [57]. Experimentally, this is not observed (Fig. 14).

Table 9. Calculated by PM3 method values IP and BDE of gossypol and its imine derivatives

Compounds	IP, ev	BDE, kcal/mol
G	8.75	74.2
GDA	7.91	78.8
GAPP	8.10	80.3
GGCP	7.82	64.8
GGCPP	8.44	65.6

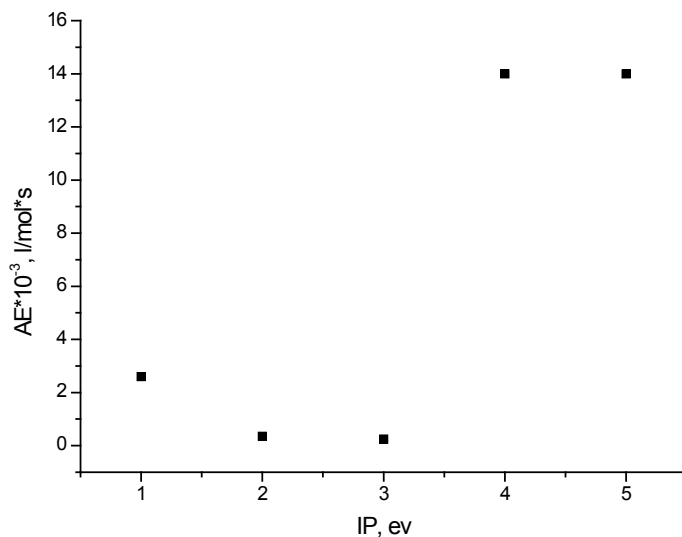


Figure 14. Plot AE vs BDE for phenols

SPLET may be suppressed by the addition of acids and, with sufficient acid, phenol ionization, and hence SPLET, can be eliminated leaving only the HAT mechanism operative [58, 59]. That leads to a considerable decreasing of reaction rate. However, the acidification of alcoholic solutions of gossypol shifts tautomeric equilibrium from aldehyd-aldehyd to lactol-lactol form [60], and in the case of Schiff bases - from enamine-enamine to imine-imine form [52-54]. Changing of the tautomeric forms has a dramatical effect on reactivity of phenolic compounds toward DPPH. This makes it impossible to make a conclusion about SPLET mechanism.

As seen from Fig. 15, there is a correlation between the values of AE and the BDE of phenolic compounds ($AE = 70.734 - 0.892 \times BDE$, $r = 0.973$). This suggests that DPPH reacts with gossypol and its imine derivatives by a single-

step hydrogen transfer mechanism (HAT).

The data in Table 8 indicate that AE values the most pronounced characterize the effect of the structure on the antioxidant properties of compounds. Therefore, obtained hydrazones of gossypol are in 5 times more active than gossypol, and Schiff bases - 5 - 10 times less active. According to ascending of antiradical activity this compounds form a sequence: GAPP <GDA <gossypol <GGCPP <GGCP. As a result, we can conclude that the modification of gossypol by introducing a hydrazone fragment is very effective and promising way to increase the antioxidant activity of the basic structure of natural polyphenol - gossypol.

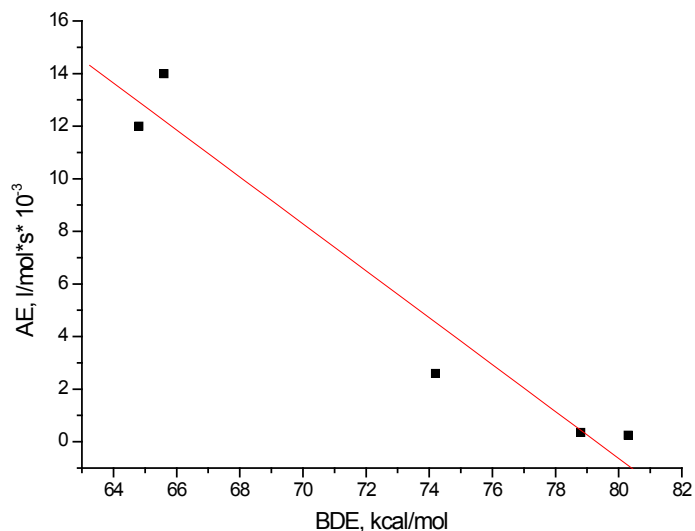


Figure 15. Correlation between AE and BDE values of investigated compounds

Effect of complexation of cations on the antioxidant properties of gossypol imine derivatives

Cation binding by amine derivatives of gossypol occurs with the participation of imino groups and one or more OH groups of gossypolic part (mostly O₁H group). It was established that the degree of involvement of O₁H group in the process of complex formation is directly proportional the size of cation [52-54]. In the series Li⁺, Na⁺, K⁺, Rb⁺, Cs⁺ cations K⁺, Rb⁺, and Cs⁺ are capable to form two types of complexes (a complex only with the imino group or a complex involving O₁H group). Since metal ions are present in all biological systems and involved in the regulation of vital processes, is also interesting to evaluate the

influence of the cations Li^+ , K^+ , Na^+ , Mg^{2+} on antiradical activity of gossypol derivatives.

In the literature there is evidence that the presence of metal ions significantly affects on the reaction rate of hydrogen atom transfer to DPPH [61]. Thus, the rate of DPPH reaction with 2,2,5,7,8-pentamethylchroman-6-ol (vitamin E model) in methanol increases significantly in the presence of $\text{Mg}(\text{ClO}_4)_2$. A similar effect was explained by the fact that this reaction in the polar solvents proceeds via two-step ET-PT mechanism.

Baciocchi et al. [62] suggested that the same mechanism is realized in the presence and in the absence of Mg^{2+} (reaction of 4-X-substituted-N,N-dimethylanilines with DPPH). Their results suggest a single-step hydrogen transfer mechanism from the N-C-H bond to DPPH which might take the form of a concerted proton electron transfer. The significant rate accelerating effect by Mg^{2+} is likely due to a favorable interaction of the Mg^{2+} ion with the partial negatively charged R-methyl carbon in the polar transition state for the hydrogen transfer process.

As seen from Fig. 16, antiradical activity of GAPP depends on the nature of cation [55].

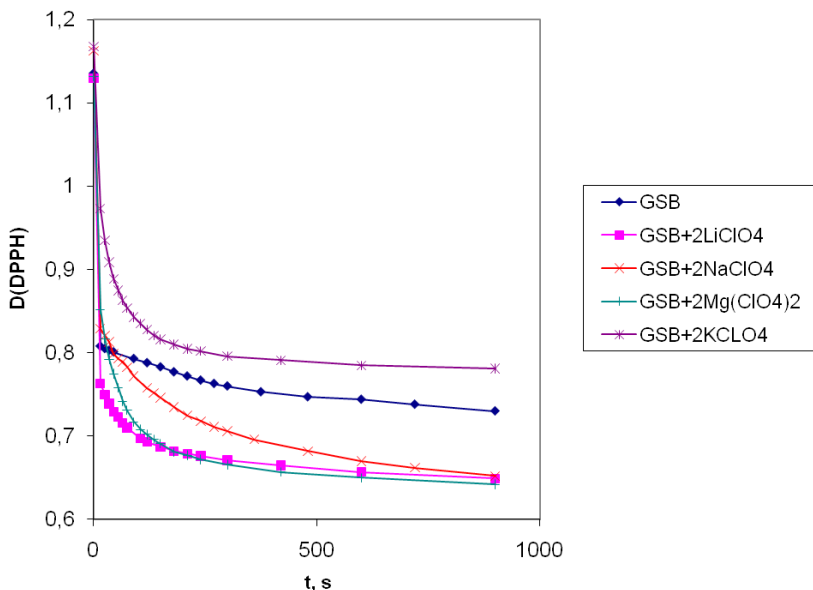


Figure 15. Decay of the visible absorbance at 518 nm of 0,18 mM DPPH solution in EtOH after addition of GAPP

Table 10 shows that in the case of GAPP presence of any of the cations (except K^+) leads to an increase of stoichiometric coefficients of reaction n_{300} and n_{tot} , as well as the values of AE.

Table 10. Characteristics of antiradical activity of GAPP and GGCP in the presence of metal cations

Compound	$EC_{50}(\times 10^5)$, mol/l	n_{300}	n_{tot}	n_{str}	$T_{1/2}^{DPPH}$, sec	$AE(\times 10^{-3})$, l/mol \times sec
GAPP+2LiClO ₄	2.70	3.19	3.38	6	30	1.23
GAPP+2NaClO ₄	2.77	2.99	3.35	6	75	0.48
GAPP+2KClO ₄	3.25	2.49	2.70	6	180	0.17
GAPP+2Mg(ClO ₄) ₂	2.69	3.15	3.39	6	30	1.24
GGCP+2LiClO ₄	1.60	4.96	5.70	8	≤ 10	≥ 6.25
GGCP+2NaClO ₄	1.73	4.96	5.42	8	≤ 10	≥ 5.78
GGCP+2KClO ₄	1.68	4.97	5.60	8	≤ 10	≥ 5.95
GGCP+2Mg(ClO ₄) ₂	1.80	4.65	5.22	8	≤ 10	≥ 5.56

Among Li^+ , Na^+ , K^+ cations maximum antiradical activity observed in the presence of Li^+ . It is known [52-54], Li^+ forms the most stable complexes with azomethine fragment of gossypol Schiff bases. The presence of Li^+ and Mg^{2+} leads to an increase of GAPP antioxidant efficiency almost 5 times. Decrease of activity in the presence of K^+ is probably due the fact that this cation interact, in addition to the azomethine fragment, with OH groups of gossypol part [52]. Binding of O_1-H or $O_1'-H$ group with the cation prevents the interaction of the hydrogen atom of this group with DPPH.

In the case of GGCP electrostatic repulsion prevents the interaction of metal cations with atoms of the azo group. The presence of any metal cations in solution only reduces the antiradical activity of phenolic OH groups. As a result, the antioxidant activity of GGCP reduced 2 - 2.5 times. On the degree of reduction of antioxidant activity and the stoichiometric coefficients of reaction cations can be arranged in the following order: $Li^+ < K^+ < Na^+ < Mg^{2+}$.

References

1. K. Dodou, Investigations on gossypol: past and present developments, Expert Opin. Investig. Drugs. - 2005. - Vol. 14, № 11. - P. 1419 – 1434
2. Coutinho E. M., Gossypol: A Contraceptive for Men, Contraception. - 2002. - Vol. 65. - P. 259 – 263
3. R. Adams, T. A. Geissman, J. D. Edwards, Gossypol, a Pigment of

- Cottonseed, Chem. Rev. - 1960. - Vol. - P. 555 – 574
4. J. A. Kenar, Reaction Chemistry of Gossypol and its Derivatives, JAOCs. – 2006. – Vol. 83, № 4. - P. 269 – 302
 5. B. Polsky, S. J. Segal, P. A. Baron, J. W. M. Gold, H. Ueno, D. Armstrong, Inactivation of Human Immunodeficiency Virus in vitro by Gossypol, Contraception. - 1989. - Vol. 39. - P. 579 – 587
 6. R. Zaidi, S. M. Hadi, Strand Scission in DNA by Gossypol and Cu(II): Role of Cu(I) and Oxygen-Free Radicals, J. Biochem. Toxicol.- 1992. - Vol. 7, № 3. - P. 213 – 217
 7. C. Dando, E. R. Schroeder, L. A. Hunsaker, The kinetic properties and sensitivities to inhibitors of lactate dehydrogenases (LDH1 and LDH2) from *Toxoplasma gondii*: comparisons with pLDH from *Plasmodium falciparum*, Mol. Biochem. Pharmacol. - 2001. - Vol. 118, № 1. - P. 23 – 32
 8. N. I. Baram, A. I. Ismailov, Biological Activity of Gossypol and Its Derivatives, Chem. Nat. Comp. - 1994. - Vol. 29, № 3. - P. 275 – 287
 9. K. Dodou, R. J. Anderson, W. J. Lough, D. A. P. Small, M. D. Shelley, P. W. Groundwater, Synthesis of gossypol atropisomers and derivatives and evaluation of their antiproliferative and antioxidant activity, Bioorg. Med. Chem. - 2005. - Vol. 13, № 13. - P. 4228 – 4237
 10. R. E. Royer, R. G. Mills, L. M. Deck, G. J. Mertz, D. L. Vander Jagt, Inhibition of Human Immunodeficiency Virus Type I Replication by Derivatives of Gossypol, Pharmacol. Res. - 1991. - Vol. 24, № 6. - P. 407 – 412
 11. M. J. Laughton, B. Halliwell, P. J. Evans, J. R. Hoult, Antioxidant and prooxidant actions of the phenolics quercetin, gossypol and myricetin, Biochem. Pharmacol. - 1989. - Vol. 38, № 17. - P. 2859 – 2865
 12. L. I. Ash, B. Bandy, S. S. Tsang, A. J. Davison, DNA-breaking versus DNA-protecting activity of four phenolic compounds *in vitro*, Free Rad. Res. - 2000. - Vol. 33. - P. 551 – 566
 13. R. Adams, C. C. Price, W. R. Dial, Structure of gossypol. V. Anilino Derivatives, J. Am. Chem. Soc. - 1938. - Vol. 60, № 9. - P. 2158 – 2160
 14. F. E. Carruth, Contribution to the chemistry of gossypol, the toxic principle of cottonseed, J. Amer. Chem. Soc. - 1918. - Vol. 40, № 1. - P. 647 – 663
 15. M. B. Abou-Donia, Physiological Effects and Metabolism of Gossypol, Residue Rev. - 1976. - Vol. 61, № 1. - P. 125 – 160
 16. V.-T. Dao, C. Gaspard, M. Mayer, G. H. Werner, S. N. Nguyen, R. J. Michelot, Synthesis and Cytotoxicity of Gossypol Related Compounds

- , Eur. J. Med. Chem. - 2000. - № 35. - P. 805 – 813
17. Kh. L. Ziyaev, F. G. Kamaev, N. I. Baram, L. Biktimirov, A. I. Ismailov, New Gossypol Imines, Chem. Nat. Comp. - 1997. - Vol. 33, № 6. - P. 545 – 547
 18. N. I. Baram, F. G. Kamaev, Kh. L. Ziyaev, L. Biktimirov, A. I. Ismailov, G. B. Nazarov, B. T. Ibragimov, Structure of Gossypol Arylimines, Chem. Nat. Comp. - 1988. - Vol. 24, № 6. - P. 550 – 553
 19. S. A. Matlin, S. Roshdy, G. B. Cass, C. G. Freitas, R. L. Longo, I. Malvestiti, Structural Investigations of Gossypol Schiff Bases, J. Brazil. Chem. Soc. - 1990.- Vol. 1, № 1. - P. 128 – 133
 20. G. B. Nazarov, B. T. Ibragimov, T. F. Aripov, X-Ray Structural Investigation of Gossypol and Its Derivatives. VII. Molecular and Crystal Structure of Dianilinegossypol, Chem. Nat. Comp. - 1988. - Vol. 24, № 5. - P. 560 – 564
 21. T. T. Quang, K. P. P. Nguyen, P. E. Hansen, Quang, T. T. Schiff bases of gossypol: an NMR and DFT study, Magn. Reson. Chem. - 2005. - Vol. 43, № 2. - P. 302 – 308
 22. А. Х. Хаитбаев, З. Тиябаев, Г. Ш. Ачилова, З. Тиябаев, Х. Х. Хаитбаев, С. А. Ауелбеков, Синтез и биологическая активность некоторых производных госсипола, Хим. прир. соед. - 1995, № 1. - С. 44 – 49
 23. T. T. Quang, K. P. P. Nguyen, P. E. Hansen, Quang, T. T. Schiff bases of gossypol: an NMR and DFT study, Magn. Reson. Chem. - 2005. - Vol. 43, № 2. - P. 302 – 308
 24. P. Przybylski, K. Jasinski, B. Brzezinski, F. Bartl, Spectroscopic Studies and PM5 Semiempirical Calculations of New Schiff Bases of Gossypol with Amino Derivatives of Crown Ethers, J. Mol. Struct. - 2002. - № 611. - P. 193 – 201
 25. P. Przybylski, M. Ratajczak-Sitarz, A. Katrusiak, W. Schilf, G. Wojciechowski, B. Brzezinski, Crystal Structure of Schiff Base Derivative of Gossypol with 3,6,9-Trioxa-decylamine, J. Mol. Struct. - 2003. - № 655. - P. 293 – 300
 26. P. Przybylski, W. Schilf, B. Brzezinski, ¹³C, ¹⁵N NMR and CP-MAS as Well as FT-IR and PM5 Studies of Schiff Base of Gossypol with l-Phenylalanine Methyl Ester in Solution and Solid, J. Mol. Struct. - 2005. - № 734. - P. 123 – 128
 27. P. Przybylski, G. Wojciechowski, W. Schilf, B. Brzezinski, F. Bartl, Spectroscopic study and PM5 semiempirical calculations of tautomeric forms of gossypol Schiff base with n-butylamine in the solid state and

- in the solution, *J. Mol. Struct.* - 2003. - № 646. - P. 161 – 168
28. G. Bejcar, P. Przybylski, B. Brzezinski, NMR, FT-IR as well as PM5 semiempirical studies of new hydrazone of gossypol with 3-oxa-n-butylhydrazine, *J. Mol. Struct.* - 2005. - № 734. - P. 45 – 49
 29. P. Przybylski, G. Bejcar, W. Schilf, B. Brzezinski, Structural and semiempirical investigations of hydrazone of gossypol and its protonated species, *J. Mol. Struct.* - 2008. - № 878. - P. 71 – 78
 30. V. Razakantoanina, N. K. P. Phung, G. Jaureguiberry, Antimalarial activity of new gossypol derivatives, *Parasit. Res.* - 2000. - № 7. - P. 479 – 498
 31. P. Kovacic, Mechanism of Drug and Toxic Actions of Gossypol: Focus on Reactive Oxygen Species and Electron Transfer, *Current Med. Chem.* - 2003. - Vol. 10, № 24. - P. 2711 – 2718
 32. D. L. Vander Jagt, L. M. Deck, R. E. Royer, Gossypol: Prototype of Inhibitors Targeted to Dinucleotide Folds, *Current Med. Chem.* - 2000. - Vol. 7, № 4. - P. 479 – 498
 33. D. L. Janero, B. Burghardt, Protection of rat myocardial phospholipid against peroxidative injury through superoxide-(xantine oxidase)-dependent, iron-promoted Fenton chemistry by the male contraceptive gossypol, *Biochem. Pharmacol.* - 1988. - Vol. 37, № 17. - P. 3335 – 3342
 34. Е. Н. Мухамеджанова, Д. Н. Далимов, З. Тилябаев, В. Б. Шнейвайс, Ф. Г. Камаев, Л. Биктимиров, А. И. Исмаилов, Синтез, строение бис-диэтиланилинимингоссиолов, их антиокислительная и антихолинэстеразная активность, *Хим. прир. соед.* - 1991. - № 1. - С. 184 – 188
 35. C. Jo, H. S. Yook, M. S. Lee, J. H. Kim, H. P. Song, J. S. Kwon, M. W. Byun, Irradiation effects on embryotoxicity and oxidative properties of gossypol dissolved in methanol, *Food Chem. Toxicol.* - 2003. - Vol. 41. - P. 1329 – 1336
 36. X. Wang, T. H. Beckham, J. C. Morric, F. Chen, J. D. Gangemi, Bioactivities of Gossypol, 6-Methoxygossypol, and 6,6'-Dimethoxygossypol, *J. Agric. Food Chem.* - 2008. - Vol. 56, № 12. - P. 4393 – 4398
 37. B. Brzezinski, J. Olejnik, S. Paszyc, T. F. Aripov, NMR Studies of Gossypol and Its Complexes with Some Organic Compounds, *J. Mol. Struct.* - 1990. - № 220. - P. 261 – 268
 38. B. Brzezinski, J. Olejnik, S. Paszyc, Fourier Transform Infrared Study on the Identification of Gossypol Tautomers, *J. Mol. Struct.* - 1990. - № 239. - P. 23 – 31
 39. Л. С. Хайкин, О. Е. Грикина, В. А. Шляпочников, Дж. Е. Боггс,

- Интерпретация колебательных спектров нитраминов на основе квантово-химических расчетов, Изв. РАН, Сер. хим. - № 12. - 1994. - С. 2106 – 2117
40. D. C. Young, *Computational Chemistry: A Practical Guide for Applying Techniques to Real-World Problems*, N. Y. : Wiley & Sons, 2001. - 381 p
 41. B. Brzezinski, J. Rozwadowski, B. Marciniak, S. Paszyc, Spectroscopic Study of Gossypol-Lanthanide Cation Complexes in Acetonitrile Solution, *J. Mol. Struct.* - 1997. - № 435. - P. 275 – 279
 42. C. L. Beisela, M. K. Dowd, P. J. Reill, Conformational analysis of gossypol and its derivatives by molecular mechanics, *J. Mol. Struct. : THEOCHEM.* - 2005. - № 730. - P. 51 – 58
 43. A. A. Tyshchenko, O. F. Filatova, S. M. Khodzhibaeva, K. D. Davranov, Free-radical gossypol derivatives for cotton *Verticillium* Wilt, *Chem. Nat. Comp.* - Vol. 40, № 1. - 2004. - P. 75 – 78
 44. К. Наканиси, Наканиси, К. Инфракрасные спектры и строение органических соединений, М. : Мир, 1965. – 210 с
 45. Н. Ількевич, М. Касянчук, Б. Бжезінський, Окиснення госсиполу та діаніліногоссиполу молекулярним киснем у диметилсульфоксиді, *Донецький вісник Наукового товариства ім. Шевченка: Хімія.* - 2006.- Т 10. - С. 23 – 28
 46. В.И. Рыбаченко, Н.С. Ількевич, Г. Шредер, А.Ф. Дмитрук, К.Ю. Чотий, В.А. Боровик, Изучение реакции госсипола с 2,2-дифенил-1-пикрилгидразилом, *Научные труды Донецкого Национального Технического Университета. Серия: Химия и химическая технология.* – 2007. - Вып. 119(9). - С. 77 – 80
 47. Н.С. Ількевич, В.І. Рибаченко, К.Ю. Чотій, Г. Шредер, Вивчення реакції діаніліногоссиполу з 2,2-дифеніл-1-пікрілгідразилом, *Донецький вісник Наукового товариства ім. Шевченка: Хімія.* - 2008. - Т 21. - С. 15 – 19
 48. Н.С. Ількевич, В.І. Рибаченко, К.Ю. Чотій, Г. Шредер, А.Ф. Дмитрук, Вивчення антирадикальної активності гідрозону госсиполу, *Донецький вісник Наукового товариства ім. Шевченка: Хімія.* - 2008. - Т 21. - С. 20 – 24
 49. Н.С. Ількевич, В.И. Рыбаченко, Г. Шредер, А.Ф. Дмитрук, К.Ю. Чотий, Антиоксидантные свойства госсипола и его некоторых имино-производных, *Научные труды Донецкого Национального Технического Университета. Серия: Химия и химическая технология.* – 2009. - Вып. 152(13). - С. 110 – 117

50. J. Lebeau, C. Furman, J.-L. Bernier, P. Duriez, E. Teissier, N. Cotelle, Antioxidant properties of di-*tert*-butylhydroxylated flavonoids, *Free Radical Biol. Med.* - 2000. - Vol. 29, № 9. - P. 900 – 912
51. H. Quan, V. Ninorimbere, Antioxidant power of phytochemicals from *Psidium guajava* leaf, *Zhejiang Univ SCI.* - 2004. - Vol. 5, № 6. - P. 676 – 683
52. P. Przybylski, N. Ilkevych, G. Schroeder, B. Brzezinski, F. Bartl, Schiff Base of Gossypol with 3,6,9-trioxa-decylamine Complexes with Monovalent Cations Studied by MS, ¹H NMR, FT-IR, as well as PM5 Semiempirical Methods, *Biopolymers (Biospectroscopy)*. - 2004. - Vol. 72. - P. 470 – 483
53. P. Przybylski, G. Bejcar, G. Schroeder, B. Brzezinski, Complexes of Schiff base of gossypol with 5-hydroxy-3-oxapentylamine and some monovalent cations studied by ESI MS as well as PM5 semiempirical methods, *J. Mol. Struct.* - 2005. - № 654. - P. 245 – 252
54. P. Przybylski, G. Schroeder, R. Pankiewicz, B. Brzezinski, F. Bartl, Complexes of Schiff base of gossypol with n-butylamine and some monovalent or bivalent cations studied by ESI MS, NMR, FT-IR as well as PM5 semiempirical methods, *J. Mol. Struct.* - 2003. - № 658. - P. 193 – 205
55. Н.С. Илькевич, В.И. Рыбаченко, Г. Шредер, А.Ф. Дмитрук, К.Ю. Чотий, Изучение реакции госсипола и его имино-производных с 2,2-дифенил-1-пикрилгидразилом, *Ж. общей химии.* – 2010. – Т. 80, № 2. – С. 276 – 282
56. M. C. Foti, C. Daquino, I. D. Mackie, G. A. DiLabio, K. U. Ingold, Reaction of Phenols with the 2,2-Diphenyl-1-picrylhydrazyl Radical. Kinetics and DFT Calculations Applied To Determine ArO-H Bond Dissociation Enthalpies and Reaction Mechanism, *J. Org. Chem.* - 2008. - Vol. 73, № 23. - P. 9270 – 9282
57. H. H. Hussian, G. Babic, T. Durst, J. S. Wright, M. Fluerau, A. Chichirau, L. Chepelev, Development of Novel Antioxidants: Design, Synthesis, and Reactivity, *J. Org. Chem.* 2003. – Vol. 68. – P. 7023 – 7032
58. G. Litwinienko, K. U. Ingold, Abnormal Solvent Effects on Hydrogen Atom Abstractions. 1. The Reactions of Phenols with 2,2-Diphenyl-1-picrylhydrazyl (dpph) in Alcohols, *J. Org. Chem.* - 2003. - Vol. 68, № 9. - P. 3433 – 3438
59. G. Litwinienko, K. U. Ingold, Abnormal Solvent Effects on Hydrogen Atom Abstraction. 2. Resolution of the Curcumin Antioxidant

- Controversy. The Role of Sequential Proton Loss Electron Transfer, *J. Org. Chem.* - 2004. - Vol. 69, № 18. - P. 5888 – 5896
60. M. Bronislaw, G. Schroeder, H. Kozubek, B. Brzezinski, Spectroscopic and Kinetic Studies of the Aldehyde-Lactol Tautomerization of Gossypol in Solution, *J. Chem. Soc. Perkin Trans. II.* -1991. - № 9. - P. 1359 – 1362
61. I. Nakanishi, T. Kawashima, K. Ohkubo, H. Kanazawa, K. Inami, M. Mochizuki, K. Fukuhara, H. Okuda, T. Ozawa, S. Itoh, S. Fukuzumi, N. Ikota, Electron-transfer mechanism in radical-scavenging reactions by a vitamin E model in a protic medium, *Org. Biomol. Chem.* - 2005. - Vol. 3. - P. 626 – 629
62. E. Baciocchi, A. Calcagni, O. Lanzalunga, Kinetic Study of the Reaction of N,N-Dimethylanilines with 2,2-Diphenyl-1-picrylhydrazyl Radical: A Concerted Proton-Electron Transfer?, *J. Org. Chem.* – 2008. – Vol. 73. – P. 4110 – 4115

Chapter 2

Synthesis methods of silica-gold (silver) matrices

Joanna Kurczewska and Grzegorz Schroeder
*Adam Mickiewicz University, Faculty of Chemistry, Grunwaldzka 6,
60-780 Poznań, Poland*

The production of nanoparticles (NPs) of metals became extremely important research area in recent years. Nanoparticles are often described as intermediate between molecules and solids but as opposed to molecules and solids, their properties are size-dependant. Nanoparticles of noble metals (Au, Ag) demonstrate significant dependence between their optical properties (color) and size and shape of the particles, which results from strong surface plasmon resonant (SPR) absorption in ultraviolet-visible region of the electromagnetic spectrum. Additionally, peak position of the plasmon resonance depends strongly on the surrounding medium, like solvents, surfactants or oxygen [1,2].

A noble metal can be deposited onto dielectric particle (like silica) and SPR peak is still observed. Silica belongs to the very popular materials applied as both shell and core in the designed core-shell nanoparticles.

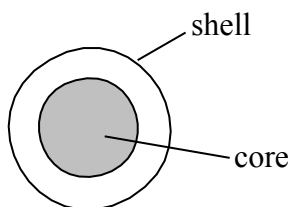


Figure 1. Schematic model of core-shell nanomaterial

The popularity of silica results from several important properties of the material, e. g. chemical and thermal stability, chemical inertness, large surface area, good compatibilities with other materials [3,4].

Core-shell structures composed of metals and dielectric could find applications in optics, photonics, surface-enhanced Raman scattering, biological sensing, electronics, magnetics and catalysis [5-11].

1. Silica-gold (silver) core-shell nanomaterials

The affinity of gold to silica matrix is insignificant therefore the initial modification of the surface is essential. The commonly applied methods use dithiols for gold substrates and aminoalkylalkoxysilanes for silica substrates.

Graf and van Blaaderen [12] developed the synthesis of colloidal gold shell with dielectric core (Figure 2). The Stöber procedure [13] was used to obtain small silica seed particles. It is one-step method based on the condensation of tetraethyl orthosilicate (TEOS) in ethanol-water mixture under alkaline conditions at room temperature. It allows the controlling of size, narrow size distribution and morphology of the silica particles. Then the particles obtained were grown in several seeded growth steps to get the desired radii. Such silica particles were next modified with 3-aminopropyltrimethoxysilane (APTMS). On the other hand, small gold particles were obtained by the reduction of chloroauric acid in the presence of tetrakis(hydroxymethyl)phosphonium chloride (THCP). Silica sphere solution was added to aqueous gold cluster solution. After that shell growth step was carried out in the presence of chloroauric acid and potassium carbonate. The authors observed that the formation of well-defined and uniform shells required simultaneous growth of all gold nanoclusters. Besides they suggested that newly added gold ions should only be reduced on the small gold nanoclusters. Taking that into consideration, the authors applied hydroxylamine to the reduction of chloroauric acid, which gave particles with a variable core radius, controlled thickness of gold shell and low polydispersity.

Westcott et al. [14] obtained clusters of gold nanoparticles on silica nanoparticles surface. First, the authors mixed water solution of gold nanoparticles with ethanolic solution of 3-aminopropyltrimethoxysilane-functionalized silica nanoparticles in order to immobilize gold on the silica. The gold particles were strongly attached and well-separated. However, when gold nanoparticles solution was prepared in water and ethanol mixture, clusters of gold (each aggregate has tens of gold nanoparticles) were attached on the silica surface. The authors applied two strategies to observe differences in the growth of gold nanoparticles. They used two different precursors for silica surface modification: 3-aminopropyltrimethoxysilane (APTMS) and propyltrimethoxysilane (PTMS) in different ratio, and varied the concentration of ethanol-water mixture for gold nanoparticles solution preparation. In general, the higher concentration of ethanol, the better association of gold nanoparticles was observed. It could be explained by the lower dielectric constant of ethanol. On the other hand, no significant differences were noticed in silica nanoparticles behaviour terminated with different ratio of APTMS (amine groups) and PTMS (methyl groups), with the exception of 5% APTMS content when lower coverage of gold was

achieved. Other organosilanes were also used to observe the influence of different functional groups and the general tendency showed that hydrophilic groups (NH_2 , SH) were conducive to the attachment of gold nanoparticles, while hydrophobic groups (CH_3 , PPh_2) demonstrated opposite behaviour.

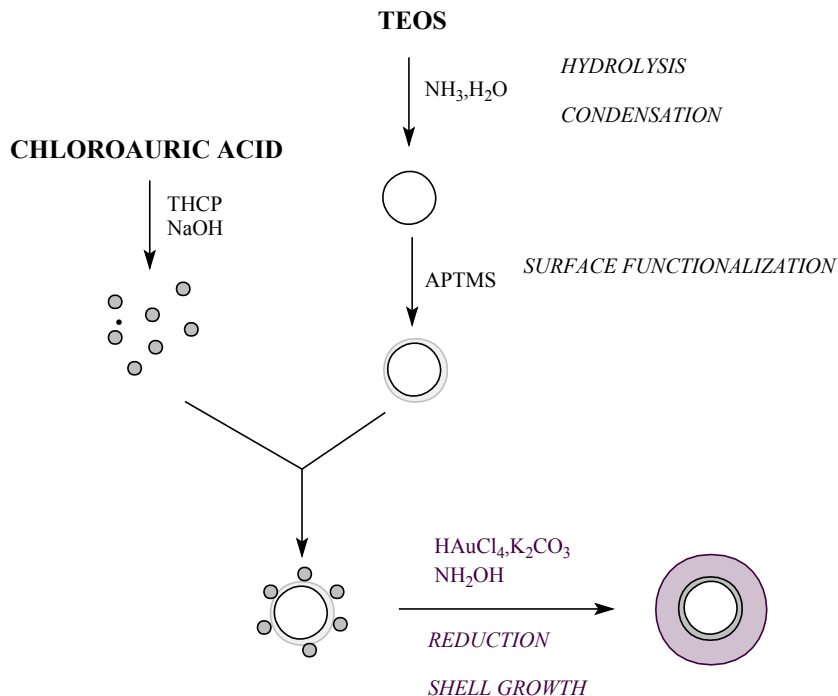


Figure 2. Synthesis of gold shell with a silica core [12]

Other improvement of the synthesis of silica-gold nanoparticles was presented by Kandpal et al. [15]. The paper focused on the comparison of two popular reducing agents of chloroauric acid-trisodium citrate and sodium borohydride, which were used for coating and for gold nucleation. Also the combination of both methods, in which borohydride method was used for coating and citrate method for gold nucleation, was tested. It was noticed that the stability of gold nanoparticles is lower for borohydride method. On the other hand, very slow reduction rate in citrate method is also undesirable. The best results were observed when sodium borohydride was used for coating (high reduction rate) and trisodium citrate for nucleation (stable gold particles).

The commonly used method of the formation of silica-gold core-shell nanomaterial is carried out in two separated steps (Figure 3A), which are the synthesis of colloidal gold and its attachment to the organofunctionalized dielectric core [12].

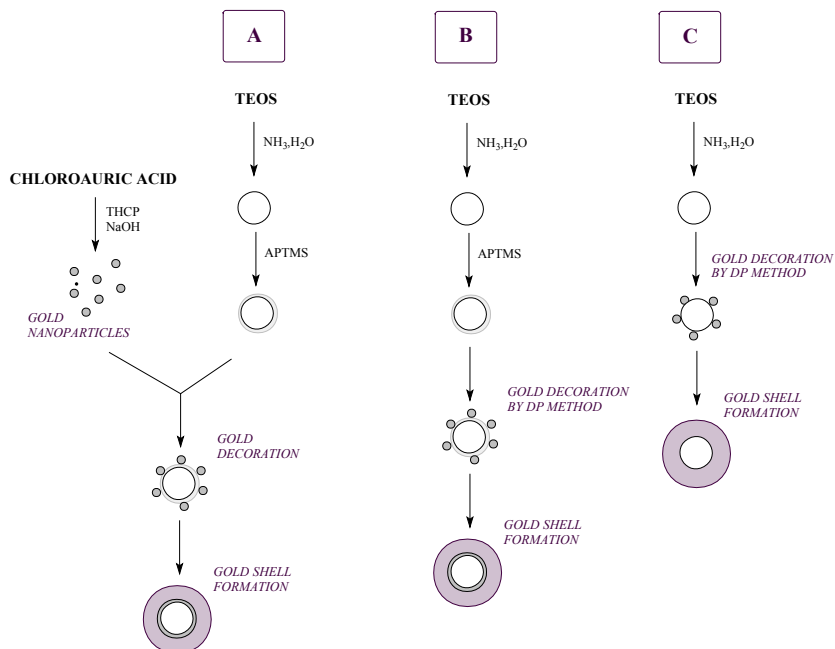


Figure 3. Commonly used (A) and alternative methods (B, C) of the synthesis of core-shell structures [16,17]

Kah et al. [16] decided to adopt deposition-precipitation (DP) process in order to eliminate the synthesis of colloidal gold in a separate step (Figure 3B). DP process is often used to form nanoparticles gold catalysts for low temperature oxidation of carbon monoxide. This method requires a contact between the support and solution of gold (III) chloride. However, the method applied in the synthesis of gold nanoshells is highly dependant from several factors: optimal pH range is rather narrow (around 8) to achieve a high density of $\text{Au}(\text{OH})_3$ loading; bare silica core is unfavorable (in comparison with amine functionalized silica) and temperature of the process should exceed 65°C . Regardless of some limitations, deposition-precipitation method is easier and less cost expensive in comparison to widely used two-step strategy.

The same scientific group worked out another simplified method of core-shell structures synthesis [17]. They again applied deposition-precipitation procedure with sodium borohydride as a reducing agent. Additionally, gold seeding was carried out on both 3-aminopropyltriethoxysilane (APTES)-grafted silica and bare silica spheres (Figure 3B,C). Under acidic conditions silica surface is positively charged so direct deposition of gold is possible from anionic complex. However, chloroauric acid is then insignificantly dissociated. On the other hand, in higher pH hydrolysis of acid increases but adsorbent becomes negatively charged. Therefore the authors used ammonia in the synthesis of silica spheres that interacted with Si-OH (hydrogen bonding) getting positively charged surface that willingly adsorbed gold anions. Even though gold decoration is better for APTS-functionalized silica core, the shorter reaction time and simplicity of the method encourage to use bare silica spheres.

Jang et al. [18] proposed another strategy of facile synthesis of core-shell particles (Figure 4). Instead of gold seeding, which requires several steps of washing and purification, they applied electroless deposition (ELD) of dendritic gold on an amine-functionalized surface. They used ascorbic acid (ASA) as reducing agent and polyvinylpyrrolidone (PVP) as a complexing agent of the gold precursor. ASA guarantees slow reduction of metal precursor and acidic reaction of the solution. Protonated amine groups of silica surface attract ASA⁻ anions. Moreover, carbonyl groups of PVP interact with protonated amine groups and form complexes with metal ions. Finally, all reagents concentrate near the silica surface that is favorable by gold reduction.

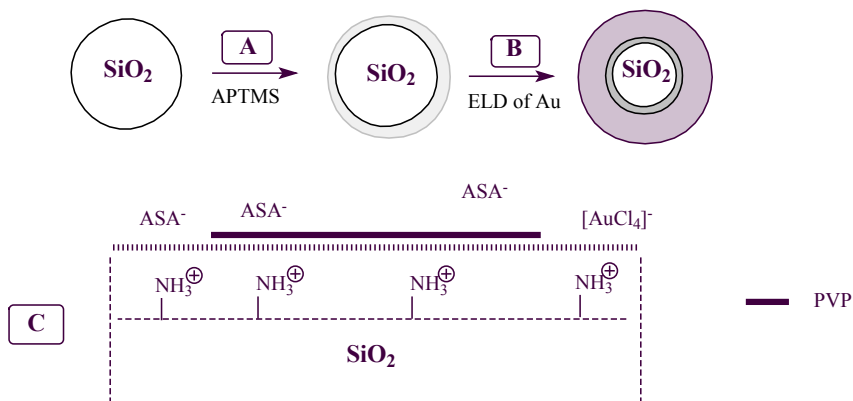


Figure 4. Synthesis procedure (A-B) and charge interactions near the amine-functionalized silica surface (C) [18]

Very interesting core-shell model was synthesized by Ji et al. [19]. A core was composed of superparamagnetic iron oxide (SPIO) and silica, while gold formed nanoshell. The synthesis procedure (Figure 5) is rather simple and similar to the previously described. The great advantage of such nanomaterial is bifunctionality, which results from photothermal properties of gold and magnetic properties of SPIO. SPIO-Au nanoshells were prepared according to Stöber synthesis and gold nanoseeds were responsible for nucleation of a gold layer growth. Finally, the nanoshells were coated with polyethylene glycol in order to retain stability in aqueous solutions.

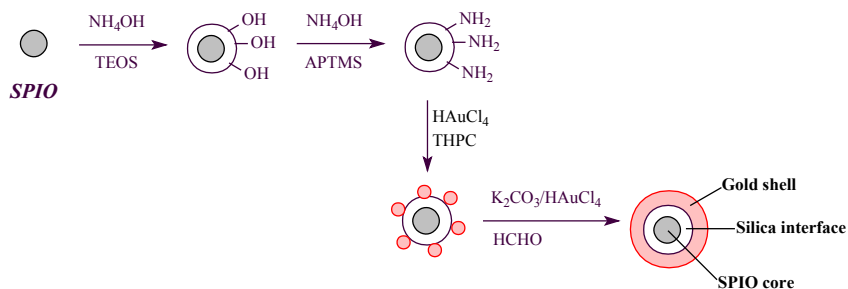


Figure 5. The synthesis procedure of bifunctional nanomaterials [19]

The above mentioned methods of gold particles deposition on silica spheres (pre-treatment of electroless deposition, functionalization, layer by layer process) are also applied for a preparation of silica-silver core shell spheres. Similarly to the above mentioned processes, the growth of silver particles depends on several parameters: temperature, concentration of reactants, pH value etc.

Jean et al. [20] proposed facile experimental procedure based on the modified Stöber method (Figure 6). They carried out the synthesis without coupling agents and a complexation of silver ions (from silver nitrate) was performed with the presence of ammonia. Owing to the control of silica and silver nanoparticles size, the nanospheres obtained demonstrated the ability of melamine detection.

On the other hand pre-treatment process was used by Zhu et al. [21] to functionalize silica surface before electroless plating. According to Figure 7, after the preparation of silica spheres by Stöber method (A), Sn^{2+} ions were adsorbed on the surface (B). Then silver ions were reduced with tin ions to give silver nuclei and act as seeds (C). Finally, the nuclei growth process took place in the mixture of formaldehyde and ammoniacal silver nitrate (D).

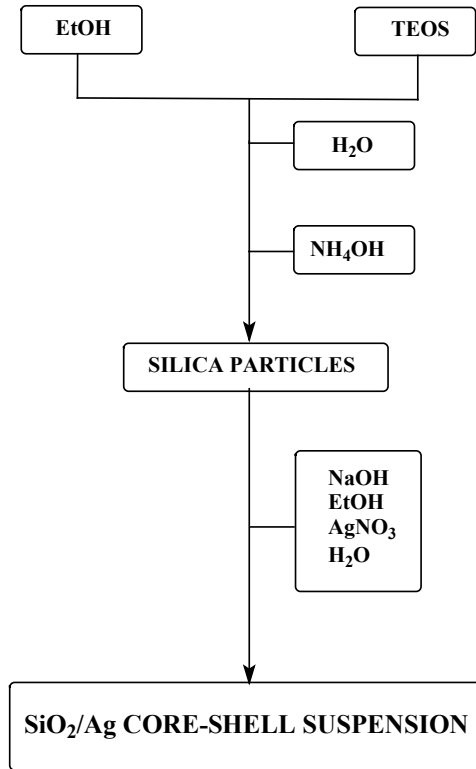


Figure 6. Schematic representation of synthesis procedure [20]

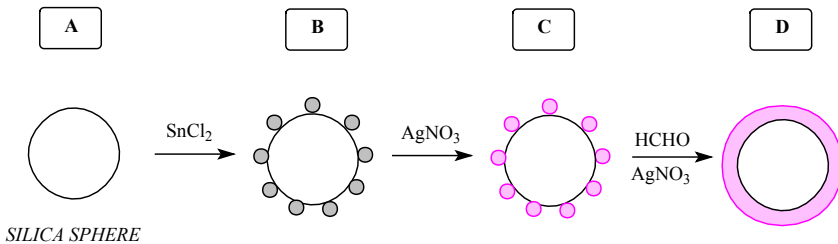


Figure 7. The fabrication process for silica-silver spheres [21]

Tuval et al. [22] used another technique to coat silica surface, prepared by modified Stöber method, with silver nanoparticles – microwave radiation. A very popular reaction used for nanoparticles preparation is polyol method [23].

Initially it was developed for divided metal powders of reducible metals (e.g., Cu, Co, Ni). However, the process carried out under reflux conditions takes long time. On the other hand, the same reaction under microwave radiation takes effect in shorter reaction time, smaller particle size, and narrow particle size distribution. The authors applied two different solvents: ethylene glycol (EG) and polyethylene glycol 400 (PEG). Firstly, deposition of Ag on silica surface failed. Therefore, silica surface was activated by ultrasonic radiation in order to convert siloxane bonds into free silanol groups. Then the activated silica was exposed to microwave radiation in the presence of silver nitrate. The best coverage was obtained using PEG that is characterized by higher boiling point than EG. Therefore, the high temperature is very important factor that determines the effectiveness of the process. Also the activated silica influences significantly the formation of the composite.

Another solution that eliminates the necessity of functionalization of silica spheres in multistep process is ultrasonic deposition of silver onto silica spheres [24]. Silica spheres were again synthesized according to the modified Stöber method. Since silver nitrate is unstable, the silver perchlorate electrolytes were also prepared. Deposition of silver nanoparticles required two-electrode arrangement with an electrochemical cell. The anode and cathode were composed of identical silver slices, while silver perchlorate solution was electrolyte. The deposition process in the electrochemical cell was carried out under continuous ultrasonic radiation. Dielectric silica cannot support electrodeposition, so the success of the process depends on silver ions, strictly speaking on bonding and reducing of ions on silica surface. Initially silver ions formed a layer as a result of electrostatic interaction between silanol surface groups and Ag ions, and chemical bond between siloxane oxygen and elemental Ag. Silica surface was activated under the ultrasonic radiation. The silver-ion-silica went to the cathode, where Ag ions were deoxidized and the bounded Ag^0 was then nucleating site. After that such nanoelectrodes attracted continuously silver ions from the anode.

Among many papers considering silica-gold (silver) nanostructures, most of them describe the synthesis procedure and their characterization. Nevertheless, two basic applications of such matrices are significant: catalytic and bactericidal activity. Qu et al. [25] studied catalytic activity of Ag/SiO_2 in CO selective oxidation in H_2 in different temperatures. On the other hand, antibacterial properties can be applied in textile industry. Nischala et al. [26] prepared successfully silica silver particles that were applied on cotton fabric in order to act as an antibacterial agent.

2. Gold (silver)-silica core-shell nanomaterials

Nanoparticles of noble metals could equally well act as core, while silica as shell in core-shell particles. Again, very little affinity of gold for silica is significant aspect. Therefore, usually silane coupling agents are used as surface primers, which is analogous approach as in case of silica core functionalization. Such method was used by Liz-Marzán et al. [27], who functionalized gold sol with APTMS (Figure 8). The process was carried out in water, while final shell growth via the Stöber method was taken in ethanol.

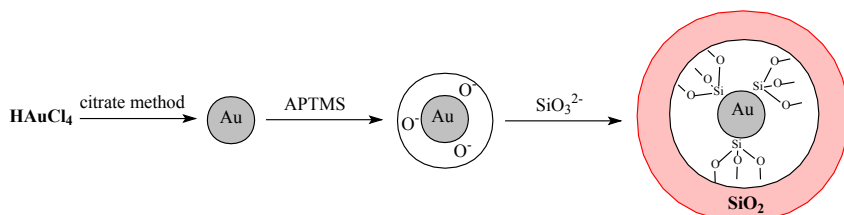


Figure 8. Formation of silica layer on gold particles [27]

The methods that require surface primer like silane coupling agent [27] or noionic polymer [28] are very effective but long and difficult to control at the same time. On the other hand direct coating of gold (silver) by silica via modified Stöber method is only possible for large metal particles. Han et al. [29] applied reverse microemulsion method of silica coated gold (silver) nanoparticles synthesis. Generally, reversed microemulsions are composed of water core surrounded by a layer of amphiphilic molecules. In the paper discussed gold was initially stabilized by oleylamine. The formation of a water-in-cyclohexane microemulsion led to silica surface coating. Analogous procedure was applied for bared silica, amino- and aldehyde- functionalized particles. Besides, the method enabled covering of small gold particles.

Other solution was proposed by Mishra et al. [30], who embedded silver particles in silica matrix by atom beam sputtering. This method consists in co-sputtering of silver and silica using fast argon atom source, giving consequently thin films of silver and silica composites. Additionally, the authors observed the sensitivity of the nanoparticles obtained towards glucose that indicated the possibility of their application in medical diagnostics.

The functionalization of silica coat gives the possibility of further modification to obtain specific desired application. Figure 9 presents gold nanoparticles with silica coating that was functionalized with primary amine [31]. Such precursors were further modified in order to obtain aptamer- and antibody-functionalized

Au nanoparticles. The materials were characterized by the ability of protein detection, very good water solubility, high buffer and colloidal stability. Other interesting medical application was presented by Zhan et al. [32], who described gold nanorods coated with mesoporous silica for cancer cell imaging.

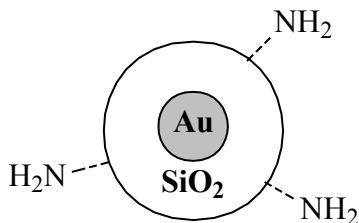


Figure 9. The precursor of Au nanoparticles for protein detection [31]

Despite general classification described above, some authors present more advanced systems, to be precise silica-coated Au nanospheres surrounded by a gold shell layer (Figure 10), [33]. The process of multilayered nanostructure formation was taken in several steps. Initially, Au nanoparticles were synthesized from chloroauric acid using CO as reducing agent. Then silica coating was formed from TEOS, which was modified with cyclic silane. Finally, electroless plating was applied to form gold layer, where small gold particles were precursors before gold shell growing around silica. Such materials could determine new direction of development of core-shell structures that similarly to previously described ones find a variety of technological applications.

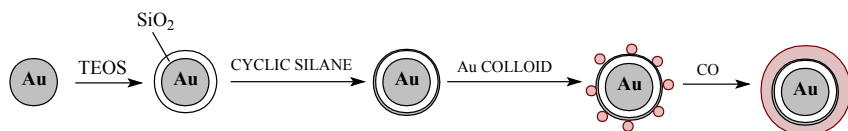


Figure 10. Synthesis of multilayered nanostructure [33]

This paper provides only an extract of varied core-shell matrices that have been studied by various research groups. Nevertheless, the same research methods are usually applied to characterize the particles, to be precise transmission electron microscopy and ultraviolet-visible spectroscopy. Other methods, which appear in some papers, complete the description of given nanomaterials, e. g. scanning electron microscopy, X-ray diffraction, Fourier transform infrared spectroscopy. The development of synthesis of core-shell matrices goes in two

general directions. The crucial aspect is related to the synthesis procedure that should be as simple as possible but effective at the same time, i. e. multistep processes are replaced by shorter methods, while control of size is still achieved. The other interest (not that much developed) concentrates on the possibility of modification of shell surface. Any further functionalization increases an amount of a possible application. Therefore, it seems that this direction should come in prominence in the nearest future.

Our attempts concentrate on silica-gold materials that can be further functionalized with thiocompounds. So far we covered silica of a new generation (spherical silica functionalized with triamine) by clusters of gold (Figure 11).

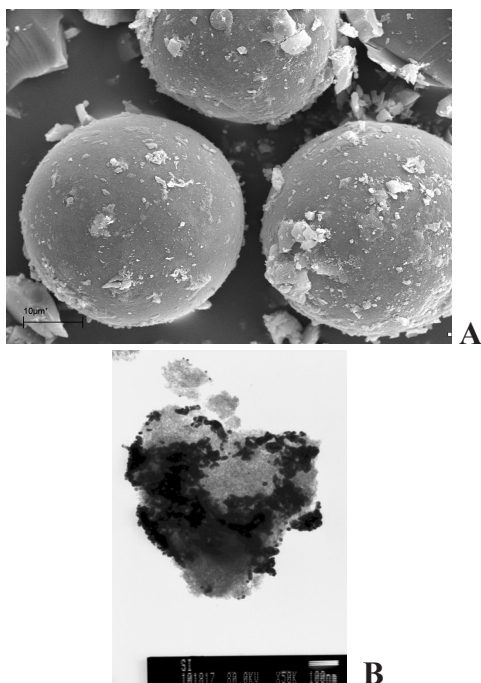


Figure 11. SEM (A) and TEM (B) images of silica-gold matrix

Spectrum XRF of silica-gold matrix shows stoichiometry elements in hybrid materials (Fig.12).

Such a hybrid material could be applied as either a molecular scavenger of trace amounts of thiocompounds or selective supporter matrix in the analysis of low molecular weight compounds by MALDI MS method [34-36].

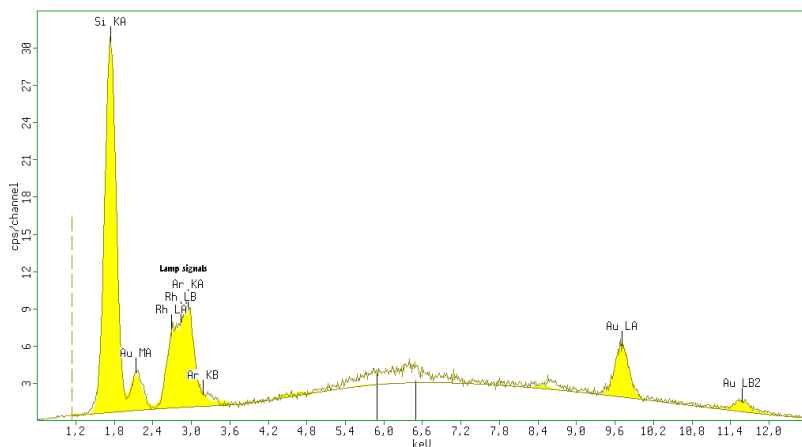


Figure 12. XRF spectrum of silica-gold matrix

Acknowledgements

This work was supported by research funds in years 2009-2012 from the Polish Ministry of Science and Higher Education as scientific grant NN 204 028636.

References

1. E. Hutter, J.H. Fendler, *Adv. Mater.*, 16, 1685 (2004)
2. A. Serra, E. Fillippo, M. Re, M. Palmisano, M. Vittori-Antisari, A. Buccelieri, D. Manno, *Nanotechnology*, 20, 165501 (2009)
3. P.K. Jal, S. Patel, B.K. Mishra, *Talanta*, 62, 1005 (2004)
4. S.K. Parida, S. Dash, S. Patel, B.K. Mishra, *Adv. Colloid Interface Sci.* 121, 77 (2006)
5. L.M. Liz-Marzán, M.A. Correa-Duarte, I. Pastoriza-Santos, P. Mulvaney, T. Ung, M. Giersig, N.A. Kotov, *Handbook of surfaces and interfaces of materials*, ed. H.S. Nalva, vol. 3, ch. 5, p. 189, Academic Press (2001)
6. S. Nie, S.R. Emory, *Science*, 275, 1102 (1997)
7. S.J. Oldenburg, G.D. Hale, J.B. Jackson, N.J. Halas, *Appl. Phys. Lett.*, 75, 1063 (1999)
8. Y. Lu, Y. Yin, Z.Y. Li, Y. Xia, *Nano. Lett.*, 2, 785 (2002)
9. G. Peto, G.L. Molnar, Z. Paszti, O. Geszti, A. Beck, L. Guzzi, *Mater. Sci. Eng.*, C19, 95 (2002)
10. M.A. El-Sayed, *Account. Chem. Res.*, 34, 257 (2001)

11. P.V. Kamat, *J. Phys. Chem. B*, 106, 7729 (2002)
12. S.L. Westcott, S.J. Oldenburg, T.R. Lee, N.J. Halas, *Langmuir*, 14, 5396 (1998)
13. C. Graf, A. van Blaaderen, *Langmuir*, 18, 524 (2002)
14. W. Stöber, A. Fink, E. Bohn, *J. Colloid Interface Sci.*, 26, 62 (1968)
15. D. Kandpal, S. Kalele, S.K. Kulkarni, *Pramana-J. Phys.*, 69, 277 (2007)
16. J.C.Y. Kah, N. Phonthammachai, R.C.Y. Wan, J. Song, T. White, S. Mhaisalkar, I. Ahmad, C. Sheppard, M. Olivo, *Gold Bulletin*, 41, 23 (2008)
17. N. Phonthammachai, J.C.Y. Kah, G. Jun, C.J.R. Sheppard, M.C. Olivo, S.G. Mhaisalkar, T.J. White, *Langmuir*, 24, 5109 (2008)
18. S.G. Jang, S.H. Kim, S.Y. Lee, W.C. Jeong, S.M. Yang, *J. Colloid Interface Sci.*, 350, 387 (2010)
19. X. Ji, R. Shao, A.M. Elliott, J. Stafford, E. Esperza-Coss, J.A. Bankson, G. Liang, Z.P. Luo, K. Park, J.T. Markert, C. Li, *J. Phys. Chem. C*, 111, 6245 (2007)
20. R.D. Jean, K.C. Chiu, T.H. Chen, C.H. Chen, D.M. Liu, *J. Phys. Chem. C*, 114, 15633 (2010)
21. M. Zhu, G. Qian, Z. Hong, Z. Wang, X. Fan, M. Wang, *J. Phys. Chem. Solids*, 66, 748 (2005)
22. T. Tuval, A. Gedanken, *Nanotechnology*, 18, 255601 (2007)
23. F. Fievet, J.P. Lagier, B. Blin, B. Beaudoin, M. Figlarz, *Solid State Ion.*, 32-33, 198 (1989)
24. S. Tang, Y. Tang, F. Gao, Z. Liu, X. Meng, *Nanotechnology*, 18, 295607 (2007)
25. Z. Qu, M. Cheng, C. Shi, X. Bao, *J. Natural Gas Chem.*, 14, 4 (2005)
26. K. Nischala, T.N. Rao, N. Hebalkar, *Colloids Surf. B Biointerfaces*, 82, 203 (2011)
27. L.M. Liz-Marzán, M. Giersig, P. Mulvaney, *Langmuir*, 12, 4329 (1996);
28. C. Graf, D.L.J. Vossen, A. Imhof, A. van Blaaderen, *Langmuir*, 19, 6693 (2003)
29. Y. Han, J. Jiang, S.S. Lee, J.Y. Ying, *Langmuir*, 24, 5842 (2008)
30. Y.K. Mishra, S. Mohapatra, D. Kabiraj, B. Mohanta, N.P. Lalla, J.C. Pivin, D.K. Avasthi, *Scripta Materialia*, 56, 629 (2007)
31. N.R. Jana, J.Y. Ying, *Adv. Mater.* 20, 430 (2008)
32. Q. Zhan, J. Qian, X. Li, S. He, *Nanotechnology*, 21, 055704 (2010);
33. R. Bardhan, S. Mukherjee, N.A. Mirin, S.D. Levit, P. Nordlander, N.J. Halas, *J. Phys. Chem. C*, 114, 7378 (2010)
34. S.Z. Qias, C.Z. Yu, Q.H. Hu, Y.G. Jin, X.F. Zhou, S.X. Zhao, G.Q. Lu,

- Micropor. Macropor. Mater., 91, 59 (2006)
35. Y. Wei, R.A. Latour, Langmuir, 24, 6721 (2008)
 36. Y. Wei, R.A. Latour, Langmuir, 25, 5637 (2009)

Chapter 3

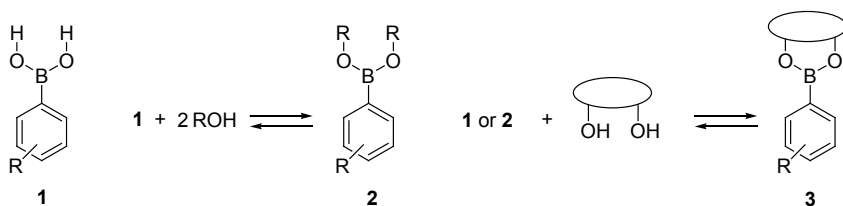
Synthesis, application and stability of phenylboronic esters

Agnieszka Adamczyk-Woźniak

*Warsaw University of Technology, Faculty of Chemistry,
Noakowskiego 3, 00-664 Warsaw, Poland*

Introduction

Phenylboronic acids (1, Scheme 1) have been applied in many fields of chemistry and medicine [1]. Their corresponding cyclic esters (3) are also widely applicable mostly due to their enhanced Lewis acidity. The much more convenient purification and characterization in comparison with boronic acids is of big importance in their applications. Phenylboronic esters (2, 3 Scheme 1) can be obtained by esterification of the boronic unit in the phenylboronic acids (1) as well as by the borylation of the corresponding halides in the presence of a catalyst. The acyclic esters (2) are easily hydrolyzed and are usually not isolated as such [2]. 2 can be transesterified by diols with formation of cyclic boronates (3). The cyclic esters (3) are much more resistant to hydrolysis and can be formed even in aqueous solutions.

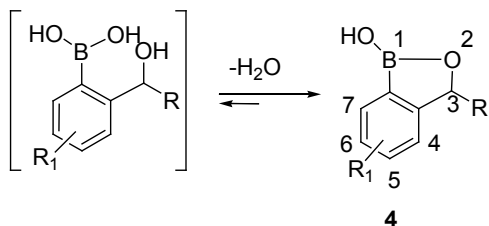


Scheme 1. Reversible formation of boronic acyclic (2) and cyclic esters (3) by esterification of boronic acids (1).

Many applications of the boronic acids (1) rely upon the reversible formation of cyclic esters (3) in their reaction with hydroxyl compounds (Scheme 1). It is the principle of boronic acids' action as sugar receptors [3]. Interestingly, recently the pinacolate ester was proposed as the active component of a sensor developed for saccharides instead of the usually used boronic acid. Sugar sensing

was possible due to the transesterification [4].

Benzoxaboroles (4, Scheme 2) are cyclic hemiesters of the unstable 2-hydroxymethyl boronic acid.



Scheme 2. Formation of benzoxaboroles (4) by dehydration of the corresponding 2-hydroxymethyl boronic acids.

Despite the fact that benzoxaboroles contain only one hydroxyl group, they reveal high receptor activity towards polyols. It happens due to the formation of cyclic esters with saccharides by the anionic form in neutral or slightly alkaline media [5, 6]. Another very important application of benzoxaboroles is their use in Suzuki coupling to give *ortho*-substituted benzyl alcohols [7]. Comprehensive review on the chemistry, structure and applications of benzoxaboroles has been recently published [8]. Series of novel benzoxaboroles has also been recently obtained and structurally characterized [9,10]. The reactivity of 3-morpholine-substituted benzoxaborole at reducing conditions has recently been investigated [11].

The aim of the current review is to evaluate possible applications of boronic esters as molecular receptors on the basis of their availability and properties. The chemistry of boronic esters, including their formation and cleavage, has been nicely and comprehensively reviewed by Duggan and Tyndall in 2002 [12]. Therefore, in current review the recent publications have been mainly focused.

1. Properties of boronic esters in comparison with those of boronic acids

Main differences in properties of boronic acids and esters are presented in Table 1. The esterification of the boronic group leads to the increased acidity of the boronic center (the pK_a lowers by about 2-4 units [13]), which enables action of boronic esters as anion receptors [14-20].

The other very important feature of the boronic ester group is the increased chemical stability of the C-B bond in comparison with the free $B(OH)_2$ group, that enables various chemical transformations of other functional groups within the boronic molecule.

Table 1. Comparison of the properties of boronic acids and esters.

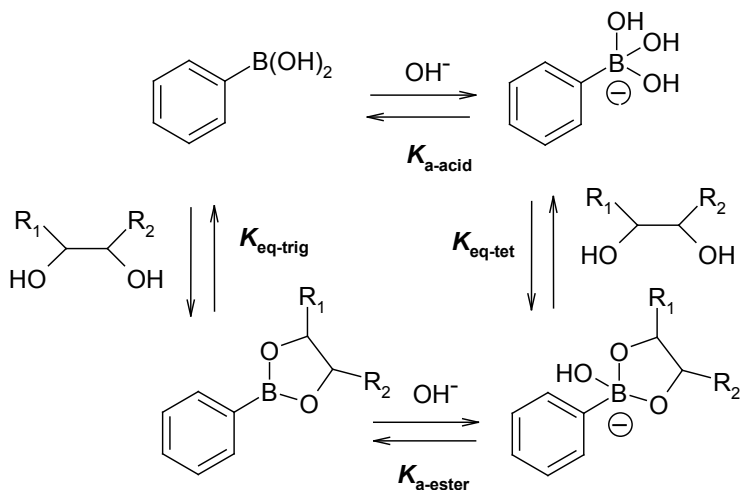
Boronic acids	Boronic esters
Higher pK_a	Lower pK_a
Lower stability of the C-B bond	Higher stability of the C-B bond
Irreversibly stick to silica gel - cannot be purified by column chromatography	Can be purified by column chromatography
Form dimers, boroxins and other anhydrides in a complex equilibrium	Easier to purify and characterize
Often sparingly soluble in organic solvents	Easily dissolved in organic solvent

Boronic esters are also easier to purify [21], handle and identify in comparison with boronic acids, that are usually in mixture with their cyclic anhydrides (boroxins) [22], other dehydrated forms [23] or dimeric species [24]. On the contrary to boronic acids, the boronate compounds (boronic esters) can easily be purified by column chromatography. Therefore, boronic compounds are very often characterized as their boronate derivatives [25, 26]. In author's opinion, it's not always justified, especially in case of pinacolate esters, which cleavage requires quite harsh conditions, that may cause decomposition of the boronic acid structure. The transformation of the free boronic group into its corresponding ester results in the increased solubility of the boronic compound in organic solvents, which is important in some applications such as Suzuki coupling or polymer electrolytes additives. The feature has also been utilized to confirm spectroscopically the structure of some sparingly soluble boronic acid in the form of their ester derivatives [27].

Benzoxaboroles exert properties of both boronic acids and esters, which make them very interesting as well as promising subject of the applied studies.

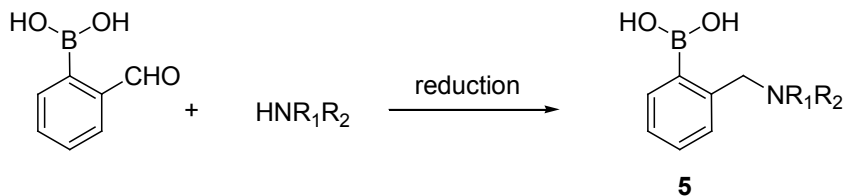
2. Reversible formation of boronic esters by esterification of boronic acids

The reaction of aromatic boronic acids and diols resulting in the formation of five- or the less stable six-membered cyclic boronate esters has been studied experimentally for many years [28]. Formation of the seven-membered esters of *trans*-diols has been recently reported [29]. Quite surprisingly, the esterification proceeds also in aqueous solution [30], which became the principle of application of boronic acids in sensing of sugars as well as other bio-molecules that are water-soluble species. The equilibrium is complex, covering both trigonal and tetragonal boronic moiety (Scheme 3) [31]. It should be clearly stated that the presence of OH^- ions influence not only kinetics yet also the equilibrium.



Scheme 3. The esterification equilibrium of boronic acids with diols in aqueous solution.

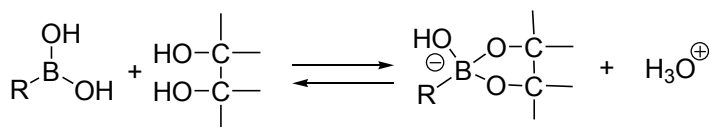
The equilibrium constant for ester formation is generally not very large at neutral pH. Higher association constants can be obtained under basic conditions (generally pH=10), where the population of the tetrahedral boronate form is greater. In order to obtain higher association constants at neutral pH, Lewis basic substituents are introduced at the appropriate position to enable donation of the lone pair into the empty boron p-orbital [32, 33]. The benzylic amine functionality at *ortho* position (as in compound 5, Scheme 4) is the most often used to enhance esterification and thus sugar sensing. It is introduced by reductive amination of the corresponding benzaldehyde (Scheme 4) or by nucleophilic displacement of a benzylic bromide [34]. The purification and subsequent synthetic manipulation of *ortho*-methylamines is often problematic due to the zwitterionic and amphoteric character of the B–N moiety [11, 35].



Scheme 4. Synthesis of *ortho*-benzylic amine boronic acids (5) in the amination-reduction reaction.

According to the works of Springsteen and Wang, the dependence of binding constants of pK_a is not as simple as it appeared. Careful studies revealed that the optimal binding pH is not always above the pK_a of the boronic acid species. The other finding is that the nature of the buffer and its concentration exert influence on the acid binding affinity [36]. Those claims have been later supported by several experiments, that also revealed that the optimal pH for binding is related to both pK_a of the acid and the diol, yet the dependence can not be precisely predicted [37]. The equilibrium is also affected by Lewis bases such as fluoride ions [38] or amines [32], which can be utilized in diols binding enhancement.

Acidic dihydroxyl ligands such as α -hydroxylic acids, dicarboxylic acids, and dihydroxybenzene react directly with trigonal boronic unit via a so-called proton transfer mechanism. When the ligand is not acidic, the boronic unit reacts mostly due to tetragonal species.

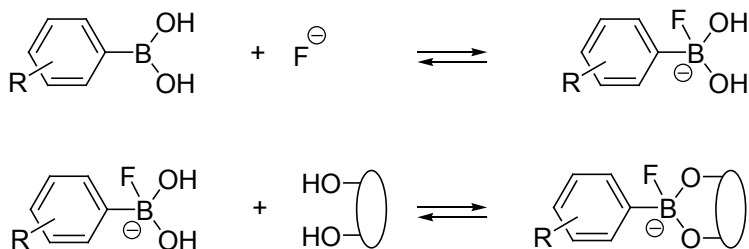


Scheme 5. Formation of four-coordinate species in the esterification reaction.

Due to the relative values of the corresponding equilibrium constants, it can be stated that boronic acids react with bidentate hydroxyl ligands to produce four-coordinate complexes (Scheme 5), however some esters are also present in the neutral form [36]. Due to the release of hydronium ions, the reaction rate can be determined by the aid of a pH indicator [39]. The so-called pH depression method measures the increase in acidity of the solution, when a diol is titrated into a solution of boronic acid [36].

3. Application of the esterification reaction

Reversible esterification of boronic acids with hydroxyl compounds is the basis of their application as molecular recognition agents, which has been recently reviewed [40]. The formation of boronic esters at basic conditions and their cleavage at acidic ones is the principle of the so-called boronate affinity chromatography (BAC). The affinity can be additionally enhanced by addition of the Lewis base to the mobile phase. Such a mechanism is favorable when the analyte is less stable at high pH conditions [38]. Schematic illustration of this effect is shown in Scheme 6.



Scheme 6. Effect of the fluoride anion on the diol's binding.

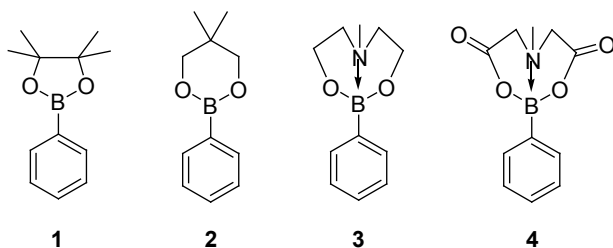
Boronic acids have been long used as derivatizing agents of ethylene glycol [41, 42]. The electrochemical detection of dopamine in the form of its boronate ester in the presence of excess ascorbic acid is an example of such application [43]. A method for the detection of sugars via the in-situ derivatization with phenylboronic acid PhB(OH)_2 using reactive desorption electrospray ionization (DESI) has been reported [44]. Improved sensitivity has recently been achieved by employing modified phenylboronic acids including 3-nitrophenylboronic acid and *N*-methyl-4-pyridineboronic acid iodide [45].

4. Synthesis of boronic esters by esterification of the corresponding acids

As it was above stated, the trigonal boron can form stable esters with the exclusion of water. It is the case in anhydrous, non-coordinating organic solvents [46]. In order to obtain boronic esters in high yields, the equilibrium should be right shifted. To achieve that, the esterification reaction is most frequently carried out on removal of water by azeotropic distillation or by application of a drying agent such as molecular sieves, anhydrous Na_2SO_4 or MgSO_4 . The reaction is carried out in such solvents as: pentane [47, 48] in refluxing CH_2Cl_2 [49], toluene with azeotropic distillation [50], in dry THF using molecular sieves 4A at reflux [25]. Pretty interesting alternative is the solid state synthesis [51], giving higher yields in comparison with the more traditional solvent method [52, 53].

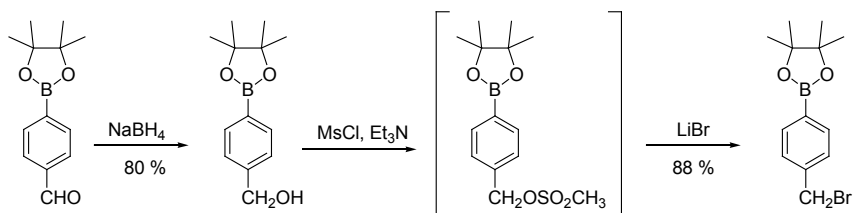
5. Protection of the free boronic group in the form of its ester

Transformation of the boronic acid functionality into the corresponding ester (*i.e.* pinacol (1) or neopentyl (2), Scheme 7) enables protection of the boronic unit. The boronic group can also be protected by a trivalent ligand as in the case of dihydroxylamines forming azaesters (3, Scheme 7) as well as the esters of *N*-methyliminodiacetic acid (MIDA) esters (4, Scheme 7).



Scheme 7. Various protected forms of the boronic unit: pinacolate (1), neopentylglycolate (2), azaester (3), MIDA ester (4).

An ideal protective group is the one that is (1) easily introduced, (2) is stable at purification conditions, (3) remains stable at reaction conditions, enabling the desired chemical transformation of other functional groups within the molecule and finally (4) can be easily removed with the restoration of the original functionality. It is worth pointing out, that only the aza and MIDA esters, that occupy the empty p-orbital of boron atom, can protect the boronic unit from nucleophilic attack. From among simple diol esters, the pinacol protected form of boronic acids is generally more useful than the neopentyl one due to its higher stability under column chromatography conditions. However, for the same reason the pinacol boronic esters are rather difficult to deprotect [54]. Azaesters are not compatible with column chromatography either, mostly due to their polar character [1]. The pinacolate turned out to be stable under reducing (NaBH_4) as well as basic conditions (Et_3N), (Scheme 8) [55].



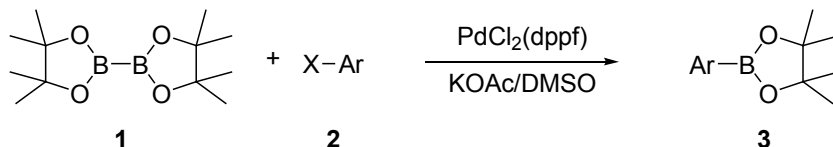
Scheme 8. Some chemical transformations of the pinacolate ester.

MIDA esters display many advantages over boronic acids as well as their other surrogates. Unlike simple boronic esters, MIDA esters are unreactive under anhydrous cross-coupling conditions [56] as well as forcing oxidizing conditions. Unlike corresponding azaesters, MIDA esters are compatible with chromatography, which is quite useful in purification. Moreover, MIDA esters

are stable to storage and tolerant to a variety of reaction conditions as well as workup/extraction media including: water, pH 7 buffer, brine, aq. HCl, aq. NH_4Cl , aq. $\text{Na}_2\text{S}_2\text{O}_3$, and aq. hydrogen peroxide at pH 6. Saturated aqueous NaHCO_3 was also well tolerated, except in the presence of alcoholic solvents. Despite this widespread stability, several MIDA boronates were conveniently transformed into the corresponding boronic acids using mild aqueous base (aq. NaOH/THF , 23°C , 10 min, or aq. $\text{NaHCO}_3/\text{MeOH}$, 23°C , 3.5 h) [57]. It was found, that MIDA boronates are generally incompatible with LiAlH_4 , DIBAL, TBAF, and a variety of metal alkoxides [58]. MIDA boronates have been alkylated on the MIDA ligand using $n\text{-BuLi}$ as base at room temperature [58]. The exceptional stability of MIDA esters in comparison with the closely related *N*-methyl azaesters results from the irreversibility of the N–B bond up to 150°C [57]. Interestingly, it is possible to slowly release boronic acids from their MIDA esters, which enables Suzuki-Miyaura coupling of otherwise unstable boronic acids substrates [59].

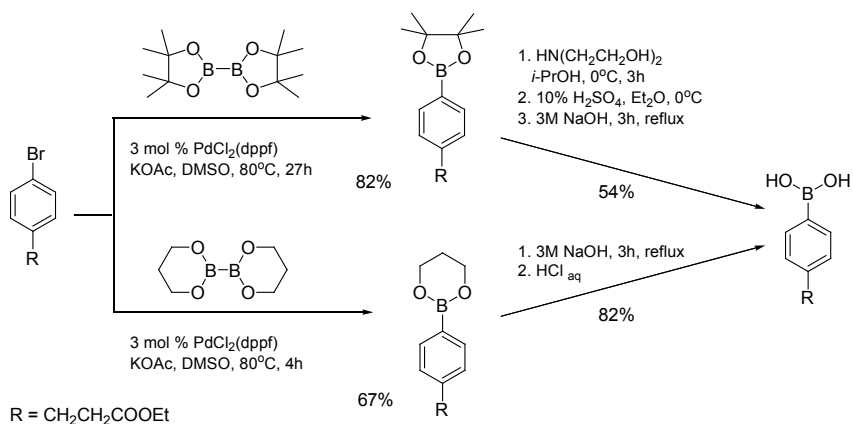
6. Direct synthesis of boronic esters

The rapid advancement of organoboron chemistry was due to the accessibility of boronic esters under mild conditions enabled by Miyaura borylation of aryl- and vinyl-halides in the presence of a palladium catalyst and bis(pinacolato) diboron (**1**, Scheme 9) [60]. Various catalysts have been used [61].



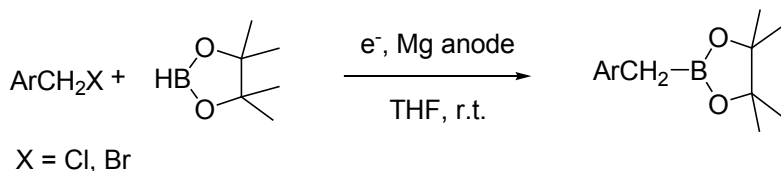
Scheme 9. Direct introduction of boronic ester unit by borylation with bis(pinacolato) diboron.

Similar conditions have been applied in the synthesis of the neopentyl derivative [62], when the bis(pinacolato)diboron was ineffective, probably due to steric hindrance caused by the *ortho*-substituent in the bromide. There are several other examples of the direct introduction of the boronate unit into the phenyl ring using pinacol [63-65] as well as neopentyl [66], or propyl diboranes [67-75]. According to the results reported by Zaidlewicz et al. formation of pinacolate is more efficient than formation of the corresponding propylester. At the deprotection step however, the reactivity is higher for propylester (Scheme 10) [76].



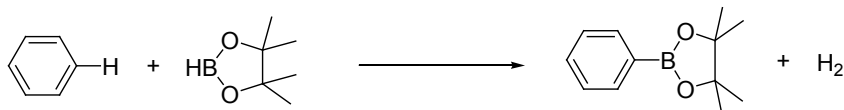
Scheme 10. Yields of catalytic borylation and of the subsequent ester cleavage of the pinacolate and propylate.

The electrosynthetic methodology for the preparation of allylboronic [77] as well as benzylic [78] esters can be the alternative to the transition-metal-catalysed procedures (Scheme 11).



Scheme 11. Electrosynthesis of boronic esters from benzyl halides and pinacolborane.

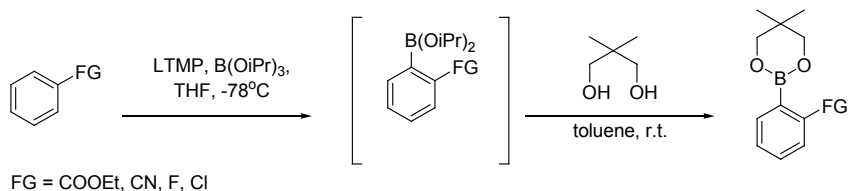
The boron pinacolate unit was also introduced by catalytic borylation of various arenes by means of HBPIn (Scheme 12) [79].



Scheme 12. Catalytic borylation of arenes with HBPIn.

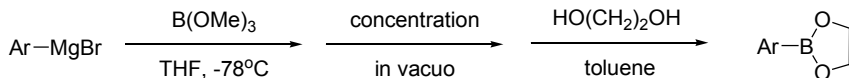
The boronic unit was also introduced directly in *ortho* position of COOEt, CN, F and Cl [80] groups of the phenyl ring by application of LTMP (lithium

2,2,6,6-tetramethylpiperidide) and the *in-situ* trapping of the resulting lithium derivative with $B(OiPr)_3$, followed by transesterification with neopentyl glycol (Scheme 13). Several esters have been obtained by this method [81-82].



Scheme 13. Direct introduction of the boronic unit by ortho-lithiation.

Grignard reagents have also been successfully applied in the “one-pot” synthesis of boronic esters (Scheme 14). Transesterification of the “ate” complex with diol established the convenient nonaqueous procedure for the preparation of boronic esters [82].



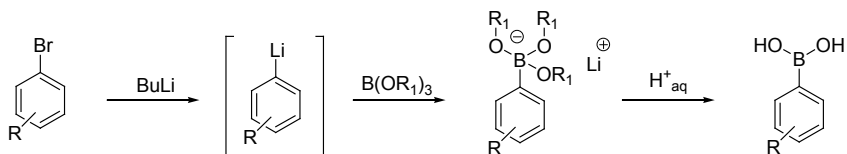
Scheme 14. One-pot, non-aqueous procedure for boronic esters starting from Grignard reagent.

7. Cleavage methods and relative stability of boronic esters

Several reactions of organoboron reagents require, or proceed most efficiently with, boronic acids [83], therefore the efficient cleavage methods are needed. The hydrolytic stability of boronic esters has frequently been discussed, yet there is very little quantitative data available. Therefore, when studying the literature concerning phenylboronic esters chemistry care should be taken, as some statements, especially in the introductory part may be unjustified or too generalized. For example, most of the researchers claim that pinacolates need forcing conditions to be cleaved, whereas others name them “readily hydrolyzed” species [84] or state: “they (boronic esters) have low hydrolytic stability both during synthetic reactions and in biological media” [85].

Searching for a transformation of esters into the corresponding boronic acids, one can find several references that cover the hydrolysis of “ate” complexes as part of the usual methodology applied for the synthesis of boronic acids (Scheme 15). The high number of such references can give a false impression that there is a lot of reports on the hydrolysis of esters as such. In the considered route, the

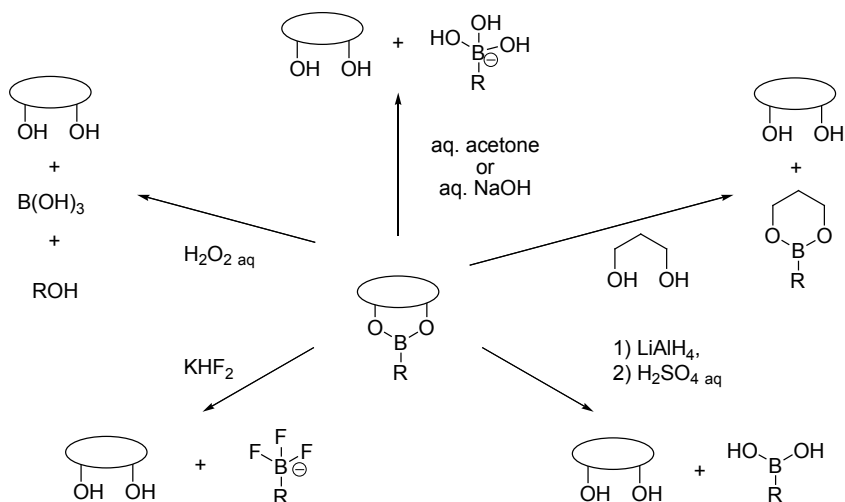
phenyl lithium intermediate reacts with electrophilic trialkoxyborate resulting in formation of the “ate” complex that is not isolated, yet is hydrolyzed during work-up at acidic conditions [23, 86-89].



Scheme 15. The usual methodology for the synthesis of boronic acids.

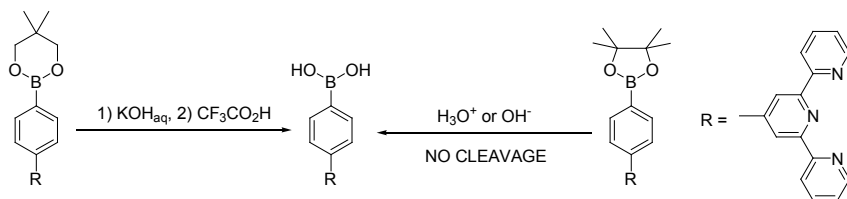
The acidic work-up conditions are usually: 10% aq HCl in THF/pentane [86], 15% HCl at 22°C in THF [90], 2M HCl [91], 10 M HCl [92], concentrated HCl [89] in THF/hexane [93]. The alternative to acidic work-up is the “in-situ” transformation of the “ate” complex into a stable cyclic ester and its subsequent isolation [49, 94-97] as well as pinanediol esters [98] have been obtained by this method.

The cleavage methods can be generally divided into the destructive ones and the deprotection ones that liberate boronic unit. Some of them have been presented at Scheme 16 [12].



Scheme 16. Some methods used to cleave boronate esters.

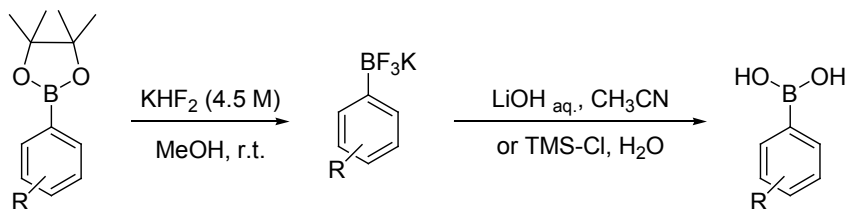
Pinacolates are claimed to be much easier to handle than the corresponding acids [97]. Due to facile synthesis of pinacolates their cleavage to obtain free boronic group has been widely studied. The pinacolates are especially resistant to hydrolysis under both acidic and basic conditions [99], therefore their synthesis and purification can not guarantee the desired free boronic group. The neopentyl glycolate analogues are more readily hydrolyzed, generating free boronic unit [100] for example by a trifluoroacetic acid [67] or 1.5 M HCl work-up [101] (Scheme 17). The neopentyl [71] and propyl [76] boronates have been transesterified with diethanolamine. The pinacol group was oxidized with H_2O_2 with the formation of a carbonyl group [70].



Scheme 17. Stability of neopentyl and pinacol boronates.

The pinacol can be effectively cleaved by application of the boronic modified polystyrene resin [48, 83]. The deprotection has also been carried out with 2 N aq. HCl in the presence of phenylboronic acid in THF–MeOH [72], NaIO_4 in THF/ H_2O and then 2 N HCl, 12 h, extraction with ethyl acetate [102].

An alternative two-step cleavage method for pinacol ester deprotection proceeds via a readily isolable potassium trifluoroborate. The liberation of the boronic unit proceeds either by basic hydrolysis or using trimethylsilyl chloride (Scheme 18) [103].



Scheme 18. A two step cleavage of pinacol boronate with KHF_2 .

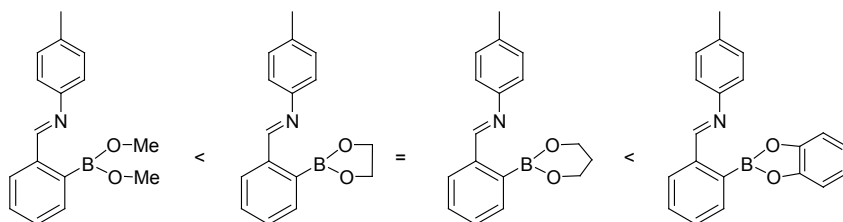
The pinacol protecting group can be either trapped with BCl_3 or destructively

remove with NaIO_4 , however those methods are not always effective [54]. Boronic acids were obtained from the corresponding pinacol esters with BBr_3 in dichloromethane at 0°C [104].

The main factor that influence the stability of boronic esters is geometrical: *cis*-diols bind more strongly than acyclic diols. The stability of the ester depends also on the steric hindrance of the B-O bond. The sterically unencumbered boronates can be easily cleaved by water [105], whereas the more hindered boronic esters such as pinacolates are quite resistant to hydrolysis and the deprotection requires rather harsh conditions. The empty p-orbital of boron is susceptible to interactions with electron donor atoms (dative bonds). Therefore, some substituents at *ortho*-position can additionally increase the stability of boronic ester by their coordination to the boronate unit [105]. The fact is probably the reason of the high binding constant of boronic acids with fructose in comparison of other sugars. It may also result in high stability of the α -hydroxy acid complexes in comparison with simple diol complexes [106, 107].

Roy and co-workers [47] showed that the trans-esterification rate of boronic esters with diols is increased by a nitrogen atom in the diol chain. Formation and stability studies of catecholates revealed that they are readily formed in CDCl_3 and C_6D_6 solutions. Heating the equimolar mixture of catechol and boronic acid at 323 K for 12 h resulted in formation of the corresponding esters in high quantities, depending on the steric hindrance of the boronic unit. Addition of an excess of D_2O (27 equiv.) to the resulting mixture and heating for 12 h resulted in partial decomposition of the ester. The study revealed that esters exert higher stability in CDCl_3 than in C_6D_6 solution [108].

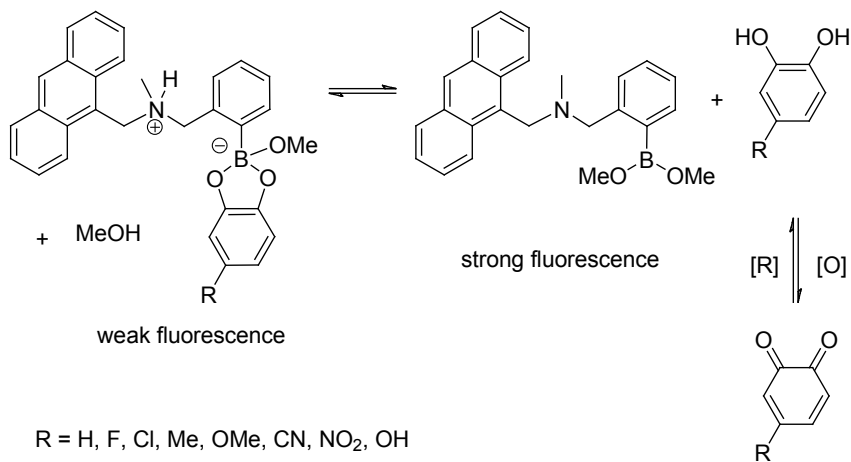
According to the paper of Hutin and coworkers [109], catechol A produces more stable boronate esters with the *ortho*-iminoboronate compounds than the more electron-rich methanol, aliphatic ethylene glycol and 1,3-propanediol (Scheme 19).



Scheme 19. Relative stability of iminoborane esters evaluated by Hutin and co-workers [109].

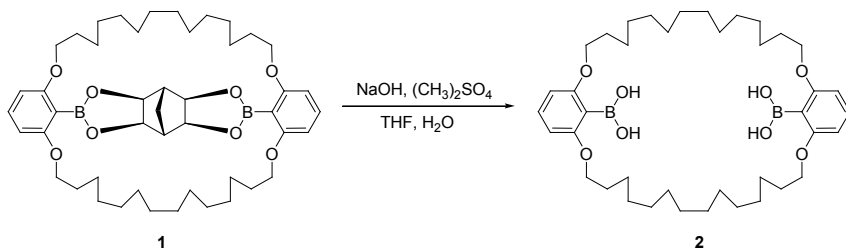
The issue was investigated by ^1H NMR. Methyl ester of the ortho-imine was obtained in deuterated methanol. The methanol was removed under vacuum and CDCl_3 was added to the resulting methyl ester. The addition of ethylene glycol to the resulting ester solution led to its complete conversion into the cyclic ester. The addition of the equimolar amount of 1,3-propanediol resulted in an equilibrium with neither of the cyclic esters predominating. The addition of catechol to the solution resulted in the quantitative displacement of the aliphatic diol with the formation of catecholate. It was stated that the driving force for the observed displacement was better stabilization of the negative charge in catecholate than in acyclic esters.

Binding constants of various catecholates with a fluorescent boronic acid in methanol were determined electrochemically (Scheme 20) [110]. Electron-withdrawing groups (EWGs) on catechol (F, CN, NO_2) enhance the affinity.



Scheme 20. Reversible boronate formation between catechol and a fluorescent boronic acid.

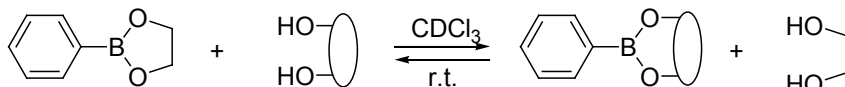
Difficulties in cleavage of the macrocyclic ester (**1**, Scheme 21) can serve as example of high resistance to hydrolysis of some boronic esters. The free acid (**2**) could not be isolated when the esters were simply hydrolyzed using various conditions. However, the addition of dimethyl sulfate, which probably scavenged the tetraol by alkylation, allowed the generation of the free boronic acid in 55% yield [93].



Scheme 21. Alkylating conditions used for cleavage of the tetraol ester (**1**).

Quite a surprising method for the deprotection of a water soluble boronic ester was developed by B. Martin and co-workers [111]. To a stirred solution of the boronic ester to be cleaved (1 mmol) in water (15 mL) phenylboronic acid (1 mmol) and ether (15 mL) were added. The phenylboronic ester was removed by several washing with ether.

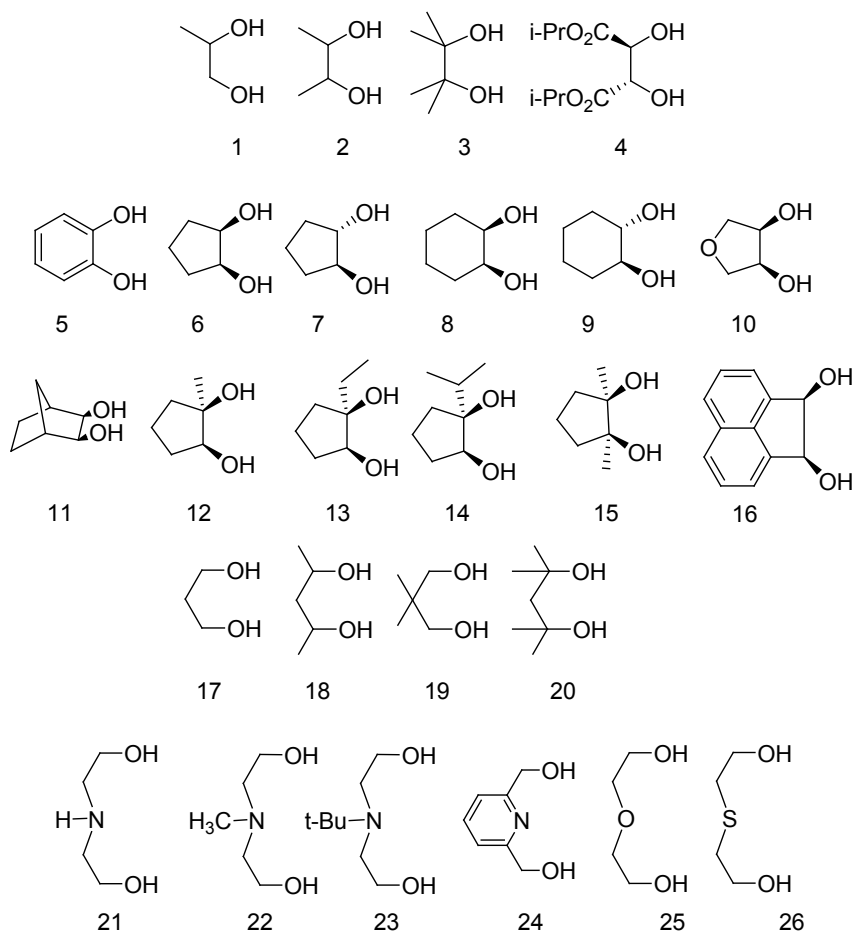
Roy and Brown investigated transesterification of a simple cyclic ethylene glycol phenylboronic acid ester with a wide variety of diols (Scheme 22) to study the relative stability of boronic esters [47]. Transesterifications were carried out in CDCl_3 solvent in NMR tubes under inert atmosphere at ambient temperature. The progress of the reactions were monitored by ^1H NMR spectroscopy. The results are summarized in Table 2.



Scheme 22. General scheme for the transesterification of 2-(phenyl)-1,3,2-dioxaborolane with various diols.

Table 2. Reaction times needed for equilibration and yields of the transesterification of 2-(phenyl)-1,3,2-dioxaborolane with a variety of diols.

Diol Nr.	1	2	3	4	5	6	7	8	9	10	11	12	13
Time [h]	0.1	0.1	94	0.1	5	0.1	47	0.1	44	0.75	0.1	0.75	1.5
Yield [%]	68.6	74.7	87.8	4.5	28	99	0	47	0	97	99.5	99	99
Diol Nr.	14	15	16	17	18	19	20	21	22	23	24	25	26
Time [h]	1.75	258	2.5	0.1	0.1	0.1	67	0.1	0.7	72	129	70	69
Yield [%]	99	99	97	88.5	98	85	91	99	70	0	9	0	0

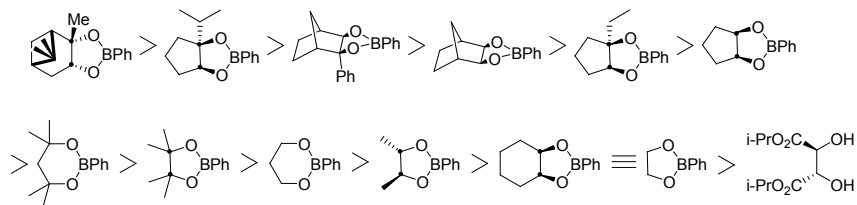


Scheme 23. Structures of diols under studies of relative stability of esters [47].

It was found that the alkyl substituents on the α -carbons of diols 1, 2 and 3 slow down the transesterification, but produce thermodynamically more stable boronic ester. Six-membered boronic esters 17, 18, 19 and 20 are thermodynamically more stable than their corresponding five-membered analogs. Amongst cyclic 1,2-diols, cis-1,2-cyclopentanediol (6) displaces ethylene glycol instantaneously whereas trans-1,2-cyclopentanediol (7) is totally unreactive, which suggests that the cis-stereochemistry of the 1,2-diol is a prerequisite for transesterification. cis-1,2-Cyclohexanediol (8) displaced ethylene glycol only

up to 48% which indicates its lower reactivity in comparison with its pentane analog which may be due to ring strain. Among the 1,5-diols, diethanolamine (21) displaces ethylene glycol quite rapidly, N-methyldiethanolamine (22) is less effective chelating agent, and N-tert-butyldiethanolamine failed to displace ethylene glycol. The oxygen atom of di(ethylene glycol) (25) and the sulfur atom of 2,2'-thiodiethanol (26) do not assist in displacing the ethylene glycol from their boronic esters.

Relative stability of a wide spectrum of achiral and chiral boronic esters (Scheme 24) has been studied employing transesterification with free diols under neutral conditions [48]. Transesterification reactions were carried out in NMR tubes under an inert atmosphere. An equimolar mixture of the boronic ester and the diol was prepared in dry CDCl_3 . The ^1H NMR spectra of various exchange reactions were frequently recorded (5–15 min to 12–24 h depending upon the speed of the reaction) to get percentage exchange accurately with time. For slow transesterifications, the reactions were followed for extended period of time (until no further exchange) even after an equilibrium had reached. The extent of ligand exchange was determined based on the NMR integrations of the relevant proton signals. On the basis of those experiments, the investigated boronic esters have been arranged according to the stability. Pinanediol phenylboronic ester was found to be the most stable whereas DIPT boronic ester appeared to be thermodynamically the least stable one. The transesterification with sterically hindered diols was observed to be relatively slow, yet afforded thermodynamically more stable boronic esters [48].



Scheme 24. Decreasing order of stability of the corresponding boronic esters.

Moreover, the resulting catechol esters are sensitive to moisture and chromatography, whereas the corresponding inert pinacol esters are more stable. This is the reason why the quantitative transesterification with pinacol was performed at room temperature in 30 min [112]. Pinanediolates have been obtained by transesterification of the corresponding pinacol esters [98] and pinacol esters into a six-membered ones [113].

The complexation of a fluorescent boronic acid with catechol in methanol has been recently investigated by Zhang *et al.* [110]. The research showed that in methanol solution the “zwitterionic” species with tetracoordinate boron atom are formed. Electron withdrawing groups in catechol moiety enhance the affinity.

8. Application of boronic esters

A macrocyclic, fluorescent receptor containing boronic ester unit has been applied as a selective H_2PO_4^- anion receptor [114]. CH_3COO^- and HSO_4^- give a much smaller impact on the fluorescence whereas Cl^- , Br^- and I^- give no impact and F^- gave a complex answer. Selective fluorine anion binding [61, 115] is due to relatively weak Lewis acidity that enables formation of complexes with fluoride and not with the potential competitive anions [14] and references cited there. Series of electron-deficient boronic esters was applied as potential anion receptors in lithium battery electrolytes [16, 17].

Boronic esters are applicable to the Suzuki–Miyaura coupling reaction in place of boronic acids [97, 116] thereby negating the need for conversion to the corresponding boronic acids. The use of boronic esters has some advantages, such as a high stability to heat and high solubility in organic solvents, when compared to boronic acids [117]. Neopentyl [117] as well as pinacol esters [117,118] have been applied in the Suzuki coupling [49, 94, 96, 97, 112, 119-122]. Boronic acid pinacol esters were less reactive in the Suzuki coupling than boronic acid neopentylglycol esters [117] as well as boronic acid itself [123].

The use of boronate esters as protecting groups for diols has been reviewed [12] with many applications to carbohydrate synthesis and the regioselective manipulation of hydroxyl groups [124].

Interestingly, the pinacolate ester and not the expected free boronic acid was proposed as the active component of a sensor developed for saccharides. Sugar sensing is possible due to the transesterification [4].

Conclusions

- The use of phenyl boronic acids esters as anion receptors is quite promising. From obvious reasons, the aza and MIDA esters are in this case excluded. Both features Lewis acidity, enabling complexation of a given anion and stability of the ester should be however taken into consideration when designing a new boronic anion receptor. Partial positive charge at the boron atom can be increased by the application of the electron-withdrawing groups in the phenyl ring. Steric hindrance of the boronic unit should also exert the influence on both the complexation ability as well as stability of the ester group.

- If it comes to application of boronic esters as sugars' or other diols' receptors, the relative stabilities of the "receptor" ester and the ester formed after complexation as well as the rate of the transesterification should be taken into account. The mentioned features are highly conditions-dependent, and only limited data has been so-far reported, therefore careful studies of the specific system should be carried out.
- Due to the exceptional stability of some *ortho*-derivatives of boronic esters, the liberation of the boronic unit can be difficult if possible. It should be considered on planning the synthetic strategy for some *ortho*-substituted boronic esters.

Acknowledgements

The author acknowledge financial support by the Ministry of Science and Higher Education (Grant N N204 127938) as well as technical support by Grzegorz Pojmaj.

References

1. Hall D.G. (Ed.), Boronic Acids. Preparation, Applications in Organic Synthesis and Medicine (VCH, Weinheim, 2005)
2. Carboni, B.; Pourbaix, C.; Carreaux, F.; Deleuze, H.; Maillard, B., *Tet. Lett.*, **1999**, 40, 7979
3. James, T. D.; Phillips, M.D.; Shinkai S., Boronic Acids in Saccharide Recognition (RSC Publishing, Cambridge, 2006)
4. Elfeke, S. A.; D'Hooge, F.; Poncel, L.; Chen, W.; Perera, S. P.; van den Elsen, J. M. H.; James, T. D.; Toby, A.; Jenkins, A.; Cameron, P. J.; Fossey, J. S., *New J. Chem.*, **2009**, 33, 1466
5. Dowlut, M.; Hall, D.G., *J. Am. Chem. Soc.* **2006**, 128, 4226
6. Bérubé, M.; Dowlut, M.; Hall, D.G., *J. Org. Chem.*, **2008**, 73, 6471
7. Gunasekera, D.S.; Gerold, D.J.; Aalderks, N.S.; Chandra, J.S.; Maanu, C.A.; Kiprof, P.; Zhdankin, V.V.; Reddy, M.V.R., *Tetrahedron*, **2007**, 63, 9401
8. Adamczyk-Woźniak, A.; Cyrański, M. K.; Żubrowska, A.; Sporzyński A., *J. Organomet. Chem.*, **2009**, 694, 3533
9. Adamczyk-Woźniak, A.; Cyrański, M. K.; Jakubczyk, M.; Klimentowska, P.; Koll, A.; Kołodziejczak, J.; Pojmaj G.; Żubrowska, A.; Żukowska, G. Z.; Sporzyński, A., *J. Phys. Chem. A*, **2010**, 114, 2324
10. Adamczyk-Woźniak, A.; Madura I.; Velders A. H.; Sporzyński, A., *Tetrahedron Lett.*, **2010**, 51, 6181
11. Adamczyk-Woźniak, A.; Madura, I.; Pawełko, A.; Sporzyński A.;

- Żubrowska, A., Żyła, J., *Cent. Eur. J. Chem.*, **2011** (in press)
12. Duggan, P. J.; Tyndall, E. M., *J. Chem. Soc., Perkin Trans. 1*, **2002**, 1325
 13. Ni, W.; Fang, H.; Springsteen, G.; Wang, B., *J. Org. Chem.*, **2004**, 69, 1999
 14. Bresner, C.; Day, J. K.; Coombs, N. D.; Fallis, I. A.; Aldridge, S.; Coles, S. J.; Hursthouse, M. B., *Dalton Trans.*, **2006**, 3660
 15. Lee, H. S.; Yang, X. Q.; McBreen, J., *J. Power Sources*, **2001**, 97-98, 566
 16. Żukowska, G.; Szczechura, M.; Marcinek, M.; Żubrowska, A.; Sporzyński A.; Wieczorek, W., *ECS Trans.*, **2009**, 16105
 17. Lee, H. S.; Ma, Z. F.; Yang, X. Q.; Sun, X.; McBreen, J., *J. Electrochem Soc.*, **2004**, 151, 1429
 18. Lee, H. S.; Yang, X. Q.; Xiang, C. L.; McBreen J.; Choi L. S., *J. Electrochem. Soc.*, **1998**, 145, 2813
 19. Cooper, C. R.; Spencer, N.; James, T. D., *Chem. Commun.*, **1998**, 1365
 20. Arimori, S.; Davidson, M. G.; Fyles, T. M.; Hibbert, T. G.; James, T. D.; Kociok-Köhn, G. I., *Chem. Commun.*, **2004**, 1640
 21. Zheng, S.-L.; Reid, S.; Lin, N.; Wang B., *Tetrahedron Lett.*, **2006**, 47, 2331
 22. Stones, D.; Manku, S.; Lu, X.; Hall, D. G., *Chem. Eur. J.*, **2004**, 10, 92
 23. Li, W.; Nelson, D. P.; Jensen, M. S.; Hoernner, R. S.; Cai, D.; Larsen, R. D.; Reider, P. J., *J. Org. Chem.*, **2002**, 67, 5394
 24. Heinrichs, G.; Schellentrager, M.; Kubik, S., *Eur. J. Org. Chem.*, **2006**, 4177
 25. Bushby, R. J.; Taylor, N.; Williams, R. A., *J. Mater. Chem.*, **2007**, 17, 955
 26. Coutts, I. G. C.; Goldschmidt, H. R.; Musgrave, O. C., *J. Chem. Soc. C*, **1970**, 488
 27. Blatch, A. J.; Chetina, O. V.; Howard, J. A. K.; Patrick, L. G. F.; Smethurstb, C. A.; Whiting, A., *Org. Biomol. Chem.*, **2006**, 4, 3297
 28. Bhat, K. L.; Howard, N. J.; Rostami, H.; Lai, J. H.; Bock, C. W., *J. Mol. Struct.*, **2005**, 723, 147
 29. Meiland, M.; Heinze, T.; Guenther, W.; Liebert, T., *Tetrahedron Lett.*, **2009**, 50, 469
 30. Lappert, M. F., *Chem. Rev.*, **1956**, 56, 959
 31. Fang, H.; Kaur, G.; Wang, B., *J. Fluoresc.*, **2004**, 14, 481
 32. Zhu, L.; Shabbir, S. H.; Gray, M.; Lynch, V. M.; Sorey, S.; Anslyn, E. V., *J. Am. Chem. Soc.*, **2006**, 128, 1222

33. Nakashima, K.; Iguchi, R.; Shinkai, S., *Ind. Eng. Chem. Res.*, **2000**, 39, 3479
34. Sporzyński, A.; Żubrowska, A.; Adamczyk-Woźniak, A. In: *Synthetic Receptors in Molecular Recognition*, V.I. Rybachenko (Ed.) (Schidnyj Wydawnyczyj Dim, Donetsk, Ukraine, 2007) pp. 51-88
35. Mulla, H. R.; Agard, N. J.; Basu, A., *Bioorg. Med. Chem. Lett.*, **2004**, 14, 25
36. Springsteen, G.; Wang, B., *Tetrahedron*, **2002**, 58, 5291
37. Yan, J.; Springsteen, G.; Deeter, S.; Wang, B., *Tetrahedron*, **2004**, 60, 11205
38. Ren, L.; Liu, Z.; Dong, M.; Yeb, M.; Zou, H., *J. Chromatogr. A*, **2009**, 1216, 4768
39. Ito, H.; Kono, Y.; Machida, A.; Mitsumoto, Y.; Omori, K.; Nakamura, N.; Kondo, Y.; Ishihara, K., *Inorganica Chim. Acta*, **2003**, 344, 28
40. Adamczyk-Woźniak, A., In: *Application of Molecular Receptors*, V.I. Rybachenko (Ed.) (Schidnyj Wydawnyczyj Dim, Donetsk, Ukraine, 2009) pp. 9-24
41. Porter, W. H.; Auansakul, A., *Clin. Chem.*, 1982, 28, 75
42. Winek, C. L.; Shingleton, D. P.; Shanor S. P., *Clin. Toxicol.*, **1978**, 13, 297
43. Strawbridge, S. M.; Green, S. J.; Tucker, J. H. R., *Chem. Commun.*, **2000**, 2393
44. Chen, H. Cotte-Rodriguez, I.; Cooks, R.G., *Chem. Commun.*, **2006**, 597
45. Zhang, Y.; Chen, H., *Int. J. Mass Spectrom.*, **2010**, 289, 98
46. Niu, W.; Rambo, B.; Smith, M. D.; Lavigne, J. J., *Chem. Commun.*, **2005**, 5166
47. Roy, C. D.; Brown, H. C., *J. Organomet. Chem.*, **2007**, 692, 784
48. Roy, C. D.; Brown, H. C., *Monatsh. Chem.*, **2007**, 138, 879
49. Bo, Z.; Schlüter, A. D., *Chem. Commun.*, **2003**, 2354
50. Niu, W.; Rambo, B.; Smith, M. D.; Lavigne, J. J., *Chem. Commun.*, **2005**, 5166
51. Kaupp, G.; Naimi-Jamal, M. R.; Stepanenko, V., *Chem. Eur. J.*, **2003**, 9, 4157
52. Wieber M.; Kunzel W., *Z. Anorg. Allg. Chem.*, **1974**, 403, 107
53. Sugihara, J. M.; Bowman, C. M., *J. Am. Chem. Soc.*, **1958**, 80, 2443
54. Yan, J.; Jin, S.; Wang B., *Tetrahedron Lett.*, **2005**, 46, 8503
55. Filippis, A.; Morin, C.; Thimon, C., *Synt. Commun.*, **2002**, 32, 2669
56. Gillis, E. P.; Burke, M. D., *J. Am. Chem. Soc.*, **2007**, 129, 6716

57. Gillis, E. P.; Burke, M. D., *J. Am. Chem. Soc.*, **2008**, 130, 14084
58. Mancilla, T.; Romo, M. A. C.; Delgado, L. A., *Polyhedron*, **2007**, 26, 1023
59. Knapp, D. M.; Gillis, E. P.; Burke, M. D., *J. Am. Chem. Soc.*, **2009**, 131, 6961
60. Ishiyama, T.; Murata, M.; Miyaura, N., *J. Org. Chem.*, **1995**, 60, 7508
61. Tan, W.; Zhang, D.; Wang, Z.; Liu, C.; Zhu, D., *J. Mater. Chem.*, **2007**, 17, 1964
62. Fang, H.; Kaur, G.; Yanb, J.; Wang, B., *Tetrahedron Lett.*, **2005**, 46, 1671
63. Milbank, J. B. J.; Knauer, C. S.; Augelli-Szafran, C. E.; Sakkab-Tan, A. T.; Lin, K. K.; Yamagata, K.; Hoffman, J. K.; Zhuang, N.; Thomas, J.; Galatsis, P.; Wendt, J. A.; Mickelson, J. W.; Schwarz, R. D.; Kinsora, J. J.; Lotarski, S. M.; Stakich, K.; Gillespie, K. K. Lam W. W.; Mutlib, A. E., *Bioorg. Med. Chem. Lett.*, **2007**, 17, 4415
64. Ahmed, V.; Liu, Y.; Silvestro, C.; Taylor, S. D., *Bioorg. Med. Chem.*, **2006**, 14, 8564
65. Giroux, A., *Tetrahedron Lett.*, **2003**, 44, 233
66. Kennedy, J. W. J.; Hall, D. G., *J. Org. Chem.*, **2003**, 680, 263
67. Aspley, C. J.; Williams, J. A. G., *New J. Chem.*, **2001**, 25, 1136
68. Itoh, T.; Hirai, K.; Tomioka H., *J. Am. Chem. Soc.*, **2004**, 126, 1130
69. Shinohara, T.; Deng, H.; Snapper, M. L.; Hoveyda, A. H., *J. Am. Chem. Soc.*, **2005**, 127, 7334
70. Dickinson, B. C.; Chang, C. J., *J. Am. Chem. Soc.*, **2008**, 130, 9638
71. Rosen, B. M.; Wilson, D. A.; Wilson, C. J.; Peterca, M.; Won, B. C.; Huang, C.; Lipski, L. R.; Zeng, X.; Ungar, G.; Heiney, P. A.; Percec, V., *J. Am. Chem. Soc.*, **2009**, 131, 17500
72. Decicco, C. P.; Song, Y.; Evans, D. A., *Org. Lett.*, **2001**, 3, 1029
73. Imanishi, M.; Tomishima, Y.; Itou, S.; Hamashima, H.; Nakajima, Y.; Washizuka, K.; Sakurai, .M.; Matsui, S.; Imamura, E.; Ueshima, K.; Yamamoto, T.; Yamamoto, N.; Ishikawa, H.; Nakano, K.; Unami, N.; Hamada, K.; Matsumura, Y.; Takamura, F.; Hattori, K., *J. Med. Chem.*, **2008**, 51, 1925
74. Pettus, L. H.; Xu, S.; Cao, G.-Q.; Chakrabarti, P. P.; Rzasa, R. M.; Sham, K.; Wurz, R. P.; Zhang, D.; Middleton, S.; Henkle, B.; Plant, M. H.; Saris, C. J. M.; Sherman, L.; Wong, L. M.; Powers, D. A.; Tudor, Y.; Yu, V.; Lee, M. R.; Syed, R.; Hsieh, F.; Tasker, A. S., *J. Med. Chem.*, **2008**, 51, 6280
75. Skaff, O.; Jolliffe, K. A.; Hutton, C. A., *J. Org. Chem.*, **2005**, 70, 7353
76. Zaidlewicz, M.; Wolan, A., *J. Organomet. Chem.*, **2002**, 657, 129

77. Godeau, J.; Pintaric, C.; Olivero, S.; Duñach, E., *Electrochim. Acta*, **2009**, 54, 5116
78. Pintaric, C.; Olivero, S.; Laza, C.; Duñach, E., *Tetrahedron Lett.*, **2004**, 45, 8031
79. Cho, J.-Y.; Iverson, C. N.; Smith, III, M. R., *J. Am. Chem. Soc.*, **2000**, 122, 12868
80. Kristensen, J.; Lysén, M.; Vedsø, P.; Begtrup, M., *Org. Lett.*, **2001**, 3, 1435
81. Lysn, M.; Hansen, H. M.; Begtrup, M.; Kristensen, J. L., *J. Org. Chem.*, **2006**, 71, 2518
82. Wong, K.-T.; Chien, Y.-Y.; Liao, Y.-L.; Lin, C.-C.; Chou, M.-Y.; Leung, M.-K., *J. Org. Chem.*, **2002**, 67, 1041
83. Pennington, T. E.; Kardiman, C.; Hutton, C. A., *Tetrahedron Lett.*, **2004**, 45, 6657
84. Deady, L. W.; Rogers, M. L.; Zhuang, L.; Baguley, B. C.; Denny, W. A., *Bioorg. Med. Chem.*, **2005**, 13, 1341
85. Bernardini, R.; Oliva, A.; Paganelli, A.; Menta, E.; Grugni, M.; De Munari, S.; Goldoni, L., *Chem. Lett.*, **2009**, 38, 750
86. Kiryanov, A. A.; Sampson, P.; Seed, A. J., *J. Mater. Chem.*, **2001**, 11, 3068
87. Jeong, K. S.; Kim, S. Y.; Shin, U.-S.; Kogej, M.; Hai, N. T. M.; Broekmann, P.; Jeong, N.; Kirchner, B.; Reiher, M.; Schalley, Ch. A., *J. Am. Chem. Soc.*, **2005**, 127, 17672
88. Routier, S.; Peixoto, P.; Mérour, J.-Y.; Coudert, G.; Dias, N.; Bailly, C.; Pierré, A.; Léonce, S.; Caignard, D. H., *J. Med. Chem.*, **2005**, 48, 1401
89. Bonvallet, P. A.; Breitkreuz, C. J.; Kim, Y. S.; Todd, E. M.; Traynor, K.; Fry, C. G.; Ediger, M. D.; McMahon, R. J., *J. Org. Chem.*, **2007**, 72, 10051
90. Percec, V.; Holerca, M. N.; Nummelin, S.; Morrison, J. J.; Glodde, M.; Smidrkal, J.; Peterca, M.; Rosen, B. M.; Uchida, S.; Balagurusamy, V. S. K.; Sienkowska, M. J.; Heiney, P. A., *Chem. Eur. J.*, **2006**, 12, 6216
91. Yoon, T.; De Lombaert, S.; Brodbeck, R.; Gulianello, M.; Krause, J. E.; Hutchison, A.; Horvath, R. F.; Ge, P.; Kehne, J.; Hoffman, D.; Chandrasekhar, J.; Doller, D.; Hodgetts, K. J., *Bioorg. Med. Chem. Lett.*, **2008**, 18, 4486
92. Harvey, R. G.; Dai, Q.; Ran, C.; Penning, T. M., *J. Org. Chem.*, **2004**, 69, 2024
93. Lüthje, S.; Bornholdt, C.; Lüning, U., *Eur. J. Org. Chem.*, **2006**, 909
94. Steinke, N.; Jahr, M.; Lehmann, M.; Baro, A.; Frey, W.; Tussetschläger,

- S.; Sauera, S.; Laschat, S., *J. Mater. Chem.*, **2009**, 19, 645
95. Zhong, Z.; Anslyn, E. V., *J. Am. Chem. Soc.*, **2002**, 124, 9014
96. Moorthy, J. M.; Venkatakrishnan, P.; Natarajan, P.; Huang, D.-F.; Chow, T. J., *J. Am. Chem. Soc.*, **2008**, 130, 17320
97. Kalinin, A. V.; Reed, M. A.; Norman, B. H.; Snieckus, V., *J. Org. Chem.*, **2003**, 68, 5992
98. Morandi, S.; Morandi, F.; Caselli, E.; Shoichet, B. K.; Prati, F., *Bioorg. Med. Chem.*, **2008**, 16, 1195
99. Ishiyama, T.; Itoh, Y.; Kitano, T.; Miyaura, N., *Tetrahedron Lett.*, **1997**, 38, 3447
100. Wang, J.; Jin, S.; Akay, S.; Wang, B., *Eur. J. Org. Chem.*, **2007**, 2091
101. Wang, Z.; Zhang, D.; Zhu, D., *J. Org. Chem.*, **2005**, 70, 5729
102. Falck, J. R.; Bondlela, M.; Venkataraman, S. K.; Srinivas, D., *J. Org. Chem.*, **2001**, 66, 7148
103. Yuen, A. K. L.; Hutton, C. A., *Tetrahedron Lett.*, **2005**, 46, 7899
104. Shimizu, K.; Maruyama, M.; Yasui, Y.; Minegishi, H.; Seung Ban, H.; Nakamura, H., *Bioorg. Med. Chem. Lett.*, **2010**, 20, 1453
105. Greene, T. W.; Wuts, P. G. M., *Protective Groups in Organic Synthesis*, (John Wiley & Sons, 1999)
106. Wiskur, S. L.; Lavigne, J. J.; Metzger, A.; Tobey, S. L.; Lynch, V.; Anslyn, E. V., *Chem. Eur. J.*, **2004**, 10, 3792
107. Bromba, C.; Carrie, P.; Chui, J. K. W.; Fyles, T. M., *Supramol. Chem.*, **2009**, 21, 81
108. Nishimura, N.; Yoza, K.; Kobayashi, K., *J. Am. Chem. Soc.*, **2010**, 132, 777
109. Hutin, A.; Bernardinelli, G.; Nitschke, J. R., *Chem. Eur. J.*, **2008**, 14, 4585
110. Zhang, L.; Kerszulis, J. A.; Clark, J. R.; Ye, T.; Zhu, L., *Chem. Commun.*, **2009**, 2151
111. Martin, B.; Possémé, F.; Le Barbier, C.; Carreaux, F.; Carboni, B.; Seiler, N.; Moulinoux, J.-P.; Delcros, J.-G., *J. Med. Chem.*, **2001**, 44, 3653
112. Claudel, S.; Gosmini, C.; Parisb, J. M.; Périchon, J., *Chem. Commun.*, **2007**, 3667
113. Kaur, G.; Fang, H.; Gao, X.; Li, H.; Wang, B., *Tetrahedron*, **2006**, 62, 2583
114. Kameta, N.; Hiratan, K., *Chem. Lett.*, **2006**, 35, 536
115. Tan, W.; Zhang, D.; Zhu, D., *Bioorg. Med. Chem. Lett.*, **2007**, 17, 2629
116. Clapham, K. M.; Batsanov, A. S.; Bryce, M. R.; Tarbit, B., *Org. Biomol.*

- Chem., **2009**, 7, 2155
117. Kitamura, Y.; Sakurai, A.; Udzu, T.; Maegawa, T.; Monguchi, Y.; Sajiki, H., *Tetrahedron*, **2007**, 63, 10596
118. Primas, N.; Bouillon, A.; Lancelot, J.-C.; Rault, S., *Tetrahedron*, **2009**, 65, 6348
119. Hutchinson, I.; Stevens, M. F. G., *Org. Biomol. Chem.*, **2007**, 5, 114
120. Sienkowska, M. J.; Farrar, J. M.; Zhang, F.; Kusuma, S.; Heiney, P. A.; Kaszynski, P., *J. Mater. Chem.*, **2007**, 17, 1399
121. Michels, J. J.; O'Connell, M. J.; Taylor, P. N.; Wilson, J. S.; Cacialli, F.; Anderson, H. L., *Chem. Eur. J.*, **2003**, 9, 6167
122. Deng, H.; Jung, J.-K.; Liu, T.; Kuntz, K. W.; Snapper, M. L.; Hoveyda, A. H., *J. Am. Chem. Soc.*, **2003**, 125, 9032
123. Nambo, M.; Noyori, R.; Itami, K., *J. Am. Chem. Soc.*, **2007**, 129, 8080
124. Hungerford, N. L.; McKinney, A. R.; Stenhouse, A. M.; McLeod, M. D., *Org. Biomol. Chem.* **2006**, 4, 3951

Chapter 4

Molecular Complexation of Ivy Saponins with Some Drugs and Biologically Active Substances

L.A. Yakovishin¹, V.I. Grishkovets², G. Schroeder³
and N.I. Borisenko⁴

¹*Sevastopol National Technical University, Universitetskaya Str., 33, Sevastopol, 99053, Crimea, Ukraine*

²*V.I. Vernadsky Taurida National University, Vernadsky Ave., 4, Simferopol, 95007, Crimea, Ukraine*

³*Adam Mickiewicz University, Faculty of Chemistry; Grunwaldzka 6, 60-780 Poznań, Poland*

⁴*Ecological and Analytical Center, Southern Federal University, Zorge Str., 7, Rostov-on-Don, 344090, Russia*

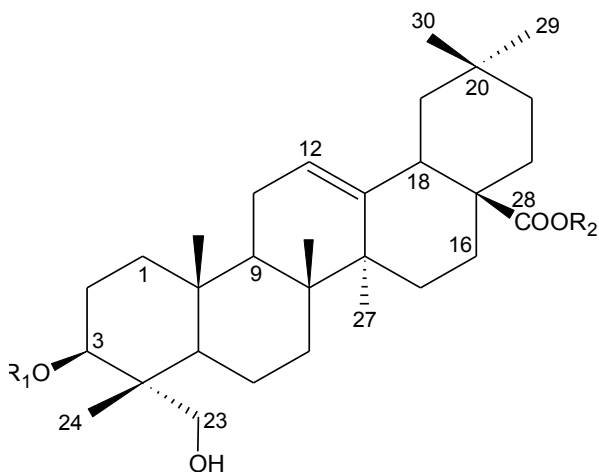
Today the molecular complexation of saponins and different biologically active molecules is widely studied. The great interest to these supramolecular products is first and foremost caused by the possibility of new drugs composition by means of drug dose reduction, bioavailability and decomposition resistance increasement, the action prolongation, and expansion of biological activity spectrum of drugs (pharmacones) [1, 2].

This approach has been examined mainly for glycyrrhizic acid (3-O- β -D-glucopyranosyl-(1 \rightarrow 2)-O- β -D-glucopyranoside of glycyrrhetic acid), the main triterpene glycoside of the licorice roots. Molecular complexes of glycyrrhizic acid with pyrimidine derivatives, nonsteroid anti-inflammatory drugs, prostaglandins, cardioactive and psychotropic drugs were prepared. Besides, the complexes of acanthophylloside B isolated from *Acanthophyllum gypsophyloides* roots were prepared with prostaglandins [1, 2].

Recently, triterpene glycosides α -hederin (glycoside 1) and hederasaponin C (glycoside 2) have been suggested as prospective molecular carrier of biologically active substances and medicines (Fig. 1) [3]. Glycoside 1 is 3-O- α -L-rhamnopyranosyl-(1 \rightarrow 2)-O- α -L-arabinopyranoside of hederagenin, and 2 is 3-O- α -L-rhamnopyranosyl-(1 \rightarrow 2)-O- α -L-arabinopyranosyl-28-O- α -L-rhamnopyranosyl-(1 \rightarrow 4)-O- β -D-glucopyranosyl-(1 \rightarrow 6)-O- β -D-

glucopyranoside of hederagenin. Glycosides 1 and 2 are one of the most widespread saponins of the plants from family Araliaceae Juss. They were discovered in different species of genus *Hedera* (Fig. 2) and *Kalopanax*, in *Aralia elata* and *Acanthopanax sieboldianus* [4–6]. Glycoside 1 is also discovered in *Polyscias dichroostachya* [4], and 2 – in *Schefflera octophylla* [7].

Triterpene glycosides 1 and 2 are the components of the cough medicines *Hedelix* [8, 9], *Prospan* [4, 8, 10], *Pektolvan Hedera helix* [11] and others. These medicines contain extract of *Hedera helix* L. leaves (Fig. 2). *Hedera helix* leaves have been used as cough medicine European ethnoscience for several centuries [4].



Glycoside 1: $R_1 = Rhap\alpha-(1\rightarrow2)-Arap\alpha\rightarrow$, $R_2 = H$;
 glycoside 2: $R_1 = Rhap\alpha-(1\rightarrow2)-Arap\alpha\rightarrow$, $R_2 = \leftarrow\beta Glcp-(6\leftarrow 1)-\beta Glcp-(4\leftarrow 1)-\alpha Rhap$;
 glycoside 3: $R_1 = Glcp\beta-(1\rightarrow2)-Glcp\beta\rightarrow$, $R_2 = H$

Figure 1. IVY Saponins

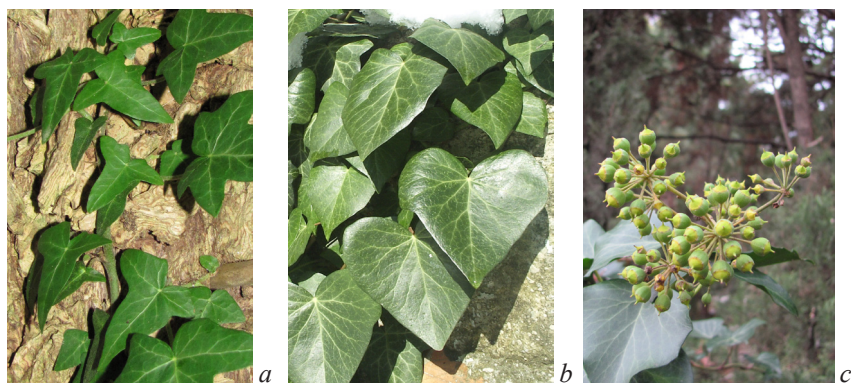


Figure 2. *Hedera helix* L. leaves (a) and *Hedera taurica* Carr: leaves (b) and fruits (c)

1. Molecular complexes of triterpene glycosides with proteinogenous amino acids and cholesterol

1.1. Complexes with cholesterol.

Complexation of steroid saponin digitonin and cholesterol (Fig. 3) was discovered in 1909 by Windaus [4]. Ability to form complexes with sterols is a characteristic feature of saponins [4, 5, 12]. Binding to them alters the permeability of all membranes, which is responsible for some of the biological activity of saponins. This effect was previously found for glycoside 1 [12], however, in [13] it was shown that it does not form complexes with cholesterol.

Complex formation of glycoside 1 and cholesterol was discovered with the help of IR spectroscopy [14]. During the complex IR spectrum analysis the changes in frequency of CO-group absorption and in absorption lines of cholesterol OH-groups and glycoside OH-groups were observed. Evidently, these changes are caused by the formation of intermolecular hydrogenous bonds between cholesterol and glycoside molecules.

Glycosides 1 and 2 complexation with cholesterol was also studied using electrospray mass spectrometry (ESI-MS) [15, 16]. In the mass spectrum the peak of protonated complex of glycoside 1 and cholesterol $[2M(1)+H+2M(\text{cholesterol})]^+$ (m/z 2274.445) was found. In positive-ion and negative-ion modes the mutual peaks of glycoside 2 and cholesterol were not observed.

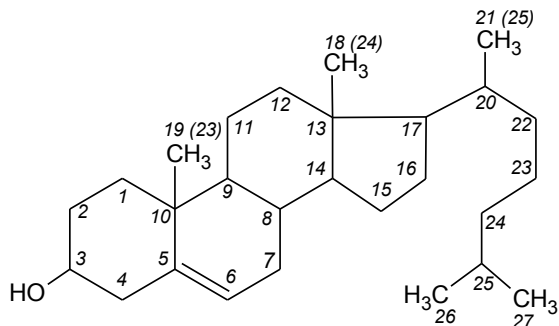


Figure 3. Cholesterol

To confirm the conclusions about the complexation of glycosides 1 and 2 with cholesterol, their toxicity to the fish *Barbus fezzonae* (Cyprinidae) was examined. The results from the study of glycosides 1 and 2, and their mixtures with cholesterol ichthyotoxicity (Table 1) confirmed the conclusions obtained from mass spectrometry.

Table 1. Effect of glycosides 1 and 2, and their complexes with cholesterol on *Barbus fezzonae*

Compound	Exposure time $t_{LD_{100}}$ until death, min
1	6.5±0.3
2	25.2±0.4
1-cholesterol	11.5±0.4
2-cholesterol	23.8±0.3

It was found that adding cholesterol to glycoside 1 and 3-O-β-D-glucopyranosyl-(1→2)-O-β-D-glucopyranoside of hederagenin (glycoside 3, Fig. 1) solutions reduces substantially their toxicity in comparison with glycoside 2 for the mollusks *Planorbis corneus*, *Planorbis corneus* var. *rubra* и *Melanoides tuberculata* (Table 2) [17]. It is probably caused by the formation of more stable complexes. Glycoside 3 is found in fruits of *Hedera helix* [18] and *Hedera colchica* [19], and fruits and leaves of *Hedera taurica* [20, 21].

Table 2. Molluscicidal activity of glycosides 1–3 and their complexes with cholesterol

Compound	LD_{100} , mol/l	Exposure time $t_{LD_{100}}$ until death, min		
		<i>Planorbis corneus</i>	<i>Planorbis corneus</i> var. <i>rubra</i>	<i>Melanoides tuberculata</i>
1	10^{-2}	3.3±0.2	3.7±0.3	2.0±0.2
2	10^{-2}	6.5±0.4	7.0±0.3	6.0±0.3
3	10^{-2}	4.5±0.3	4.7±0.1	2.0±0.1
1–cholesterol	10^{-2}	5.0±0.1	4.6±0.1	3.5±0.2
2–cholesterol	10^{-2}	7.9±0.2	8.3±0.4	7.2±0.1
3–cholesterol	10^{-2}	6.9±0.4	7.0±0.2	3.3±0.2

While testing glycosides effect on fish *Brachydanio rerio* it was shown [22] that adding cholesterol to incubatory mixture reduces glycosides 1 and 3 activity for 2 times, and glycoside 2 activity to a lesser degree (Table 3). It can be explained by the lack of stable complexation between them.

The effect of triterpene glycosides 1 and 3, and of their molecular complexes with cholesterol on fish *Brachydanio albolineatus* and *Poecilia reticulata* was examined (Table 4) [14]. The study of ichthyotoxicity of cholesterol mixtures with glycosides 1 and 3 also confirms complexation between them, as for the

complexes $t_{LD_{100}}$ turned to be greater than for the pure glycosides.

Table 3. Ichthyotoxicity effect of glycosides 1–3 and their complexes on *Brachydanio rerio*

Compound	LD_{100} , mol/l	Exposure time $t_{LD_{100}}$ until death, min
1	10^{-2}	3.0±0.3
2	10^{-2}	11.5±0.4
3	10^{-2}	2.5±0.2
1–cholesterol	10^{-2}	5.0±0.2
2–cholesterol	10^{-2}	15.0±0.2
3–cholesterol	10^{-2}	6.0±0.2
1–Gly	10^{-4}	12.0±0.3
1–Val	10^{-4}	Within 60 min is not toxic
1–Ala	10^{-4}	10.0±0.4

Obviously, cholesterol binds better to monodesmosidic triterpene glycosides (1 and 3) with a carbohydrate chain on C-3 and a free C-17 COOH group of aglycone (hederagenin). And it does not form stable complexes with bidesmosidic glycosides (glycoside 2).

Table 4. Ichthyotoxicity of glycosides 1–3 and their complexes

Compound	LD_{100} , mol/l	Exposure time $t_{LD_{100}}$ until death, min	
		<i>Brachydanio albolineatus</i>	<i>Poecilia reticulata</i>
1	10^{-2}	4.1±0.2	6.2±0.3
2	10^{-2}	12.1±0.2	14.7±0.3
3	10^{-2}	3,1±0.3	5.7±0.2
1-cholesterol	10^{-2}	6.2±0.2	7.3±0.2
2-cholesterol	10^{-2}	14.0±0.2	17.5±0.5
3-cholesterol	10^{-2}	7.3±0.1	6.7±0.3
1-Gly	10^{-4}	19.0±0.4	20.2±0.3
1-Val	10^{-4}	Within 60 min is not toxic	Within 60 min is not toxic
1-Ala	10^{-4}	11.5±0.3	19.1±0.4

1.2. Complexes of glycosides and proteinogenous amino acids

1.2.1. Complexes with aliphatic amino acids.

The complexes of glycoside 1 with proteinogenous amino acids glycine (Gly), L-alanine (Ala) and L-valine (Val) were prepared (Fig. 4) [3, 23]. Complexation was confirmed using IR spectrometry. The complexation occurs through amino acid zwitterion and COO⁻-group of glycoside aglycone. The effect of the complexes prepared on *Avena sativa* L. seeds germination was examined. Analysis of germination activity of glycoside 1 and its complexes showed complexes toxicity reduction in comparison with pure glycoside. Possibly, it is caused by the partial involvement of glycoside carboxyl group into interaction with amino acids, as the high activity of the pure glycoside is caused by the presence of free COOH-group in its aglycone part.

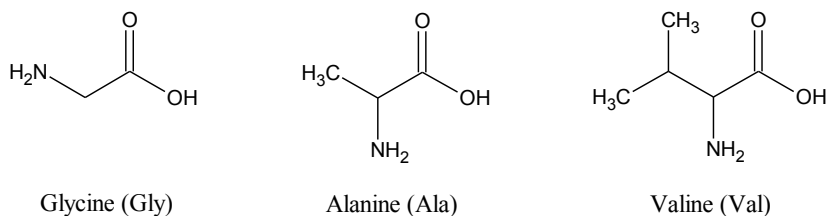


Figure 4. Aliphatic amino acids

Ichthyotoxic and molluscicidal activities of glycoside 1 complexes with Gly, Ala and Val were studied before (Table 3, 4). For the fish *Brachydanio rerio* (Cyprinidae) glycoside 1 complexes with Gly and Ala proved to be more toxic than the pure glycoside [22]. The complexes with Gly and Ala turned to be less toxic for *Brachydanio albolineatus* than for *Brachydanio rerio* [14]. The complex of glycoside 1 and Val did not effect on *Brachydanio albolineatus* [14], *Brachydanio rerio* [22] and *Poecilia reticulata* (Poeciliidae) [14] for 60 min. Compared with *Brachydanio albolineatus* and *Brachydanio rerio*, *Poecilia reticulata* turned to be more resistant to complexes of glycoside 1 with Gly and Ala [14].

Molecular complexes of glycoside 1 with Gly and Ala proved to be more toxic for the mollusks *Planorbis corneus*, *Planorbis corneus* var. *rubra* and *Melanoides tuberculata* than the pure glycoside [17]. The complex with Ala is more toxic. The complex of glycoside 1 and Val did not show up molluscicidal activity for 60 min.

1.2.2. Complexes of glycosides and hydrophilic amino acids.

Molecular complexation of glycoside 1 and *L*-asparagine (Asn) and *D,L*-aspartic acid (Asp) (Fig. 5) was examined using IR spectroscopy [24]. Complexation of Asn and glycoside occurs through interaction of ionized carboxyl group of hederagenin aglycone and NH_3^+ -group amino acid zwitterion form. Contribution of Asn amide group to additional H-bonds formation with OH-groups of glycoside in the complex. The complex of Asp and glycoside occurs through aglycone COO^- -group and amino acid NH_3^+ -group. This is confirmed by the respective amino acid line II and carboxylate shift in IR spectrum.

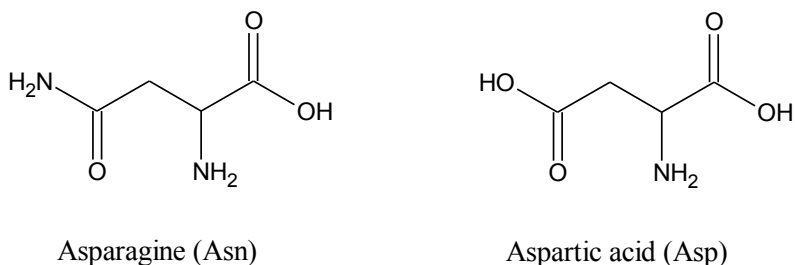


Figure 5. Hydrophilic amino acids

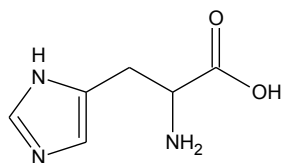
1.2.3. Complexes of glycosides and aromatic amino acids.

Molecular complexes of glycosides 1 and 2 with *L*-tryptophan (Trp) in aqueous solution were prepared (Fig. 6) [25]. As the glycosides 1 and 2 concentration increases at constant Trp concentration, the optical density of their solutions increases (hyperchromic effect). Besides, for the range of solutions containing glycoside 2 and Trp a low bathochromic shift was shown. Complexes composition was defined by the method of isomolar series. Glycosides form complexes with a 1:1 molar ratio.

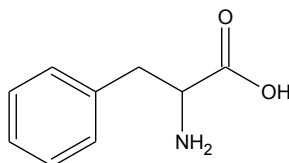
The formation of complexes with analogical composition between Trp and glycosides 1 and 2 has recently been confirmed using electrospray-ionization mass spectrometry [26]. The glycoside 1 complex is more stable. Glycoside 1 and Trp also form unstable complexes with a 3:1 and 4:2 molar ratio, for which ions $[3M^1+M^{\text{Trp}}+2H]^{2+}$ and $[4M^1+2M^{\text{Trp}}+2H]^{2+}$ were observed in mass spectrum.

Using the method of isomolar series it was established that in aqueous solutions *L*-phenylalanine (Phe) (Fig. 6) forms 1:1 complexes with glycosides 1 and 2 [27]. Intermolecular interaction results in hyperchromic effect. It was supposed that NH_3^+ -group contributes to binding to glycosides. The effect of glycosides 1 and 2 complexes with Phe on *Avena sativa* L. seeds germination was examined. The complexes are less toxic than pure glycosides. They increase seeds germination and influence the germination of their roots and sprouts.

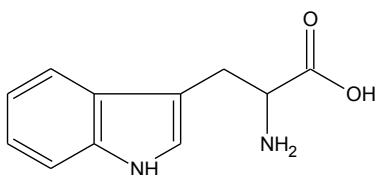
Complexation of Phe with glycosides 1 and 2 was also studied using electrospray-ionization mass spectrometry [26]. In mass spectrum the peaks of ions $[M^1+M^{\text{Phe}}-H]^-$, $[M^1+M^{\text{Phe}}+H]^+$ and $[M^2+M^{\text{Phe}}-H]^-$ were found. It indicates the composition of complexes is 1:1. As in case of glycoside 1 and Trp low-intensity peaks of protonated molecules of the complexes with more complicated composition ($[4M^1+2M^{\text{Phe}}+2H]^{2+}$, $[5M^1+M^{\text{Phe}}+2H]^+$ and $[5M^1+2M^{\text{Phe}}+2H]^{2+}$) were found in the mixtures of glycoside 1 and Phe.



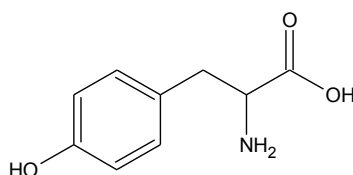
Histidine (His)



Phenylalanine (Phe)



Tryptophan (Trp)



Tyrosine (Tyr)

Figure 6. Aromatic amino acids

Amino acids *L*-tyrosine (Tyr) and *L*-histidine (His) (Fig. 6), like Trp and Phe form mainly molecular complexes with a 1:1 molar ratio. This was confirmed by the method of electrospray-ionization mass spectrometry [26]. In the mass spectrum the peak $[M^2+M^{\text{His}}-H]^-$ (m/z 1374.7) was observed. Its intensity was 28.16%. This value is the greatest one among peak intensities of complexes, which were previously found for glycosides 1 and 2 with aromatic amino acid [26].

Complexation of glycoside 1 and His was confirmed by IR spectroscopy [24]. It was shown that in their intermolecular complex the interaction of zwitterion form of amino acid and COO⁻-group of glycoside was observed.

2. Molecular complexes of triterpene glycosides with drugs

2.1. Complexes with sildenafil

Citrate of sildenafil (Viagra) (Fig. 7) is one of the most widespread drugs for treating erectile-dysfunction today [28]. Molecular complex of glycoside 1 with sildenafil (in the basic form) was prepared (Fig. 7) [29]. The result of intermolecular interaction in the IR spectrum of complex is the shift of absorption line of glycoside 1 and sildenafil CO-group.

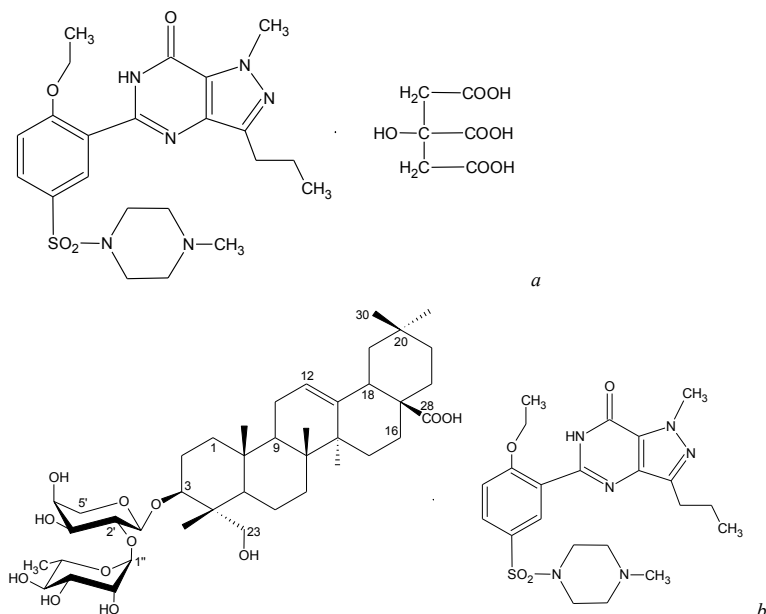


Figure 7. Sildenafil (a) and molecular complex of glycoside 1 with sildenafil (b)

In the complex spectrum analysis the decrement of valence oscillations frequencies of OH- and NH-groups, the increasement of amide line II frequency and change of $\nu_{\text{as}}(\text{SO})$ and $\nu_{\text{s}}(\text{SO})$ absorption frequencies were observed. This indicates the possible association of molecules at the expense of intermolecular H-bonds formation occurring through glycoside OH-groups, and sildenafil NH- and SO-groups as well.

With the help of intracellular diversion the effect of citrate of sildenafil and its complexes with glycosides 1 and 2 on electrical activity non-identified neurons of *Helix albescens* Rossm. visceral ganglion was examined [30]. Opposite neurotropic effects of citrate of sildenafil and its complexes were demonstrated. Citrate of sildenafil application resulted in neurons activation, while glycoside complex on neurons soma provoked their activity depression.

Previously it was shown that bidesmosidic triterpene glycosides did not effect on neurons electrical potentials [31, 32]. However, it is proved that citrate of sildenafil binding to bidesmosidic glycoside 2 results in development of neurotropic effects manifesting in changes of neurons electrophysiological rate. This effect is not characteristic for the use of pure citrate of sildenafil and glycoside 2 [30].

2.2. Complexes with caffeine

The complexation of glycosides 1 and 2 with caffeine (Fig. 8) in aqueous solutions was confirmed by UV spectroscopy [33, 34]. If glycosides concentration increases at constant caffeine concentration (0.50×10^{-4} M), the increase of solutions optical density is observed (hyperchromic effect) (see Fig. 9). While solutions λ_{\max} decreases a little (hypsochromic shift). For the glycoside 1 a bit greater shift was observed. It was also recently reported that a hyperchromic effect occurred upon formation of the clathrate complex of β -cyclodextrin with caffeine [35].

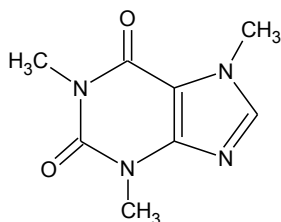


Figure 8. Caffeine

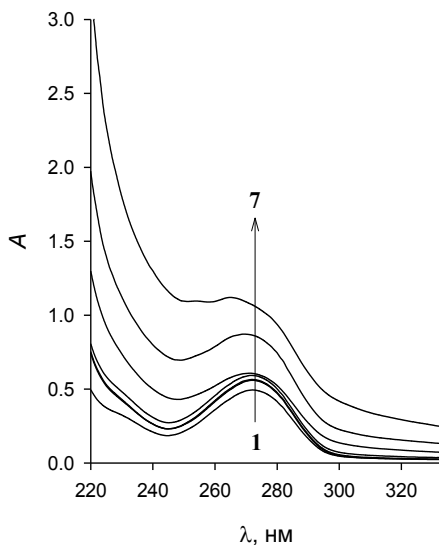


Figure 9. UV spectrum of caffeine aqueous solutions (0.50×10^{-4} M = const) with different concentrations of glycoside 1: 0 M (1), 0.25×10^{-4} M (2), 0.50×10^{-4} M (3), 10^{-4} M (4), 0.25×10^{-3} M (5), 0.50×10^{-3} M (6) and 10^{-3} M (7)

The complexes composition was defined by the method of isomolar series and of molar ratios (saturation method). It was established that glycosides 1 and 2 form complexes with caffeine in a 2:1 molar ratio (Fig. 10). The same ratio was found for nanostructures of glycyrrhizic acid and some pharmacocones [1, 2].

It was supposed that the complexation leads to disruption the self-association of caffeine. Clathrate complex between glycosides and caffeine formed by hydrophobic interactions of the glycosides aglycon with the heterocyclic system and methyls of caffeine. The formation of intermolecular H-bonds involving the pyrimidine C=O and the imidazole N-atom of caffeine and the OH groups of the glycosides monosaccharide units was also possible.

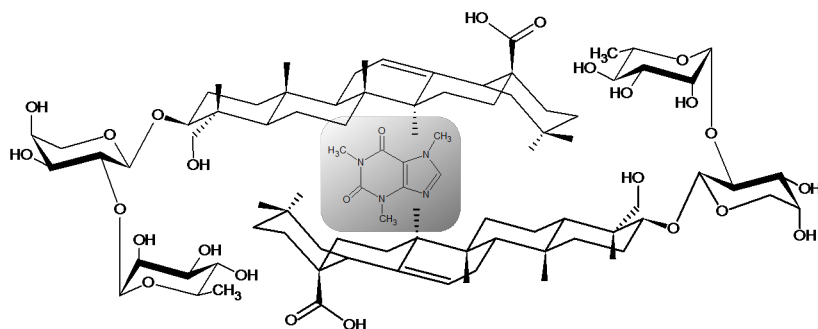


Figure 10. Clathrate structure of glycoside 1 with caffeine

The toxicity of glycoside 1, caffeine, and their complex for mollusks *Planorbis corneus* (*Planorbidae*) and of glycoside 2, caffeine, and their complex for fish *Poecilia reticulata* (*Poeciliidae*) was studied [33, 34]. The complex of glycoside 1 turned to be less toxic with the pure glycoside and more toxic than caffeine. The biological activity of caffeine complexed with glycoside 2 was reduced.

It was shown by electrospray-ionization mass spectrometry that big aggregates of caffeine (trimers and hexamers) can not occupy the space formed by two molecules of glycosides 1 and 2 [36], and complexation does not occur in this case.

The effect of triterpene glycosides 1 and 2 in their complexes with caffeine on the electrical activity of the grape snail visceral ganglion non-identified neurons was studied (Fig. 11) [37]. The complexes activated electrophysiological neurons rate, and they had an opposite kinetics of entering and outgoing currents. Thus, while glycoside 1 complex activity the entering currents were increasing and the outgoing ones decreased, and while using glycoside 2 complex both entering and

outgoing transmembranous ionic currents decreased. Previously it was found that bidesmosidic triterpene glycosides do not effect on the neurons background activity [31, 32]. Thus, complexation with caffeine activates neurotropic effect of bidesmosidic glycoside 2.

2.3. Complexes with paracetamol

The molecular complexation of paracetamol (*para*-acetaminophenol) (Fig. 12) with glycosides 1 and 2 was studied by electrospray-ionization mass spectrometry [38]. In mass spectrum of mixture of glycoside 1 with paracetamol a low intensity peak $[M^1+M^{Par}-H]^-$ (m/z 900) was observed, and of mixture of glycoside 2 with paracetamol there were the peaks $[M^2+M^{Par}-H]^-$ (m/z 1371) and $[M^2+M^{Par}+H]^+$ (m/z 1372). It is noteworthy that the intensities for peaks of the complexes $[M^{1(2)}+M^{Par}-H]^-$ differed by 1.7 times. In such a way it was established that glycosides form unstable complexes in a 1:1 molar ratio with paracetamol. Glycoside 2 complex turned to be a bit more stable. Supramolecular structures are formed by means of H-bonds through paracetamol O–H, N–H and C=O groups and O–H-groups of glycosides monosaccharide units. The greater stability of the complex of glycoside 2 can be explained by the presence in its structure of the trisaccharide chain on C-28 of aglycone (hederagenin).

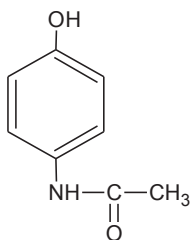


Figure 12. Paracetamol

2.4. Complexes with antibiotic laevomycetin (chloramphenicol)

It was shown that glycosides 1 and 2 form complexes with antibiotic laevomycetin (chloramphenicol) (Fig. 13) in a 1:1 molar ratio [39]. In mass spectrum (electrospray-ionization) the complexes peaks $[M^1+M^{LaeV}-H]^-$ (m/z 1072), $[M^2+M^{LaeV}-H]^-$ (m/z 1544) and $[M^2+M^{LaeV}+H]^+$ (m/z 1545) were observed. Molecular complex of laevomycetin with monodesmosidic glycoside 1 turned to be more stable one as the peaks of glycoside 2 complexes have a low intensity. Previously the complex with laevomycetin was prepared for triterpene glycosides with glycyrrhizic acid only [40].

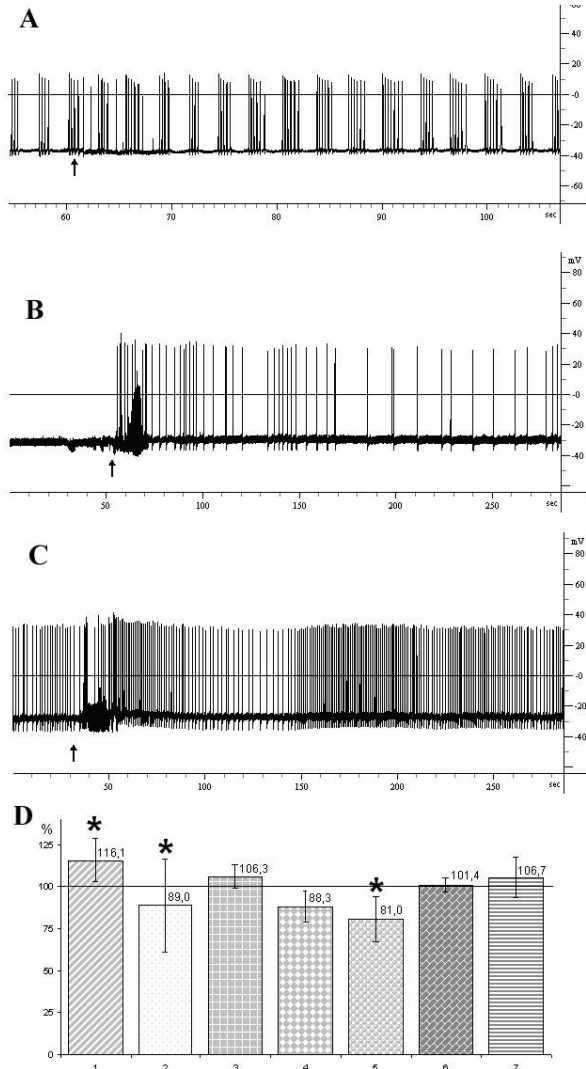


Figure 11. Effects of glycoside 2 complex with caffeine on pacemaker activity (A), silent neuron (B), monomodal activity (C). D – Average data (%), $n = 21$. Asterisks indicate the cases of reliable differences from background indexes. 1 – Frequency of impulse generation; 2 – interimpulse intervals; 3 – duration of action potential; 4 – total entering currents; 5 – total outgoing currents; 6 – amplitude of action potential; 7 – membranous potential.

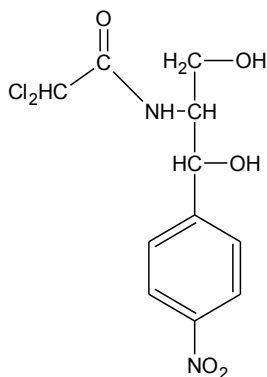


Figure 13. *Laevomycesin (chloramphenicol)*

2.5. Complexes with streptocid (sulfanilamide)

Complexation of streptocid (sulfanilamide) (Fig. 14) with glycosides 1 and 2 was studied by electrospray-ionization mass spectrometry [39]. The complex of glycoside 1 proved to be less stable as its peak $[M^1+M^{Str}-H]^-$ (m/z 922) is of low intensity. For the glycoside 2 the ions $[M^2+M^{Str}-H]^-$ (m/z 1394), $[2M^2+M^{Str}+K-3H]^{2-}$ (m/z 1325), and $[2M^2+2M^{Str}+K+H_2O-3H]^{2-}$ (m/z 1423) were found in mass spectrum. The first one dominates among them. It was shown that the free carboxyl group of glycoside 1 does not take part on complexation. Hydroxyl group of monosaccharide units, and NH_2 - and SO_2 -groups of streptocid are involved into intermolecular interactions. Molecular complex of glycoside 2 with streptocid turned to be more stable compared with the previously prepared complexes of this glycoside with paracetamol and laevomycesin [38, 39].

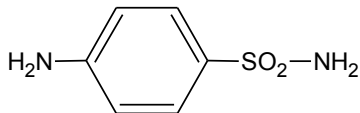


Figure 14. *Streptocid (sulfanilamide)*

References

1. Tolstikov G.A., Baltina L.A., Grankina V.P., Kondratenko R.M., Tolstikova T.G., Licorice: biodiversity, chemistry and application in medicine. – Novosibirsk: Geo, 2007. – P. 311
2. Tolstikova T.G., Tolstikov A.G., Tolstikov G.A., On the way to low-

- dose drugs, *Vestn. Ross. Acad. Nauk.* – 2007. – Vol. 77, No 10. – P. 867–874
3. Yakovishin L.A., Pugovkin A.M., Markova P.A., Formation of complex triterpene glycoside a-hederin with aliphatic amino acids of proteins, *Materials of the Second Intern. conf. “Forest bioactive resources”* (21–23 Sept. 2004, Khabarovsk, Russia). – Khabarovsk, 2004. – P. 219–222
 4. Hostettmann K., Marston A., Saponins. – Cambridge: Cambridge University Press, 1995. – P. 548
 5. Dekanosidze G.E., Chirva V.Ya., Sergienko T.V., Biological role, distribution, and chemical structure of triterpene glycosides. – Tbilisi: Metsniereba, 1984. – P. 349
 6. Grishkovets V.I., Chirva V.Ya., Kachala V.V., Shashkov A.S., Triterpene glycosides of Araliaceae: the structures of isolated triterpene glycosides, *Tr. Nikit. Bot. Sada.* – 2007. – Vol. 128. – P. 90–102
 7. Maeda C., Ohtani K., Kasai R., Yamasaki K., Duc N.M., Nham N.T., Cu G.K.Q. Oleanane and ursane glycosides from *Shefflera octophylla*, *Phytochemistry.* – 1994. – Vol. 37, № 4. – P. 1131–1137
 8. Zuzuk B.M., Kutsik R.V., Zuzuk L.I., Ivy creeping *Hedera helix L.*, *Provizor.* – 2003. – No 12. – P. 13–14
 9. Yakovishin L.A., Grishkovets V.I., Triterpene glycosides of the medicinal preparation Hedelix[®], *Chem. Nat. Comp.* – 2003. – Vol. 39, No. 5. – P. 508–509
 10. Yakovishin L.A., Vozhzhova M.A., Kuznetsova A.L., Grishkovets V.I., Study of triterpene glycosides of the drug “prospan[®]”, *J. Org. Pharm. Chem.* – 2005. – Vol. 3, No 1 (9). – P. 57–59
 11. Yakovishin L.A., Grishkovets V.I., Korzh E.N., Triterpene glycosides of the medicinal preparation “Pectolvan *Hedera helix*”, *Pharm. J.* – 2010. – No 3. – P. 56–60
 12. Anisimov M.M., Chirva V.Ya., About of the biological role of triterpene glycosides, *Usp. Sovrem. Biol.* – 1980. – Vol. 6, No 3. – P. 351–364
 13. *Chemical Analysis of Medicinal Plants*, N.I. Grinkevich and L.N. Safronich (eds.), – Moscow: Vysshaya Shkola, 1983. – P. 50
 14. Yakovishin L.A., Rubinson M.A., Korzh E.N., Influence of the triterpene glycosides and their molecule complexes on *Brachydanio albolineatus*, *Poecilia reticulata* and *Chironomus plumosus*, *Vestn. Zapor. Nat. Univ., Biol. Sci.* – 2007. – No. 1. – P. 223–228
 15. Yakovishin L.A., Borisenko N.I., Rudnev M.I., Vetrova E.V., Grishkovets V.I., Self-association and complexation of triterpene glycosides and cholesterol, *Chem. Nat. Comp.* – 2010. – Vol. 46, No

1. – P. 49–52
16. Lekar A.V., Yakovishin L.A., Vetrova E.V., Rudnev M.I., Borisenko N.I., Mass spectrometry of complexes formation and self-association between triterpenoid saponins and cholesterol, *Mass-spektrom.* – 2010. – Vol. 7, No 3. – P. 213–216
17. Yakovishin L.A., Ertahova V.A., Bazyura E.A., Influence of the triterpene glycosides and their complexes on mollusks, *Ukr. Bioorg. Acta.* – 2006. – Vol. 4, No 2. – P. 22–26
18. Hostettmann K., Saponins with molluscicidal activity from *Hedera helix* L., *Helv. Chim. Acta.* – 1980. – Vol. 63, No 60. – P. 606–609
19. Mshvildadze V., Elias R., Faure R., Debrauwer L., Dekanosidze G., Kemertelidze E., Balansard G., Triterpenoid saponins from berries of *Hedera colchica*, *Chem. Pharm. Bull.* – 2001. – Vol. 49, No 6. – P. 752–754
20. Loloiko A.A., Grishkovets V.I., Shashkov A.S., Chirva V.Ya., Triterpene glycosides of *Hedera taurica* III. Structures of hederosides A₃, B, E₂ and F from the berries of Crimean ivy, *Chem. Nat. Comp.* – 1988. – Vol. 24, No 5. – P. 614–618
21. Grishkovets V.I., Tolkacheva N.V., Shashkov A.S., Chirva V.Ya., Triterpene glycosies of *Hedera taurica* VIII. Taurosides F₁, F₂, and F₃ and a triterpenoid sulfate, *Chem. Nat. Comp.* – 1991. – Vol. 27, No 6. – P. 760–761
22. Yakovishin L.A., Bazyura E.A., Ertahova V.A., Korzh E.N., Rubinson M.A., Influence of the triterpene glycosides and their complexes with cholesterol and amino acids on *Brachydanio rerio*, *Prirod. Almanah, ser. Biol. Sci.* – 2006. – No. 8. – P. 329–335
23. Yakovishin L.A., Rubinson M.A., Molecular complexes of the triterpene glycoside α -hederin with aliphatic proteinogenous amino acids, *Ukr. Bioorg. Acta.* – 2009. – Vol. 7, No 1. – P. 32–35
24. Yakovishin L.A., Grishkovets V.I., Rubinson M.A., Korzh E.N., The complex's formation of triterpene glycoside α -hederin with hydrophilic proteinogenous amino acids, *Sci. Not. V.I. Vernadsky Taurida Nat. Univ., ser. Biol. Chem.* – 2009. – Vol. 22, No 1. – P. 208–213
25. Yakovishin L.A., Grishkovets V.I., Epishina N.V., Kurtametov I.S., Molecular complexation of the triterpene glycosides with tryptophan in water solutions, *Sci. Not. V.I. Vernadsky Taurida Nat. Univ., ser. Biol. Chem.* – 2010. – Vol. 23, No 2. – P. 270–275
26. Vetrova E.V., Lekar A.V., Yakovishin L.A., Borisenko N.I., Mass spectrometry research of complexes of triterpene glycosides

- (hederosides) with amino acids, X Intern. workshop on magnetic resonance (spectroscopy, tomography and ecology) (2–7 Mar. 2010, Rostov-on-Don, Russia). – Rostov-on-Don, 2010. – P. 30
27. Yakovishin L.A., Grishkovets V.I., Sergienko U.I., Korzh E.N., Molecular complexation of triterpene glycosides with L-phenylalanine in water solutions, *Sci. Not. V.I. Vernadsky Taurida Nat. Univ., ser. Biol. Chem.* – 2010. – Vol. 23, No 3. – P. 255–261
 28. Drewes S.E., George J., Khan F., Recent findings on natural products with erectile-dysfunction activity, *Phytochemistry.* – 2003. – Vol. 62. – P. 1019–1025
 29. Yakovishin L.A., Rubinson M.A., Kuznetsova A.L., Grishkovets V.I., Korzh E.N., Molecule complex of triterpene glycoside α -hederine and sildenafil (viagra), *Sci. Not. V.I. Vernadsky Taurida Nat. Univ., ser. Biol. Chem.* – 2006. – Vol. 19, No 1. – P. 179–182
 30. Kolotilova O.I., Yakovishin L.A., Koreniuk I.I., Grishkovets V.I., Husainov D.R., Gamma T.V., Influence of viagra and complex triterpence glycosides with viagra on parameters of the electrical activity of neurons *Helix albescens*,/ *Sci. Not. V.I. Vernadsky Taurida Nat. Univ., ser. Biol. Chem.* – 2010. – Vol. 23, No 2. – P. 96–103
 31. Kostyuchenko O.V., Grishkovets V.I., Sobolev E.A., Korenyuk I.I., The effect of triterpene glycosides on electrical activity changes of identified mollusk neurons, *Chem. Nat. Comp.* – 2001. – Vol. 37, No 1. – P. 43–46
 32. Kostyuchenko O.V., Grishkovets V.I., Korenyuk I.I., The effect of the plant saponins on the mollusk neurons, *Fiziol. Zh.* – 2001. – Vol. 47, No 4. – P. 42–48
 33. Yakovishin L.A., Molecular complexation of the triterpene glycoside hederasaponin C and caffeine in aqueous solution, *Chem. Nat. Comp.* – 2010. – Vol. 46, No 5. – P. 746–749
 34. Yakovishin L.A., Grishkovets V.I., Korzh E.N., Supramolecular structures of triterpene glycosides with caffeine in aqueous solution, VIII Rus. conf. with intern. particip. “Chemistry and medicine”. – (6–8 Apr. 2010, Ufa, Russia). – Ufa, 2010. – P. 358–359
 35. Mejri M., BenSouissi A., Aroulmoji V., Rogé B., Hydration and self-association of caffeine molecules in aqueous solution: comparative effects of sucrose and β -cyclodextrin, *Spectrochim. Acta Part A.* – 2009. – Vol. 73, No 1. – P. 6–10
 36. Yakovishin L.A., Borisenko N.I., Vetrova E.V., Rudnev M.I., Grishkovets V.I., Mass-spectrometry research of self-association of caffeine and possibility of it complex’s formation with triterpene

- glycosides, *Chem. Plant Raw Material.* – 2010. – No 3. – P. 67–70
37. Kolotilova O.I., Yakovishin L.A., Koreniuk I.I., Grishkovets V.I., Katjushina O.V., Influence of molecular complex triterpence glycosides with caffeine on parameters of the electrical activity of neurons *Helix albescens*, *Sci. Not. V.I. Vernadsky Taurida Nat. Univ., ser. Biol. Chem.* – 2010. – Vol. 23, No 1. – P. 32–39
 38. Lekar A.V., Vetrova E.V., Borisenko N.I., Yakovishin L.A., Grishkovets V.I., Electrospray-ionization mass spectrometry of mixtures of triterpene glycosides with paracetamol, *J. Appl. Spectrosc.* – 2010. – Vol. 77, No. 5. – P. 615–618
 39. Vetrova E.V., Lekar A.V., Yakovishin L.A., Borisenko N.I., Research of complexes of plants triterpene glycosides from *Araliaceae* Juss. with medical products, X Intern. workshop on magnetic resonance (spectroscopy, tomography and ecology) (2–7 Mar. 2010, Rostov-on-Don, Russia). – Rostov-on-Don, 2010. – P. 29
 40. Kondratenko R.M., Baltina L.A., Mustafina S.R., Ismagilova A.F., Zarudii F.S., Davydova V.A., Bazekin G.V., Suleimanova G.F., Tolstikov G.A., Complex compounds of glycyrrhizic acid with antimicrobial drugs, *Pharm. Chem. J.* – 2003. – Vol. 37, No 9. – P. 485–488

Chapter 5

Dye-sensitized solar cells

Maciej Zalas

*Faculty of Chemistry, Adam Mickiewicz University, ul. Grunwaldzka 6,
60-780 Poznań, Poland*

1. Introduction

Each process taking place in the Universe is related to exchange or transformation of energy. The simplest description of the energy's nature, is the ability to perform work. Energy may occur in quite a few forms such as: thermal energy, chemical energy, nuclear energy, magnetic energy, radiant energy, electrical energy, etc. Every type of energy can be transformed into to another one, but unfortunately this process is always accompanied by dissipation of energy. The Sun is the main energy source for the Planet Earth, the energy supplied by the Sun to the Earth is really huge and has been estimated as around 3×10^{24} J per year [1] (approximately 1.7×10^{17} W per year). Only a small part of this energy, about 1×10^{14} W per year [2], is used by the flora for accumulation of chemical energy, in the process of photosynthesis. The energy stored by the flora is the primary source of energy for any other organism living on the Earth. Of course human civilization, from its early beginning, is based on the energy consumption, mainly as food (i.e. plants and/or animals), and fuels (firstly by burning plants, than coal, oil and finally natural gas). In the initial phase of civilization development, wood was the most important fuel, but increasing energy demand stimulated to exploration of other energy carriers such as peat, lignite or hard coal. At the turn of the 18th and 19th centuries, witnessing the industrial revolution, the use of coal sharply increased. Ever-increasing energy demand caused, at the end of the 19th century, the exploitation of oil and natural gas deposits, which are still the main energy sources for our civilization. The rapid development of the automotive industry, which is now the largest consumer of fuels in all sectors of global economy, began at that time. The most part of the 20th century was characterized by careless exploitation of the benefits afforded by the nature. Fuels overexploitation led to permanent devastation of virgin areas of Earth, by deforestation and/or by converting them to the oil fields or mines. Moreover the use of fossil fuels generates a lot of air pollutants, especially

carbon dioxide which, together with water vapour, is seen as the main cause of the greenhouse effect and probably has a great influence on global warming.

The beginning of the 1970s brought the first warning signal indicating that the Earth's natural wealth is not boundless and inexhaustible. This was a signal of global fuel crisis. Long-term problems with oil supply revealed that the energy dependent civilization can plunged into the chaos and destruction due to the lack of access to its sources. The depletion of the energy resources is estimated at the turn of 21st and 22nd century [3]. These facts led to a worldwide discussion about finding and utilization of some new energy sources that will reduce the civilization dependence on fossil fuels. In a short time a number of suggestions for generating energy from renewable conventional fuel-independent sources, have been made, indicating the following energy sources:

- Wind turbines
- Hydropower
- Wave and tidal power
- Solar thermal
- Solar cells
- Photocatalytic hydrogen generation
- Biomass conversion

Photovoltaic technology based on the use of solar energy is considered as the most promising one among all the renewable technologies listed above [3].

The global energy consumption rate in the year 2000 was estimated as about 1.3×10^{13} W. This consumption will increase more than two times, to approximately 2.8×10^{13} W, within the next 50 years. This enormous amount of energy is, however, about 10,000 times less than the energy reaching the Earth's surface from the Sun. That means that covering of the 0.1 % of the Earth's surface with solar cells working with an efficiency only of 10 % will satisfy the needs of our civilization for many years [1, 4]. However, to create such a large and efficient network of solar panels which will provide the humanity with the energy needed, is an extremely difficult challenge that requires many years of research and development of new technologies.

2. A bit of solar cell history

The beginning of the solar cell development stems from the discovery of the photoelectric effect by a French scientist Edmond Becquerel in 1839. He discovered that the photocurrent is observed when platinum electrode is coated with silver chloride or bromide and illuminated in aqueous solution [1, 5-7].

The first working solar cell was made by american inventor Charles Fritts in 1883. The cell used the junction formed by coating selenium semiconductor

with an ultrathin gold layer. The device he constructed was able to convert light to electricity with an efficiency less than 1 % [8].

In 1905 Albert Einstein published his description of the phenomenon of the photoelectric effect, and in 1921 he was awarded the Nobel Prize in Physics. The Royal Swedish Academy motivated the Prize for Einstein with this words: “For his services to Theoretical Physics, and especially for his discovery of the law of the photoelectric effect” [9].

The first silicon solar cell was patented by an American inventor R.S. Ohl in 1941 [10]. The energy conversion efficiency of this cell was less than 1 %, but its technology was a milestone in the solar cells development. Over the years the silicon solar cells performance has reached 25 % [11].

The commercial career of the solar cells was initiated by the Bell Telephone Laboratories in 1954, which introduced the first inorganic solar cell on the market [3, 5]. This device was based on a silicone homojunction and its efficiency was about 6 % at room temperature [3, 5, 12].

Before the global fuel crisis in the 1970s the main recipient and driving force of solar cells industry development was the space program of the National Aeronautic and Space Administration (NASA). The first solar cells powered artificial satellite launched from the Earth’s surface into space, was Vanguard I on March 17th, 1958. Vanguard I carried aloft a solar array, which was assembled of six panels and every panel consisted of a number of single crystal silicone cells with 10 % efficiency each. This array produced about 1 W of energy during the satellite mission for over six years [13].

The last 25 years of the 20th century and the first 10 years of the 21st century brought an explosion of popularity of the silicone solar cells. The demand for solar energy has grown rapidly, with growth rates between 20 and 25 % per every year [5]. Today the standard efficiency of commercial silicone solar cell is between 15 and 20 %. However, the silicone solar cells still account for less than 0.1 % of the total world energy production. The relatively high production costs of silicone photovoltaics, and the fact that their production process needs ultraclean materials, are the main reason that prevents their widespread use. Moreover, toxic chemicals are used in their manufacturing [1, 3-5].

The low-cost alternative for typical silicon solar cells was reported in 1991 by O’Regan and Grätzel [14]. These cells, called dye-sensitized solar cells (DSC’s, Grätzel cells), were based on low- or medium purity materials prepared in a standard laboratory conditions without using any hi-clean technologies. The efficiency of the first reported DSC’s was approximately 7.9 – 7.12 per cent, which is a much promising result. In 2010 Michael Grätzel was awarded “The 2010 Millennium Technology Grand Prize” for his ground-breaking research

that has led to the practical application of dye-sensitized solar cells [15].

3. How does DSC's works?

The typical dye-sensitized solar cell, see Fig. 1, consists of two plates of the conducting glass (tin oxide conducting glass – TCO, indium-tin oxide conducting glass – ITO, fluorine doped tin oxide conducting glass – FTO). The conducting side of the first glass plate (anode) is covered by a nanocrystalline porous semiconductor layer (mostly TiO_2 , rarely ZnO [4]) about $10\ \mu\text{m}$ thick. The porous layer is obtained from the paste containing semiconductor particles, polymer additives and water and/or organic solvent. This paste is spread on the conducting glass surface and an electrode is sintered at various temperatures (usually $723\ \text{K}$) to remove organic components and improve electrical connection between semiconductor particles. On the semiconductor surface a monolayer of organic charge-transfer dye is adsorbed, which plays a role of surface sensitizer. The conducting side of the other glass plate (anode) is covered with a thin layer of red-ox catalyst (mostly platinum films or carbon films, rarely conducting polymers or CoS [4]) and is called the “counter electrode”. The cell is assembled with both electrodes in sandwich-like construction, and the liquid electrolyte is injected between the electrodes. A large majority of the electrolytes consist of I^-/I_3^- red-ox couple solution in an organic solvent (for example, KI and I_2 solution in acetonitrile).

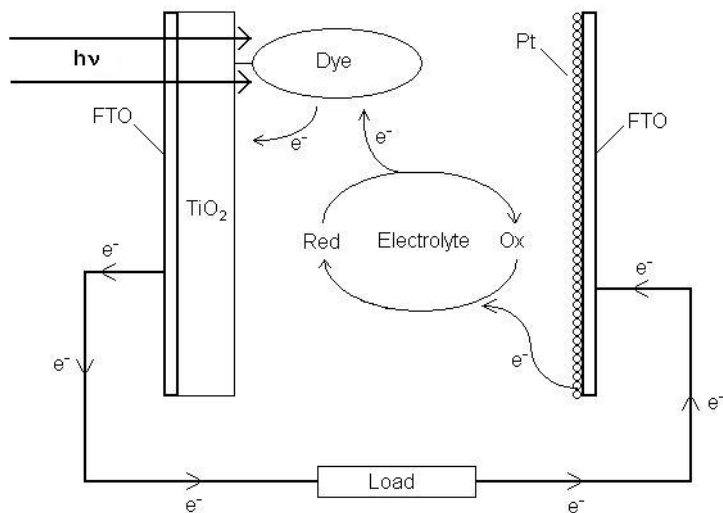
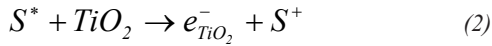


Figure 1. Schematic overview of a dye-sensitized solar cell

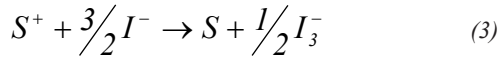
The first step of the dye-sensitized solar cell working cycle is the photoexcitation of the dye molecule (S). During this process the dye absorbs photons and in consequence its electrons are transferred from the ground to the excited state (S*) (see Eq. 1).



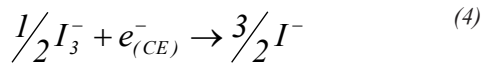
The excited electrons can be injected to the conducting band of the porous oxide layer, and the dye is going to get oxidized (S⁺) (eq. 2).



Electrons from the porous layer migrate to the FTO substrate, and are transferred to the counter electrode through the external circuit. The ground state of the dye is restored by electron transfer from the reduced form of the red-ox medium (I⁻) existing in the electrolyte, simultaneously the oxidized form of red-ox medium is formed (I₃⁻) (Eq. 3).



The I₃⁻ ions formed during the dye reduction process diffuse through the electrolyte to the counter electrode, where they are reduced by the electrons transferred from the electrode and the I⁻ ions are regenerated (Eq. 4), which is the final step of the DSC's working cycle. The above-described process continues as long as illumination is applied or until all parts of the cell are deactivated.



Unfortunately, the desirable electron transfer pathways are accompanied by some loss reactions, decreasing the cell efficiency. One of such process is direct recombination of the excited dye, related to a particular dye excited state lifetime. Another one is the use an electron injected into the semiconductor conduction band to regenerate the ground state of the dye molecule rather than transfer it to the external circuit. There is also the use of electron located in

the conduction band of the anode material to regenerate the reduced forms of the red-ox couple present in the electrolyte. These two last processes are called “internal short-circuit” of the cell.

Since the publication of the first paper about DSCs, much attention has been devoted to solutions of these problems and stopping unwanted processes taking place in the DSC’s mechanism of action. Ongoing research resulted in the discovery of thousands of new dyes, hundreds of electrolyte systems and countless mesoporous electrode materials, which had a more or less positive influence on the light harvesting and light-to-electricity conversion efficiency in the cells constructed. In this paper we present a general scheme of the solutions proposed in this field.

4. Anode semiconductors (on TiO_2 example)

O’Regan and Grätzel were not the inventors of the dye-sensitized solar cells. Research works on such systems were carried out much earlier, however, a fundamental problem was the use of semiconductors with a smooth surface to construct an anode [4]. These materials were characterized by a relatively low surface area and, in consequence, low dye adsorption, which resulted in low photoelectric conversion yields, not exceeding a value of 1 % [4]. Numerous attempts have been made to improve the efficiency of solar cells e.g. through the use of multilayer adsorption of the dye, but it also did not bring the desired results. The use of a mesoporous titania electrode, characterized by a high internal surface area, was a milestone for the DSCs development. It brought about 1000 times increase in the dye load, in the form of a monolayer on the surface of a porous electrode, in comparison with the result of non-porous semiconductor materials applied earlier. The increase in cell efficiency was almost by one order of magnitude, from less than 1 % to almost 8 % [14].

The typical way of preparing a porous anode for DSC is by sintering of TiO_2 nanoparticles prepared via hydrolysis of a titanium precursor [1,4,7,16]. Hydrolysis of titanium precursors can be carried out under different conditions of temperature, pH or at different water content. All of these conditions have a significant impact on the properties of the resulting titanium oxide, such as the shape or size of nanoparticles, crystallinity, porosity, etc. Hydrolysis in different pH conditions gives materials with different particle shapes and properties. Hore et. al found that DSC’s assembled using TiO_2 prepared in basic conditions has a better charge separation properties and, in consequence, shows lower recombination effect, moreover gives higher voltage, but exhibit lower dye adsorption in comparison of those TiO_2 prepared in acidic media [17]. The porosity of electrodes obtained can be easy controlled by addition of the specific

amount of polymer additives to the titania paste before sintering. Porosity determines the amount of adsorbed dye, so it should be as high as possible, but on the other hand too high porosity leads to poor interconnection between semiconductor particles, and in consequence to a decrease in the ability of anode to transfer electrons which is the main reason for reduction in the electron lifetime and increase in the negative recombination process [4].

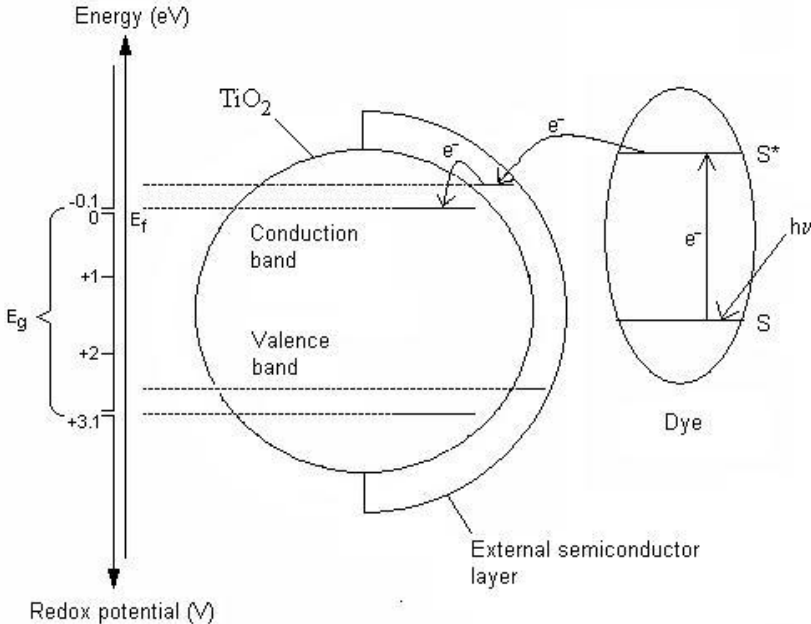


Figure 2. Modification of the TiO_2 electrode via external semiconductor layer

For improvement of electron injection efficiency or electron lifetime in the electrode, some post-synthesis-treatment methods were applied. The most common method was deposition of a thin layer TiO_2 on the electrode external surface using TiCl_4 aqueous solution treatment or TiCl_3 electrodeposition. The increase in the dye adsorption after the modifications described above were simultaneously reported [4].

Modification of TiO_2 electrodes by covering them with a thin layer of an insulator or other semiconductor can generate an energetic barrier for the electron back-transfer and improves the photoelectrical properties of DSC (Fig. 2.) [18-21]. If the modifying semiconductor has a slightly more negative

potential of the conduction band level than TiO_2 , but less negative than the excited state of the sensitizing dye, the photoinduced electrons can be still easily injected into the TiO_2 conduction band through the external modification of the semiconductor layer. After the injection process, the energy of the electrons present in TiO_2 conduction band corresponds to that of the bandgap of the external semiconductor and the recombination process is stopped. The electrons trapped in the conducting band of the TiO_2 can be easily transferred to TCO and used for the next steps of the photoelectric process, taking place in DSC.

Since 2005 the vertically orientated titania nanotubes “brush-like” arrays (Fig. 3.) have been often studied [4, 22-23]. Typical synthesis of TiO_2 nanotubes involves a titanium foil or titanium thin film deposited on FTO. The nanotubes growth is achieved by the potentiostatic anodization of metallic Ti substrate in fluoride-based solutions. TiO_2 nanotubes can also be prepared using alumina templates. The templates are prepared the conditions as mentioned above, using aluminium films deposited on FTO. The obtained alumina brushes are immersed in the titanium precursor solution and sintered at 673 K. The alumina templates are removed by extraction with 6 M NaOH solution and finally titania nanotubes or nanorod arrays are obtained [4].

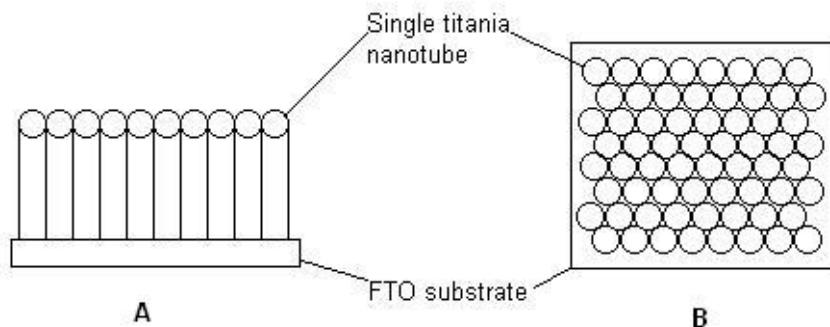


Figure 3. Schematic diagram of the TiO_2 nanotube “brush-like” array side view (A) and top view (B)

The length of the prepared nanotubes (up to $1000\ \mu\text{m}$), wall thickness (5-34 nm) and tube-to-tube spacing (0-10 nm) can be easily controlled by changing the preparation conditions such as anodization potential, time and temperature of the process and fluoride-based electrolyte composition [4].

5. Dyes and sensitizers

Not only mesoporous anode material was of key importance for the O'Regan and Grätzel's success with the first DSC in 1991. Huge influence on their discovery performance had the trimeric ruthenium complex (see Fig. 4. D) used as a sensitizer. The most important advantage of this sensitizer is its relative high stability with the turnover number measured as 5×10^6 [4, 14]. However, similarly as for the mesoporous electrode, O'Regan and Grätzel were not the first who used ruthenium dyes for DSC. The Ru-complexes with carboxylated bipyridine were for the first time used as sensitizers in 1979 by Anderson et al. for sensitizing TiO_2 single crystals [4, 24]. The brilliant idea behind the first highly efficient DSC was a combination of the advantages of the high surface area of porous TiO_2 with the stability and light absorption properties of the ruthenium dye, which produced desired results and brought a great success to O'Regan and Grätzel.

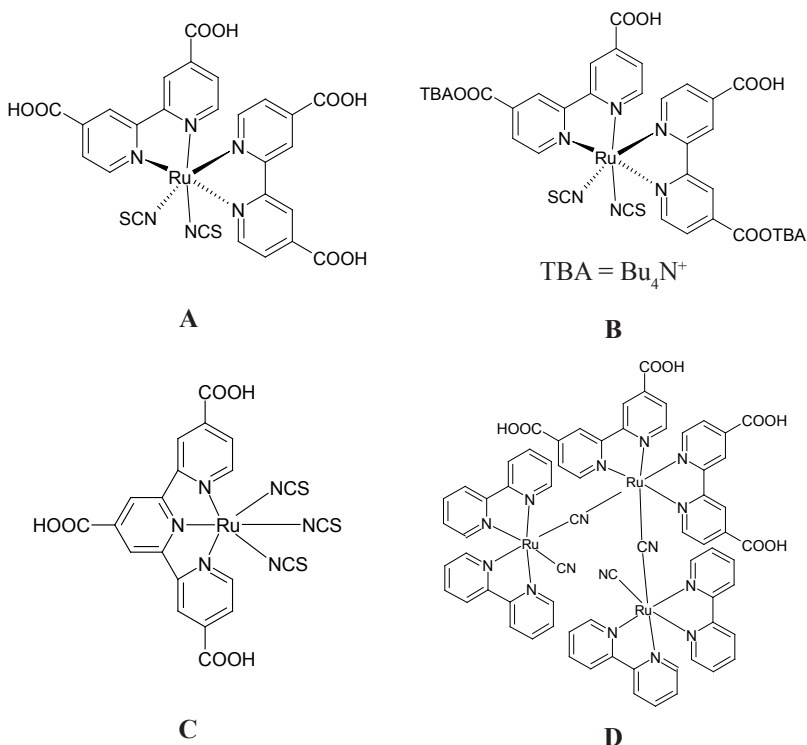


Figure 4. Exemplary structures of ruthenium dyes; N3-dye (A), N719-dye (B), "black dye" (C) and trimeric Ru complex (D)

The most important properties of dyes used in DSC's are [25]:

- broad and strong absorption, covering the widest possible range of electromagnetic radiation from visible light up to near-infrared;
- maximum stability of its excited state and resistance to deactivation by the emission of light and/or heat;
- strong and irreversible binding to the semiconductor surface and high electronic coupling of its excited state to the semiconductor conduction band;
- high chemical stability of the ground, excited and oxidized state;
- for effective electron injection, the reduction potential should be 150 – 200 mV higher than the semiconductor band edge;
- for rapidly regeneration, oxidation potential should be 200 – 300 mV lower than the red-ox potential of the electrolyte electron mediator species.

For last 20 years a great number of dyes (from natural, extracted from various plants, through synthetic metal complexes, to various organic compounds) have been tested as the DSCs sensitizers, however the best photovoltaic performance was obtained for Ru(II) polypyridyl complexes [4, 25]. Introduced in 1993 by Grätzel and co-workers N3 dye (Fig. 4. A) was a sensitizer used in the first dye-sensitized solar cell, which achieved a photovoltaic conversion efficiency of 10 % [4, 25-26]. The partly deprotonated form of N3 was presented by the same group and called N719 (Fig. 4. B). The cell obtained by using this sensitizer has reached overall photon-to-current conversion efficiency of 11.2 % [4, 25, 27]. These two dyes were characterized by such excellent properties as broad visible light absorption spectrum up to 800 nm, suitable long excited state lifetime (around 20 ns), strong adsorption on the semiconductor surface, and relatively long lifetime in photovoltaic process conditions. These advantages made N3 and N719 the reference dyes for DSC, and are used as a basis for designing other more or less efficient Ru-containing sensitizers [4].

A good example of the importance of using of the dye meeting all the criteria listed above is tri-thiocyanato terpyridyl Ru(II) complex N749, also known as the “black dye” (Fig. 4. C) designed by the same researchers who developed N3 and N719 [28]. This sensitizer absorption spectrum covers the whole visible range extended to near-IR region up to 920 nm. Another interesting property of the “black dye” is that its absorption and emission maxima show a bathochromic shift which depends on pH. This feature shows that the excited state lifetime is strongly related to pH values [25]. Such properties of this dye suggest that it could be a very efficient sensitizer, however, the DSC sensitized with N749 shows conversion efficiency of 10.4 %, which is much lower than

that characteristic of N719, and only slightly higher than the achieved with N3 [4, 7, 25, 28] (according to the first reported N3-sensitized DSC [26], afterwards more efficient N3-sensitized cells were obtained [25], so the “black dye” became less efficient than N3 in the same conditions). The reason for this unexpected relatively low efficiency of the “black-dye” containing DSC is low semiconductor surface coverage by N749, and its low extinction coefficient [25].

Despite efficient performance of Ru(II) complexes as sensitizers in Grätzel’s cells, organic dyes are also very intensively studied. The main reason for the search for a replacement of ruthenium complexes is their relatively high price resulting from the content of rare metal, and significant difficulties in purification of dye after its synthesis. The main advantages of the organic dyes are: wide range of possibilities of designing their physicochemical properties via appropriate molecular modeling, well known synthetic methods with easy purification procedures, and finally high molar absorption coefficients. However, their relatively low photostability or insufficient light harvesting in visible region caused by sharp absorption bands in the visible spectrum should be pointed to as the main disadvantage [25]. To this date the highest performance of organic-dye sensitized solar cells is 10.3 % obtained by Weng et al. using an orderly conjugated ethylenedioxythiophene and dithienosilole blocs containing a dye named C219 [29].

6. Electrolyte systems

The electrolyte is “the weakest link” of the dye-sensitized solar cells. The most effective devices use liquid electrolytes, which generate problems such as probability of solvent evaporation or leaking when the cell is not perfectly sealed, or water and/or oxygen permeation into the cell and their reactions with the DSC components. The consequences of the above mentioned effects is a significant reduction in the cell performance and/or time of its stability. Moreover liquid electrolytes are a source of problems in manufacturing of the commercial multi-cell modules, because the single cells, which make a module, must be electrically connected and simultaneously chemically separated but still located on a single conducting glass substrate. To minimize those effects, solvent free ionic liquids, solid or quasi-solid state (both organic and inorganic) hole conductors or conductive polymers are used, however, the performance of the cells using these alternative electrolytes is still lower than that of the cells with liquid electrolytes [3-4, 6, 25, 30].

In the first DSC constructed in 1991 the authors used an electrolyte based on tetrapropylammonium iodide and iodine dissolved in a mixture of ethylene carbonate and acetonitrile [14]. For the last nearly 20 years, different solvents,

redox couples and additives have been tested to tune up the electrolytes properties to improve DSC performance, but, in fact, we are still using the same categories of electrolytes based on I/I³⁻ redox couple [4]. The main disadvantages of the iodine/iodide redox mediator are high corrosive properties and photochemical activity. There are two common approaches to replace iodine-based electrolytes. The first is to use molecular species of similar type as iodine, for example Br/Br₃⁻, SCN⁻/(SCN)₃⁻ or SeCN⁻/(SeCN)₃⁻, and the second is to use the transition metal systems, such as cobalt(II)/(III), copper(I)/(II) or nickel(III)/(IV). Unfortunately all these alternative redox couples show much faster recombination reaction than iodine/iodide couple, which is probably its greatest advantage, and makes its hard to replace [4].

7. Conclusions

Dye-sensitized solar cells are seen as an alternative for traditional silicon photovoltaics. Today their main advantage is a low price in comparison with that of silicon cells. Unfortunately there are still many issues that must be solved before DSCs will be commercially available. The efficiency of the known DSCs is relatively low, moreover enlarging scale of single cell or module leads to decreased photon-to-current conversion efficiency (the working area of the most of high-effective cells reported, does not exceed 1 sq. cm). Another challenge is to extend the durability time and thermal stability of the cells for household devices. In summary, there is still much to be done, but 20 years ago there were no indicators that it would be possible to achieve a photovoltaic conversion efficiency over 1 %, and now it is easy to exceed the limit of 10 %, so it can be expected that further work on the development of DSC technology will lead to achieve stable, efficient, and at the same affordable devices based on dye-sensitized technology and applicable in the daily green energy raising.

Aknowledgments

This work was supported by the Polish Ministry of Science, grant No. N N204 023538.

References

1. M. Grätzel; *Nature*, 414 (2001) 338
2. K.H. Nealon, P.G. Konrad; *Philos. Trans. R. Soc. Lond. B: Biol. Sci.*, 354 (1999) 1923
3. B. Li, L. Wang, B. Kang, P. Wang, Y. Qiu; *Sol. En. Mater. Sol. Cells*, 90 (2006) 549
4. A. Hagfeldt, G. Boschloo, L. Sun, L. Kloo, H. Pettersson; *Chem. Rev.*,

- in press, DOI 10.1021/cr900356p
5. H. Spanggaard, F.C. Krebs; *Sol. En. Mater. Sol Cells*, 83 (2004) 125
 6. A. Goetzberger C. Hebling, H.-W. Schock; *Mat. Sci. Eng. R: Reports*, 40 (2003) 1
 7. M. Grätzel; *J. Sol-Gel Sci. Techn.*, 22 (2001) 7
 8. S.J. Fonash, R.T. Fonash, S. Ashok; *Encyclopedia Britannica*, online edition: <http://eb.com>
 9. <http://nobleprize.org>
 10. R. S Ohl, US Patent 2,443,542; May 27 1941.
 11. M.A. Green; *Prog. Photovot.: Res. Appl.*, 17 (2009) 183
 12. D.M. Chapin, C.S. Fuller, G.L. Pearson; *J. Appl. Phys.*, 25 (1954) 676
 13. D.J. Flood; *Mod. Phys. Lett. B*, 15 (2001) 561
 14. B. O'Regan, M. Grätzel; *Nature*, 353 (1991) 737
 15. G.J. Meyer; *Nano Focus*, 4 (2010) 4337
 16. A. Hagfeldt, M. Grätzel; *Acc. Chem. Res.*, 33 (2000) 269
 17. S. Hore, E. Palomares, H. Smit, N.J. Bakker, P. Comte, K.R. Thampi, J.M. Kroom, A. Hinsch, J. R. Durant; *J. Mater. Chem.*, 15 (2005) 412
 18. C. Kim, K-S Kim, H.Y. Kim, Y.S. Han; *J. Mater. Chem.*, 18 (2008) 5809
 19. B.C. O'Regan, S. Scully, A.C. Mayer, E. Palomares, J. Durant; *J. Phys. Chem. B*, 109 (2005) 4616
 20. Y.-M. Lee, C.-H. Hsu, H.-W. Chen; *Appl. Surf. Sci.*, 255 (2009) 4658
 21. S. Yang, H. Kou, S. Song, H. Wang, W. Fu; *Colloids Surf. A: Physicochem. Eng. Aspects*, 340 (2009) 182-186
 22. G.K. Mor, K. Shankar, M. Paulose, O.K. Varghese, C.A. Grimes; *Nano Lett.*, 6 (2005) 215
 23. N.N. Bwana; *Nano Res.*; 1 (2008) 483
 24. S. Anderson, E.C. Constable, M.P. Daredwards, J.B. Goodenough, A. Hamett, K. R. Seddon, R.D. Wright; *Nature*, 280 (1979) 571
 25. G.C. Vougioukalakis, A.I. Philippopoulos, T. Stergioopoulos, P. Falaras; *Coord. Chem. Rev.*, (2010) DOI: 10.1016/j.ccr.2010.11.06
 26. M.K. Nazeerudin, A. Kay, I. Rodicio, R. Huphry-Baker, E. Mueller, P. Liska, N. Vlachopoulos, M. Grätzel; *J. Am. Chem. Soc.*, 115 (1993) 6382
 27. M.K. Nazeerudin, S. Zakeeruddin, R. Huphry-Baker, M. Jirousek, P. Liska, N. Vlachopoulos, V. Shklover, C.H. Fisher, M. Grätzel; *Inorg. Chem.*, 38 (1999) 6298
 28. M.K. Nazeerudin, P. Pechy, M. Grätzel; *Chem. Commun.*, (1997) 1705

29. W. Zeng, Y. Cao, Y. Bai, Y. Wang, Y. Shi, M. Zhang, F. Wang, C. Pan, P. Wang; *Chem. Mater.*, 22 (2010) 1915
30. M. Grätzel; *J. Photochem. Photobiol. C: Photochem. Rev.*, 4 (2003) 145

Chapter 6

Application of noble gases NMR in supramolecular and material chemistry Complexes with supramolecular ligands

Błażej Gierczyk

*Faculty of Chemistry, Adam Mickiewicz University,
Grunwaldzka 6, 60-780 Poznań, Poland*

1. Introduction

Since the discovery of the nuclear magnetic resonance phenomenon in 1946, it becomes one of the most important analytical technique, used in many branches of chemistry, biology, medicine, physics and various applied science. At the beginning of this method evolution the most important and the widest studied aspect was the application of the ^1H NMR spectroscopy in organic chemistry (mainly for determination of the compounds structures). However, the intensive development of the NMR spectrometer has caused the increasing of the number of available techniques, nuclei which could be measured, experiments sensitivity etc. Among 84 naturally occurring chemical elements only three (Ar, Ce and Th) are not suitable for NMR measurements because of absence on natural isotopes of nuclear spin number $I > 0$. Although also some others elements, possessing magnetically active isotopes, could not be used for NMR experiments, for example because of huge quadruple moment (i.e. Au, In, Ir etc.), or the paramagnetism of their compounds (i.e. Pr, Eu, Gd and some others lanthanides), NMR of less common studied, so called “exotic” nuclei is one of the most interesting branch of the spectroscopy. Nowadays multinuclear magnetic resonance of the “exotic” isotopes is important tool for inorganic, metalorganic as well as supramolecular and material chemistry.

2. Nuclear magnetic resonance of the noble gases – an introduction

Among noble gases only argon is not suitable for NMR measurements because of no stability and magnetical activity of this element isotope. Also the only one radon isotope with nuclear spin > 0 (^{219}Rn) is not useful for NMR experiments due to its short life half-time (3.96 s). The basic NMR properties of

the other noble gases isotopes were summarized in Table 1.

Table 1. Basic nuclear properties of NMR-suitable noble gases isotopes

Nuclei	Spin	Natural abundance (%)	Receptivity ($^{13}\text{C} = 1.00$)	Quadrupole moment (10^{-30} m^2)	Resonant frequency (MHz) at 2.348T	Chemical shift standard
^3He	1/2	0.00014	0.00326	-	76.178	He^a
^{21}Ne	3/2	0.27	0.0036	9	7.894	Ne^a
^{83}Kr	9/2	11.50	1.23	15	3.847	Kr^a
^{129}Xe	1/2	26.4	31.8	-	27.660	XeOF_4 Xe^a
^{131}Xe	3/2	21.2	3.31	-12	8.199	XeOF_4 Xe^a

^a extrapolated to zero pressure

As it could be seen, only two of noble gases have an isotope of the spin $I = \frac{1}{2}$ and, in consequence, their spectra could be measured without disturbance by quadrupole interactions. First of them, ^3He is rarely used for NMR studies. Once, helium does not form any covalent or ionic compounds, so the tools for their studies are not necessary. Additionally, very low natural abundance of this isotope causes its extremely small receptivity. On the other hand, the experiments with enriched samples are very expensive because of the prices of ^3He (about 1000 \$/L). Moreover, its resonance frequency is not available on most commercial spectrometers. In consequence, helium-3 NMR studies are quite sparse, and concentrate on He encapsulated in fullerenes and application of helium as the probe for studying of porous materials. The second $I = \frac{1}{2}$ isotope is ^{129}Xe . The intensive development in the xenon chemistry causes an increasing of the importance of ^{129}Xe NMR. Because of the sensitivity of the xenon chemical shift on the electronic effects (it covers the range of about 7000 ppm), this method is an excellent tool for the studying of covalent and ionic compounds of xenon and mechanisms of any reactions involving them. Also the spin-spin couplings, easily observed in the ^{129}Xe NMR spectra give a useful information about the structure of the Xe compounds. The high receptivity of ^{129}Xe NMR experiments, favorable relaxation times similar to that of ^{13}C and the fact, that the ^{129}Xe spectra could be measured on most of the spectrometers produced in present days cause, that a large number of ^{129}Xe NMR data (chemical shifts, coupling constants etc.) are available. The excellent, comprehensive reviews about the application of this technique for the studying of xenon compounds structure and their reactivity were published¹⁻⁴. The other areas where the ^{129}Xe NMR spectroscopy is widely

used are the characterization of porous inorganic and organic materials and chemistry of xenon atoms containing fullerenes as well as the supramolecular complexes of Xe with organic ligands. The huge range of ^{121}Xe chemical shifts and the sensitivity of this parameter on intramolecular interactions make xenon an excellent probe on van der Waals forces in gases and liquids.

The quadrupolar nuclei of noble gases (^{21}Ne , ^{83}Kr and ^{131}Xe) were much more extensively studied. Only few papers, mainly confined to physics, involving their application for NMR spectroscopy were published. The ^{131}Xe NMR signals were strongly widened in the result of fast relaxation due to quadrupolar mechanism. Although such effects make this isotope useless for studies of xenon compounds, it becomes an interesting probe for studying the order, structure and electric field gradients of liquid crystals, micelles and solid materials surfaces. Differences between gyromagnetic ratios of both xenon isotopes make them a good tool for an identification of frequency-dependent interactions.

Even though krypton chemistry is not so intensively developed as xenon one, large number of Kr containing compounds were synthesized. On the other hand no ^{83}Kr NMR data of covalent or ionic krypton compounds were given^{4,5}. The NMR studies of this nuclide focused on the characterization of porous materials and surfaces. The ^{21}Ne isotope was not studied during chemical NMR investigation until nowadays.

3. ^{129}Xe NMR studies of xenon complexes with organic supramolecular ligands

Xenon atom van der Waals radius is 216 pm, therefore, xenon may form supramolecular complexes with a wide spectrum of ligands: cyclodextrins, crown ethers, cryptophanes, cucurbiturils, hemicarcerands and calixarenes.

The earliest NMR data of supramolecular xenon complexes were given for crown ethers in chloroform solutions^{6,7}. The authors observed significant changes of ^{129}Xe NMR chemical shift of xenon signal obtained for CHCl_3 solutions containing 12-crown-4 or 15-crown-5 (Fig. 1A, B) ethers in comparison with pure chloroform. Such shifts were not recorded if other ethers (1,4-dioxane, triglyme or tetraglyme) were used instead of crown ethers. In both cases only one signal in the ^{129}Xe NMR spectrum was observed, which indicated on fast exchange of the xenon atom between the complex and free form. The chemical shifts calculated from fitting of the results obtained for various ligand concentrations were collected in Table 2. The studies of complexes of Xe with other crown ethers or cryptands were not performed.

Table 2. ^{129}Xe NMR chemical shifts and stability constants for complexes of xenon with supramolecular ligands

Ligand number	Ligand name	^{129}Xe NMR chemical shift	Stability constant ^a [M^{-1}]	Conditions
1A	12-crown-4	249.0	0.082	CHCl_3
1B	15-crown-5	256.1	0.082	CHCl_3
1C	α -cyclodextrin	196.0 195.6 192 199	22.0 2.2 -	H_2O ; 298 K DMSO; 298 K solid state, hydrated crystals solid state, anhydrous
2A	cucurbit[6]uril	122.0	210	0.2 M Na_2SO_4 in D_2O ; 298 K
2B	-	97.0 132.0	1300 (ITC) 180 (ITC)	H_2O ; 295 K 0.2 M Na_2SO_4 in H_2O ; 295 K
2C	cucurbit[5]uril dihydrochloride octahydrate	230	-	solid state
2F	-	196	-	CDCl_3
2G	p- <i>tert</i> -butyl calix[4]arene	59; 64	-	solid state
2H	p-hexanoyl calix[4]arene	90; 190	-	solid state; 293 K
2I	p-octanoyl calix[4]arene	100; 190	-	solid state; 293 K
2J	p-decanoyl calix[4]arene	105	-	solid state; 293 K
2K	p-dodecanoyl calix[4]arene	120; 200	-	solid state; 293 K
2M	p-hexadecanoyl calix[4]arene	75; 210	-	solid state; 293 K
2O	4-sulfothia calix[4]arene sodium salt	117.7	13.6	D_2O ; 298 K
2P	-	114	200	CDCl_3
3A	cryptophane-A	61.0 54.1	3900 -	$(\text{CDCl}_3)_2$; 278 K $(\text{CDCl}_2)_2$ /toluene (1:1); 238 K
3B	cryptophane-223	53.5	2800	$(\text{CDCl}_2)_2$; 278 K
3C	cryptophane-233	45.0	800	$(\text{CDCl}_2)_2$; 278 K
3D	cryptophane-224	73.5	9.5	$(\text{CDCl}_2)_2$; 278 K
3E	cryptophane-111	32.0 -	10000 28000	$(\text{CDCl}_2)_2$; 293 K (Ref.16) $(\text{CDCl}_2)_2$; 278 K (Ref.17)
3F	cryptophane-E	32.0	<10	$(\text{CDCl}_2)_2$; 278 K
3G	-	47.0	1400	$(\text{CDCl}_2)_2$; 278 K
3H	-	68.5	-	$(\text{CDCl}_2)_2$; 278 K
3I	-	61.0	-	$(\text{CDCl}_2)_2$; 278 K
3J	-	61.5	-	$(\text{CDCl}_2)_2$; 278 K

3K	cryptophane-C	54.0	-	(CDCl ₂) ₂ ; 278 K
3L	cryptophane-D	68.5	-	(CDCl ₂) ₂ ; 278 K
5B	-	53.7	-	(CDCl ₂) ₂ /toluene (1:1); 238 K
5C	-	53.5	-	(CDCl ₂) ₂ /toluene (1:1); 238 K
5D	-	53.4	-	(CDCl ₂) ₂ /toluene (1:1); 238 K
5E	-	53.2	-	(CDCl ₂) ₂ /toluene (1:1); 238 K
5F	-	52.9	-	(CDCl ₂) ₂ /toluene (1:1); 238 K
5G	-	52.0; 53.2	-	(CDCl ₂) ₂ ; 228 K
7A	-	77.5	3400-4400	(CDCl ₂) ₂ ; 283 K
7B	-	71.2	3400-4400	(CDCl ₂) ₂ ; 283 K
8A	-	62.3; 63.1	-	D ₂ O; 298 K
8B	-	62.5; 63.5	-	D ₂ O; 298 K
8C	-	62.2; 62.8	-	D ₂ O; 298 K
8D	-	64.5; 65.2	-	D ₂ O; 298 K
8E	-	64.3; 65.0	-	D ₂ O; 298 K
8F	-	63.9; 64.1; 64.7; 65.0	-	D ₂ O; 298 K
9A	-	64.0	6800	D ₂ O; 293 K
9B	-	52.0	2200	D ₂ O; 293 K
9C	-	42.0	2200	D ₂ O; 293 K
9D	-	35.0	1000	D ₂ O; 293 K
9F	-	- 64.6 - -	17300 (ITC) - 30100 (ITC) 21900 (ITC)	1 mM phosphate buffer, pH 7.2; 293 K 1 mM phosphate buffer, pH 7.2; 300 K 1 mM phosphate buffer, pH 7.2; 310 K human plasma; 310 K
10A	-	65.0; 65.9	-	H ₂ O/D ₂ O (1:1); 296 K
10B	-	62.3; 62.9	-	H ₂ O/D ₂ O (1:1); 293 K
10C	-	66.1; 66.9	-	H ₂ O/D ₂ O (1:1)
10D	-	61.8; 62.4	-	D ₂ O; 291 K
10E	-	61.4; 62.2	-	D ₂ O; 291 K
10F	-	63.3	-	PBS buffer, pH 7.4
10G	-	68.5	-	D ₂ O, 310 K
10I	-	41.8	-	(CDCl ₂) ₂ /toluene (75:25); 298 K
11A	-	63.5	-	50 mM Tris buffer, pH 8.0; 293 K
11B	-	63.9	-	50 mM Tris buffer, pH 8.0; 293 K
11C	-	62.9	-	50 mM Tris buffer, pH 8.0; 293 K
13A	-	62.0 73.0	-	H ₂ O/D ₂ O (3:1); 298 K Intralipid®; 298 K
13B	-	62.7; 63.0	-	D ₂ O; 295K

^a) unless otherwise noted, stability constants were determined by ¹²⁹Xe NMR

The only cyclodextrin studied as the ligand for xenon is α -cyclodextrin, an homologue composed from six glucopyranose units (Fig. 1C). The complex formation was carried out in water and in DMSO⁸ as well as in solid state⁹. In liquids, the nonlinearity of the $\delta^{129}\text{Xe}$ plotted as the function of α -CD concentration indicates on the three-site model of the xenon complexation. The authors assume that the xenon atoms may be complexed inside the α -CD, may stay in the close environment of the oligosaccharide molecule or exist in the bulk phase. The exchange between these three sites is fast, therefore only one signal is observed in the spectrum. The binding constants and chemical shifts of the complexed xenon atom were calculated from fitting of the experimental chemical shift results, obtained for various concentration of Xe as well as ligand molecule. Additional experiments with linear, not cavity forming oligosaccharides, containing 1 to 6 glucose units were also performed. The K values obtained for α -CD complexes with xenon are 22.9 M⁻¹ (in water) and 2.2 M⁻¹ (in DMSO). The complex formation were confirmed by ^{129}Xe - ^1H heteronuclear nOe experiments. The irradiation of the sample with resonance frequency of H-3 protons signal caused the change of the ^{129}Xe NMR signal intensity, the enhancement factor was -0.23. The values of chemical shifts of xenon atom binded inside the cyclodextrin are similar for solid and liquid samples (Table 2).

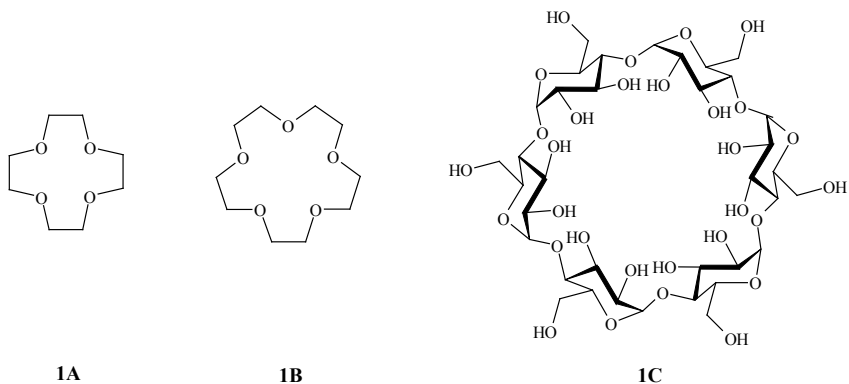


Figure 1. Structures of 12-crown-4 (1A), 15-crown-5 (1B) and α -cyclodextrin (1C)

The cucurbit[6]uril (Fig. 2A) 1:1 complex with xenon was also studied by ^{129}Xe NMR spectroscopy¹⁰. As for α -cyclodextrin, cucurbituril forms a stable host-guest compound with Xe in the effect of weak London energies. Because of the limited solubility of the ligand, the studies were performed in 0.2 M solution of Na_2SO_4 in water, at pH = 2.2. The spectra were recorded for different Xe/

host molecule ratios. At the low xenon concentrations, one resonance line was observed at 122 ppm. After the increasing of the xenon amount in the sample the second signal at 195 ppm, which corresponded to water solvated Xe atom, built up. This indicates on the slow (in the NMR time-scale) exchange between the encapsulated and free xenon position, however this process influents effectively on the relaxation times *via* scalar mechanism. The ^{129}Xe signals recorded for the cucurbiturils containing samples were significantly broadened in comparison with the signal of Xe dissolved in water (800 Hz vs. 10 Hz). The line-width of both signal obtained from the cucurbituril containing samples increased with the increasing of Xe/ligand ratio. The binding constants of this complex was calculated from the ^1H NMR titration as well as from competition experiments with cucurbit[6]uril/xenon/tetrahydrofuran system and estimated to be 210-240 M^{-1} . Further studies of cucurbituril-xenon complexes were performed on this system in more acidic solutions (0.5 M D_2SO_4 in water)¹¹. The K value obtained in this system is similar to that for the previously described (220 M^{-1}) but, in ^{129}Xe NMR spectrum, only one signal with chemical shift typical for uncomplexed xenon is observed. Authors explain this as the effect of the chemical exchange – the signal of the bonded xenon is too broad to be observed in the spectrum.

The water soluble cucurbit[6]uril analogue (Fig. 2B) was also checked as the xenon binding molecule¹². The stability constant, determined in water solution with isothermal titration calorimetry, was over one order of magnitude larger than for not modified cucurbituril molecule (3400 M^{-1}). The ^{129}Xe NMR spectra, recorded in water using hyperpolarized xenon, show two signals – one of unbonded and one of complexed Xe atom (190 ppm and 97 ppm respectively). As for unsubstituted cucurbituril, the exchange process is sufficiently slow in the NMR time scale. The spectra obtained for this ligand in 0.2 M water solution of Na_2SO_4 showed three significant changes, in comparison with those recorded in pure water: a) the signal of encapsulated Xe was shifted downfield to about 125 ppm; b) the ratio of the bonded/unbonded Xe resonance line was smaller for the samples of the same Xe/ligand ratios; c) the signals were significantly narrower. The ^{129}Xe chemical shift characterizing the sample containing the Na_2SO_4 is very similar to that obtained for the complexes with unsubstituted cucurbituril. The differences between the $\delta^{129}\text{Xe}$ in spectra recorded with the presence or absence of salt in the solution indicate on the interaction of encapsulated Xe atom with the cations on the ligand portals. The decreasing of the bonded/unbonded Xe signals ratio is the effect of the decreasing of the affinity of the xenon to the ligand molecule. The K value for the Xe interaction with 2B ligand in sodium sulfate containing solution, determined by ^{129}Xe NMR is 180 M^{-1} , so it is significantly smaller than for solutions in water (and similar to that of Xe-cucurbit[6]uril

complex in water/ Na_2SO_4). Signal narrowing suggests slower exchange of Xe atoms between bonded and free positions. It was confirmed with 2D ^{129}Xe EXSY spectra. The calculated rate constants of the complexation (ingression) and decomplexation (egression) processes in water were one order of magnitude higher than in water/ Na_2SO_4 system ($k_{\text{ing}} = 3.0 \times 10^6 \text{ M s}^{-1}$, $k_{\text{egr}} = 2.3 \times 10^3 \text{ s}^{-1}$ vs. $k_{\text{ing}} = 5.4 \times 10^4 \text{ M s}^{-1}$, $k_{\text{egr}} = 3.1 \times 10^2 \text{ s}^{-1}$). The slowing of the chemical exchange is probably caused by the presence of Na^+ ions at the portal. The authors determine also the ^{129}Xe spin-lattice relaxation time (T_1) for the complex in water solution. The value of these parameters, calculated from experimental, is about 40 s.

The cucurbit[5]uril hydrochloride hydrate (Fig. 2C) was studied by ^{129}Xe MAS NMR in solid state³². The signal observed at 205 ppm was assigned to the xenon atom inside tight cage of the host, the one at 105 ppm to the Xe in interstitial sites, while at 10 ppm to the xenon adsorbed in interparticle pores.

Branda et al. have studied the complexes of xenon gas with self-assembling dimers (Fig. 2D-F)²⁶. They shown that the encapsulation process might be controlled by the protonation of the ligand. Only for one host (2F) the ^{129}Xe NMR data were given. For the CDCl_3 solution of the ligand two signals, one corresponding to free xenon, second to the complexed one, were observed. The encapsulated Xe atom gave the resonance line about 19 ppm upfield shifted (i.e. at 196 ppm) that the non-bonded xenon. No stability constants or other thermodynamic or kinetic parameters were given.

The first calixarene-xenon complexes NMR data were obtained for crystalline *p-tert*-butylcalix[4]arene-nitrobenzene-xenon system (Fig. 2G)²⁷. It was also the first example of gas inclusion to calix[4]arene cavity. The XRD analysis has showed, that in crystalline sample of studied complex about 17% of the host cavities were occupied by xenon atoms, while the rest of them by nitrobenzene molecules. The ^{129}Xe MAS NMR consists of two signals (δ_{iso} 59 and 64 ppm) of slightly different intensities (0.6:0.4). This indicates that Xe is bonded in two inequivalent sites, possessing slightly different xenon occupancies and void space volumes. The fitting of static ^{129}Xe spectra gave the values of the chemicals shifts anisotropy (CSA) tensors for both sites. Their δ_{11} and δ_{22} parameters differ (49 ppm vs. 64 ppm and 54 ppm vs. 60 ppm) while the δ_{33} values are the same (76 ppm). The asymmetry of both powder patterns CSA tensors reflect to the departure from the axial symmetry of calix[4]arene cage. The δ_{33} component corresponds to the anisotropy along *z*-axis. The fact that for both ^{129}Xe signals this parameter has the same value, indicates that the both xenon occupied cavities have the same dimension along this axis. The differences in the cavities dimensions, sampled by Xe atom, are in the *xy* plane. As it was proved on the basis of XRD measurements, the disorder of the one of

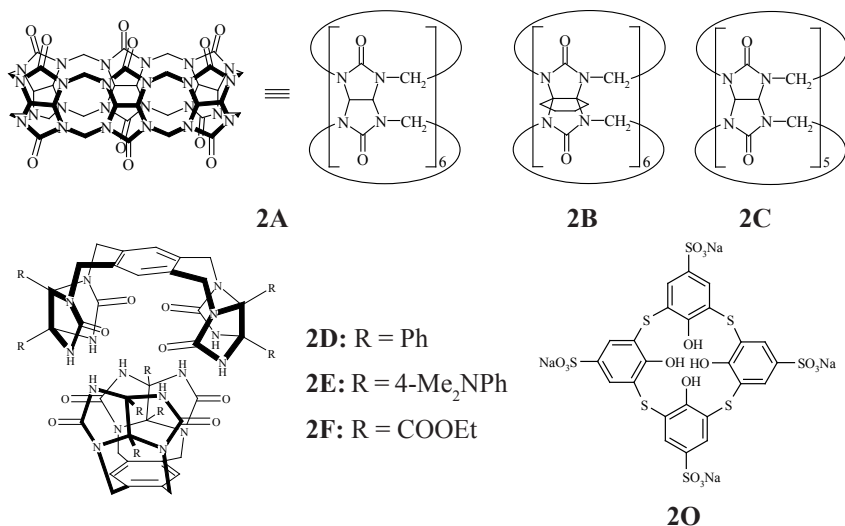
tert-butyl group influenced on the cavity *xy* dimensions, while it did not disturb its along *z* axis. The presence of two ^{129}Xe signal indicates on the static character of this disturbance.

The further studies of calixarene xenon complexes focus on the solid lipid nanoparticles of 4-acylcalix[4]arenes (Fig. 2H-M) and their sorption properties, studied with hyperpolarized ^{129}Xe NMR²⁸. The colloidal suspensions of solid particles of the mean diameter equal to 150 nm in water were used for the studies. For all studied ligands the ^{129}Xe spectra showed four signals, originating from free Xe (0 ppm), the xenon in interparticle space (~20 ppm), the Xe atom in calix[4]arene cavity (80-130 ppm) and the noble gas atom located between the aliphatic, hydrophobic chains of the molecule (approximately 190 ppm). The linear dependence of ^{129}Xe chemical shift of the xenon atom inside the ligand cavity and the length of the acyl substituents chain length was observed. This indicates on the decreasing of the reduction of the void space of the calixarene cage with the increasing of hydrophobic chain length. Authors explain this effect by folding of the chains over the cavity as well as into it, which reduces or completely fills the void space and disturbs the Xe encapsulation. The MAS NMR spectra for the studied compounds complexes with Xe, recorded after the pulse of methylene chloride, show the disappearing of the signal corresponding to the xenon atom located inside the host molecule cavity. This proves the displacement of the noble gas atom by CH_2Cl_2 molecule. After some time, the signal at 80-100 ppm rebuilt, that indicated the return of the Xe to the host cavity as methylene chloride was stripped out. The signal obtained after this cycle shows some differences in comparison with that before CH_2Cl_2 pulse: a) it is upfield shifted (about 15 ppm for 2H); 2) it is split into two resonance lines (at 78.6 and 73.6 ppm for ligand 2H); 3) the intensity of recovered signal is distinctly higher than that for material before methylene chloride action. Authors explain this phenomena on the basis of two effects. The deshielding of the signal and its intensity increasing are the result of the exclusion of substituents chains from the calixarene cavities, which increases the void space and the accessibility of the host cage. The splitting of signal is the effect of statistically disordered substituents. Special interest was dedicated to the host 2I which formed the nanocapsules in solid state²⁹. The static ^{129}Xe NMR studies of its complex with xenon show a signal at approximately 100 ppm, which exhibited an axial anisotropy of chemical shift. The calculated void space and crystallographic structure indicate that the cavity of calixarene part is not accessible for Xe atom because of its occupancy by one of the C8 chains, therefore the xenon is located in the channel formed between the two calixarenes, limited by the aliphatic chains of the host molecule.

The only results of the Xe complexes with calixarene in solution were

presented for 4-sulfothiacalix[4]arene sodium salt (Fig. 2O) in D_2O^{30} . For the studied complex, one signal at 130–200 ppm, depending on ligand concentration, was observed. It is shifted to higher field with increasing of 2O concentration. The absence of the signal corresponding to soluble Xe gas indicates on fast exchange between complexed and free xenon atoms, which could be explained by the flexibility of a host molecule. The calculated on the basis of ^{129}Xe NMR titration experiments chemical shift for $\text{Xe}@2\text{O}$ complex is 117.7 ppm, while the stability constant is 13.6 M^{-1} (298 K). The temperature variable ^{129}Xe measurements permit to determine the K values at different temperatures as well as thermodynamic parameters of complexation process.

Hemicarcerands form a unique group of supramolecular ligands (Fig. 2P). The complexation of Xe by ligand 2P was successfully studied by ^{129}Xe NMR³¹. The saturation of the CDCl_3 solution of host with xenon gas caused the formation of signal at 114 ppm. The kinetics of complex formation in chloroform solution were studied (the second-order rate constant were estimated to be $9.2 \times 10^{-4} \text{ s}^{-1} \text{ M}^{-1}$), as well as for the decomplexation process ($k_d = 4.2 \times 10^{-4} \text{ s}^{-1}$; in CD_2Cl_2). The estimated K value is 200 M^{-1} .



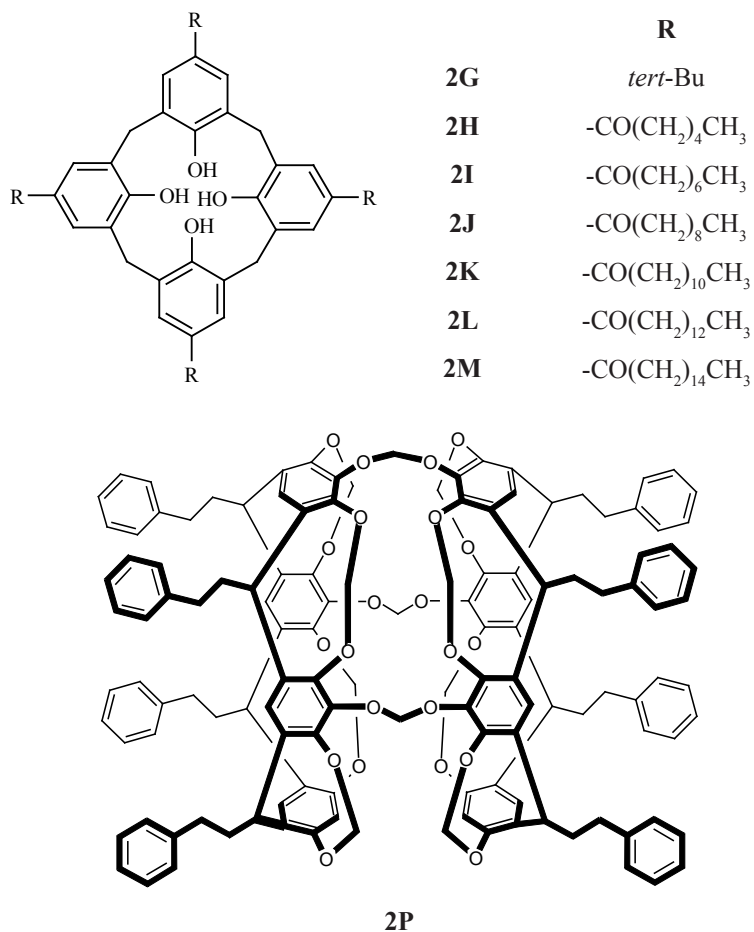


Figure 2. Cucurbituril (2A-C), glucuril (2D-F), calixarene (2M-O) and hemicarcerand (2P) xenon complexing ligands

The largest group of xenon binding supramolecular ligands are cryptophanes. The earliest studies focused on cryptophane-A (Fig. 3A), a cage molecule forming stable complexes with various neutral guests, i.e. methane or chloroform.

The largest group of xenon binding supramolecular ligands are cryptophanes. The earliest studies focused on cryptophane-A (Fig. 3A), a cage molecule forming stable complexes with various neutral guests, i.e. methane or chloroform.

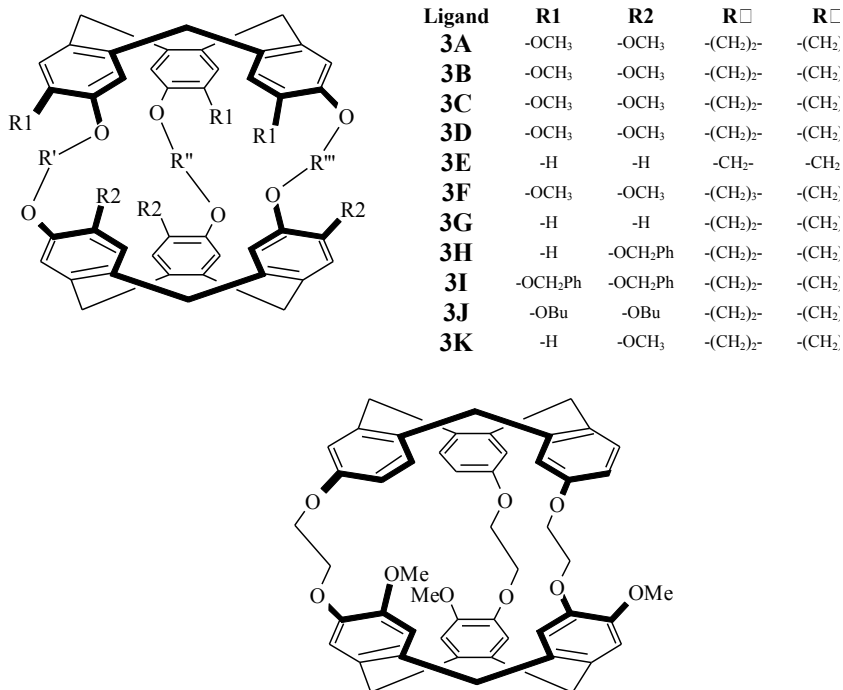


Figure 3. Cryptophane ligands

The cryptophane may adopt various conformation and fit to the size and shape of the guest molecule. The measurements were made in 1,1,2,2-tetrachloro-1,2-dideuteroethane, which molecule did not incorporate in the cryptophane-A cage¹³. The ¹²⁹Xe NMR spectra of the solution containing a ligand show the downfield shifted signal of the encapsulated Xe atoms and the second, corresponding to free xenon, present in the solution (62.3 ppm and 229.5 ppm respectively). It indicates on slow, in the NMR time-scale, exchange between these two species, however this process influences on the broadening of the both signals. The large difference of the bounded and free xenon chemical shifts comes from the strong intramolecular interactions (mainly van der Waals forces) of the host molecule with highly polarizable electron cloud of xenon guest atom. The ring current effects contribute much weaker on the complexation induced shift. The authors present also detailed studies of temperature and host/guest ratio dependence of the line-widths and chemical shifts of the both signals observed in the spectrum.

The following observations are important for the studied system: a) the chemical shift of the free xenon is the same, within the experimental error, in pure solvent as well as in the presence of the ligand in wide temperature range; b) the chemical shifts of encapsulated xenon do not depend on xenon/ligand ratio and change linearly in the wide temperature ranges; c) the line widths of the encapsulated and free xenon signals are the same in low temperatures (240-250 K). It indicates that, at lower temperatures, the situation of infinitely slow chemical exchange occurs. Additionally, the chemical shifts changes may not originate from the slowing down of the exchange process, but it should be intrinsic to the structure of the complex formed. They are explained by the changes of the cryptophane cavity dimensions due to the dynamics of $\text{OCH}_2\text{CH}_2\text{O}$ units and the deshielding effects of repulsive configurations, characteristic for xenon atom in confined cavity space. The affinity of the xenon to the cryptophane-A molecule was determined by ^1H NMR in the competition experiments with xenon/ligand/ CHCl_3 system, and it was established to be larger than 3900 M^{-1} .

Further studies of the Xe/cryptophane-A complexes took the advantages of the hyperpolarized ^{129}Xe NMR technique and used the heteronuclear Overhauser effect to determine the structure of the host-guest system¹⁴. The spectra recorded with SPINOE sequence, for the sample with positively and negatively hyperpolarized xenon, show the significant enhancement of the all of the ligand protons' signals after irradiation of the sample with the frequency of ^{129}Xe resonance line, and vary from 3 to 13%, depending on the proton position. The results of this experiment were collected in Table 3. As it comes from the discussion presented by the authors, the xenon atom is included into the cavity of the ligand and the spacer bridges are in gauche conformation. Additionally, the T_1 relaxation times for ^{129}Xe and ^1H nuclei of the host and guest were determined (approximately 16 s for encapsulated xenon, hundreds of second for free Xe dissolved in $(\text{CDCl}_2)_2$).

Table 3. The SPINOE experiment results for cryptophane-A/xenon system

Proton	T_1 [s]	SPINOE [%]	$\sigma_{\text{HXe}}/\sigma_{\text{H(aromatic)Xe}}$ ¹	$\langle r_{\text{HXe}}^{-6} \rangle / \langle r_{\text{H(aromatic)Xe}}^{-6} \rangle$
Ar-H	0.80	11.0	1.00	1.00
ArCH ₂ Ar ax.	0.27	3.0	0.47	0.3-0.4
ArCH ₂ Ar eq.	0.35	2.7	0.35	0.3-0.4
OCH ₂ CH ₂ O	0.36; 0.41	5.2; 13.0	0.67; 1.55	0.3; 1.5-1.8
OCH ₃	0.83	2.6	0.23	0.1-0.3

¹ relative H-Xe cross relaxation rates

In following years the chemistry of cryptophane-xenon complexes were concentrated on two scopes – optimizing of the cages to the xenon complexation process and modification of the ligand properties (binding constants, solubility) by molecule modifications by substituents. In the work of Brotin and Dutasta¹⁵ three new cryptophane ligands with different length of spacer bridges were presented (Fig. 3B-3D). All compounds were characterized by ^{129}Xe NMR spectroscopy in $(\text{CDCl}_2)_2$. The compounds 3B and 3C show separated signals of free and encapsulated xenon atoms in the NMR spectra that indicates the slow exchange between these species. In the spectrum of 3D/xenon system, only one, broad line of the chemical shift close to that of free Xe occurs. It is the effect of fast exchange and relatively short residence time of guest atom in host cage. The ligands 3A, 3B and 3C show a significant difference in $\delta^{129}\text{Xe}$ values, which increases upon temperature decreasing. The differences between free and encapsulated Xe chemical shifts at 293 K were 156.0 ppm for 3A, 164.0 ppm for 3B and 177.0 ppm for 3C, while at 238 K they were 189.0, 201.0 and 211.0 ppm, respectively. It is the effect of various cavities volume changes with temperature decreasing for above ligands and, in consequence various confining of Xe atom. The binding constants were determined by the ^{129}Xe NMR experiments performed for mixtures of studied ligands with cryptophane-A, their values were given in Table 2. The kinetic of the chemical exchange for compounds 3B and 3C was studied by 1D ^{129}Xe EXSY experiments in various temperatures and the activation parameters were determined.

Fogarty et al.¹⁶ has synthesized the smallest cryptophane (3E) and determined its xenon encapsulating properties by standard and hyperpolarized ^{129}Xe NMR. The host shows enormously high affinity to the xenon, the binding constant, obtained from competition experiments with cryptophane-A is close to 10000 M^{-1} . Also the kinetic parameters, the decomplexation rate and the mean residence time are quite high, distinctly higher than that determined for cryptophane-A, which indicates on the high stability of the complex formed. It effects in the shape of the signals in the xenon NMR spectrum – the lines are significantly narrower than for the complexes with hosts 3A-D. The T_1 relaxation time for Xe@3E is 18.8 s, which value is smaller than that obtained for cryptophane-A, due to the smaller proton-xenon distances and increased correlation times.

The systematic studies of xenon complexation by cryptophanes were made by Huber et al.¹⁷. The series of new, modified ligands (Fig. 3F-L) were obtained and their ^{129}Xe NMR spectroscopic properties as well as complexating properties were studied. The results were compared with that for known ligands (3A-E), for which some spectral parameters were redetermined. The studies concentrate on the influence of the cage size and the character of the phenyl rings substituents

on the ligand properties. The thermal and light polarized xenon was used for their characterization. All measurements were made for $(\text{CDCl}_2)_2$ solutions. The following parameters were determined for all studied host molecules: xenon binding constants (K), the ^{129}Xe chemical shifts and their temperature dependence, decomplexation (release) rate of the encapsulated xenon and longitudinal relaxation times (T_1) of encapsulated xenon nucleus. Xenon forms 1:1 complexes with studied ligands. The stability constants were collected in Table 2. They were determined from competition ^1H and ^{129}Xe NMR experiments as well as ^1H NMR titration of the ligand with xenon gas. The ligands forming the series 3A-D and 3F differ only in the length of the chains linking two cyclotribenzylene (CTB) parts. As it could be seen, the increasing of the length of these spacer bridges resulted in the decreasing of the xenon to ligand affinity. It is the effect of the weakening of the host-guest London forces due to the increasing of noble gas atom – ligand atom distances. Also the higher flexibility of the ligand may influent on the entropic part of the affinity constant and decrease the K value. The third reason of the stability constant decreasing with the increasing of the spacers length may be stronger solvent molecules-encapsulated xenon atom interactions via larger, more flexible ligands portal. These interactions could also explain lower stability of the complexes with 3G ligand than this with cryptophane-A, because the absence of the methoxy substituents allows to contact of the Xe atom with solvent molecules. The xenon-129 chemical shifts of the complexes were collected in Table 2. The authors confirm previous observation, that for ligand-xenon systems, showing slow chemical exchange (in NMR time-scale), the ^{129}Xe chemical shift is independent from the concentration of ligand or xenon partial pressure. The influence of the sphericity of the cage and the arrangements of the linking bridges on the ^{129}Xe chemical shifts are clearly seen for the pair of ligands 3K and 3L, for which the less spherical ligands complex (3L) shows the downfield shifted signal in comparison with 3K. The studied ligands confirm also the previously described tendency of the decreasing of the chemical shift of encapsulated xenon atom with the increase of the size of the portal as well as the cage dimensions. The deshielding of the xenon nucleus increases upon the minimizing of the distances between the guest and hosts atoms. The detailed analysis of the ^{129}Xe chemical shifts dependence on the solvent used for complex preparation leads the authors to state, that for the ligands with greater cavity the influence of the solvent molecules on the xenon shielding take a significant role. By comparing of the δ ^{129}Xe values of the ligands differs only in the substituents at the phenyl rings (3A, 3G-3K), the following observations could be made: a) the signal of xenon encapsulated by ligand 3G is significantly shielded in comparison with the other ones; b) the ^{129}Xe chemical shifts observed for xenon

bound by ligands 3A, 3H-3J are very close to each other; c) the $\delta^{129}\text{Xe}$ of Xe@3K is the intermediate between the 3G and the 3A. The strongest upfield shift of the Xe@3G is the effect of the absence of the alkoxy substituents in the host molecule. This causes the increasing of the electronic density in the phenyl rings and, in consequence, larger shielding of the xenon atom. For complex with 3K host, which molecule has methoxy groups bonded to the half of the phenyl rings, the observed xenon-129 shift is the intermediate value.

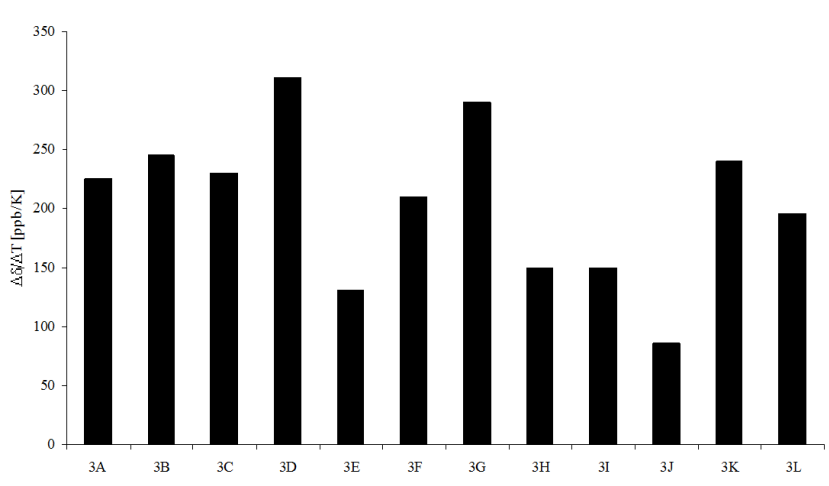


Figure 4. Temperature dependence of ^{129}Xe chemical shifts for ligands 3A-L

The temperature dependences of the ^{129}Xe chemical shifts of the studied complexes were collected in Fig. 4. The strongest influence of the temperature was recorded for ligands 3D and 3G. The first one contains the relatively flexible butanedioxy linker, which allows to the significant changes between host molecule conformations. The second one shows the small energy barrier of cage distortions, due to the absence of the alkoxy substituents at phenyl rings. The smallest effect, recorded for ligand 3J is explained by the presence of flexible butoxy substituents. The van der Waals interactions between them may minimize the cage conformational freedom. They could also hinder the interactions of the Xe atom with solvent molecules. The release rate of the xenon was calculated from the line-widths for the systems showing slow chemical exchange. The following observations should be pointed out: a) the presence of alkoxy substituents decreases the rate of the exchange due to hindering of xenon release; b) the significant differences between 3K and 3J indicate on the

strong influence of conformational spaces on the releasing of Xe atoms from the ligands cavities. The longitudinal relaxation rates of encapsulated xenon nucleus were determined by inversion-recovery method or the monitoring of the area of the ^{129}Xe NMR signal (assuming the very slow relaxation of the xenon in “free” position).

The cryptophane-A molecule was also modified by successive deuterium labeling of ethylenedioxy bridges and/or methoxy groups¹⁸. The structures of the obtained ligands were presented in Fig. 5A-F. In the spectrum recorded for equimolar solution of 5A (unlabeled cryptophane-A) and $[\text{H}]_{30}$ -cryptophane-A (compound 5F) in a presence of xenon, recorded at 238 K in $(\text{CDCl}_2)_2$, three signals were observed – one originated from free xenon soluted in tetrachloroethane (224.8 ppm) and two well separated signals (54.1 and 52.9 ppm), first corresponding to Xe@5A, second to Xe@5F. At 298 K the exchange between these three species results in collapsing of the signals of encapsulated xenon and broadening of both signals visible in the spectrum. Also for mixture of hosts 5C and 5D, which differs only by change of one CH_3 group on CD_3 , the splitting of high field signal onto two lines could be seen. The authors show the linear dependence of the chemical shift and the number of deuterium atoms in ethylenedioxy bridges or methoxy groups (these two lines differs in slopes). The ^{129}Xe 2 D EXSY spectra recorder for the mixture containing xenon and hosts 5A and 5F permits to determine the rate constants of the exchange processes between the xenon-containing species present in the solution. The results of these experiments were presented in Fig. 6 (in brackets). The redetermination of these parameters with ^{129}Xe 1D EXSY spectra gave slightly different results¹⁹. Contrary to the previously described model, which assumed both exchange between the free and complexed species as well as direct Xe atom transfer between the ligands present in solution, the further measurements prove, that the second process did not occur. The rate constants determined with 1 D EXSY spectra were also given in Fig. 6. On the basis of variable temperature 1 D EXSY experiments, the activation parameters were calculated.

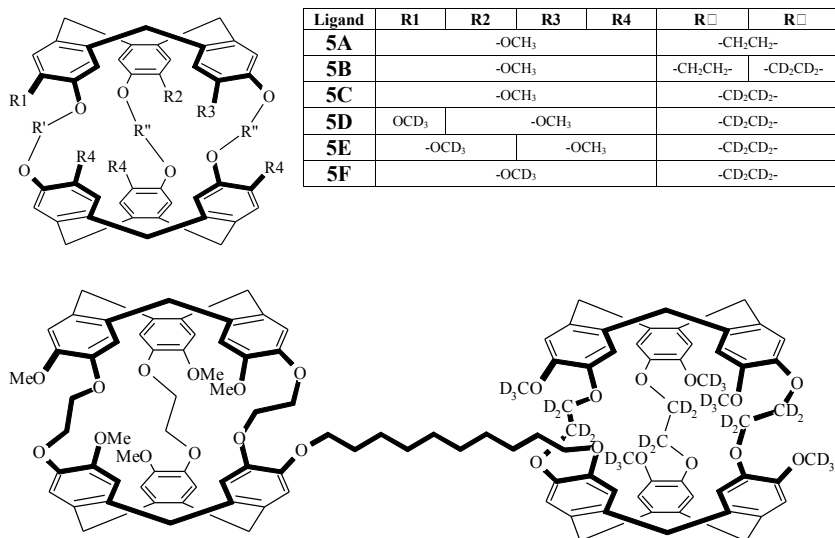
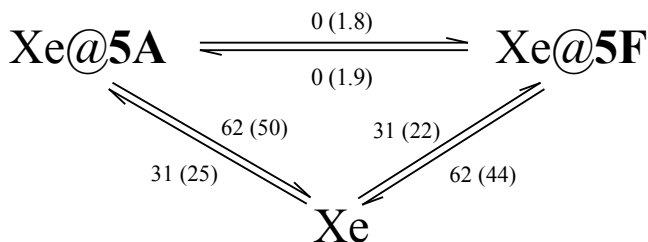


Figure 5. Deuterated cryptophane-A analogues


 Figure 6. Rate constants (s^{-1}) for exchange processes of xenon between free and encapsulated species according to Ref. 18 and 19 (in brackets)

Very similar results were obtained for bis-cryptophane complexes²⁰. The studied ligand contains two cryptophane-A units connected by 1,10-decylene linker. One of the complexing parts was deuterium labeled (Fig. 5G). The Xe complexes of ligand synthesized were studied by ¹²⁹Xe NMR spectroscopy, involving 1D EXSY spectra. As for the mixture of deuterated and undeuterated ligands, two signals of encapsulated xenon atom were observed at low temperature, first one corresponding to the guest in deuterium labeled cage, second one to the xenon binded by protonated one. The calculated rate constants

of the xenon exchange are similar to those described for not-connected ligands. Also in these studies the direct exchange of xenon atom between the cages were not observed.

The chemical shifts of ^{129}Xe isotope encapsulated by unfunctionalized cryptophane hosts were studied also by theoretical calculations²¹. The authors obtain a good reproduction of chemical shifts of $\text{Xe}@$ cryptophane systems, the sign and the order of magnitude of thermal dependence of the $\delta^{129}\text{Xe}$, the changes upon the successive deuteration of the host molecule as well as discuss the effects of cage distortions on this value.

The D_3 symmetry of cryptophane-A molecule causes its chirality and, in consequence, existence of two enantiomers of these ligands (Fig. 6A). It was showed, that the signal of encapsulated Xe atom inside the cryptophane-A cavity split into two lines after adding of chiral shift reagent – tris[3-(heptafluoropropylhydroxymethylene)-(+)-camphorato] europium(III) (Fig. 6B)^{24,25}. The diastereomeric chemical shifts of the Xe atom encapsulated in the cage of the cryptophane-A molecule, modified by the chiral substituent, were reported.

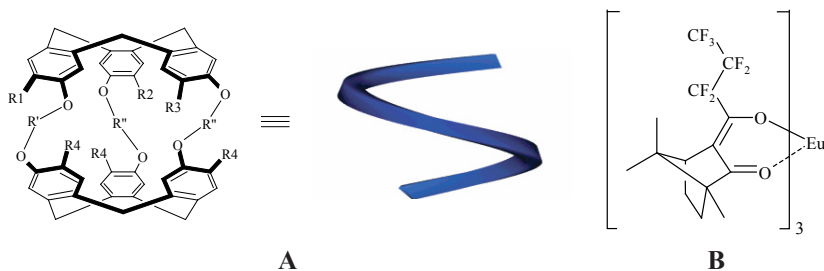


Figure 6. Cryptophane-A chirality (A) and the chiral europium shift reagent structure (B)

First studied example were the cryptophanol esters with (–)-camphanic acid²². Two diastereomeric host molecules (Fig. 7A, B) were obtained. The xenon complexes of those ligands were studied in $(\text{CDCl}_2)_2$. In the ^{129}Xe NMR spectrum of the mixture containing both ligands two distinctly resolved signals (chemical shift difference of 7 ppm) corresponding to encapsulated xenon were obtained and the third one, originated from the free Xe in solution. This indicates on the slow exchange between xenon-containing species. Such variation in xenon chemical shifts was explained as the result of the cavities volume change or small difference in shielding effects of the camphanyl substituents. The binding constants of xenon to ligands 7A and 7B were not determined (but their values was estimated to be similar to that for cryptophane-A, i.e. 3400–4400 M^{-1}), although the differences in the intensities of the ^1H and ^{129}Xe signals

permitted to state that binding of Xe to **7B** was more favorable than **7A** is. The ^1H - ^{129}Xe SPINOE spectra confirm the location of the xenon atom inside the cryptophane cavity and that the camphanic acid moiety does not participate in complex formation (after xenon signal irradiation, only the enhancement of cryptophane units protons was observed, the signals of camphanyl substituent hydrogen atoms were suppressed).

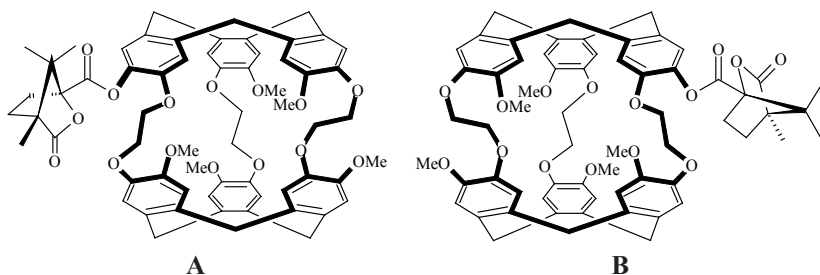
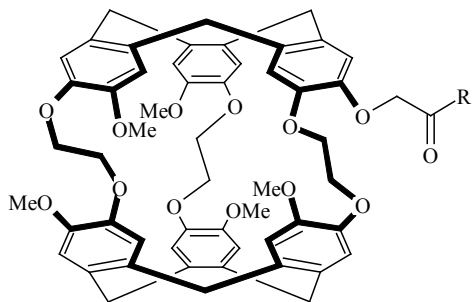


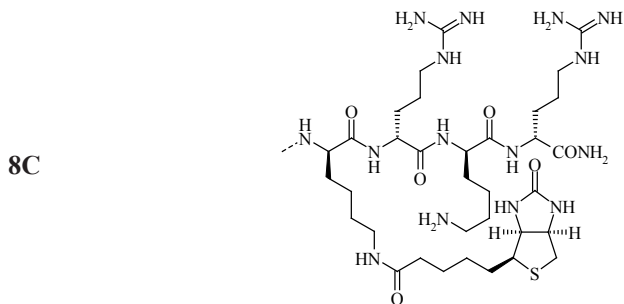
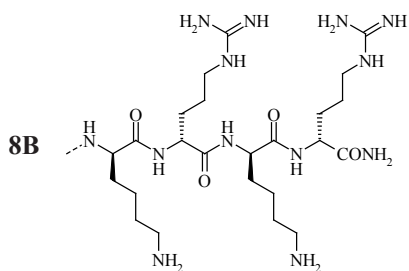
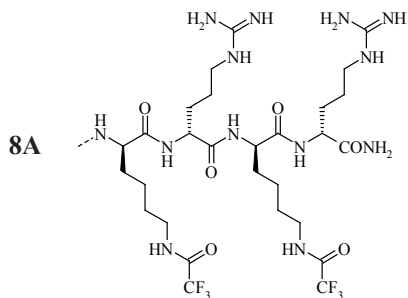
Figure 7. Diastereomeric analogues of cryptophane-A: (-)-camphanic acid esters (**7A**, **B**)

The second described diastereotopic complexes of cryptophane analogues with xenon were the ligands built from cryptophane derivatized by tripeptide substituent (Fig. 8A-F) or tripeptide substituent and 2-mercaptosuccinylimide moiety (Fig. 8G)²³. The ligands 8A-F exist in form of diastereomers (enantiopure peptide part and racemic cryptophane cage), while the ligand 8F as a mixture of four isomers (enantiopure peptide chain and racemic cryptophane cage and 2-mercaptosuccinylimide moiety). For the first compound (**8A**), the ^{129}Xe spectrum recorded for solution of the ligand in D_2O saturated with xenon is composed from two signals separated by 0.84 ppm. The ligand **8F** shows four signals, corresponding to four diastereomers present. The other peptide containing ligand **8B**, studied as the mixture of two diastereomers, shows also the two lines separated by 1.00 ppm. The protection of its free NH_2 groups by trifluoroacetyl substituted (ligand **8A**) causes the decreasing of the signals splitting to 0.84 ppm. Also the other ligands studied, containing the biotin connected to the cryptophane cage via peptide unit, show the diastereotopic chemical shifts of xenon atom. It was shown that the small modification of the host molecule (e.g. changing of the CONH_2 substituent to methyl ester, ligands **8D** and **8E**) caused a measurable differences in $\delta^{129}\text{Xe}$ values. This indicates on the high sensitivity of the encapsulated xenon atoms chemical shift on small changes in the ligand structure, also if they are introduced in the part of ligand molecule far from the Xe complexation centre. For the compounds studied the calculation of ^{129}Xe chemical shifts was also presented. All ligands synthesized

were presented in Fig. 8 and the obtained chemical shifts were collected in Table 2. Achiral ligand 10I was used as the model compound.



R =



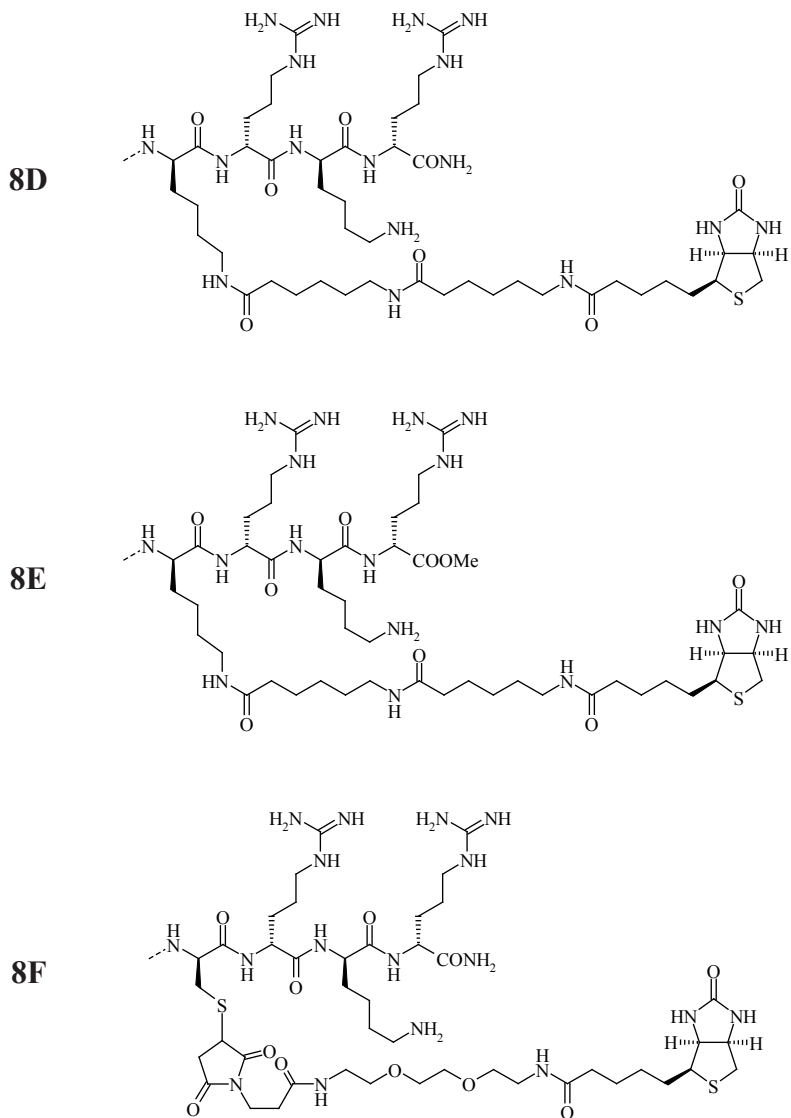


Figure 8. Peptide containing diastereomeric cryptophane ligands.

Water soluble cryptophane analogues were obtained for a possible purpose as the ^{129}Xe MRI contrast agents and substrates for biosensors synthesis. Huber et al. have studied the series of O-carboxymethyl substituted cryptophanes (Fig. 9A-E)³³. On the basis of ^{129}Xe NMR measurements the following parameters were determined: a) the chemical shifts of complexed xenon atom; b) the stability constants of complex formed; c) the kinetics of the encapsulation process; d) hyperpolarization life-time. All measurements were performed for D_2O solutions. The observed ^{129}Xe chemical shifts were similar, but slightly smaller than those of the methoxy analogues (parent hosts 5A; studied in $(\text{CDCl}_2)_2$). The only exception is compound 9E, for which the signal is downfield shifted and sharper in comparison with 5F. It is probably the result of simultaneous complexation of Xe and D_2O and, in effect, reducing of the volume occupied by xenon atom and slowing its exchange with free Xe present in solution. In the case of the ligand 5F the binding of $(\text{CDCl}_2)_2$ together with Xe is impossible. The affinity of xenon to ligands was determined by proton and xenon magnetic resonance. Both approaches gave the results staying in good agreement. The stability constants determined by ^{129}Xe NMR were collected in Table 2. As for methoxy analogues, the stability of the complexes decreases with increasing of the cavity dimensions. Generally, the Xe@9A-E complexes are more stable than that of parent hosts. It is the result of lower affinity of xenon to water than to $(\text{CDCl}_2)_2$, as well as unfavorable entropy of water inside hydrophobic cryptophane cavity. The exchange rates were estimated on the basis of the resonance line width, and increased with increasing of the spacer bridge length (larger portal permits on the faster exchange). The relaxation time T_1 was determined only for ligands 9A and 9E. The replacement of the all aliphatic hydrogen atoms to deuterium causes the decrease of the relaxation (T_1 values 12.1 and 17.6 s^{-1} respectively).

Another example of water soluble cryptophane ligand is the host 9F, containing three triazole rings, synthesized via click-chemistry methods³⁴. Although the ^{129}Xe NMR spectra of Xe@9F were recorded (Table 2), the stability constants were determined by other methods (fluorescence quenching and ITC).

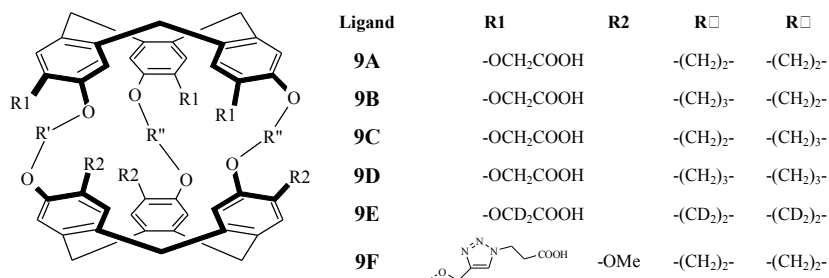
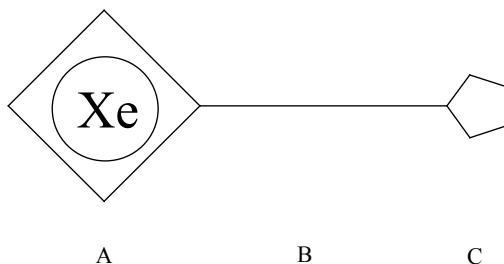


Figure 9. The water soluble cryptophane ligands

The idea of the ^{129}Xe NMR biosensor is presented on Scheme 1. The xenon-binding part of the molecule (A) is connected via a long linker (B) with a unit (C), which could be binded to the protein or other biomolecule with high affinity and specificity.



Scheme 1. Scheme of xenon-containing biosensor

The Xe complexing part of the molecule should encapsulate the guest with a high stability constant and the complex formed should be stable in physiological conditions. The biomolecule-recognizing arm should form stable complexes with species detected. Two basic applications of such biosensors should be mentioned:

a) ^{129}Xe MRI imaging – after an injection the xenon-biosensor complex is accumulated in organ or tissue proportionally to the concentration of the biomolecule its interact. In consequence, it plays the role of contrast agent.

b) Bioanalytical applications – if the ^{129}Xe NMR chemical shift of xenon-biosensor complex differs from the value for xenon-biosensor-biomolecule system, the ^{129}Xe NMR spectroscopy could be used as an excellent method

for a selective detection and determination of selected bioanalyte in complex mixtures.

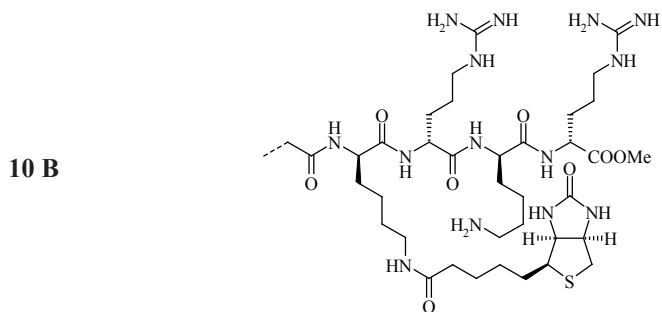
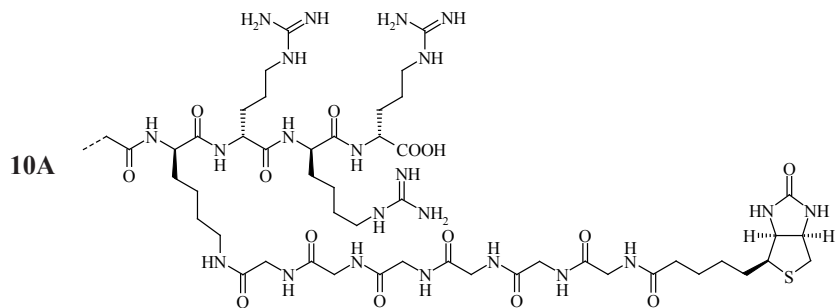
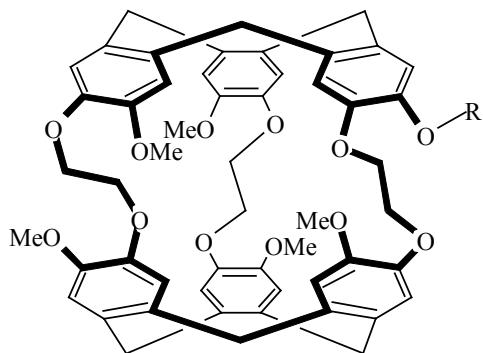
Because of the excellent affinity to xenon, cryptophane hosts were used as the carriers for xenon atoms. The enhancement of the sensitivity of the experiments with xenon-containing biosensors could be obtained if the hyperpolarized xenon was used. The concept of xenon-containing biosensors was described by Spence et al.³⁵ and the nicely micro-review on the xenon MRI contrast agents was published by Taratula and Dmochowski³⁶.

The first results of the usage of the functionalized xenon as biosensor were obtained for biotin substituted cryptophane (Fig. 8G), which interacted with avidin – the tetrameric biotin-binding protein produced in oviducts of oviparous animals and deposited in whites of their eggs³⁵. The spectra recorded in D₂O for free xenon-biosensor complex show one signal at 70.3 ppm. After avidin addition, the new resonance line, downfield shifted (at 72.7 ppm) was built. It comes from the xenon atom encapsulated in cage of the 8G host, bonded to the protein. Using of the biotin saturated avidin instead of free protein does not cause the formation of the signal at 72.7 ppm. The later studies of the same biosensor concentrated on the titration studies of the biotinylated ligand with the avidin and the kinetic of the exchange process between the protein-bonded and free form of the sensor³⁷. The further works were focused on the optimization of the avidin biosensor. The group of the biotin-containing cryptophane derivatives 8F, 10A-C were obtained and their interaction with avidin were studied by ¹²⁹Xe NMR spectroscopy. The following observations should be pointed out:

1. The diastereomeric splitting observed for studied ligands is higher for the complex with protein than for free biosensor;
2. The binding of the protein cause the increasing of the line width due to the change of the cryptophane cage motions after biosensor binding as well as the exchange process between free and bounded sensor. The observed line width values are 20-50 Hz;
3. For ligand 10A with rigid six-glycine linker ¹²⁹Xe NMR spectrum recorded for sample with excess of avidin shows four sharp signals. It probably comes from the existence of two independent biotin binding sites in the protein molecule. The ligands with more flexible linkers allows for more independent motions of the cryptophane units, thus reduce the effects of the neighborhoods and influence of the ligands on one another.
4. The decreasing of the linker length restricts the cage motions to the proximity of the protein surface. It causes larger effect on the ¹²⁹Xe chemical shifts, therefore the chemical shift sensitivity on the biosensor-

protein interactions for the short-linker ligands is much distinct then for that with longer one. The ligands with shorter linkers show also the higher line width values after binding by avidin. The biosensor 10C with the cage-biotin distance larger than 5.5 nm does not show any changes in ^{129}Xe NMR spectrum in the presence of avidin.

5. Partially deuterium-labeled analogues of sensor 8G show no effect of the deuterium on the ^{129}Xe NMR line width both in free ligand as well as in its complex with avidin. Therefore the dipole-dipole couplings contribution to the line width of ^{129}Xe signal was estimated to less than 1 Hz.
6. The signals show the significant temperature dependence. Both chemical shift and line width change with temperature variation. For all biosensors studied and their complexes with avidin, the δ ^{129}Xe values depend linearly on temperature (slope 0.27 ppm K^{-1}), similarly to the variations observed for unsubstituted cryptophane A xenon complex. This indicates on the similar interactions of encapsulated xenon atom with the ligand's cage, independently on the solvent used for NMR studies, the cage substitution and binding of the biosensor by avidin. The line width of the avidin-free biosensors 8F, 10A and 10C as well as for protein-bonded molecules 8F and 10C increases with the temperature increasing above 25-35°C. This indicates that the xenon exchange occurs for the systems studied with the rate constant $>30 \text{ s}^{-1}$. Therefore, above 25°C the exchange dependent relaxation contributes to the total relaxation time and, in consequence, to the line width of xenon atom. The line broadening due to exchange was estimated on 7 Hz. Below this temperature the xenon signal line width does not depend on the temperature variation, so the signal broadening must be connected with some of correlation time dependent mechanisms. For 10A-avidin system the ^{129}Xe NMR resonance line is the narrowest at 23°C and the line width increases above and below this value. The authors does not discuss this behavior. For ligand 8F the activation energy for the exchange process was calculated. It is about three times larger than for cryptophane-A/xenon system in $(\text{CDCl}_2)_2$, which could be explained by a higher enthalpic costs of xenon in water dissolution. The authors try to estimate also the contribution of chemical shift anisotropy relaxation to the signal width and state, that the effect observed could not be explained by this relaxation mechanism. They proposed an effect of the slow conformational exchange between multiply bound conformations as the possible explanation of this unexpected line width of Xe signals.



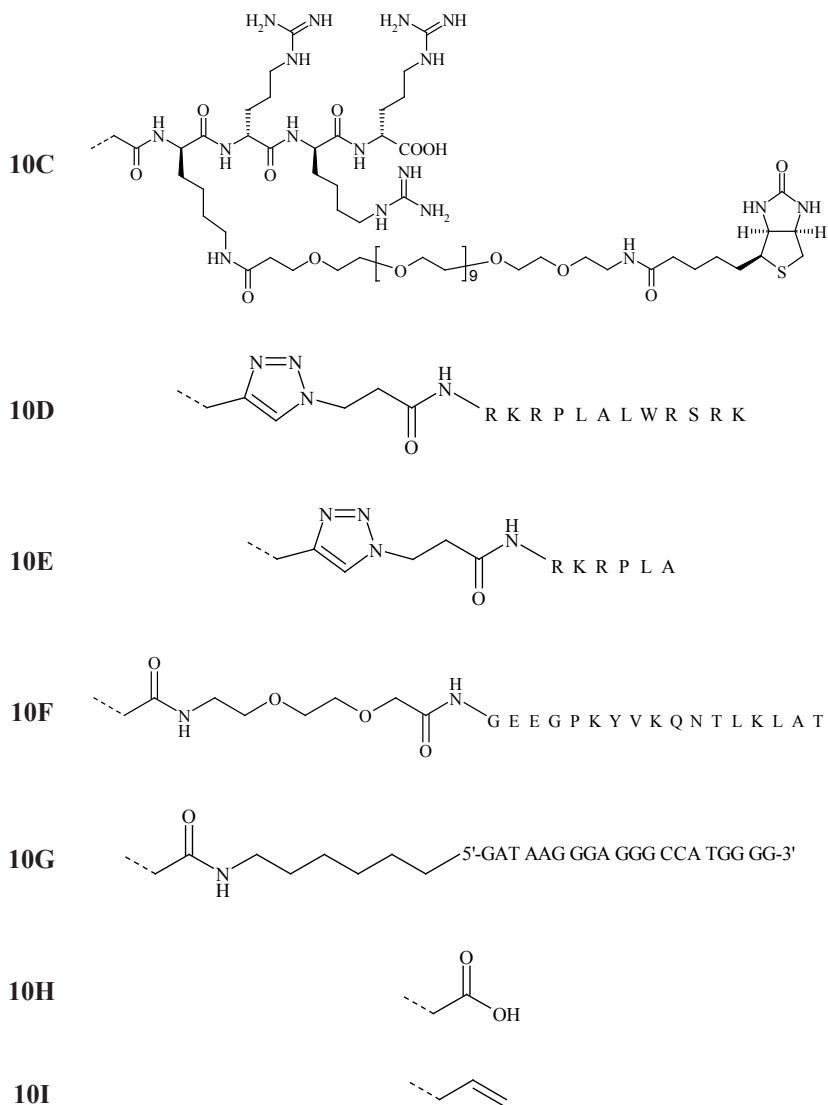


Figure 10. Peptide and DNA biosensors

The next examples of protein xenon biosensor are the molecules 11A-C, containing the sulfonamide moieties³⁸. They interact with human carbonic

anhydrase (CA), a protein involved in many physiological and biochemical processes, mainly the transport of carbon dioxide and the pH homeostasis. The interactions with two isozymes (CAI and CAII) were studied. The complex of biosensor 11B with CAII was obtained as single crystal and studied by X-ray diffraction³⁹. The dissociation constants of the biosensor-protein complexes were determined by ITC. The biosensors obtained contain no stereocenters in the linker part of the molecule to avoid the splitting of the Xe signal and, in consequence, the lowering of the signal intensity and increasing of its width due to diastereomers formation. All biosensor obtained were bounded by CAI and CAII, however the affinity to the CAII is higher for all studied molecules than for CAI. The ^{129}Xe NMR spectra recorded in water solutions of biosensors studied show single signals (Table 2). CA addition causes the formation of new signals, corresponding to the bonded biosensor. For some systems (CAI with 11C, CAII with 11B and 11C) two ^{129}Xe signals were observed due to the diastereomeric shift (diastereomers were formed in consequence of interaction of chiral ligand and chiral protein). For the rest of the systems both diastereomers have the same chemical shift value. The absence of this splitting could be explained as the result of the short distance between the xenon containing cage and the protein surface. This close proximity causes the partial desolvation of the cryptophane part. In consequence the net environmental changes felt by the Xe atom dominate the observed change of the $\delta^{129}\text{Xe}$ values over the diastereomeric considerations. The chemical shifts changes upon interaction with protein are 3.0-7.5 ppm, while the diastereomeric splittings are 1.3-4 ppm. The line widths of the biosensors studied only slightly increase in the presence of the anhydrase in comparison with those for free ligands (25-79 Hz vs. 23-50 Hz).

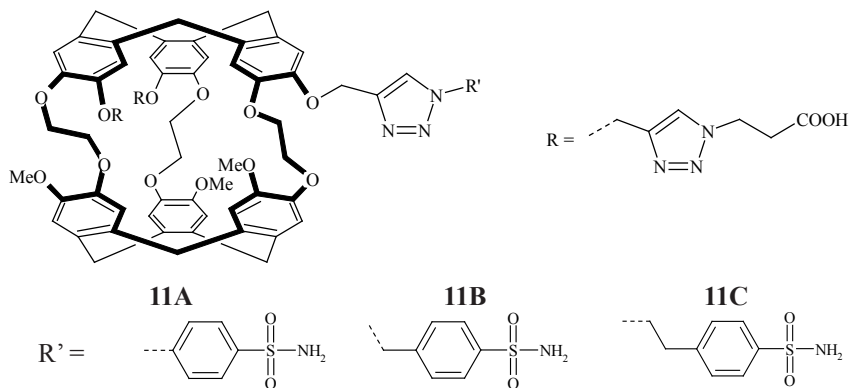


Figure 11. Anhydrase targeted biosensors

The metalloproteinase biosensors (Fig. 10D, E) were also studied⁴⁰. They are composed from the cryptophane A cage modified by oligopeptide chain. The matrix metalloproteinase MMP-7 was targeted for these studies. This enzyme is overexpressed and extracellularly localized in many oncologic diseases. Biosensor 10E is formed in the result of the 10D hydrolysis by MMP-7. The affinity of 10D to protein was estimated on the basis of fluorescence titration. The ^{129}Xe chemical shifts of Xe@10D and Xe@10E in water were given (Table 2). The spectra show the pair of signals due to the diastereomeric splitting. The difference in the chemical shifts of xenon encapsulated in both ligands was not fully elucidated, but the authors suggest that the difference of the charge of the both peptide chains results in the observed shift. No ^{129}Xe NMR data for biosensor-MMP-7 systems were given.

Another example of protein biosensors in the molecule 10F, which interacts with major histocompatibility complex (MHC) class II protein⁴¹. MHC class II molecules are cellular surface proteins of immunological relevance and participate in T cell mediated immune response. They play the significant role in autoimmune syndromes. The authors design the oligopeptide-containing ligand for detecting human leukocyte antigen DR1. The oligopeptide part of the biosensor molecule was the hemagglutinin peptide. The sensor-protein interaction was proved by ELISA assay as well as by ^{15}N - ^1H HSQC spectra. The ^{129}Xe NMR spectra of the biosensor show the single signal corresponding to encapsulated Xe atom (Table 2). After DR-1 protein addition the signal is shifted downfield by 1 ppm and its width increases slightly (37 Hz vs. 31 Hz for free sensor).

The biosensor for specific nucleotide sequence was described by Roy et al.⁴². The cage of cryptophane-A host was functionalized by 20-mer length oligonucleotide and the sensor obtained was used for DNA detection (Fig. 10G). To avoid the splitting of ^{129}Xe NMR signal due to diastereomeric interactions, the optical-pure (-)-cryptophane-A derivative was used for synthesis. The spectra were recorded for the biosensor mixtures with complementary or non-complementary DNA strands at micromolar concentrations. The hybridization was confirmed by ^1H NMR spectra – for the mixture of biosensor with complementary strand the NH signals at 13 ppm were detected. The spectrum of the free sensor shows one signal at 68.5 ppm. For the samples containing non-complementary strands no shift of the ^{129}Xe NMR signal of the encapsulated xenon in comparison with that of unbonded sensor was observed. The interactions with complementary strand cause the upfield shift of the signal of about 1.5 ppm. The ^{129}Xe NMR spectrum recorded at higher, milimolar concentrations, shows different, peculiar features. The spectrum of the unbonded ligand consists of three broad peaks

(71.0, 69.0 and 67.7 ppm). The similar spectrum was obtained for the mixture with non-complementary strand, but the relative intensities of those resonance lines were different. The signals ratio depends also on the ionic strength of the solution – the addition of NaCl to the solution containing biosensor and non-complementary strand causes the diminishes of the central signal, does not influence on the intensity of the signal at 67.7 ppm and it causes a predomination of the downfield shifted peak. The spectrum of the mixture with complementary strand shows only one peak. Such behavior could be explained by two effects:

- micelles formation, with the cryptophane cages associated as a core;
- bilayer vesicles formation, with the cages forming the internal layer.

The increasing of the NaCl concentration causes the micellar form replacement by larger aggregates (vesicles). The hybridization with the complementary strand causes the stabilization of the monomeric form.

Quite different approach of the biosensor-labeling of the biomolecule was shown by Mynar et al.⁴³. The carboxylic analogue of cryptophane-A ligand (Fig. 10H) was non-covalently bonded by PPI and PAMAM dendrimers (Fig. 12A-D). The PAMAM G5 dendrimer containing the biotin moiety (Fig. 12E) was also obtained. The authors determine the maximal number of the cryptophane cages encapsulated by dendrimer molecule (2 for PPI G4, 4 for PPI G5, 7 for PAMAM G4 and 11 for PAMAM G5, respectively) and discuss the ¹²⁹Xe NMR properties of that systems. For PPI/Xe@10H systems the signal was observed at 63 ppm, while for PAMAM/Xe@10H at 59 ppm. The signals line widths are 12 Hz and 80 Hz, respectively. These parameters did not vary with change of dendrimer/cage ratios and dendrimer generation. This indicates on high mobility of Xe@10H complexes inside the dendrimer sphere. The biotin containing host could bound up to three Xe@10H molecules. This value decreases to two, when this construct interacts with avidin molecule, probably due to unfavorable interactions of cage-dendrimer complex with protein surface. However, the signal-to-noise ratio of the ¹²⁹Xe NMR spectra for 12E/Xe@10H/avidin system is about 8 time better than for the previously described avidin biosensors. This is the result of the doubling of the Xe atoms per one protein molecule, avoiding of the diastereomeric splitting and decreasing of the line width. Additionally, interactions of uncomplexed xenon with dendrimer could cause an increasing of the xenon concentration around the dendrimer-bounded cages.

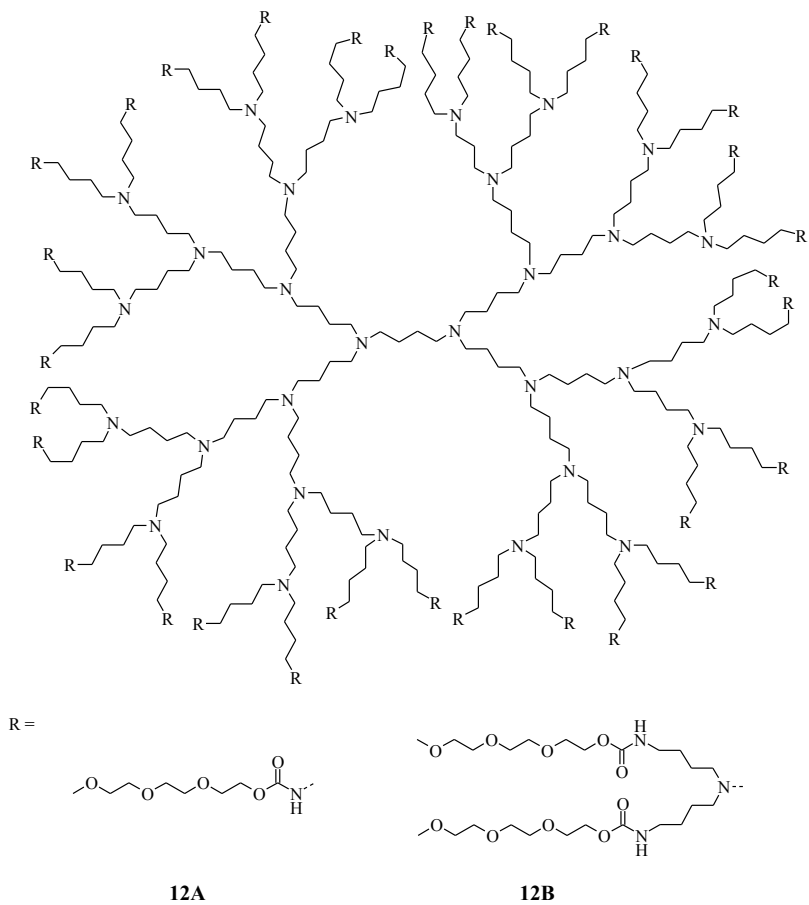


Figure 12. Dendrimers used as cryptophane carriers

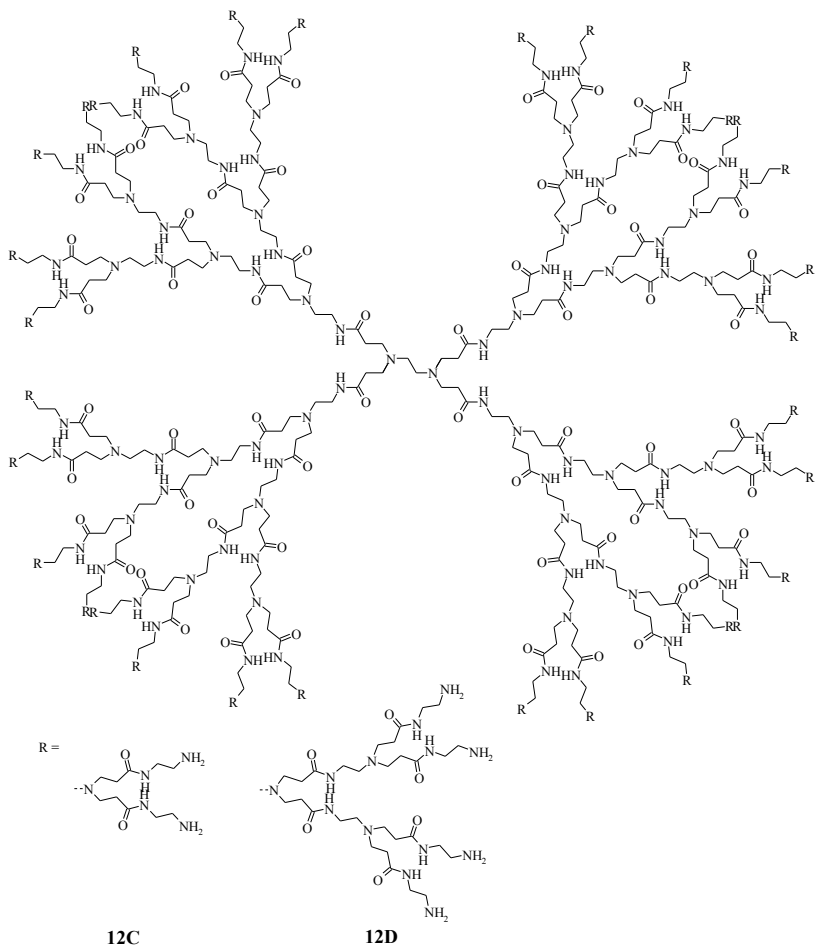


Figure 12 (cont.). Dendrimers used as cryptophane carriers

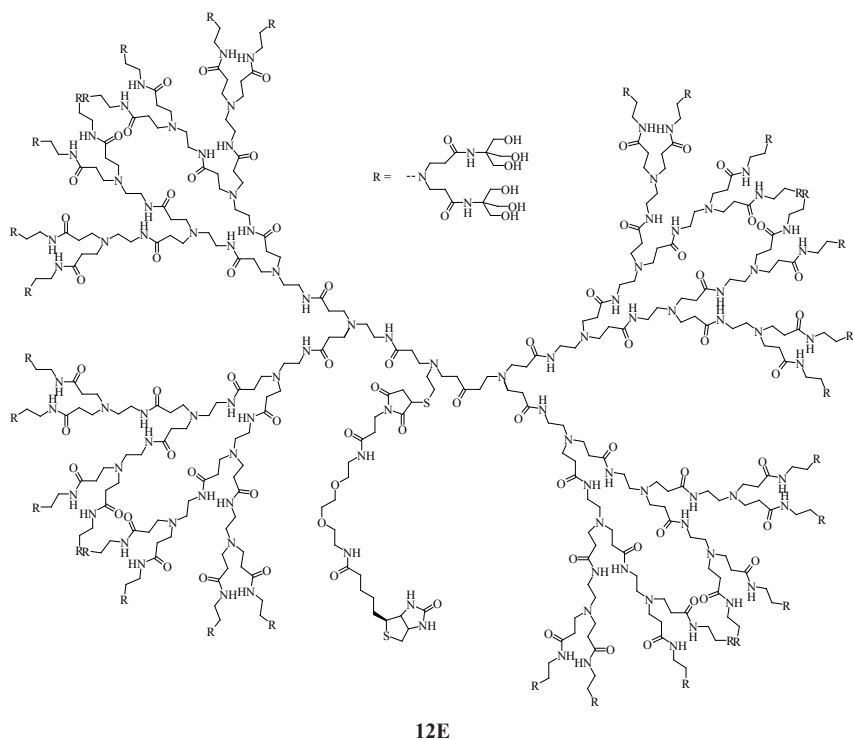
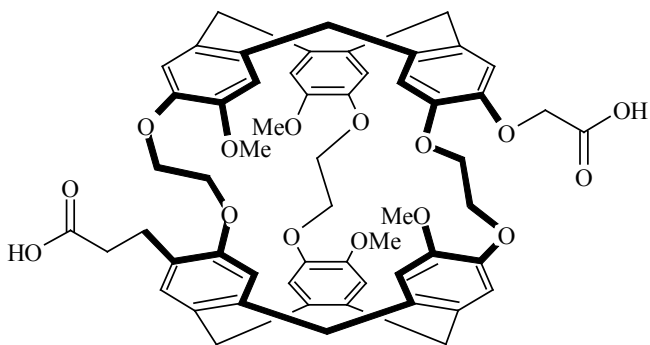


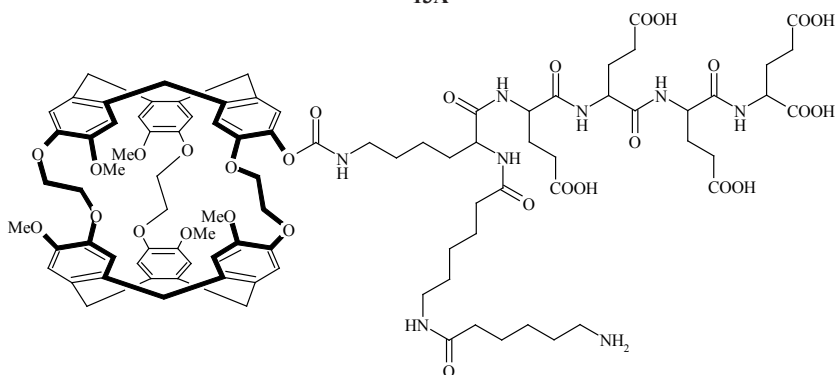
Figure 12 (cont.) Dendrimers used as cryptophane carriers.

The interactions of xenon-based molecular sensors in lipid suspensions were studied by Meldrum et al.⁴⁴. It is important from the *in vivo* biosensors application point of view. The interaction of hydrophobic part of their molecules with lipid membranes could affect the signal and sensing of the specific molecules. The studies were performed for diacid cryptophane analogue (Fig. 13A) as the xenon binder. At 298 K the spectra of 13A obtained in xenon saturated water saturated shows two signals – first one corresponding to water dissolved Xe (189 ppm), second one to the Xe@13A complex (62 ppm; Table 2). The experiments performed for 13A in 1% lipid/water suspension containing Xe, show three signals – two of them at the chemical shifts values the same as for Xe/13A/water system and additional one at 73 ppm, which corresponds to Xe@13A in lipid environment. The integration of the signals indicates on the about 50 times greater affinity of Xe@13A to lipids than to water. The increasing of the lipid/

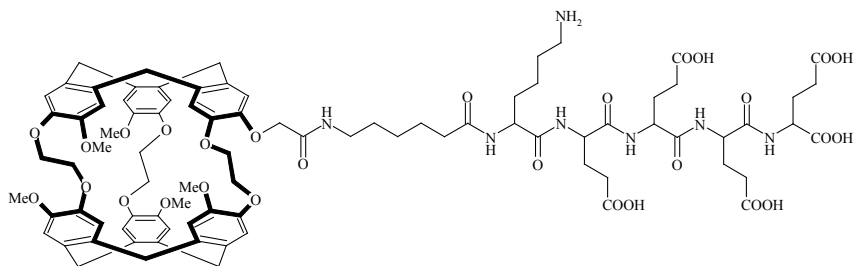
water ratio causes the decreasing of $\text{Xe}@13\text{A}_{aq}$ signal, which disappears when the lipid content is more than 10%. The signal of free xenon shifts downfield with the increasing of the lipid concentration in the sample, also its width increases significantly. The fitting of this signal with two Lorentzian curves gives the two signals resolved by about 1 ppm. More downfield shifted peak of these resonances is broader and was assigned as lipid-soluted xenon. The difference in chemical shifts of the $\text{Xe}@13\text{A}$ encapsulated in water and lipid systems is about 10 times larger than for free xenon. Below the 298 K the signals of Xe_{aq} and Xe_{lipid} were distinguishable and showed different temperature dependence ($\delta^{129}\text{Xe}_{aq} \sim T^2$ while $\delta^{129}\text{Xe}_{lipid} \sim -T$). Both signals of $\text{Xe}@13\text{A}$ show the linear temperature dependence, the slope for $\text{Xe}@13\text{A}_{aq}$ is 0.31 ppm K^{-1} , for $\text{Xe}@13\text{A}_{lipid}$ 0.18 ppm K^{-1} . The experimental conditions (saturation frequency) effect on the saturation transfer and MR images were also studied.



13A



13B



13C

Figure 13. Functionalized cryptophane-A ligands

The molecule 13B was used for studies of hyperpolarized nuclei chemical exchange saturation transfer (hyper-CEST) applications for ultrasensitive NMR detection and the temperature response of ^{129}Xe depolarization transfer⁴⁵. It was shown that the detection of the cryptophane biosensor at the 10 nM concentration was possible, which was far below the detection limit of UV-Vis spectroscopy.

The xenon containing supramolecular biosensors were used for magnetic resonance imaging. The molecule 10A was chosen for MRI images obtaining of avidin-modified agarose beads^{46,47}. The chemical shift imaging of two-phase (water/tetrachloroethane) system containing 3E and 9A was also presented⁴⁸.

Schielling et al. have shown the utility of ^{129}Xe NMR spectroscopy of encapsulated, hyperpolarized xenon as the MRI thermometer. The sensor (Fig. 13C) was used as a model compound. For the studied cryptophane construct huge temperature shift of ^{129}Xe resonance was observed (0.29 ppm K⁻¹). The authors present the temperature mapping of the sample (phantoms), using direct NMR detection (sensor concentration 150 μM) or indirect experiment (hyper-CEST sequence).

References

1. M. Gerken, G.J. Schrobilgen, The impact of multi-NMR spectroscopy on the development of noble-gas chemistry, *Coord. Chem. Rev.*, **197**, **2000**, 335-395
2. C.I. Ratcliffe, Xenon NMR, *Ann. Rep. NMR Spectroscopy*, **36**, **1998**, 123-221
3. D. Raftery, Xenon NMR Spectroscopy, *Ann. Rep. NMR Spectroscopy*, **57**, 2006, 205-270
4. G.J. Schrobilgen, Noble gas elements. w: D.M. Grant, R.K. Harris

- (red.), *The Encyclopedia of Nuclear Magnetic Resonance*, Willey, New York, **1996**, 3251-3262
5. J.F. Lehmann, H.P.A. Mercier, G.J. Schrobilgen, The chemistry of krypton, *Coord. Chem. Rev.*, 233-234, **2002**, 1-39
 6. J. Reisse, M. Claessens, O. Fabre, G. Michaux, M.L. Stien, D. Zimmermann, Heterocycles and intermolecular interactions, *Bull. Soc. Chim. Belg.*, 92, **1983**, 819-824
 7. M. Claessens, O. Fabre, D. Zimmermann, J. Reisse, NMR study of molecular interactions between xenon and crown ethers, *Bull. Soc. Chim. Belg.*, 93, **1984**, 983-989
 8. K. Bartik, M. Luhmer, S.J. Heyes, R. Ottinger, J. Reisse, Probing molecular cavities in α -cyclodextrin solutions by xenon NMR, *J. Magn. Reson. B*, 109, **1995**, 164-168
 9. J.A. Ripmeester, C.I. Ratcliffe, J.S. Tse, The nuclear magnetic resonance of ^{129}Xe trapped in clathrates and some other solids, *J. Chem. Soc. Faraday Trans. 1*, 84, **1988**, 3731-3745
 10. M.E. Haouaj, M. Luhmer, Y.H. Ko, K. Kim, K. Bartik, NMR study of the reversible complexation of xenon by cucurbituril, *J. Chem. Soc. Perkin Trans. 2*, **2001**, 804-807
 11. M.E. Haouaj, Y.H. Ko, M. Luhmer, K. Kim, K. Bartik, NMR investigation of the complexation of neutral guests by cucurbituril, *J. Chem. Soc. Perkin Trans. 2*, **2001**, 2104-2107
 12. B.S. Kim, Y.H. Ko, Y. Kim, H.J. Lee, N. Selvapalm, H.C. Lee, K. Kim, Water soluble cucurbit[6]uril derivative as a potential Xe carrier for ^{129}Xe NMR-based biosensors, *Chem. Commun.*, **2008**, 2756-2758
 13. K. Bartik, M. Luhmer, J.-P. Dutasta, A. Collet, J. Reisse, ^{129}Xe and ^1H NMR study of the reversible trapping of xenon by cryptophane-A in organic solution, *J. Am. Chem. Soc.*, 120, **1998**, 784-791
 14. M. Luhmer, B.M. Goodson, Y.Q. Song, D.D. Laws, L. Kaiser, M.C. Cyrier, A. Pines, Study of xenon binding by cryptophane-A using laser-induced NMR polarization enhancement, *J. Am. Chem. Soc.*, 121, **1999**, 3502-3512
 15. T. Brotin, J.-P. Dutasta, Xe@cryptophane complexes with C_2 symmetry: synthesis and investigations by ^{129}Xe NMR of the consequence of the size of the host cavity for xenon encapsulation, *Eur. J. Org. Chem.*, **2003**, 973-984
 16. H.A. Fogarty, P. Berthaut, T. Brotin, G. Huber, H. Desvaux, J.-P. Dutasta, A cryptophane core optimized for xenon encapsulation, *J. Am. Chem. Soc.*, 129, **2007**, 10332-10333

17. G. Huber, L. Beguin, H. Desvaux, T. Brotin, H.A. Fogarty, J.-P. Dutasta, P. Berthault, Cryptophane-xenon complexes in organic solvents observed through NMR spectroscopy, *J. Phys. Chem. A*, 112, **2008**, 11363-11372
18. T. Brotin, A. Lesage, L. Emsley, A. Collet, ^{129}Xe NMR spectroscopy of deuterium labeled cryptophane-A xenon complexes: investigation of host-guest complexation dynamics, *J. Am. Chem. Soc.*, 122, **2000**, 1171-1174
19. T. Brotin, T. Devic, A. Lesage, L. Emsley, A. Collet, Synthesis of deuterium labeled cryptophane-A and investigation of Xe@cryptophane complexation dynamics by 1D EXSY NMR experiments, *Chem. Eur. J.*, 7, **2001**, 1561-1573
20. M. Darzac, T. Brotin, L. Rousset-Arzel, D. Bouchu, J.-P. Dutasta, Synthesis and applications of cryptophanol hosts: ^{129}Xe NMR spectroscopy of a deuterium-labeled (Xe)₂@bis-cryptophane complex, *New J. Chem.*, 28, **2004**, 502-512
21. D.N. Sears, C.J. Jameson, Theoretical calculations of the Xe chemical shifts in cryptophane cages, *J. Chem. Phys.*, 119, **2003**, 12231-12244
22. J.G. Huber, L. Dubois, H. Desvaux, J.-P. Dutasta, T. Brotin, P. Berthault, NMR study of optically active monosubstituted cryptophanes and their interactions with xenon, *J. Phys. Chem. A*, 108, **2004**, 9608-9615
23. E.J. Ruiz, D.N. Sears, A. Pines, C.J. Jameson, Diastereomeric Xe chemical shifts in tethered cryptophane cages, *J. Am. Chem. Soc.*, 128, **2006**, 16980-16988
24. K. Bartik, M. El Haouaj, M. Luhmer, A. Collet, J. Reisse, Can monoatomic xenon become chiral?, *ChemPhysChem*, 221-224, **2000**, 221-224
25. K. Bartik, M. Luhmer, A. Collet, J. Reisse, Molecular polarization and molecular chiralization: the first example of a chiralized xenon atom, *Chirality*, 13, **2001**, 2-6
26. N. Branda, R.M. Grotzfeld, C. Valdés, J. Rebek, Jr., Control of self-assembly and reversible encapsulation of xenon in self-assembling dimer by acid-base chemistry, *J. Am. Chem. Soc.*, 117, **1995**, 85-88
27. E.B. Brouwer, G.D. Enright, J.A. Ripmeester, Solid-state NMR and diffraction studies of p-tert-butylcalix[4]arene-nitrobenzene-xenon. *Chem. Commun.*, **1997**, 939-940
28. A. Dubes, I.L. Moudrakovski, P. Shahgaldian, A.W. Coleman, C.I. Ratcliffe, J.A. Ripmeester, Distribution and modification of sorption sites in amphiphilic calixarene-based solid lipid nanoparticles from

- hyperpolarized ^{129}Xe NMR spectroscopy, *J. Am. Chem. Soc.*, 126, **2004**, 6236-6237
29. G.S. Ananchenko, I.L. Moudrakovski, A.W. Coleman, J.A. Ripmeestes, A channel-free soft-walled capsular calixarene solid for gas adsorption, *Angew. Chem. Int. Ed.*, 47, **2008**, 5616-5618
 30. J. Fukutomi, Y. Adachi, A. Kaneko, A. Kimura, H. Fujiwara, Inclusion complex formation of thiacalix[4]arene and Xe in aqueous solution studied by hyperpolarized ^{129}Xe NMR, *J. Includ. Phenom. Macrocycl. Chem.*, 58, **2007**, 115-122
 31. D.J. Cram, M.E. Tanner, C.B. Knobler, Guest release and capture by hemicarcerands introduces the phenomenon of constrictive binding, *J. Am. Chem. Soc.*, 113, **1991**, 7717-7737
 32. D. Bardelang, K.A. Udachin, R. Anedda, I. Moudrakovski, D.M. Leek, J.A. Ripmeester, C.I. Ratcliffe, Single-crystal to single-crystal phase transition of cucurbit[5]uril hydrochloride hydrates: large water-filled channels transforming to layers of unusual stability, *Chem. Commun.*, **2008**, 4927-4929
 33. G. Huber, T. Brotin, L. Dubois, H. Desvaux, J.-P. Dutasta, P. Berthaut, Water soluble cryptophanes showing unexpected affinity for xenon: candidates as NMR-based biosensors, *J. Am. Chem. Soc.*, 128, **2006**, 6239-6246
 34. P. Aru Hill, Q. Wei, R.G. Eckenhoff, I.J. Dmochowski, Thermodynamics of xenon binding to cryptophane in water and human plasma, *J. Am. Chem. Soc.*, 129, **2007**, 9262-9263
 35. M.M. Spence, S.M. Rubin, I.E. Dimitrov, E.J. Ruiz, D.E. Wemmer, A. Pines, S.Q. Yao, F. Tian, P.G. Schultz, Functionalized xenon as a biosensor, *Proc. Natl. Acad. Sci. USA*, 98, **2001**, 10654-10657
 36. O. Taratula, I.J. Dmochowski, Functionalized ^{129}Xe contrast agents for magnetic resonance imaging, *Curr. Opt. Chem. Biol.*, 14, **2010**, 97-104.
 37. M.M. Spence, E.J. Ruiz, S.M. Rubin, T.J. Lowery, N. Winssinger, P.G. Schultz, D.E. Wemmer, A. Pines, Development of a functionalized xenon biosensor, *J. Am. Chem. Soc.*, 126, **2004**, 15287-15294
 38. J.M. Chambers, P.A. Hill, J.A. Aaron, Z. Han, D.W. Christianson, N.N. Kuzma, I.J. Dmochowski, Cryptophane xenon-129 nuclear magnetic resonance biosensors targeting human carbonic anhydrase, *J. Am. Chem. Soc.*, 131, **2009**, 563-569
 39. J.A. Aaron, J.M. Chambers, K.M. Jude, L. Di Costanzo, I.J. Dmochowski, D.W. Christianson, Structure of a ^{129}Xe -cryptophane biosensor complexed with human carbonic anhydrase II, *J. Am. Chem.*

- Soc.*, 130, **2008**, 6942-6943
40. Q. Wei, G.K. Seward, P.A. Hill, B. Patton, I.E. Dimitrov, N.N. Kuzma, I.J. Domochoowski, Design ^{129}Xe NMR biosensors for matrix metalloproteinase detection, *J. Am. chem. Soc.*, 128, **2006**, 13274-13283
 41. A. Schlundt, W. Kilian, M. Beyermann, J. Stich, S. Günther, S. Höpner, K. Falk, O. Roetzschke, L. Mitschang, C. Freud, A xenon-129 biosensor for monitoring MHC-peptide interactions, *Angew. Chem. Int. Ed.*, 48, **2009**, 4142-4145
 42. V. Roy, T. Brotin, J-P. Dutasta, M-H. Charles, T. Delair, F. Mallet, G. Hubert, H. Desvaux, Y. Boulard, P. Berthault, A cryptophane biosensor for the detection of specific nucleotide targets through xenon NMR spectroscopy, *ChemPhysChem*, 8, **2007**, 2082-2085
 43. J.L. Mynar, T.J. Lowery, D.E. Wemmer, A. Pines, J.M.J. Frecht, Xenon biosensor amplification via dendrimer-cage supramolecular constructs, *J. Am. Chem. Soc.*, 128, **2006**, 6334-6335
 44. T. Meldrum, L. Schröder, P. Denger, D.E. Wemmer, A. Pines, Xenon-based molecular sensor in lipid suspensions, *J. Magn. Reson.*, 205, **2010**, 242-246
 45. L. Schröder, T. Meldrum, M. Smith, T.J. Lowery, D.E. Wemmer, A. Pines, Temperature response of ^{129}Xe depolarization transfer and its application for ultrasensitive NMR detection, *Phys. Rev. Lett.* 100, **2008**, 257603(4)
 46. C. Hilty, T.J. Lowery, D.E. Wemmer, A. Pines, Spectrally resolved magnetic resonance imaging of a xenon biosensor, *Angew. Chem. Int. Ed.*, 45, **2006**, 70-73
 47. L. Schröder, T.J. Lowery, C. Hilty, D.E. Wemmer, A. Pines, Molecular imaging using a targeted magnetic resonance hyperpolarized biosensors, *Science*, 314, **2006**, 446-449
 48. P. Berthault, A. Bogaert-Buchmann, H. Desvaux, G. Huber, Y. Boulard, Sensitivity and multiplexing capabilities of MRI based on polarized ^{129}Xe biosensors, *J. Am. Chem. Soc.*, 130, **2008**, 16456-16457
 49. F. Schilling, L. Schröder, K.K. Palaniappan, S. Zapf, D.E. Wemmer, A. Pines, MRI thermometry based on encapsulated hyperpolarized xenon, *ChemPhysChem*, DOI: 10.1002/cphc.201000507

Chapter 7

Applications of matrix-assisted laser desorption ionization mass spectrometry to synthetic polymers

Grażyna Bartkowiak and Grzegorz Schroeder

*Faculty of Chemistry, Adam Mickiewicz University, Grunwaldzka 6,
60-780 Poznań, Poland*

1. Introduction

Synthetic polymers became inseparable part of our life, providing the most common packaging materials, fibers of fabric, disposable dishes, artificial glass and wood, components of instruments and many other applications. They present very desired features like lightness, softness, transparency, mechanical properties and durability. However, the increasing use of plastics causes serious ecological problems due to their accumulation in the environment. Therefore, among synthetic polymers, the biodegradable ones play very important role in many fields of our life. They are considered as “eco-friendly”¹ and became indispensable in medical usage for drug delivery and for the manufacture of dissolvable sutures^{2,3,4,5}.

However, polymers are not homogenous materials: they possess various structures, may have straight linear or branched chains, contain cyclic structures, can be homopolymers, copolymers or mixtures of homo- and co-polymers. The complex nature of polymers structure causes problems with their characterization.

The first step in the analysis of polymeric materials is the identification of their molecular structure. The structure and degradation of polymers may be studied by different techniques. Many factors, which affect polymer properties, are important, such as particle size and shape, molecular weight and molecular weight distribution, polydispersity, the number and sequencing of repeat units, terminal functionalities, presence of cyclic structures, residual monomer concentration, isomeric percentage, recognition of polymer additives (like antioxidants or plasticizers), metal impurities from the catalyst and others.

Methods of polymer analysis include⁶:

1. for molecular mass evaluation: gel permeation chromatography (GPC)/size exclusion chromatography (SEC), osmometry, viscometry, light

- scattering;
2. for determination of repeat units sequence: nuclear magnetic resonance;
 3. for end-groups analysis: titration, NMR and FT-IR spectroscopy;
 4. for the evaluation of polymer purity: elemental analysis, NMR and FT-IR spectroscopy;
 5. for other physicochemical parameters (decomposition temperature, crystallinity, glass transition temperature T_g , melting temperature T_m) evaluation: thermo-gravimetric analysis (TGA), differential scanning calorimetry (DSC).

As shown above, there is no single technique which could be applied for complete characterization of a polymer sample. A powerful tool to study polymer structure appeared mass spectrometry. Mass spectrometric analysis has frequently been used to determine many polymer parameters, i.e. average molecular mass, molecular mass distribution (MMD), polydispersity (PD), terminal functional groups and others, often difficult to obtain by NMR or IR. However, the application of MS to large molecules of synthetic polymers has been limited due to low volatility and thermal instability of these materials. These difficulties have been overcome through the development of soft ionization techniques, such as chemical ionization (CI)^{7,8}, secondary-ion mass spectrometry (SIMS)^{7,8}, fast atom bombardment (FAB)^{7,8}, electrospray ionization (ESI) or matrix-assisted laser desorption/ionization (MALDI).

First of all, an effective ionization technique for high molecular weight synthetic polymers appeared to be MALDI-MS^{9,10,11,12}. This technique allows for the mass determination of large molecules of synthetic polymers by ionization and vaporization without degradation.

In MALDI-MS technique the matrix (circa 100-fold molar excess) and polymer are mixed in the appropriate solvent and placed onto the MALDI target. The solvent evaporates, allowing co-crystallization of polymer sample with matrix molecules. During the co-crystallization, polymer molecules are homogeneously dispersed within matrix molecules, which are able to absorb extensively ultraviolet laser light and transfer the absorbed energy to the analyte. As a result of this process, intact charged polymer molecules are transferred into the gas phase. The laser energy is spent mainly in volatilizing matrix and analyte and not in fragmenting the polymer chain. The crucial factor in MALDI MS application to synthetic polymers is a choice of an appropriate polymer/matrix mixture. Conventionally used matrix materials proved not to be compatible with organic-soluble polymers, which caused analytical complications, because the matrices working well for polar biopolymers are not useful for nonpolar synthetic polymers. Water-soluble synthetic polymers turn out to be capable of

analysis in similar conditions as large biomolecules, whereas the organic-soluble ones frequently demand special types of matrices. A specific kind of matrix, i.e. a fine metal (Co) powder dispersed in glycerol, has been used by Koichi Tanaka and his co-workers¹³ to achieve at the first time desorption of PEG 20000 in MALDI MS measurement. Nowadays, a broad spectrum of matrices have been used for polymer analysis (Table 1).

Organic-soluble synthetic polymers often do not have a proper concentration of ionized species and need an addition of cationizing agent to increase a number of ions in the analyte¹⁴. As the cationizing species are utilised often alkaline salts (LiCl, NaCl, KCl) and silver trifluoroacetate¹⁴.

The fundamental works concerning MALDI MS application to the polymer analysis did M. Karas and F. Hillenkamp (with co-workers)^{14,15}. They obtained MALDI mass spectra for poly(ethylene glycol)s PEG and poly(propylene glycol)s PPG with well resolved oligomers peaks, mainly sodiated and potassiated, with the distance between oligomer peaks corresponding to the expected values respective to the repeat unit mass (44 Da for PEG and 58 Da for PPG – Fig. 1.).

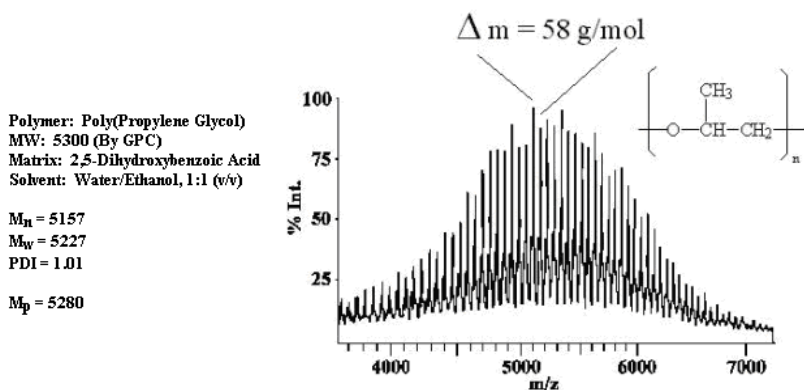


Figure 1. MALDI spectrum of PPG 5300, matrix: DHB. The spectrum consists of number of peaks with the constant distance, i.e. constant mass difference $\Delta m = 58 \text{ Da}$, corresponding to the mass of repeat unit $[-O-CH(CH_3)-CH_2-]$.¹⁴

The authors¹⁴ found that Na^+ and K^+ cations become attached to the polymer molecules even without doping with alkaline salts (NaCl, KCl). The alkali cations may originate from solvent impurities or glassware. It turned out that oligomers are desorbed intact, without fragmentation, from analyte/matrix

mixture. This phenomenon allowed for average molecular weight calculation from the MALDI mass spectra of polymers.

Karas and Hillenkamp obtained as first mass spectra for as large polymer molecules as polystyrene PS46000 and polystyrene PS70000¹⁴, the largest polymer molecules analyzed by MALDI at that time (Fig.2).

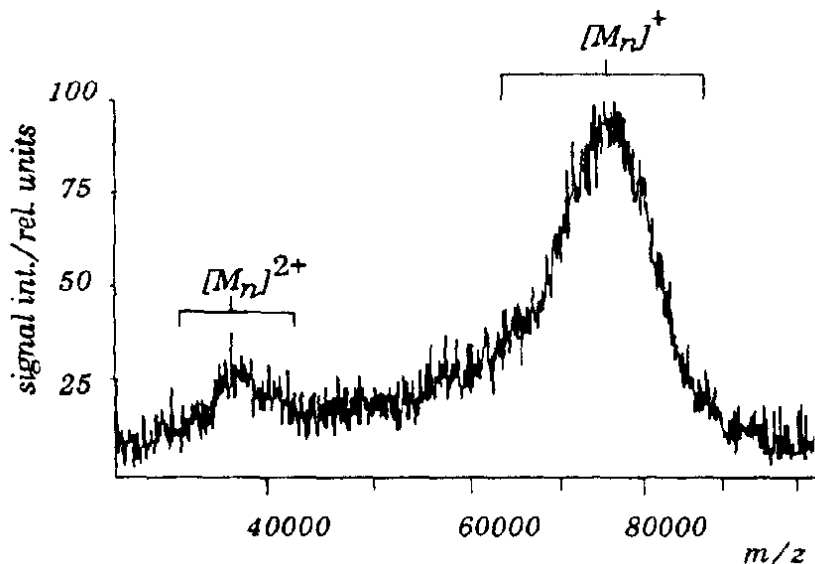


Figure 2. MALDI mass spectrum of polystyrene PS70000, the largest polymer successfully investigated by Karas and Hillenkamp¹⁴ to 1992.

They proved usefulness of silver cationization for the nonpolar polymers (they applied PS cationization with $\text{CF}_3\text{COO}\cdot\text{Ag}^+$) and the presence of dimers, trimers and tetramers in the PS spectrum (Figure 3). As a matrix for polystyrenes 2-nitrophenyl octyl ether (NPOE), a highly viscous liquid, was used, because commonly used 2,5-dihydroxy-benzoic acid (DHB) showed a separation of matrix crystals and polymer. The authors conclude that the crucial problem is a selection of the proper matrix, which should be satisfactory miscible with the polymer sample. The expanded part of the spectrum (Fig. 3) displays that the mass of repeat unit (104 Da) can still be distinguished from the peak distance in the spectrum.

Poly(Styrene)
MW: 20 000 (by GPC)
matrix: 2-nitrophenyl
octyl ether
cat. agent: silver
trifluoroacetate

Mn = 19 337
Mw = 19 509
PD = 1.01

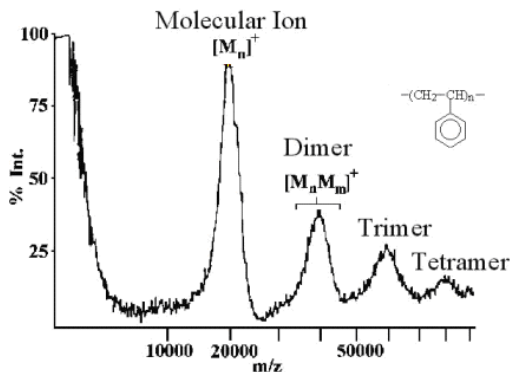


Figure 3. MALDI MS spectrum of PS 20000, laser wavelength: 337 nm, instrument LAMMA1000.¹⁴

2. Factors influencing the quality of MALDI mass spectra of synthetic polymers

2.1. Solvents

Many factors are important for the quality of the MALDI MS spectrum of synthetic polymers, mainly concerning the sample preparation^{14,16,17,18,19,20,21}. The critical factors are: the type of matrix, the cationization reagent, their concentrations, the type of solvent or solvent mixture, the spotting technique, the cocrystallization of analyte and matrix. There are many works devoted to the choice of the optimal solvent^{19,20,21,22,23,24,25}. The main conclusion is that the best results are obtained by using the same solvent for every component of the sample²⁶, i.e. polymer, matrix, and cationizing agent. For non-polar polymers tetrahydrofuran (THF), toluene and chloroform are frequently used as solvents, whereas for polar ones acetone, methanol, acetonitrile and water or their mixtures are chosen. The caution must be retained with THF because of the presence of peroxides which may cause the oxidation of chemically active groups²⁷. Brandt et al.²⁵ checked a wide range of solvents for polystyrene PS7600 and poly(ethylene glycol) PEG4820, from polar ones such as water, alcohols and DMSO to non-polar ones such as toluene, benzene and n-alkanes. Especially for PS7600 some solvent other than THF, e.g., acetone, dimethyl carbonate, and methyl ethyl ketone turned out to be appropriate.

The choice of solvent is often based on experience, trial-and-error and traditional rules such as “like dissolves like”. There are many factors involved, like evaporation rate, solution viscosity, environmental aspects, the effectiveness

of dissolution the given materials as well as solubility scales, like heptane number or Hildebrand and Hansen solubility parameters²⁸. The three-dimensional solubility parameter system, employed by Hansen²⁸, based on three parameters: the dispersion force component (δ_d), the polar component (δ_p) and the hydrogen bonding component (δ_h), was shown to be most useful²⁵.

A new approach to the solvent in MALDI techniques for polymers is the development of solvent-free sample preparation^{29,30,31}, which appeared useful for solubility-restricted compounds, like polyamides (<5000 Da) and many high-molecular weight polymers, e.g., poly(methyl methacrylate) and polystyrene.

2.2. MALDI matrices for polymer analysis

MALDI matrix for polymers, in positive mode of operation, must protonate the analyte so that it is charged, but such ionization must be done without degradation. Acidic matrices, acidic solvents or addition of any acid to the matrix/analyte solution may initiate the polymer degradation, especially the biodegradable ones^{32,33}. The resulting spectrum of a degraded polymer shows increasing of peaks intensity with the decreasing of ion masses, leading to the “wedge shape” toward the low-mass region of the spectrum³⁴.

As a consequence, some information about the average molecular weight of the polymer may be limited or biased. To overcome this problem, new type of matrices has been developed, namely ionic liquid matrices (ILMs).³⁴

The choice of a matrix tailored for a specific kind of polymer sample is critical for successful MALDI analysis. There are two steps of selection of a proper matrix:

1. a search in literature, where suggested optimal matrices for a particular type of compounds can be found;
2. the recording of spectra with 3-4 matrices chosen to match the best one.

To accelerate the selection process, one can use the tabulations of MALDI matrices, which appear for example at the NIST website³⁵.

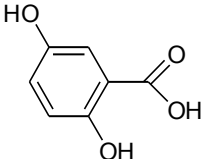
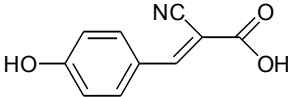
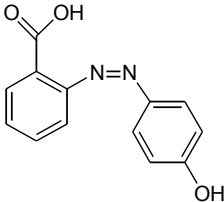
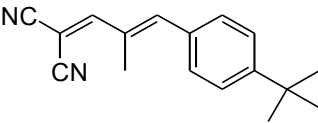
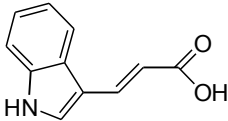
There are some empirical facts about the known matrices, which can be useful for their proper choice:

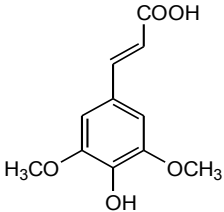
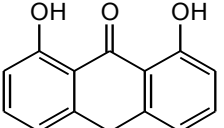
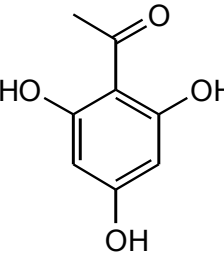
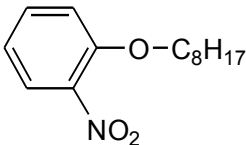
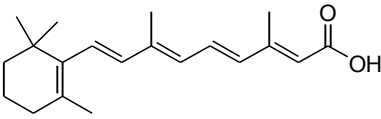
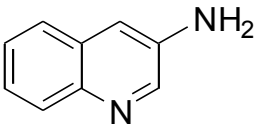
- α -cyano-4-hydroxycinnamic acid (CHCA) is considered as a “hot matrix”, stimulating the molecule’s destruction, so it is used for fragmentation experiments;
- 3-amino-4-hydroxybenzoic acid and POPOP (i.e. 1,4-bis(5-phenyloxazol-2-yl)benzene) have a high irradiance threshold, so they need high laser energy;
- all-*trans*-retinoic acid is more sensitive for impurities as other matrices (like HABA and dithranol);

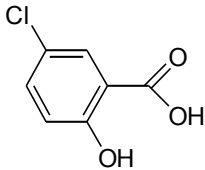
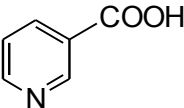
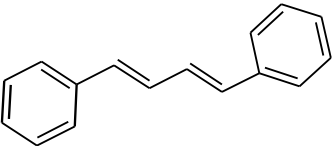
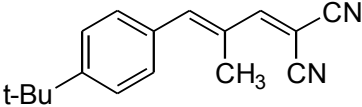
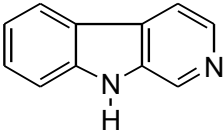
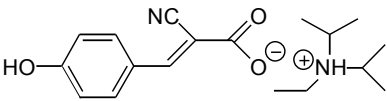
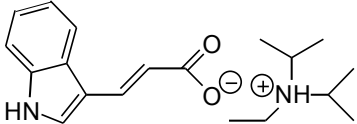
- 5-chlorosalicylic acid is preferred for nonpolar polymers, whereas trihydroxyacetophenone and norharmane³⁶ are general-purpose matrices;
- all-*trans*-retinoic acid is proper for polystyrene, but must be doped, preferably with Ag salts.

Most commonly used and novel matrices for polymers are presented in Table 1.

Table 1. Common matrices, used for polymer analysis and second-generation ionic liquid matrices (ILMs)^{16,25,37,38}.

Matrix (Formula)	Abbreviation	Structure	MW (Da)
Common matrices			
2,5-dihydroxybenzoic acid (C ₇ H ₆ O ₄)	DHB		154
α -cyano-4-hydroxycinnamic acid (C ₁₀ H ₇ NO ₃)	CHCA		189
2-(4-hydroxyphenylazo)benzoic acid (C ₁₃ H ₁₀ N ₂ O ₃)	HABA		242
1,1-dicyano-4-(4- <i>tert</i> -butylphenyl)-3-methylbuta-1,3-diene (C ₁₇ H ₁₈ N ₂)	DCTB		250
<i>trans</i> -3-indole acrylic acid (C ₁₇ H ₉ NO ₂)	IAA		187

Sinapinic acid (sinapic acid, 3,5-dimethoxy- 4-hydroxy- cinnamic acid) (C ₁₁ H ₁₂ O ₅)	SA		224
Dithranol (C ₁₄ H ₁₀ O ₃)	DIT		226
2,4,6-trihydrokso- acetophenone (C ₈ H ₈ O ₄)	THAP		168
2-nitrophenyl octyl ether (C ₁₄ H ₂₁ NO ₃)	NPOE		251
All- <i>trans</i> -retinoic acid (C ₂₀ H ₂₈ O ₂)	RA		300
3-aminoquinoline (C ₉ H ₈ N ₂)	AQ		144

5-chlorosalicylic acid (C ₇ H ₅ ClO ₃)	5-CSA		172
Nicotinic acid (C ₆ H ₅ NO ₂)	NA		123
<i>trans,trans</i> -1,4-Diphenyl-1,3-butadiene (C ₁₆ H ₁₄)	DPBD		206
<i>trans</i> -2-[3-(4- <i>tert</i> -Butylphenyl)-2-methyl-2-propenylidene]malononitrile (C ₁₇ H ₁₈ N ₂)	DCTB		250
Norharmaline (C ₁₁ H ₈ N ₂)			168
Ionic liquid matrices			
<i>N,N</i> -diisopropylethylammonium α -cyano-4-hydroxy cinnamate [C ₁₈ H ₂₆ N ₂ O ₃]	DEA-CHCA		318
<i>N,N</i> -diisopropylethylammonium <i>trans</i> -3-indole acrylate [C ₁₉ H ₂₈ N ₂ O ₂]	DEA-IAA		316

2.3. Doping agents

For successful characterization of polymers by MALDI-MS the effective formation of ions is required. It has been proved that for synthetic polymers cationization via metal ion attachment is more preferred than via protonation^{39,40}. As cationizing reagents have been used alkali metal cations, i.e. Na⁺, K⁺ or Li⁺, introduced as alkaline salts solutions (NaCl, KCl, LiCl) or such cations as Ag⁺ (introduced as silver trifluoroacetate), Cu⁺ or Cu²⁺. The usage of other metal salts, like Pd(II), Zn(II), Cd(II), Pt(III), Cr(III) or Al(III), for polystyrene cationization failed⁴¹. It seems probable that only metal cations in the oxidation state of +1 are effective and that Cu²⁺ undergo reduction to the Cu⁺ before cationization.

As an example, the effectiveness of cationization of poly(vinyl pyrrolidone) with different cationizing agents (Na, K, Li and Ag)⁴² is shown in Figure 4. The best S/N (signal-to-noise) ratio exhibits PVP cationized by sodium.

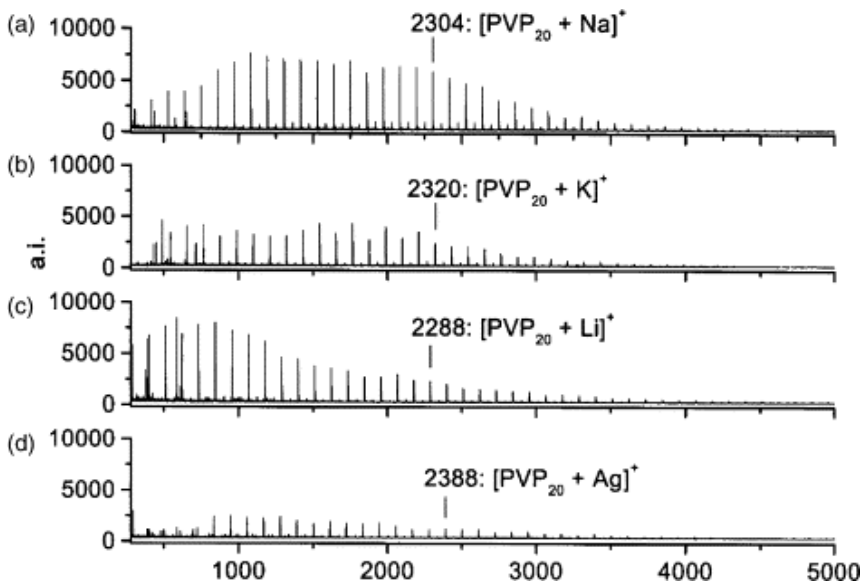


Figure 4. MALDI spectrum of poly(vinyl pyrrolidone) with different cationizing agents (Na, K, Li and Ag).⁴²

3. Molar mass (MM) and polydispersity (PD) determination

Important factors for polymers, which can be calculated from their mass spectra, are molar mass (MM) and molar-mass distribution (MMD). Polymers are collections of molecules of different chain lengths and sizes. Synthetic

polymers always possess certain polydispersity, because the numbers of monomers creating a polymer molecule can differ, sometimes significantly. The crucial feature to determine is the molar-mass distribution (MMD), i.e. the number and weight of macromolecular chains at size (or length) s , at size $(s+1)$, at size $(s+2)$, at size $(s+3)$ and so on. Knowing MMD, one can compute MMD averages^{43,44,45,46}.

The MM and MMD of a polymer are vital criteria for its practical applications, since the size and weight of molecules are essential for polymer properties. The possible types of molar mass distribution are illustrated in Figure 5. The MMD measurements may reveal narrow (Fig. 5a), broad (Fig. 5b) or bimodal (when distribution displays two maxima, Fig. 5c) distribution.

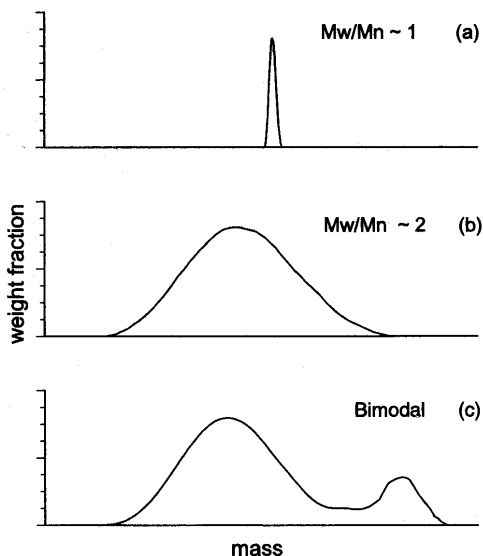


Figure 5. Different types of molar mass distributions: (a) narrow, (b) broad, (c) bimodal.⁴⁷

The mass spectrometric methods of molar mass measure are based on the fact that ions strike the detector and produce a current that reflects the number of ions. *The number of ions* of a given mass M is proportional to *the number of molecules* at that mass, which means that the detector measures *the molar fraction* of molecules of mass M .

The number-average molar mass M_n is defined⁴⁷:

$$M_n = (\sum m_i N_i) / (\sum N_i) \quad [1]$$

where N_i stands for the number of chains with mass m_i .

The weight-average molar mass M_w is defined as:

$$M_w = (\sum m_i^2 N_i) / (\sum m_i N_i) \quad [2]$$

Assuming direct linear relationship between spectral peak intensity and number of ions responsible for formation of this peak (when the detector response is proportional to molar fraction) we can calculate M_n , M_w and PD as follows, indicating by M_i molar mass of oligomeric component and by I_i – its signal intensity:

$$M_n = \frac{\sum M_i I_i}{\sum I_i} \quad [3]$$

$$M_w = \frac{\sum M_i^2 I_i}{\sum M_i I_i} \quad [4]$$

Practically, to calculate M_n and M_w using equations above, it is necessary to record the MS spectrum and tabulate the mass spectral peaks intensities. Providing these intensities values to the respective equations we obtain M_n and M_w .

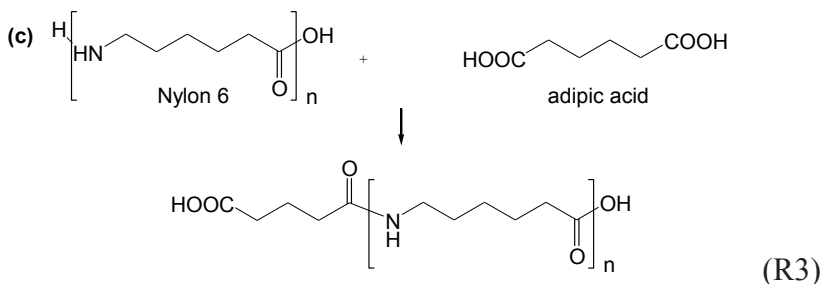
The polydispersity (PD) is calculated by dividing M_w by M_n :

$$PD = \frac{M_w}{M_n} \quad [5]$$

4. Identification of polymer end-groups

Synthetic polymers show various kinds of heterogeneity. Aside from different types of molar mass distribution they can possess various structures (linear, branched, cyclic, grafted), monomer sequence and different functional end-groups. These features of synthetic polymers construction are not easy to

c) adipic acid $\text{HOOC}-(\text{CH}_2)_4-\text{COOH}$,



d) water in methanesulfonic acid (hydrolysis).

This way the authors synthesized four samples of modified Nylon6, each terminated by different end groups, i.e. diamino terminated (a), monoamino terminated (monocapped, b), dicarboxyl terminated (c) and amino-carboxyl terminated (d) oligomers. The products were analyzed on MALI-TOF Bruker Reflex mass spectrometer, equipped with nitrogen laser, using 2-(4-hydroxy phenylazo)benzoic acid (HABA) as a matrix and trifluoroethanol (TFE) as a solvent.

Respective MALDI-TOF mass spectra^{47,57} of resulting polymers are given in Figures 6(ab) and 6(cd) as representative examples.

Nylon6, reacted with diamino-hexamethylene $\text{H}_2\text{N}-(\text{CH}_2)_6-\text{NH}_2$, forms oligomers bearing NH_2 groups at both chain ends as shown in reaction equation (R1).

The formula $\text{H}-[\text{NH}(\text{CH}_2)_5\text{CO}]_n\text{NH}(\text{CH}_2)_6\text{NH}_2$ describes the structure of created oligomers, in which the repeat unit, $[\text{NH}(\text{CH}_2)_5\text{CO}]_n$ or $\text{C}_6\text{H}_{11}\text{NO}$, corresponds to the mass 113,1 Da. The mass spectrum of the Ny6-diamino terminated displays sets of three intense peaks, marked as A, B and C (see insert in Fig. 6a), corresponding to protonated (A), sodiated (B) and potassiated (C) species. The most intense peaks in the mass spectrum (Fig. 6a) should be assigned to the sodiated species B $\text{H}-[\text{NH}(\text{CH}_2)_5\text{CO}]_n\text{NH}(\text{CH}_2)_6\text{NH}_2 \cdots \text{Na}^+$, ($n \cdot 113.1 + 116 + 23$), with $n = 11-52$.

Figure 6b displays mass spectrum of Ny6 reacted with decylamine $\text{C}_{10}\text{H}_{21}\text{NH}_2$, which gave oligomers amino terminated at one end with general formula



The MALDI spectrum (see insert in Fig. 6b) shows intense sodiated ions D and less intense protonated ions C. The species marked as 1 and 2 correspond to sodiated and potassiumated ions of Ny6 cyclic oligomers.

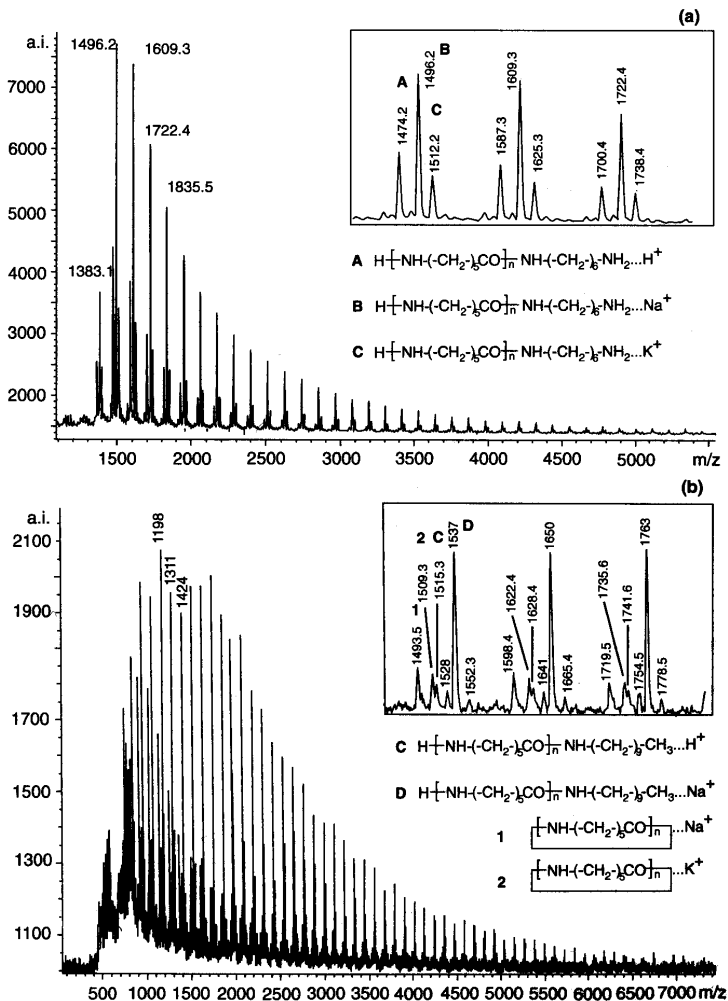


Figure 6(ab). MALDI-TOF mass spectrum of Nylon6 reacted with diaminohexamethylene (a) and decylamine (b).^{47,57}

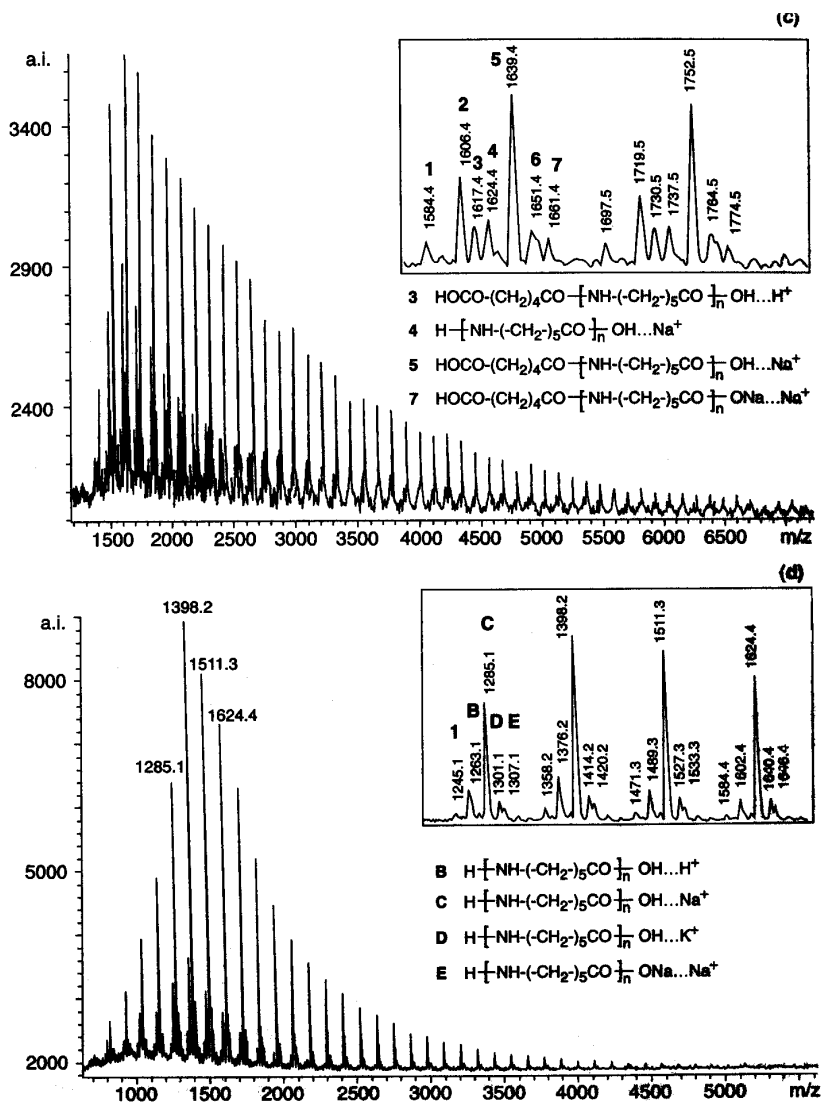


Figure 6(cd). MALDI-TOF mass spectrum of Nylon6 reacted with adipic acid (c) and hydrolyzed with water/methanesulfonic acid (d).^{47,57}

Nylon6, reacted with adipic acid, gave Ny6-dicarboxy terminated (Fig. 6c) with general formula



The MALDI-TOF spectrum (Fig. 6c) displays a series of intense peaks in the region from 1000 to 7000 Da. The most intense peaks labeled as 5 (insert of Fig. 6c) correspond to the sodiated oligomers bearing two $-\text{COOH}$ end-groups. The analogous protonated oligomers 3 and Ny6 cyclic oligomers protonated 1 and sodiated 2 as well as sodiated ions of the monosodium salt of dicarboxy terminated oligomers 7 are clearly seen in the spectrum.

Nylon6 hydrolyzed in aqueous methanesulfonic acid gave NH_2/COOH -terminated oligomers, displayed as a series of intense sodiated peaks C in the MALDI spectrum (inset of Fig. 6d). Protonated (peaks B) and potassiated (peaks D) ions of these oligomers appear with low intensity, like protonated cyclic oligomers 1 and sodiated ions of sodium salt (peaks E).

5. Investigation of fragmentation process

The examination of fragmentation process provides valuable information about the structure of polymer studied. Although the MALDI process is considered as “soft” ionization method, fragmentation of ions is possible under specific instrumental and experimental conditions:

1. Fragmentation may be triggered off in the ion-source region by the higher laser fluences. This type of fragmentation is called “prompt fragmentation”⁵⁸.
2. Another type of fragmentation is referred to as “in-source decay” (ISD) and is characteristic for delayed extraction ion sources. The ion decomposition takes place during the delay time before extraction and is caused by a great number of collisions in the expanding plume.^{35,59} ISD fragmentation has been used in analysis of poly(propylene glycol) PPG and poly(ethylene glycol) PEG³⁵.
3. In contrast to the previous methods, which can be performed in both the linear and reflection modes, metastable fragmentation called “post source decay” (PSD) occurs only in the field-free region of the instruments with reflectron detector. In the linear TOF mode parent and daughter ions are indistinguishable because of the same velocity, whereas in the reflection mode these two types of ions can be differentiated due to their different kinetic energy. The main advantage of PSD process is the possibility of precursor ion selection and obtaining of daughter ion

spectrum⁶⁰.

The MALDI-PSD measurements are useful for controlled fragmentation study, such as required for end-group identification in synthetic polymers. Placing the additional collisional cell in the field-free region of MALDI-TOF system is effective in obtaining additional fragments which means more structural information about polymer studied (PSD/CID). Several papers on the application of MALDI-PSD and PSD/CID can be found in literature concerning the analysis of synthetic polymers, i.e. PSD-MALDI and CID-MALDI investigation of polystyrene^{61,62}, poly(methyl methacrylate)s^{63,64,65}, poly(ethylene glycol) s⁵⁷, poly(ethylene terephthalate)⁵⁷, polyisobutylene⁶⁶ and poly(bisphenol-A carbonate, PC)⁶⁷.

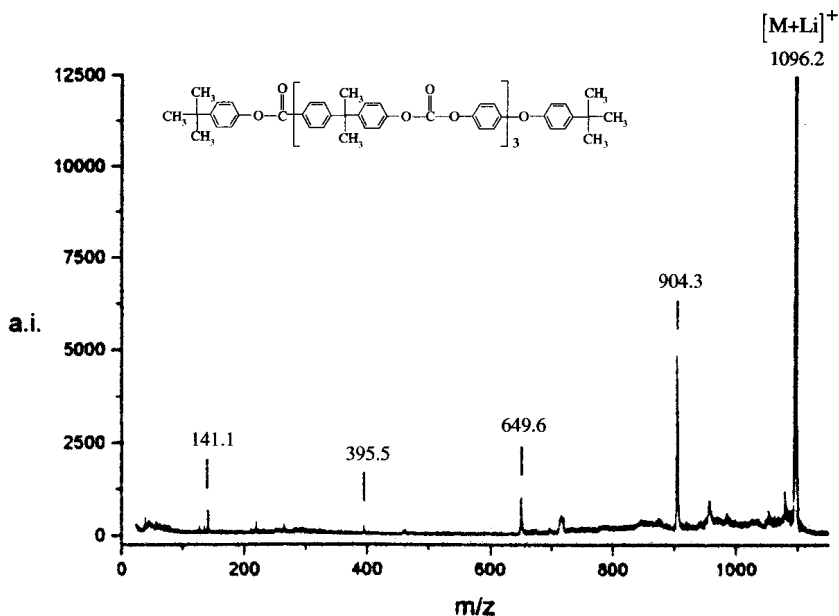


Figure 7. PSD-MALDI-TOF mass spectrum of the lithiated trimer from poly(bisphenol-A carbonate, PC)^{47,67}.

As an example, PSD-MALDI mass spectrum of the lithiated trimer (m/z 1096.2) from poly(bisphenol-A carbonate, PC) capped with 4-*tert*-butylphenol at both ends, is shown in Figure 7. In this spectrum one series of fragment ion peaks (m/z 904.3, 649.6, 395.5 and 141.1), corresponding to the oligomers with only one end-group and lithium cation, is clearly seen. The PSD measurement

demonstrated that the fragmentation behaviour of such a type of polycarbonates depends on the substituents bound to the central carbon atom of the bisphenol unit.

6. Composition and sequence of copolymers

The mass spectral analysis of copolymers is more complex than for homopolymers, since the number of peaks observed is increasing with chain size. In the case of more than two different monomers the number of peaks grows exponentially, so a higher mass resolution (as compared to homopolymers) is required to detect the individual oligomers signals as separate peaks. Nevertheless, the large number of papers on analysis copolymers by MALDI can be found^{68,69,70,71,72,73,74,75,76,77} in recent literature.

The proper MALDI peak assignment for copolymers is a challenging task, however the procedure is the same as in the case of homopolymers:

1. propose hypothetical chemical structures that may be present in the sample;
2. calculate the masses of all possible chains and checking if expected peaks are present in the spectrum.

In copolymers of the type AB (with two different monomers), two repeat units with masses m_1 and m_2 may interchange along the polymer backbone. The two masses (m_1 and m_2) differ in most cases, because the coincidence that m_1 and m_2 are equal is extremely rare, so MALDI spectrum allows the identification of the copolymer backbone structure.

On condition that the MS ionization/desorption method used to ionize and desorb the oligomers does not produce significant ion fragmentation, peak intensities from the MALDI mass spectrum can be used to determine copolymer composition^{68, 78}. The method is based on the assumption that the intensities of peaks appearing in MALDI spectrum of copolymer are directly proportional to the relative abundance of oligomers existing in the copolymer^{68,72,75}.

There are some interesting examples of using MALDI MS for copolymer characterization. Vitalini⁷⁹ analyzed MALDI-TOF mass spectrum (in the negative mode) of a copolymer constructed from bisphenol units (A) and derivatized fullerene units (B). The mass spectrum (Fig. 8) extends in the wide mass range of 1600-14 000 Da. The calculation of mass values indicate that the observable peaks originate from the cyclic ions of the type $A_n B$, where $n = 1-15$.

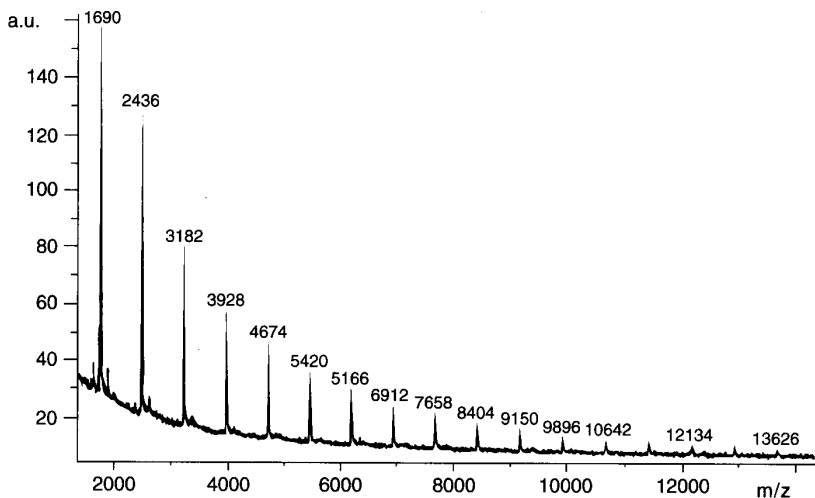


Figure 8. MALDI-TOF mass spectrum of a copolymer containing bisphenol units BPA-CH₂ and units of derivatized fullerene.⁷⁹

Viala et al.⁸⁰ studied the copolymerization of methyl methacrylate (MMA) and 1,1-diphenylethylene (DPE) in the presence of ammonia, sodium dodecylsulfate and ammonium peroxodisulfate. Depending on the reactants, various end groups are expected, i.e. -H terminal group due to disproportionation, -SO₄ terminal groups originating from initiation with sulfate ion radicals, -OH terminal groups from hydrolysis or initiation with hydroxyl radicals and more complex end groups from termination with DPE. The recorded spectrum of copolymer revealed all the expected products.

Impallomeni et al.⁸¹ heated poly(4-hydroxybutarate) (PHB) and poly(ϵ -caprolactone) (PCL) with *p*-toluenesulfonic acid (PTSA) as a catalyst. Produced copolymer possessed two different end-group sets, namely H/COOH and PTSA/COOH. The products were submitted to SEC and MALDI-TOF analysis. The MALDI-TOF spectrum (Fig. 9) revealed two ion distributions: the first, centered at $m/z = 3700$ (due to sodiated ion of the co-oligomers terminated with PTSA and COOH, species 1 in Fig. 9) and the second, centered at $m/z = 4600$ (due to sodiated ion of the co-oligomers terminated with OH and COOH groups, species 2 in Fig. 9).

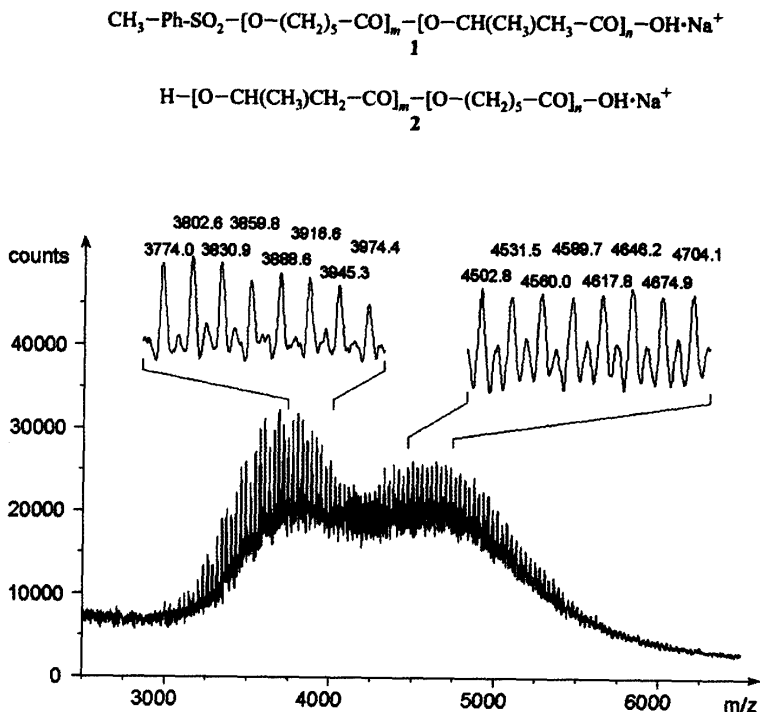


Figure 9. MALDI-TOF mass spectrum of SEC fraction of P(HB-co-47% mol CL). The spectrum revealed copolymer chains of structures shown in the upper part⁸¹.

7. Dendrimers growth control

Dendrimers can be considered to be monodisperse polymers with controlled molecular structure. Their growth is following step-by-step creating in each step new stratum, so called “generation” (G). An example for MALDI MS application to the investigation of dendrimer growth is shown in Figure 10. A presented dendrimer grows on a star-shaped nucleus made of PEG, by subsequent reactions. Initial mass about 25000 (Star PEG, line a) increases in the next stage to 28000 (PEG-[G-2]₄, line b), then to 33000 (PEG-[G-3]₄, line c) and finally to 39000 (PEG-[G-4]₄, line d)⁸².

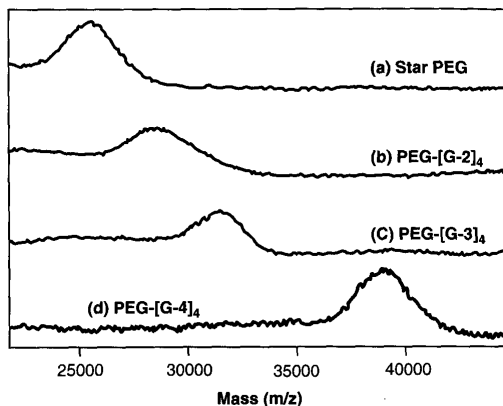


Figure 10. MALDI-TOF mass spectra of a dendrimer growing on a star-shaped core made of PEG (various stages of growth).⁸²

8. Summary

Matrix-assisted laser desorption/ionization mass spectrometry along with fragmentation analysis have been shown to be valuable tools for detailed polymer characterization. The MALDI-TOF MS technique is widely used in the analysis of synthetic organic polymers as a general method of independent determination of the chain length distribution as well as for the determination of the end groups structure and their sequences. This method is concerned as a highly sensitive, non-averaging procedure that provides detailed structural information about the individual molecules present in a polymer sample. It has been shown that MALDI-TOF is promising and very rapidly developing analytical technique.

Abbreviations used:

AQ - 3-aminoquinoline

CCD – chemical composition distribution

CHCA - α -cyano-4-hydroxy-cinnamic acid

CID – collision-induced dissociation

5-CSA - 5-chlorosalicylic acid

DEA-CHCA - *N,N*-diisopropyl ethylammonium α -cyano-4-hydroxy cinnamate

DEA-IAA - *N,N*-diisopropyl ethylammonium *trans*-3-indole acrylate

DHB - 2,5-dihydroxy-benzoic acid

DCTB - 1,1-dicyano-4-(4'-*tert*-butylphenyl)-3-methyl-buta-1,3-diene

DPBD - *trans,trans*-1,4-diphenyl-1,3-butadiene

DSC - differential scanning calorimetry
 EG – end group
 FTD – functionality distribution
 HABA - 2-(4-hydroxy-phenylazo)benzoic acid
 IAA - *trans*-3-indole acrylic acid
 ILM – ionic liquid matrix
 ISD – in-source decay
 MALDI – matrix-assisted laser desorption/ionization
 MM – molar mass
 MMA – methyl methacrylate
 MMD - molar mass distribution
 M_n – number-average molar mass
 M_w – weight-average molar mass
 NIST – National Institute of Standards and Technology
 NPOE - 2-nitrophenyl octyl ether
 NA – nicotinic acid
 PA – polyamide
 PC – polycarbonate
 PCL - poly(ϵ -caprolactone)
 PE – polyethylene
 PEG – polyethyleneglycols
 PET – polyethylene terephthalate
 PHB - poly(4-hydroxybutarate)
 PMMA – poly(methyl methacrylate)
 POPOP - 1,4-bis(5-phenyloxazol-2-yl)benzene
 PP – polypropylene
 PS- polystyrene
 PSD – post source decay
 PTSA - *p*-toluenesulfonic acid
 PVC – polyvinyl chloride
 RA – all-*trans*-retinoic acid
 SA - sinapic acid or 3,5-dimethoxy-4-hydroxy-cinnamic acid
 SEC – size exclusion chromatography
 TFE - trifluoroethanol
 TGA – thermo-gravimetric analysis
 THAP - 2,4,6-trihydroxyacetophenone
 TOF – time of flight

Acknowledgements

The authors thank the Polish Ministry of Science and Higher Education for financial support in years 2009-2012 as scientific grant No. N 204 028636.

References

1. Siracusa V, Rocculi P, Romani S, Dalla Rosa M; Biodegradable polymers for food packaging: a review; *Trends Food Sci. Technol.* 2008, **19**, 634
2. Zhao Z, Wang J, Mao H, Leong KW; Polyphosphoesters in drug and gene delivery; *Adv. Drug Deliv. Rev.* 2003, **55**, 483
3. Huang S, Zhuo R; Recent advances in polyphosphoester and polyphosphoramidate-based biomaterials; *Phosphorus Sulfur Silicon Relat. Elem.* 2008, **183**, 340
4. Lee W, Park J, Jung S, Yang CW, Kim W, Kim H, Park J, Park J; Preparation and characterization of biodegradable nanoparticles entrapping immunodominant peptide conjugated with PEG for oral tolerance induction; *J. Controlled Release* 2005, **105**, 77
5. Krogman NR, Weikel AL., Nguyen NQ, Nair LS, Laurencin CT, Allcock HR; Synthesis and characterization of serine- and threonine-containing polyphosphazenes and poly(L-lactic acid) grafted copolymers, *Macromolecules* 2008, **41**, 7824
6. <http://www.psrc.usm.edu/mauritz/maldi.html>, accessed Dec. 2010
7. Silverstein RM, Bassler GC, Morrill TC; in: *"Spectrometric Identification of Organic Compounds"*, John Wiley&Sons Pub., 1991, Chapt. 2
8. Braun RD; in: *"Introduction to instrumental analysis"*, McGraw-Hill Pub., 1987, Chapt. 21
9. Montaudo G, Sampieri F, Montaudo MS; Characterization of synthetic polymers by MALDI-MS, *Prog. Polym. Sci.* 2006, **31**, 277
10. Hanton SD; Mass spectrometry of polymers and polymer surfaces; *Chem. Rev.* 2001, **101**, 527
11. Nielen MWF; MALDI Time-of-flight mass spectrometry of synthetic polymers; *Mass Spectrom. Rev.* 1999, **18**, 309
12. Weidner SM, Trimpin S; Mass spectrometry of synthetic polymers; *Anal. Chem.* 2008, **80**, 4349
13. Tanaka K, Wak H, Ido Y, Akita S, Yoshida Y, Yoshida T; Protein and polymer analysis up to m/z 100 000 by laser ionization time-of-flight mass spectrometry; *Rapid Commun. Mass Spectrom.* 1988, **2**, 151
14. Bahr U, Deppe A, Karas M, Hillenkamp F, Giessmann U; Mass spectrometry of synthetic polymers by UV-matrix-assisted laser

- desorption/ionization, *Anal. Chem.* 1992, **64** (22), 2866
15. Karas M, Hillenkamp F; Laser desorption ionization of proteins with molecular masses exceeding 10 000 Daltons; *Anal. Chem.* 1988, **60**, 2299
 16. Danis PO, Karr DE; A facile sample preparation for the analysis of synthetic organic polymers by MALDI; *Org. Mass Spectrom.* 1993, **28**, 923
 17. Arakawa R, Watanabe S, Fukuo T; Effects of sample preparation on MALDI-TOF mass spectra for sodium polystyrene; *Rapid Commun. Mass Spectrom.* 1999, **13**, 1059
 18. Schriemer DC, Li L; Mass discrimination in the analysis of polydisperse polymers by MALDI time-of-flight mass spectrometry. 2. Instrumental issues; *Anal. Chem.* 1997, **69**, 4176
 19. Yalcin T, Dai Y, Li L; Matrix-assisted laser desorption/ionization time-of-flight mass spectrometry for polymer analysis: solvent effects in sample preparation; *J. Am. Soc. Mass Spectrom.* 1998, **9**, 1303
 20. Zhang Z, Deng H, Deng Q, Zhao S; Effect of matrix and solvent on the analysis of novel poly(phenylenevinylene) derivatives by matrix-assisted laser desorption/ionization time-of-flight mass spectrometry; *Rapid Commun. Mass Spectrom.* 2004, **18**, 2146
 21. Wetzel SJ, Guttman CM, Flynn KM, Filliben JJ; Significant parameters in the optimization of MALDI-TOF-MS for synthetic polymers; *J. Am. Soc. Mass Spectrom.* 2006, **17**, 246
 22. Liu J, Loewe RS, McCullough RD, Employing MALDI-MS on polyalkylthiophenes: analysis of molecular weights, molecular weight distributions, end group structures, and end group modifications; *Macromolecules* 1999, **32**, 5777
 23. King RC, Goldschmidt R, Xiong Y, Owens KG; *Proc. 43rd ASMS Conf. Mass Spectrometry and Allied Topics*, Atlanta, GA, 1995
 24. Chen H, Guo B; Use of binary solvent systems in the MALDI-TOF analysis of poly(methyl methacrylate); *Anal. Chem.* 1997, **69**, 4399
 25. Brandt H, Ehmann T, Otto M; Solvent selection for matrix-assisted laser desorption/ionization time-of-flight mass spectrometric analysis of synthetic polymers employing solubility parameters; *Rapid Commun. Mass Spectrom.* 2010, **24**, 2439
 26. Li L; in: „*MALDI Mass Spectrometry for Synthetic Polymer Analysis*”, John Wiley, Hoboken, 2010, 144
 27. Zagorevskii DV, Nasrullah MJ, Raghunadh V, Benicewicz BC, The effect of tetrahydrofuran as solvent on matrix-assisted laser desorption/

- ionization and electrospray ionization mass spectra of functional polystyrenes; *Rapid Commun. Mass Spectrom.* 2006, **20**, 178
28. Hansen CM; „*Hansen Solubility Parameters – A User’s Handbook*”, CRC Press, Boca Raton, 2007
 29. Trimpin S, Keune S, Räder HJ, Müllen K; Solvent-free MALDI-MS: Developmental improvements in the reliability and the potential of MALDI in the analysis of synthetic polymers and giant organic molecules; *J. Am. Soc. Mass Spectrom.* 2006, **17**, 661
 30. Trimpin S, Weidner S, Falkenhagen J, McEwen CN; Fractionation and solvent-free MALDI-MS analysis of polymers using liquid adsorption chromatography at critical conditions in combination with a multisample on-target homogenization/transfer sample preparation method; *Anal. Chem.*, **2007**, **79**(19), 7565
 31. Hanton SD, Parees DM; Extending the solvent-free MALDI sample preparation method, *Journal of the American Society for Mass Spectrometry* 2005, **16**(1), 90.
 32. Goepferich A, Mechanisms of polymer degradation and erosion; *Biomaterials* 2006, **17**, 103
 33. Siparsky GL, Voorhees KJ, Miao F; Hydrolysis of polylactic acid (PLA) and polycaprolactone (PCL) in aqueous acetonitrile solutions: autocatalysis; *J. Environ. Polymer Degradation* 1998, **6**, 31
 34. Berthod A, Crank JA, Rundlett KL, Armstrong DW; A second-generation ionic liquid matrix-assisted laser desorption/ionization matrix for effective mass spectrometric analysis of biodegradable polymers; *Rapid Commun. Mass Spectrom.* 2009, **23**, 3409
 35. Guttman CM, Wetzel S, Blair WR, Fanconi BM, Girard JE, Goldschmidt RJ et al., NIST-sponsored interlaboratory comparison of polystyrene molecular mass distribution obtained by matrix-assisted laser desorption/ionization time-of-flight mass spectrometry: statistical analysis, *Anal. Chem.* 2001, **73**, 1252
 36. Erra-Balsells R, Nonami H; UV-matrix-assisted laser desorption/ionization time-of-flight mass spectrometry analysis of synthetic polymers by using nor-harmane as matrix, *Arkivoc*, 2003, 517
 37. Enjalbal C, Ribière P, Lamaty F, Yadav-Bhatnagar N, Martinez J, Aubagnac J.-L.; MALDI-TOF MS analysis of soluble PEG based multi-step synthetic reaction mixtures with automated detection of reaction failure; *J. Am. Soc. Mass Spectrom.* 2005, **16**, 670
 38. Reinhold M, Meier RJ, de Koster CG; How feasible is matrix-assisted laser desorption/ ionization time-of-flight mass spectrometry analysis

- of polyolefins?; *Rapid Commun. Mass Spectrom.* 1998, **12**, 1962
39. Liu HMD, Schlunegger UP; Matrix-assisted laser desorption/ionization of synthetic polymers with azo compound matrices; *Rapid Commun. Mass Spectrom.* 1996, **10**, 483
 40. Macha SF, Limbach PA, Savickas PJ; Application of nonpolar matrices for the analysis of low molecular weight nonpolar synthetic polymers by matrix-assisted laser desorption/ionization time-of-flight mass spectrometry; *J. Am. Soc. Mass Spectrom.* 2000, **11**, 731
 41. Rashidezadeh H, Baochuan G; Investigation of metal attachment to polystyrenes in matrix-assisted laser desorption ionization, *J. Am. Soc. Mass Spectrom.* 1998, **9**, 724
 42. Trimpin S, Eichhorn P, Rader HJ, Mullen K, Knepper TP, Recalcitrance of poly(vinylpyrrolidone): evidence through matrix-assisted laser desorption/ionization time-of-flight mass spectrometry, *J. Chromatogr. A*, 2001, **938**, 67
 43. Flory P; in: “*Principles of Polymer Chemistry*”, Cornell University Press, Ithaca, New York, 1971
 44. Billmeyer FW Jr., in: “*Textbook of Polymer Science*”, Wiley, New York, 1971.
 45. Painter PC, Coleman MM; in: “*Fundamentals of Polymer Science*”, Technomic Publ., Lancaster, 1997
 46. Boyd RH, Phillips PJ; in: “*The Science of Polymer Molecules*”, Cambridge University Press, New York, 1993
 47. Montaudo G, Lattimer R; in: “*Mass Spectrometry of Polymers*”, CRC Press: Boca Raton, 2002, 584
 48. Pasch H, Ghahary R; Analysis of complex polymers by MALDI-TOF mass spectrometry; *Macromol. Symp.* 2000, **152**, 267
 49. Montaudo G, Montaudo MS, Puglisi C, Samperi F, Sepulchre M; End-group characterization of poly(methylphenylsilane) by alkali metal salts doped MALDI-TOF mass spectra, *Macromol. Chem. Phys.* 1996, **197**, 2615
 50. Skelton R, Dubois F, Zenobi R; A MALDI sample preparation method suitable for insoluble polymers; *Anal. Chem.* 2000, **72**, 1707
 51. Jackson AT, Yates HT, Lindsay CI, Didier Y, Segal JA, Scrivens JH, Brown J; Utilizing time-lag focusing matrix-assisted laser desorption/ionization mass spectrometry for the end-group analysis of synthetic polymers; *Rapid Commun. Mass Spectrom.* 1997, **11**, 520
 52. De Koster CG, Duursma MC, van Rooji GJ, Heeren RMA, Boon JJ; Endgroup analysis of polyethylene glycol polymers by matrix-assisted

- laser desorption/ionization Fourier-transform ion cyclotron resonance mass spectrometry; *Rapid Commun. Mass Spectrom.* 1995, **9**, 957
53. Montaudo G, Montaudo MS, Puglisi C, Samperi F; Characterization of polymers by matrix-assisted laser desorption/ionization- time of flight mass spectrometry. End-group determination and molecular weight estimates of poly(ethylene glycols), *Macromolecules* 1995, **28**, 4562
54. Yamanaka K, Kimura Y, Aoki T, Kudo T; End-group analysis of bacterially produced poly(3-hydroxybutyrate): discovery of succinate as the polymerization starter; *Macromolecules*, 2009, **42** (12), 4038
55. Weidner SM, Falkenhagen J, Knop K, Thünemann A; Structure and end-group analysis of complex hexanediol-neopentylglycol-adipic acid copolyesters by matrix-assisted laser desorption/ionization collision-induced dissociation tandem mass spectrometry, *Rapid Commun. Mass Spectrom.* 2009, **23**, 2768
56. Chen H, He M, Pei J, Liu B; End-group analysis of blue light-emitting polymers using matrix-assisted laser desorption/ionization time-of-flight mass spectrometry; *Anal. Chem.* 2002, **74**(24), 6252
57. Montaudo G, Montaudo MS, Puglisi C, Samperi F; Characterization of end-groups in Nylon 6 by MALDI-TOF mass spectrometry; *J. Polym. Sci. A, Polym. Chem.* 1996, **34**, 439
58. Mowat IA , Donovan RJ, Maier RRJ ; Enhanced cationization of polymers using delayed ion extraction with matrix-assisted laser desorption/ionization; *Rapid Commun. Mass Spectrom.* 1997, **11**, 89
59. Völcker NH, Klee D, Hanna M, Höcker H, Bou JJ, Martinez de Ilarduya A, Muñoz-Guerra S; Synthesis of heterotelechelic poly(ethylene glycol) s and their characterization by MALDI-TOF-MS; *Macromol. Chem. Phys.* 1999, **200**, 1363
60. Lee H, Lubman DM; Sequence-specific fragmentation generated by matrix-assisted laser desorption/ionization in a quadrupole ion trap/ reflectron time-of-flight device; *Anal. Chem.* 1995, **67**, 1400
61. Jackson AT, Yates HT, MacDonald WA, Scrivens JH, Critchley G, Brown J, Deery MJ, Jennings KR, Brookes C; Time-lag focusing and cation attachment in the analysis of synthetic polymers by matrix-assisted laser desorption/ionization time-of-flight mass spectrometry, *J. Am. Soc. Mass Spectrom.* 1997, **8**, 132
62. Jackson AT, Yates HT, Scrivens JH, Green MR, Bateman RH; Matrix-assisted laser desorption/ionization-collision induced dissociation (MALDI-CID) of poly(styrene), *J. Am. Soc. Mass Spectrom.* 1998, **9**, 269

63. Jackson AT, Yates HT, Scrivens JH, Critchley G, Brown J, Green MR, Bateman RH; The application of matrix-assisted laser desorption/ionization combined with collision-induced dissociation to the analysis of synthetic polymers; *Rapid Commun. Mass Spectrom.* 1996, **10**, 1668
64. Jackson AT, Yates HT, Scrivens JH, Green MR, Bateman RH; Utilizing matrix-assisted laser desorption/ionization – collision induced dissociation for the generation of structural information from poly(alkyl methacrylate)s; *J. Am. Soc. Mass Spectrom.* 1997, **8**, 1206
65. Scrivens JH, Jackson AT, Yates HT, Green MR, Critchley G, Brown J, Bateman RH, Bowers MT, Gidden J; The effect of the variation of cation in the matrix-assisted laser desorption/ionization collision induced dissociation (MALDI-CID) spectra of oligomeric systems; *Int. J. Mass Spectrom. Ion Process.*, 1997, **165**, 363
66. Selby TL, Wesdemiotis C, Lattimer RP; Dissociation characteristics of $[M+X]^+$ ions ($X = H, Li, K$) from linear and cyclic polyglycols; *J. Am. Soc. Mass Spectrom.* 1994, **5**, 1081
67. Przybilla L, Räder H-J, Müllen K; Post-source decay fragment ion analysis of polycarbonates by matrix-assisted laser desorption/ionization time-of-flight mass spectrometry, *Eur. Mass Spectrom.* 1999, **5**, 133
68. Wilczek-Wera G, Danis PO, Eisenberg A; Individual block length distributions of block copolymers of polystyrene-block-poly(α -methylstyrene) by MALDI/TOF mass spectrometry; *Macromolecules* 1996, **29**, 4036
69. Montaudo MS; Sequence constraints in a glycine-lactic acid copolymer determined by matrix-assisted laser desorption/ionization mass spectrometry; *Rapid Commun. Mass Spectrom.* 1999, **13**, 639
70. Willemsse RX., Staal BBP, Donkers EHD, van Herk AM; Copolymer fingerprints of polystyrene-block-polyisoprene by MALDI-ToF-MS; *Macromolecules*, 2004, **37**, 5717
71. Schädler V, Spickermann J, Räder H-J, Wiesner U; Synthesis and characterization of α,ω -macrozwitterionic block copolymers of styrene and isoprene; *Macromolecules* 1996, **29**, 4865
72. Wilczek-Wera G, Yu Y, Waddell K, Danis PO, Eisenberg A; Analysis of diblock copolymers of poly(α -methylstyrene)-block-polystyrene by mass spectrometry; *Macromolecules* 1999, **32**, 2180
73. Montaudo MS, Samperi F; Determination of sequence and composition of poly(butyleneadipate-co-butylene terephthalate) by matrix-assisted laser desorption/ionization time-of-flight mass spectrometry; *Eur. Mass*

- Spectrom.* 1999, **4**, 459
74. Montaudo MS, Puglisi C, Samperi F, Montaudo G; Structural characterization of multicomponent copolyester by mass spectrometry; *Macromolecules* 1998, **31**, 8666
 75. Cox JF, Johnston MV, Qian K, Peiffer DG; Compositional analysis of isobutylene/*p*-methylstyrene copolymers by matrix-assisted laser desorption/ionization mass spectrometry; *J. Am. Soc. Mass Spectrom.*, 2004, **15**, 681
 76. Polce MJ, Klein DJ, Harris FW, Modarelli DA, Wesdemiotis C; Structural characterization of quinoxaline homopolymers and quinoxaline/ether sulfone copolymers by MALDI mass spectrometry; *Anal Chem*, 2001, **73**, 1948
 77. Puglisi C, Samperi F, Di Giorgi S, Montaudo G; Exchange reactions occurring through active chain ends. MALDI-TOF characterization of copolymers from Nylon 6,6 and Nylon 6,10; *Macromolecules*, 2003, **36**, 1098
 78. Montaudo M.S., Mass spectra of copolymers, *Mass Spectrom. Rev.*, 2002, **21**, 108
 79. Vitalini D, Mineo P, Scamporrino E; Synthesis and characterization of some copolyformals containing different amounts of fullerene units; *Macromolecules* 1999, **32**, 4247
 80. Viala S, Tauer K, Antonietti K, Krüger R.-P, Bremser W; Structural control in radical polymerization with 1,1-diphenylethylene. I. Copolymerization of 1,1-diphenylethylene with methyl methacrylate; *Polymer*, 2002, **43**, 7231
 81. Impallomeni G, Giuffrida M, Barbuzzi T, Musumarra G, Ballistreri A; Acid catalyzed transesterification as a route to poly(3-hydroxybutyrate-co- ϵ -caprolactone) copolymers from their homopolymers; *Biomacromolecules*, 2002, **3**, 835
 82. Yu D, Vladimirov N, Frechet JMJ; MALDI-TOF in the characterization of dendritic-linear block copolymers and stars; *Macromolecules* 1999, **32**, 5186

Chapter 8

Nano-systems and soft materials for anion complexation

Bogusława Łęska and Radosław Pankiewicz

*Faculty of Chemistry, A. Mickiewicz University, Grunwaldzka 6,
60-780 Poznań, Poland*

Introduction

Non-covalent anion coordination chemistry was relatively slow to develop in comparison with the development of hosts for cations and even neutral molecules. But last decades we could observed the increase of interesting of this theme [1-5]. The applications of anion - binding ligands are very broad. Interest and developments in non-covalent anion coordination chemistry continued sporadically throughout the 1970s and early 1980s, with the synthesis of several hosts of crucial conceptual importance (mainly of cryptand type, analogous to the katapinands) by the groups of P. Schmidtchen and J.-M. Lehn [6, 7]. This short review-article is intended to highlight novel receptors for anions complexation and modern “bases”, defined as nano and soft materials.

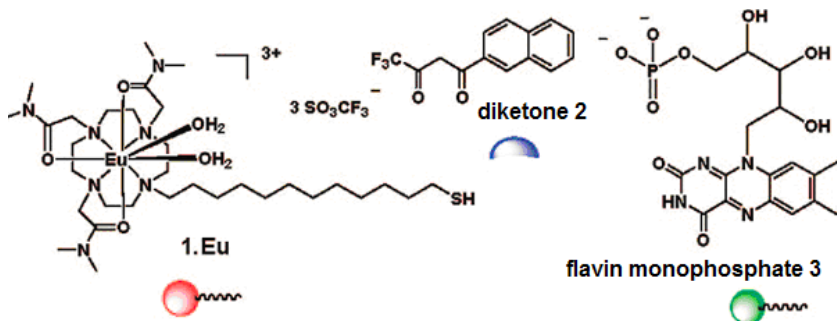
The development of chemical sensors continues to be of great interest in modern analytical chemistry [8, 9]. Demands arise from clinical diagnostics, environmental and food analysis or in the detection of illicit drugs, explosives and chemical warfare agents. A molecular chemical sensor typically consists of the analyte binding site and a signaling unit, which transposes the binding event into a macroscopically observable output, for example, a color change or a light emission. For the development of devices it is often useful to immobilize the sensor molecule on surfaces, in membranes, gels or on nanoparticles.

Nanoparticles in anion sensing

The functional hybrid nanomaterials and supramolecular systems are more interest [10-12], particularly for molecular recognition and sensing [13-16], as drug delivery systems [17] and for catalysis [18]. Gold nanoparticles (AuNPs), have attracted much attention in the development of such devices, because of their biocompatibility, unique size- and shape-dependence, and optoelectronic properties [19-22]. The complexes of lanthanide ion have been studied as tools for optical imaging and sensing of biological species [23-25]. The lanthanides

have many unique photophysical properties and these are particularly attractive features as they overcome autofluorescence and light scattering often associated with commonly used fluorophores employed in chemical biology [26, 27].

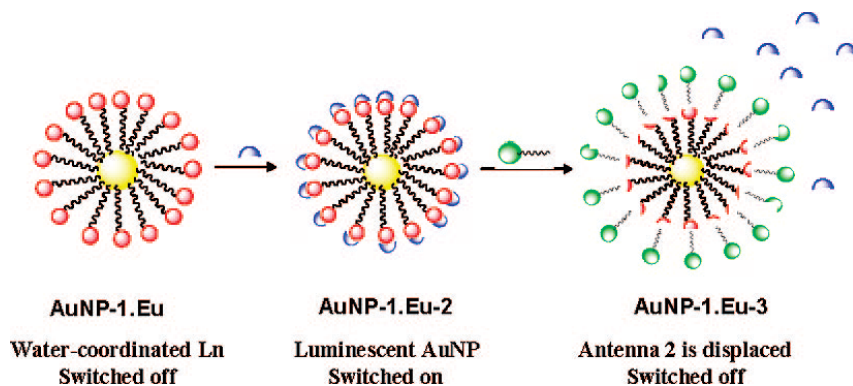
The use of nanoparticles in anion sensing, it is interesting to note, that Massue *et al.* have synthesised gold nanoparticles with appended Eu(III)–cyclen complexes 1.Eu as sensors for biologically relevant phosphates such as flavin monophosphate 3 (Scheme 1).



Scheme 1. Eu(III)–cyclen complexes 1.Eu as sensors for biologically relevant phosphates such as flavin monophosphate 3 [28].

Authors [28] present 1.Eu, a heptadendate macrocyclic Eu(III) cyclen conjugate possessing an alkyl thiol group, which enables the adsorption of 1.Eu onto the surface of gold nanoparticles for the formation of water soluble gold nanoparticles AuNP-1.Eu. The formation of ternary complexes or a self-assembly, between AuNP- 1.Eu and the β -diketone antenna 2, at pH 7.4 (0.1 M HEPES 4-(2-hydroxyethyl)-1-piperazineethanesulfonic acid) gives rise to the formation of AuNP-1.Eu-2, which is highly luminescent upon excitation of the antennae. We demonstrate that these luminescent AuNPs can be used in the sensing of biologically relevant phosphates such as flavin monophosphate 3, through the displacement of 2 (β -diketone antenna) by flavin monophosphate 3.

The functionalized nanoparticles were a β -diketone antenna 2 which coordinates to the Eu(III) centre and switches on fluorescence. This is displaced by phosphate species such as flavin monophosphate 3, which consequently causes fluorescence to be switched off as the antenna has been displaced (Scheme 2) in buffered aqueous solution. In this paper the first example of structurally defined luminescent lanthanide AuNP and demonstrated the sensing of anions through the displacement of sensitizing antennae at the surface of the AuNP have been developed [28].



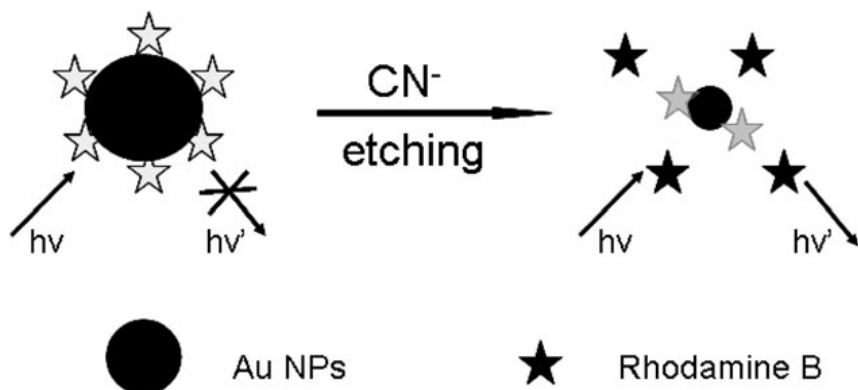
Scheme 2. The self-assembly formation between the nonluminescent AuNP-1.Eu and 2 to give AuNP-1.Eu-2. The sensing of flavin 3 occurs by the displacement of 2 and the formation of AuNP-1.Eu-3 [28].

Increasing attention is being given to the detection of anions, cyanide anion is one of the most lethal poisons to humans, that can be potentially harmful to the environment or humans [29, 30]. In addition to being found in many foods and plants, cyanide has been extensively used in industry, which correspondingly raises the potential contamination to the ground water and even drinking water [31, 32]. Therefore, pursuing an efficient and reliable analytical method for cyanide determination is of particular importance and has been the focus of much research in recent years [33-35].

Shang *et al.* have reported a new simple method for sensing cyanide involving Rhodamine-B (RB) adsorbed onto the surface of citrate stabilised gold nanoparticle. This method based on the depletion of the quencher by the analyte combined with the use of a sensitive fluorescent probe. It allows the detection of cyanide in aqueous media in a very simple approach with high sensitivity and selectivity at the same time [36]. Rhodamine B (RB) was chosen as the model fluorophore, because it is strongly fluorescent, photostable, and water-soluble. Moreover, positively-charged RB can be readily adsorbed on the surfaces of citrate-stabilized AuNPs *via* electrostatic interactions and highly efficient fluorescent resonance energy transfer is expected to occur between them.

As shown in Scheme 3, when adsorbed onto the surface of the nanoparticles the system RB-Au NPs fluoresces weakly mainly due to the efficient energy transfer from the fluorophore (RB) to the gold nanoparticle Au NPs, while the inner filter effect also contributes to the observed fluorescence decrease but to a much less extent. When in the presence of cyanide, Au NPs will be gradually dissolved. Then the fluorescence of RB is expected to be restored due to the loss

of quencher, based upon which cyanide can be detected.



Scheme 3. Schematic illustration of turn-on fluorescent cyanide detection based on the dissolution of RB-Au NPs [36].

In particular this method [36] allowed the selective detection of cyanide as low as 8.0×10^{-8} M in aqueous solution in a very simple approach. The sensing mechanism occurred through three routes:

- desorption of fluorophores from the surface of Au NPs;
- decreased fluorescence quenching ability of Au NPs with smaller size;
- diminished fluorescence inner filter effect of Au NPs upon dissolution.

Therefore, the fluorescence of RB-adsorbed Au NPs could be greatly enhanced in response to cyanide. The present principle can be generalized to develop other sensing systems by virtue of the analyte-induced depletion of the quencher. These studies demonstrates the well known interaction between cyanide and metal, thus a new avenue for the design of sensors based on a similar reaction might open up in the analytical and related fields.

The same group has also reported the development of a new cyanide sensor based on copper ion-modified CdTe quantum dots (QDs) in aqueous media [37]. This sensor functions by the ability of CN^- to bind and remove copper ions from the surface of QDs which recovers the photoluminescence (PL) that has been quenched by Cu^{2+} . The enhanced fluorescence nature, strong fluorescence quenching ability of Cu^{2+} , much higher stability constant of the complex of CN^- and copper ions and high quantum yields of QDs ensure a sensitive and selective response of the present sensor system to CN^- . Under the optimal conditions, a good linear relationship between the PL intensity and the concentration of CN^- can be obtained in the range of 3.0×10^{-7} to 1.2×10^{-5} M, with a detection

limit as low as 1.5×10^{-7} M. Additionally, the present fluorescent sensor possesses remarkable selectivity for cyanide over other anions, and negligible influences were observed on the cyanide detection by the coexistence of other anions or biological species. The proposed copper ion-modified QDs could be an efficient and reliable sensing system to monitor cyanide concentration in environmental or clinical applications.

Mesoporous solids functionalized with anion-binding groups

For years the recognition of chemical species of varying complexity has been one of the most intensively studied areas of supramolecular chemistry. Much work has been devoted to synthesis of sophisticated coordination subunits arranged in certain topologies with the aim of achieving a high degree of complementarity with the target guests [38-40].

Recently, supramolecular chemistry becomes interested in the use of coordination subunits for the preparation of molecules in such a way that the presence of target guests was transformed into a change in color [41, 42], fluorescence [43-45] or redox potential [46-48]. The recognition and signaling of chemical species is now one of the most fruitful areas of contemporary supramolecular chemistry. In this area chromogenic and fluorogenic sensors for anions [49, 50] have been developed and there is a timely increasing interest in the design of chemosensors for neutral species [51]. Although, the chromogenic and fluorogenic sensors for cations have been the most developed and expended stream in present supramolecular chemistry [52-53].

Generally the supramolecular signaling process comprises two steps:

1. the selective coordination of the target guest by using selective coordinating groups;
2. a transduction of the coordination event through modulation of the optical or electrochemical signal.

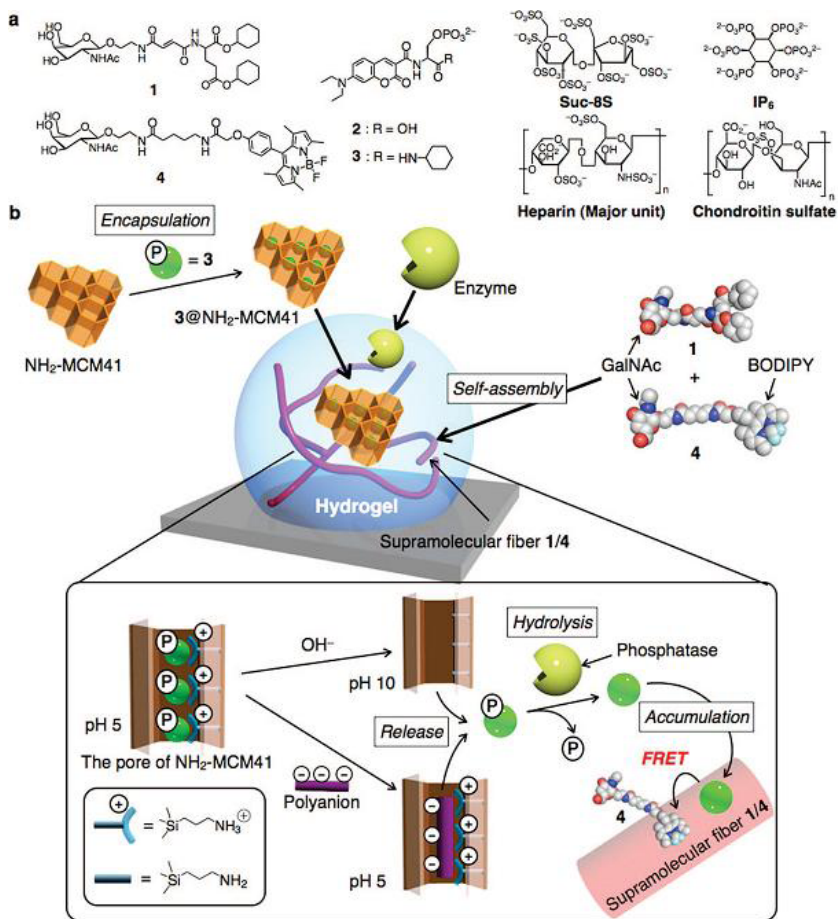
This two-step process requires adequate integration, generally into a superstructure of both components, of the signaling unit and the coordination or binding sites. Additionally, besides fluorescence or electrochemical outputs, colorimetric recognition is especially attractive because it offers the possibility of “naked eye detection” and the systems are usually easy to handle and can be applied, for instance, to the design of rapid screening semi-quantitative determinations. Many examples reported in the chemosensing field are based on relatively simple molecular systems; receptors displaying sensing features only in organic solvents are relatively common. Moreover, the milestone of selectivity in water usually necessitates extensive synthetic chemistry to prepare multitopic highly pre-organized systems.

Polyanions such as polysulfates, including heparin, chondroitin sulfate, sucrose octasulfate (Suc-8S), polyphosphates, including adenosine triphosphate (ATP), 1,4,5-inositol triphosphate (IP3), inositol hexaphosphate (IP6), phosphorylated proteins, polynucleotides such as DNA and RNA, and phospholipids, are ubiquitous in nature. They are important sensing targets because of their wide variety of biological activities [54-60]. The development of rapid, convenient, and high sensing systems for such polyanions is of considerable significance. Particularly, contamination by oversulfated chondroitin sulfate found in certain lots of heparin was recently reported to cause serious side effects presumably due to anaphylactoid response [61, 62].

The good example is gel-based sensing systems, developed by Hamachi *et al.* (fluorescence sensing system for polyanions based upon MCM-41 mesoporous silica particles modified with aminoethyl groups, enzymes and a supramolecular hydrogel) [63]. Authors presented a novel polyanion-selective fluorescence sensing system composed of a hybrid material of supramolecular hydrogel, enzymes, and aminoethyl-modified MCM41-type mesoporous silica particles (NH_2 -MCM41) encapsulating anionic fluorescent dyes. The rational combination of the polyanion-exchange ability of NH_2 -MCM41 and semi-wet supramolecular hydrogel matrix successfully produced three distinct domains; namely, cationic nanopores, hydrophobic nano/microfibers, and aqueous bulk gel phase, which are orthogonal to each other.

The coupling of anion-selective probe release from NH_2 -MCM41 with translocation of the probe facilitated by enzymatic reaction enabled fluorescence resonance energy transfer type sensing in the hybrid materials for polyanions, such as heparin, chondroitin sulfate, sucrose octasulfate, and so on. The enzymatic dephosphorylation catalyzed by phosphatase (alkaline phosphatase or acid phosphatase) that is embedded in gel matrix with retention of activity also contributed to improving the sensing selectivity toward polysulfates relative to polyphosphates. It is clear that the orthogonal domain formation of these materials and maintaining the mobility of the fluorescent dyes between the three domains are crucial for the rapid and convenient sensing provided by this system [63].

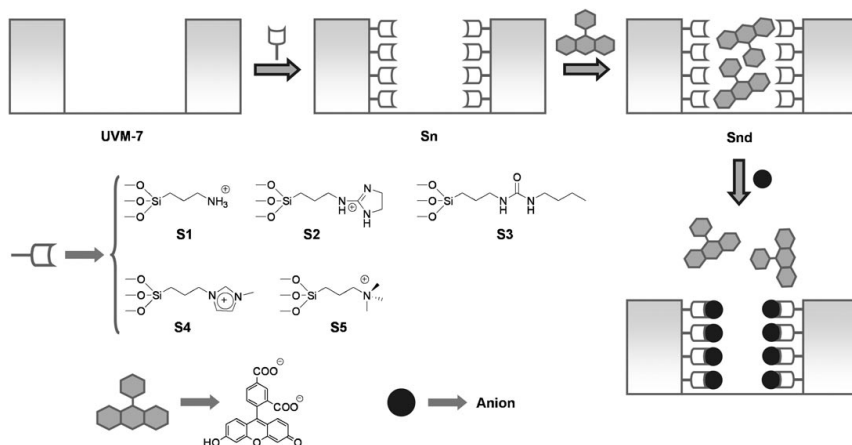
Scheme 4 illustrates author's strategy for the construction of the MCM-enzyme-supramolecular hydrogel hybrid sensor. The anion exchange within NH_2 -MCM41 took place even in the supramolecular hydrogel matrix, owing to its semi-wet environment similar to aqueous solution [63].



Scheme 4. (a) Chemical structures of compounds 1-4, Suc-8S, IP6, heparin, and chondroitin sulfate and (b) construction and mechanism operating in fluorescent dye encapsulated MCM-enzyme-supramolecular hydrogel hybrid sensory system [63].

The succeeding example of use mesoporous solids functionalized with anion-binding groups is presented by Martinez-Manez *et al.* [64]. They have employed mesoporous solids to produce new anion sensing devices that function in water *via* a displacement assay approach. UVM-7 was chosen as the support for the devices. A mesoporous MCM41-type support characterized by the presence of nanometric mesoporous particle conglomerates, was selected

as inorganic scaffolding. Reaction of the template-free UVM-7 solid with 3-aminopropyltriethoxysilane yielded solid S1, from which the derivatives S2 and S3 were obtained by reaction with 2-methylthio-2-imidazoline hydroiodide and butyl isocyanate, respectively. Solids S4 and S5 were prepared by reaction of the starting mesoporous UVM-7 scaffolding with N-methyl-N'-propyltrimethoxysilyl imidazolium chloride and with 3-(trimethoxysilyl)propyl-N,N,N-trimethylammonium chloride, respectively. The solids synthesized contain mesoporous binding pockets that can interact with anions through electrostatic attractive forces (S1, S2, S4, S5) and hydrogenbonding interactions (S1, S2, S3, S4). The solids produced contain pockets containing either positive charges, hydrogen bond donors or both.



Scheme 5. Protocol for anion sensing in water using mesoporous MCM-41-like solids containing nanoscopic binding pockets and suitable dyes [64].

These functionalized solids were loaded with a dye (d) capable of interacting coordinatively with the anchored binding sites (5-carboxyfluorescein) to yield the hybrid materials S1d, S2d, S3d, S4d and S5d. These dye-containing solids are the signaling reporters (Scheme 5). Their sensing ability towards a family of carboxylates, namely acetate, citrate, lactate, succinate, oxalate, tartrate, malate, mandelate, glutamate and certain nucleotides, has been studied in pure water at pH 7.5 (HEPES, 0.01 mol dm⁻³). In the sensing protocol, a particular analyte may be bonded preferentially by the nanoscopic functionalized pocket, leading to delivery of the dye to the solution and resulting in colorimetric detection of the guest. The response to a given anion depends on the characteristics of the

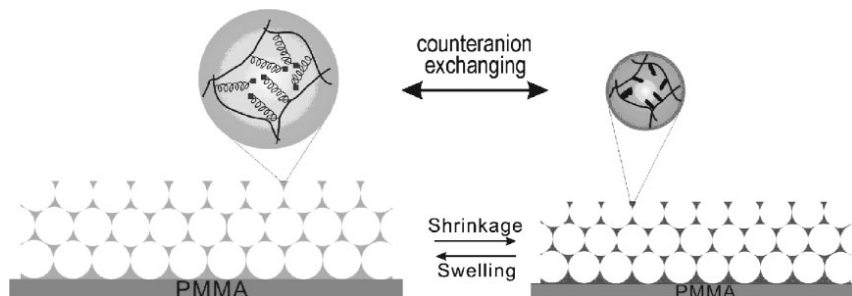
binding pockets and the specific interaction of the anion with the binding groups in the mesopores [64].

Upon addition of anion, depending on the characteristics of the functionalised binding pocket, the carboxyfluorescein may be displaced. For example S1d proved to be very selective for citrate in pure water. These conclusions can open new perspectives in the use of solids as hosts in new solid-state-supramolecular chemistry concepts. Particularly, the possibility of using a large number of mesoporous materials functionalized with different binding sites makes the approach suitable for the design of new chromo/fluorogenic probes for target guests

Other approaches to anion sensing

Other approaches to anion sensing include the production of photonic polymers from ionic liquid precursors which undergo colour changes due to anion exchange resulting in swelling or shrinking of the nanostructure [65].

Ionic liquids (ILs), mainly involving imidazolium cation, have attracted increasing interest due to their unique physicochemical properties and ever-expanding applications [66-68]. Recently, a number of literatures have described the use of imidazolium-based ILs for the regeneration of biopolymers, anion sensing, protein detection and sensitive nanomaterials [66-70]. Authors demonstrate that based on the combination of the unique properties of both ILs and photonic crystals this new concept can be efficiently employed for handy, rapid, and sensitive naked-eye detection of anions (Scheme 6) [65].

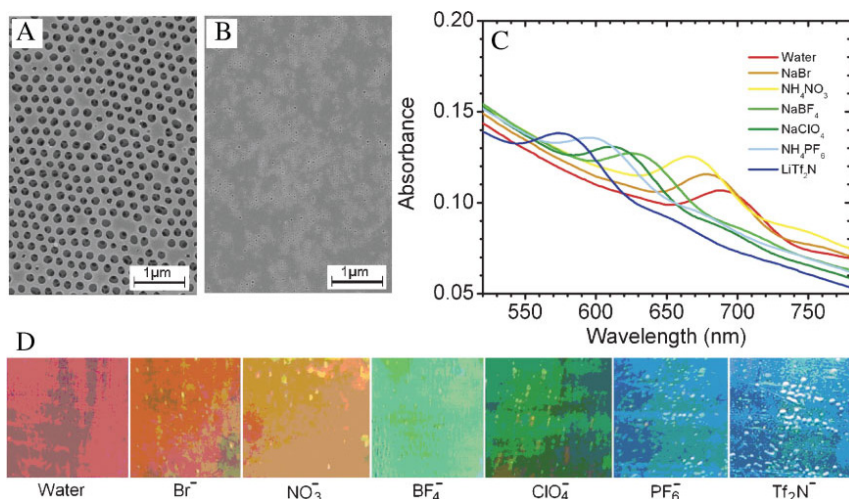


Scheme 6. Schematic illustration of the concept for anion detection based on the combination of the unique properties of both ILs and photonic crystals [65].

The initial structure of the fabricated photonic IL film is shown as Scheme 7A. The interconnected, highly ordered porous structure cannot only directly generate optical signals due to Bragg diffraction, but also be favorable for the rapid

counter-anion exchanging within IL films. Since different anion of imidazolium moiety greatly affects the hydrophilicity or hydrophobicity of IL units [66-70] when a photonic IL film is soaked in an anion aqueous solution, counteranion exchanging will induce its volume change[71] and as a consequence, cause well-defined shift of the stop band of the photonic IL film depending on the type of counteranion.

As shown in Scheme 7C, the prepared photonic IL film selectively exhibits different stop band shifts upon soaking in diversified aqueous anion solutions. More interestingly, these stop band shifts can be directly observed by the naked eye because of the substantial color changes (Fig. 2D). For example, the original photonic IL film is pink in deionized water, but changes to blue upon exposure to an aqueous solution of lithium bis(trifluoromethylsulfonyl) imide (LiTf_2N). Moreover, with the increase of the hydrophobicity of IL units upon counteranion exchange, the photonic IL film changes gradually from the transparent into semitransparent, even opaque, probably due to the increased light scattering of the interface between water phase and hydrophobic gel. Correspondingly, the opened pores become closed, due to the strong shrinkage of IL film (Scheme 7B).



Scheme 7. SEM images of the fabricated photonic ionic liquid film with opened pore structure (A) and closed pore structure (B). C) Stop band shifts of the photonic ionic liquid film upon soaking in diversified 0.02M anions aqueous solutions. D) The induced color changes of the photonic ionic liquid film upon soaking in diversified 0.02 M anions aqueous solutions [65].

It is interesting to note, that based on the system of the unique properties of both ILs and photonic crystals, this paper demonstrates a new concept for anion detection in a easy, rapid and sensitive way. Through simple counter anion exchanging of the imidazolium IL units the 3D highly ordered IL porous structure can directly sense different anions and easily convert the anion detection events into readable optical signals with color changes. The constructed photonic IL also shows promise for the detection of solvents with different polarities. This combination of the unique properties of both ILs and photonic crystals could open immense opportunities for constructing novel advanced materials [65].

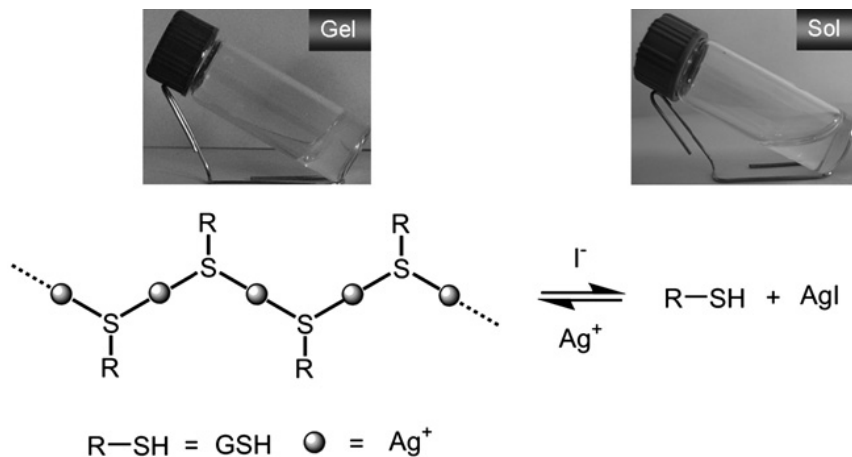
Anions, especially halides, play important roles in both environment and life sciences. For example, iodide (I^-) can induce depolymerization of actin filaments and the corresponding transition from a gel-like state to a sol state, possibly by influencing the hydration shell that is thought to surround and stabilize the actin filaments polymer [72]. Therefore, developing selective and feasible detection strategies for anions are undoubtedly crucial. Actually, anion recognitions have indeed received much attention during past decades [2]. However, only few investigations involve I^- recognition, and most of which were conducted by colorimetric and fluorimetric methods [73-75].

Applicable example we could find in the paper of Jiang and co-workers [76]. The authors demonstrate for the first time a highly selective recognition of anions based on gel-sol state transition of supramolecular hydrogel of Ag(I)-glutathione (GSH) coordination polymers, which allows for facile and selective visual recognition of I^- *via* naked eyes even in a strongly colored and/or fluorescent background. Such a strategy overcomes the drawback of spectral interferences which are often encountered in conventional colorimetric and fluorimetric means. Illustration of reversible gel-sol state transition of supramolecular hydrogel of Ag(I)-GSH coordination polymers triggered by alternately adding I^- into hydrogel and Ag(I) into the resulting sol solution has been shown in Scheme 8. It was rationalized that I^- functioned as a depolymerizing agent for the Ag(I)-GSH supramolecular hydrogels. A feasible quantitative assay for I^- was established that afforded satisfactory results for simulated wastewater samples.

This strategy [77] can in principle be applicable to other species by following a smart gel-sol state transition in designed supramolecular hydrogel.

Immobilization can be achieved, among other methods [77-79] by the incorporation of receptors into self-assembled monolayers or bilayer membranes [7] Polydiacetylene (PDA) is a particular interesting material in this respect, as diacetylene surfactants will selfassemble in water to form vesicles that can be photopolymerized to generate PDA in situ [80-83] The polymers conjugated backbone provides absorbance and fluorescence properties which are useful for

the transduction of the analytical signal [84, 85] Functionalized polydiacetylene films and vesicles have been used as chemosensors to monitor metal ions [84] glucose [86] proteins [9] and for the colorimetric detection of the influenza virus [87].

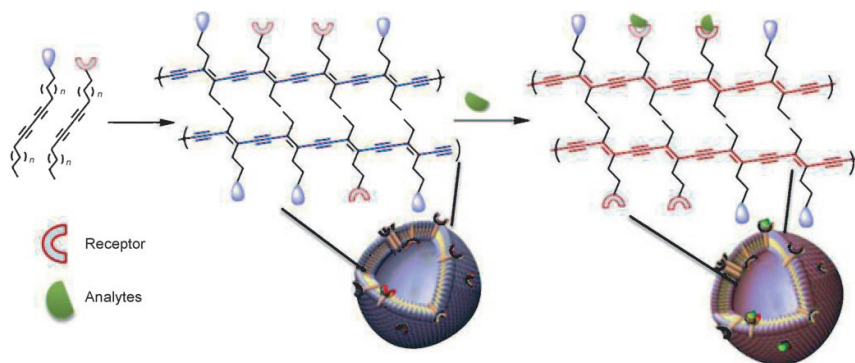


Scheme 8 Illustration of reversible gel-sol state transition of supramolecular hydrogel of Ag(I)-GSH coordination polymers triggered by alternately adding I⁻ into hydrogel and Ag(I) into the resulting sol solution [76].

Koenig and co-workers have assembled vesicles from polydiacetylene molecules functionalised with metal complexes [88]. This group describes the preparation of self-assembled vesicular polydiacetylene (PDA) particles with embedded metal complex receptor sites. The particles respond to the presence of ATP and PPi (pyrophosphate) in buffered aqueous solution by visible changes of their color and emission properties. Blue PDA vesicles of uniform size of about 200 nm were obtained upon UV irradiation from mono- and dinuclear zinc(II)-cyclen and iminodiacetato copper [CuII-IDA] modified diacetylenes, embedded in amphiphilic diacet- Glylene monomers. Addition of ATP and PPi to the PDA vesicle solution induces a color change from blue to red observable by the naked eye. The binding of ATP and PPi changes the emission intensity.

Other anions such as ADP, AMP, H₂PO₄⁻, CH₃COO⁻, F⁻, Cl⁻, Br⁻ and I⁻, failed to induce any spectral changes. The zinc(II)-cyclen nanoparticles are useful for the facile detection of PPi and ATP in millimolar concentrations in neutral aqueous solutions, while CuII-IDA modified vesicular PDA receptors are able

to selectively discriminate between ATP and PPi. Scheme 9 shows schematically the assembly and analyte response of the vesicular metal complex sensor system.



Scheme 9. Schematic representation of the preparation and the analyte response of self-assembled polydiacetylene vesicles with embedded metal complex binding sites for anions [88].

The vesicular receptors obtained from ZnII–cyclen functionalized polydiacetylene monomers respond to the presence of ATP and PPi at neutral pH at millimolar concentrations with visible changes of their color and emission. Other anions, such as halides, do not induce an analytic response. Polymerized vesicular receptors with metal complex binding sites may find applications for simple analytic tasks

Conclusions

In recent years we could observe advances in a number of areas of supramolecular chemistry. Anion recognition's problems pertain to one of them. This short review focuses on anion binding systems are representative by examples based on gel–sol state transition of supramolecular hydrogel, use of nanoparticles and mesoporous materials in sensing and self-assembled vesicular anion receptors, functionalised with metal complexes. Chemical sensors have been necessary and demanded for clinical diagnostics, environmental and food analysis or in the detection of illicit drugs, explosives and chemical warfare agents, ect. Anion complexation continues to be a stimulating and fruitful area of cross-disciplinary research and we could expect significant steps forward in the coming years.

Acknowledgements

Authors thank the Polish Ministry of Science and Higher Education for financial support under Grants No. NN 204 338237 and N 204 005536 in the years 2009–2012.

References

1. The Supramolecular Chemistry of Anions, ed. A. Bianchi, K. Bowman-James, E. García-España, Wiley-VCH, Weinheim, 1997
2. P. D. Beer, P. A. Gale, *Angew. Chem. Int. Ed.* 40 (2001) 486
3. J. M. Llinares, D. Powell, K. Bowman-James, *Coord. Chem. Rev.* 240 (2003) 57
4. V. McKee, J. Nelson, R. M. Town, *Chem. Soc. Rev.* 32 (2003) 309
5. Core Concepts in Supramolecular Chemistry and Nanochemistry, ed. J.W. Steed, D.R. Turner, K. J. Wallace, John Wiley&Sons, 2007
6. F. P. Schmidtchen, M. Berger, *Chem. Rev.* 97 (1997) 1609
7. Comprehensive Supramolecular Chemistry, ed. J. L. Atwood, J. E. D. Davies, D. D. MacNicol, F. Voegtle, J.-M. Lehn and G. W. Gokel, Elsevier Science, Oxford, 1996, vol. 1
8. A. Ojida, M. Yoshifumi, W. Jirarut, T. Shun-ichi, K. Sada, I. Hamachi, *Chem. Asian J.* 1 (2006) 555
9. A. P. de Silva, H. Q. N. Gunaratne, T. Gunnlaugsson, A. J. M. Hauxley, C. P. McCoy, J. T. Rademacher, T. E. Rice, *Chem. Rev.* 97 (1997) 1515
10. C. M. Niemeyer, *Angew. Chem., Int. Ed.*, 42 (2003) 5796
11. M. P. Moloney, Y. Gun'ko, J. M. Kelly, *Chem. Commun.* (2007) 3900
12. A. Verma, J.M. Simard, J. W.E. Worrall, V. M. Rotello, *J. Am. Chem. Soc.* 126 (2004) 13987
13. A. Labande, J. Ruiz, D. Astruc, *J. Am. Chem. Soc.* 124 (2002) 1782
14. S. J. Hurst, M. S. Han, A. K. R. Lytton-Jean, C. A. Mirkin, *Anal. Chem.* 79 (2007) 7201
15. U. Drechsler, B. Erdogan, V. M. Rotello, *Chem. Eur. J.* (2004) 10
16. Y. Chen, Y. Chi, H. Wen, Z. Lu, *Anal. Chem.* 79 (2007) 96
17. J. D. Gibson, B. P. Khanal, E. R. Zubarev, *J. Am. Chem. Soc.* 129 (2007) 11653
18. C. O'Dalaigh, S. A. Corr, Y. Gun'ko, S. Connon, *J. Angew. Chem., Int. Ed.* 46 (2007) 4329
19. M. Montalti, N. Zaccheroni, L. Prodi, N. O'Reilly, S. L. James, *J. Am. Chem. Soc.* 129 (2007) 2418
20. N. Tucitto, V. Torrisi, M. Cavazzini, T. Morotti, F. Puntoriero, S. Quici, S. Campagna, A. Licciardello, *ChemPhys Chem.* 8 (2007) 227

21. C. Li, X. Liu, M. Yuan, J. Li, Y. Guo, J. Xu, M. Zhu, J. Lv, H. Liu, Y. Li, *Langmuir* 23 (2007) 6753
22. K. G. Thomas, P. V. Kamat, *Acc. Chem. Res.* 36 (2003) 888
23. J. P. Leonard, C. B. Nolan, F. Stomeo, T. Gunnlaugsson, *Top. Curr. Chem.* 281 (2007) 281
24. S. E. Plush, T. Gunnlaugsson, *Org. Lett.* 9 (2007) 1919
25. A. Beeby, I. M. Clarkson, R. S. Dickens, S. Faulkner, D. Parker, L. Royle, A. S. de Sousa, J. A. G. Williams, M. J. Woods, *Chem. Soc., Perkin Trans. 2* (1999) 493
26. B. I. Ipe, K. Yoosaf, K. G. Thomas, *J. Am. Chem. Soc.* 128 (2006) 1907;
27. D. J. Lewis, T. M. Day, J. V. Macpherson, Z. Pikramenou, *Chem. Commun.* (2006) 1433
28. J. Massue, S. J. Quinn and T. Gunnlaugsson, *J. Am. Chem. Soc.* 130 (2008) 6900
29. R. Martinez-Manez, F. Sancenon, *Chem. Rev.* 103 (2003) 4419
30. T. Gunnlaugsson, M. Glynn, G. M. Tocci, P. E. Kruger and F. M. Pfeffer, *Coord. Chem. Rev.* (2006) 250
31. N. Gimeno, X. Li, J. R. Durrant, R. Vilar, *Chem.–Eur. J.*, 14 (2008) 3006
32. Zhang, W., Liu, W., Lv, Y., Li, B., Ying, W., *J. Haz. Mat.*, 184 (2010), 135-140
33. A. R. Surleva, V. D. Nikolova and M. T. Neshkova, *Anal. Chim. Acta*, 583 (2007) 174
34. W. J. Jin, M. T. Fernandez-Arguelles, J. M. Costa-Fernandez, R. Pereiro and A. Sanz-Medel, *Chem. Commun.* (2005) 883
35. A. Touceda-Varela, E. I. Stevenson, J. A. Galve-Gasion, D. T. F. Dryden and J. C. Mareque-Rivas, *Chem. Commun.* (2008) 1998
36. L. Shang, L. H. Jin, S. J. Dong, *Chem. Commun.* (2009) 3077
37. L. Shang, L. H. Zhang, S. J. Dong, *Analyst* 134 (2009) 107
38. J. L. Atwood, K. T. Holman, J. W. Steed, *Chem. Commun.* (1996) 1401
39. V. McKee, J. Nelson, R. M. Town, *Chem. Soc. Rev.* 32 (2003) 309
40. P. A. Gale, *Acc. Chem. Res.* 39 (2006) 465
41. Suksai, T. Tuntulani, *Top. Curr. Chem.* 255 (2005) 163
42. R. Martinez-Manez, F. Sancenon, *Coord. Chem. Rev.* 250 (2006) 3081
43. P. D. Beer, P. A. Gale, *Angew. Chem.* 113 (2001) 502
44. D. Parker, *Coord. Chem. Rev.* 205 (2000) 109
45. L. Fabbrizzi, M. Licchelli, G. Rabaioli, A. Taglietti, *Coord. Chem. Rev.* 205 (2000) 85
46. P. D. Beer, J. Cadman, J. M. Lloris, R. Martinez-Manez, J. Soto, T.

- Pardo, M. D. Marcos, *J. Chem. Soc. Dalton Trans.* (2000) 1805
47. F. Sancenon, A. Benito, F. J. Hernandez, J. M. Lloris, R. Martinez-Manez, T. Pardo, J. Soto, *Eur. J. Inorg. Chem.* (2002) 866
 48. P. D. Beer, S. R. Bayly, *Top. Curr. Chem.* 255 (2005) 125
 49. P. de Silva, H. Q. N. Gunaratne, T. Gunnlaugsson, A. J. M. Huxley, C. P. McCoy, J. T. Rademacher, T. E. Rice, *Chem. Rev.* 97 (1997) 1515
 50. S. L. Wiskur, H. Ait-Haddou, E. V. Anslyn, J. J. Lavigne, *Acc. Chem. Res.* 34 (2001) 963
 51. G. J. Mohr, *Anal. Bioanal. Chem.* 386 (2006) 1201
 52. B. Valeur, I. Leray, *Coord. Chem. Rev.* 205 (2000) 3
 53. J. F. Callan, A. P. de Silva, D. C. Magri, *Tetrahedron* 61 (2005) 8551
 54. P. S. Damus, M. Hicks, R. D. Rosenber, *Nature* 246 (1973) 355
 55. D. O. Clegg, et al. *N. Engl. J. Med.* 354 (2006) 795
 56. M. Fannon, K. Forsten-Williams, M. A. Nugent, K. J. Gregory, C. L. Chu, A. L. Goerges-Wildt, D. Panigrahy, A. Kaipainen, C. Barnes, C. Lapp, Y. J. Shing, *Cell. Physiol.* 215 (2008) 434
 57. H. Abelson, *Science* 283 (1999) 2015
 58. B. K. Yeh, A. V. Eliseenkova, A. N. Plotnikov, D. Green, J. Pinnell, T. Polat, A. Gritli-Linde, R. J. Linhardt, M. Mohammadi, *Mol. Cell. Biol.* 22 (2002) 7184
 59. S. M. Butterfield, D. H. Tran, H. Zhang, G. D. Prestwich, S. J. Matile, *J. Am. Chem. Soc.* 130 (2008) 3270
 60. J. Cho, K. Choi, T. Darden, P. R. Reynolds, J. N. Petite, S. B. Shears, *J. Biotechnol.* 126 (2006) 248
 61. M. Guerrini et al. *Nat. Biotechnol.* 26 (2008) 669
 62. T. K. Kishimoto, et al. *N. Engl. J. Med.* 358 (2008) 2457
 63. A. Wada, S. Tamaru, M. Ikeda and I. Hamachi, *J. Am. Chem. Soc.* 131 (2009) 5321
 64. M. Comes, E. Aznar, M. Moragues, M. D. Marcos, R. Martinez-Manez, F. Sancenon, J. Soto, L. A. Villaescusa, L. Gil and P. Amoros, *Chem.–Eur. J.* 151 (2009) 9024
 65. X. B. Hu, J. Huang, W. X. Zhang, M. Li, C. G. Tao, G. T. Li, *Adv. Mater.*, 20 (2008) 4074
 66. *Ionic Liquid in Synthesis*, ed. P. Wasserscheid, T. Welton, Wiley-VCH, Weinheim, Germany 2003
 67. Z. Fei, T. J. Geldbach, D. Zhao, P. J. Dyson, *Chem. Eur. J.* 12 (2006) 2122
 68. D. R. Rogers, G. A. Voth, *Acc. Chem. Res.* 40 (2007) 1077
 69. K. Fukumoto, M. Yoshizawa, H. Ohno, *J. Am. Chem. Soc.* 127 (2005)

2398

70. D. Batra, D. N. T. Hay, M. A. Firestone, *Chem. Mater.* 19 (2007) 4423
71. F Yan, J. Texter, *Angew. Chem. Int. Ed.* 46 (2007) 2440
72. I S. R. Kabir, K. Yokoyama, K. Mihashi, T. Kodama and M. Suzuki, *Biophys. J.* 85 (2003) 3154
73. Z. Rodriguez-Docampo, S. I. Pascu, S. Kubik and S. Otto, *J. Am. Chem. Soc.*, 128 (2006) 11206
74. K. Ghosh, T. Sen, *Tetrahedron Lett.*, 49 (2008) 7204
75. Z. B. Shang, Y. Wang, W. J. Jin, *Talanta*, 78 (2009) 364
76. J. S. Shen, D. H. Li, Q. G. Cai and Y. B. Jiang, *J. Mater. Chem.*, 19 (2009) 6219
77. E. Palomares, R. Vilar, A. Green, J. R. Durrant, *Adv. Funct. Mater.* 14 (2004) 111
78. A. B. Descalzo, R. Martinez-Manez, F. Sancenon, K. Hoffmann, K. Rurack, *Angew. Chem.* 2006, 118, 6068–6093; *Angew. Chem. Int. Ed.* 45 (2006) 5924
79. E. Kim, H. E. Kim, S. J. Lee, S. S. Lee, M. L. Seo, J. H. Jung, *Chem. Commun.* (2008) 3921
80. D. J. Ahn, J.-M. Kim, *Acc. Chem. Res.* 41 (2008) 805
81. H. Ringsdorf, B. Schlarb, J. Venzmer, *Angew. Chem.* 100 (1988) 117
82. K. Morigaki, T. Baumgart, U. Jonas, A. Offenhausser, W. Knoll, *Langmuir* 18 (2002) 4082
83. H. He, M. A. Mortellaro, M. J. P. Leiner, R. J. Fraatz, J. K. Tusa, *J. Am. Chem. Soc.* 125 (2003) 1468
84. M. A. Reppy, B. A. Pindzola, *Chem. Commun.* (2007) 4317
85. J. Yoon, Y. S. Jung, J. - M. Kim, *Adv. Funct. Mater.* 19 (2009) 209
86. Q. Cheng, R. C. Stevens, *Adv. Mater.* 9 (1997) 481
87. S. Kolusheva, R. Zadnard, T. Schrader, R. Jelinek, *J. Am. Chem. Soc.* 128 (2006) 13592
88. D. A. Jose, S. Stadlbauer and B. Koenig, *Chem.–Eur. J.* 15 (2009) 7404

Chapter 9

Selective fluorescent chemosensors

Radosław Pankiewicz, Grzegorz Schroeder and Bogusława Łęska
*Adam Mickiewicz University, Faculty of Chemistry, Grunwaldzka 6,
60-780 Poznań, Poland*

Introduction

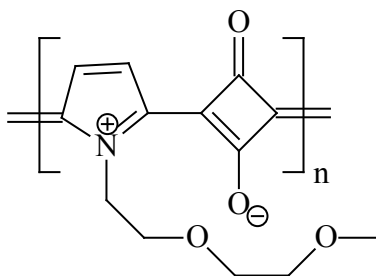
Chemosensors are molecules or supramolecular devices that signal interactions with analytes. Sensors can detect wide range of cations, anions both simple inorganic and organic as well as many different uncharged particles. Detection, in the most cases, be holds in solutions. Even in cases of detection of gases molecules or ions are first caught to solution and after that sensing. In time projecting of sensor we must solve two problems: good interaction between analyzed particle and after that easy recognizable signal. The solution is creation bifunctional molecules, one part coordinate particle, second part is responsible for signaling. Fluorescence offers high sensitivity among the many signal types available. [1, 2] So this mode of signal transduction has been used widely in the detection of a number of transition metal ions. [3, 4] Detection of individual metal ions with high specificity under physiologically relevant conditions is an important aspect in the design of fluorescent chemosensors for biological and environmental applications. Therefore peptide based sensors offer several advantages over other systems as they are biocompatible and could be conjugated to appropriate systems of biological interest such as proteins or nucleic acids.

There are known many of fluorescent sensors [5] that would merit discussion in general introductory review of that kind. Most of these were already featured in the review literature [6]. For this reason we presented only few selected, representative examples.

A fluorescent sensor for Li⁺

The pyrrole derivative was prepared as 2~³6 polycondensation reaction with squaric acid. The molecular wire was (SMW) obtained in 62% yield. Addition of micromolar quantities of alkali metal ions such as Li⁺, K⁺ and Na⁺ to a DMSO solution enhanced the absorption maxima with a marginal red shift. On the other hand, the squaraine molecular wire SMW showed significant change in

its fluorescence emission behaviour upon addition of micromolar quantities of Li^+ . Interestingly, addition of micromolar quantities of K^+ and Na^+ did not show any considerable change to the emission property. The squaraine molecular wire showed a 92% enhancement in the fluorescence quantum yield. The observed specificity of SMW towards Li^+ can be attributed to the optimum chain length of the binding sites and the electron affinity of Li^+ [7].



A fluorescent sensor for Na^+

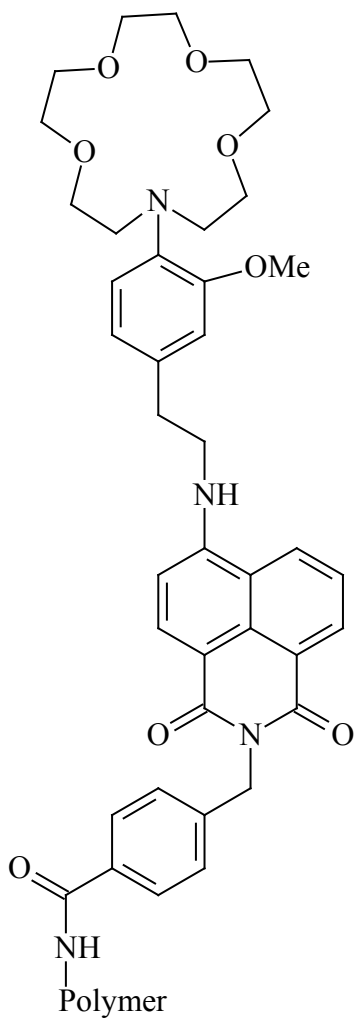
A good Na^+ sensor would have the following properties. Na^+ should bind with a dissociation constant of 5-50 mM at pH 7 in aqueous solution with no organic solvents permitted. Such a K would approximately match the expected range for sodium cations and maximize sensitivity. Excessive Na^+ affinity would be undesirable, since the indicator would then either be Na^+ saturated, or if applied in excess would depress $[\text{Na}^+]$. A good indicator should have enough discrimination against K^+ , H^+ , Mg^{2+} and Ca^{2+} . The sensor should show strong fluorescence, character able by a product of extinction coefficient and fluorescence quantum yield exceeding $10^3 \text{ M}^{-1}\text{cm}^{-1}$.

The sensor 2 made by Leiner and coworkers [8] fulfils all above mentioned conditions.

Monoaza-15-crown-5 ether has similar preferences for binding sodium and potassium cations besides sufficient attraction toward H^+ [9]. Connections of the phenyl ring with azacrown nitrogen drastically lower the attraction toward H^+ under these conditions. The three-dimensional pseudocryptand environment give higher selectivity [10,11] toward the size-complementary Na^+ than the larger K^+ (Figure 1).

Group of fluorescent PET sensor which 2 is a good example shows clear conformational changes upon binding sodium cations which decouple the electron systems of the 2-methoxyphenyl unit and of the nitrogen atom [13]. This has important ramification in a PET sensing content, because the oxidation

potential of the receptor jumps from 0.8 V to >1.2 V upon Na⁺ binding [5].



2

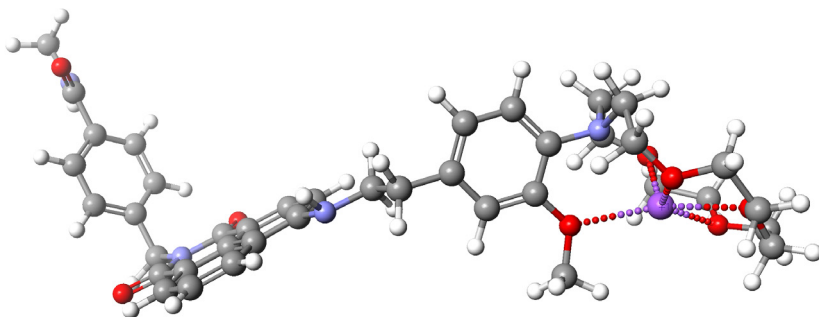
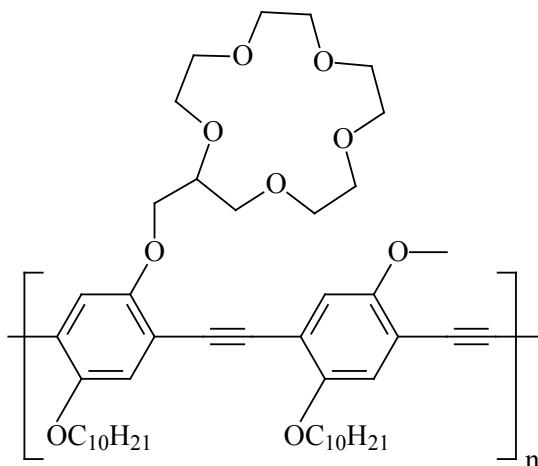


Figure 1. Structure of 2 with Na^+ calculated by PM5 semiempirical method [12].

A fluorescent sensor for K^+

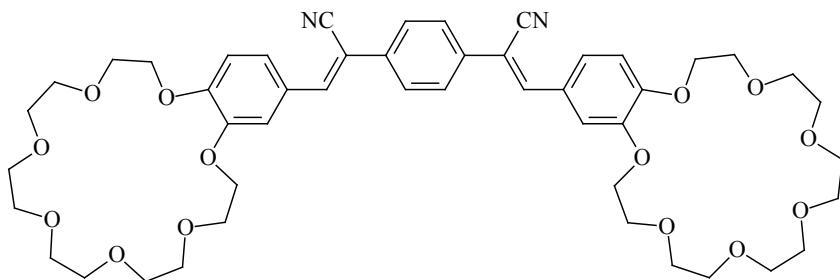


Kim and coworkers [14] has reported a new transduction mechanism based on the aggregation of conjugated sensory polymers induced by K^+ ions. This system displays enhanced sensitivity because of energy migration processes and high selectivity for K^+ over Na^+ ions.

Li^+ or Na^+ ions form 1:1 complexes with [15]-crown-5, and show no observable effect on any of the spectroscopic properties of the polymer. The absorbance and fluorescence spectra of polymer in solution are essentially

unchanged even after the addition of a 1500-fold excess of Li^+ or Na^+ ions. In contrast, addition of K^+ ions to a solution of sensor produced a new red-shifted peak at 457 nm in the absorption spectra and also fluorescence quenching was evident.

A fluorescent sensor for Cs^+

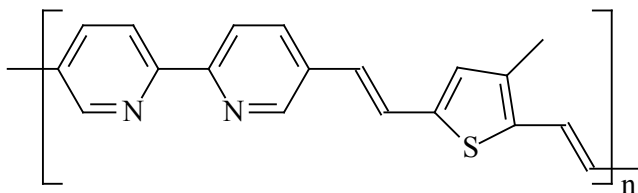


New dicyano-substituted distyrylbenzene derivative and two 18-crown-6 rings (L) was synthesized. In acetone solution, L shows a broad absorption at 380 nm. With the addition of Cs^+ ion, a slight decrease of the absorption is observed. However, a significant change is observed in fluorescence spectra of L when Cs^+ ions are added. The fluorescence intensity is enhanced significantly and the fluorescent peak redshifts from 482 to 526 nm. Stoichiometry studies indicate that L forms a 1:1 complex with caesium ion, indicating that each Cs^+ ion coordinates to two 18-crown-6 moieties. At saturation in acetone solution the maximum fluorescence intensity of L complexed with Cs^+ is about 20 times that of free L. Other alkali metal ions such as Li^+ , Na^+ and K^+ were also examined. No significant fluorescent enhancement was observed with any of these, even though 18-crown-6 is known to bind K^+ strongly [15].

A fluorescent sensor for Mg^{2+}

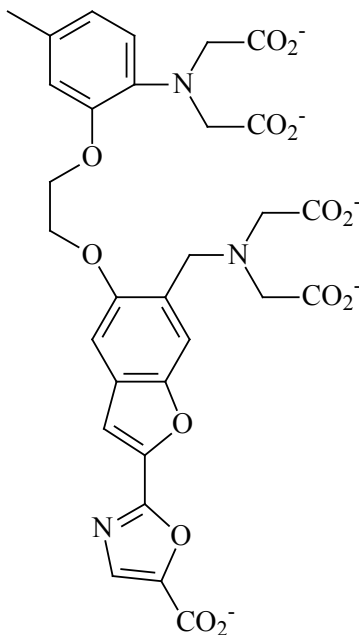
Conjugated polymers containing 2, 29-bipyridylene (P) was synthesized by Pei and coworkers [16] and studied their capability to detect metal ions. When aqueous solutions of Mg^{2+} , Ca^{2+} , Ba^{2+} , and Sr^{2+} ions were added to a solution of polymer P, Ca^{2+} , Ba^{2+} and Sr^{2+} did not change the appearance of the polymer solution. Only, the addition of Mg^{2+} changed the color of the solution from yellow to orange. Spectral studies indicated that both absorption spectra and fluorescence spectra of the polymer solution remained unchanged upon the addition of Ca^{2+} , Ba^{2+} , and Sr^{2+} , but the addition of Mg^{2+} resulted in a red shift in

the absorption spectrum of 12 nm. The fluorescence of the P solution was also gradually quenched upon adding Mg^{2+} up to a nearly complete quenching at a concentration of 30 ppm. The selective response to alkali earth metal ions thus allows the selective detection of Mg^{2+} .



A Fluorescent sensor for Ca^{2+}

Important evaluation of the role of calcium as an intracellular messenger requires quantitative measurement of cytosolic free Ca^{2+} concentrations and comparison with varied stimuli and cell responses [17]. The best example of calcium indicator is “fura” 3 synthesized by Tsien and coworkers [18].



UV absorption spectra of 3 at various levels of free Ca^{2+} are shown in Figure 2. The absorbance spectra are much as one would expect for stilbene chromophores. In the absence of, the spectrum shows a maximum at about 340 nm. Ca^{2+} binding causes a major shift toward shorter wavelengths.

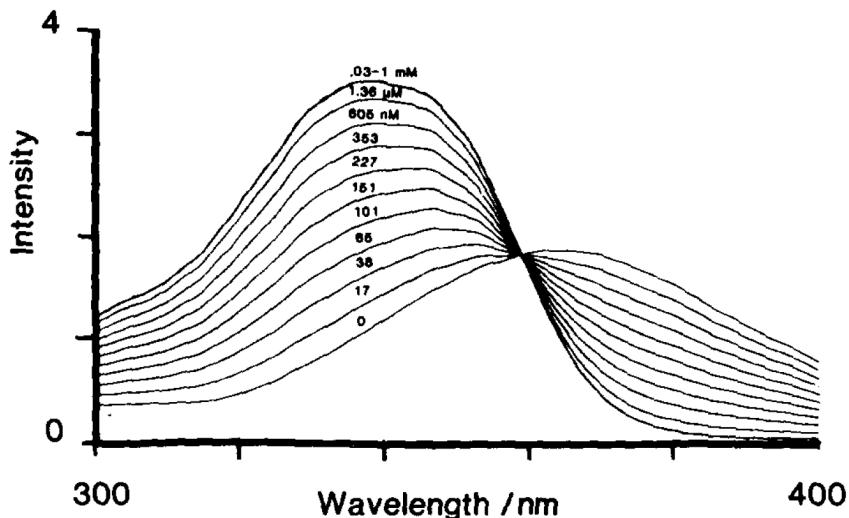


Figure 2. Excitation spectra for $1 \mu\text{M}$ 3 at $20 \text{ }^\circ\text{C}$ in buffers with free Ca^{2+} values ranging from $<1\text{ nM}$ to $>10 \mu\text{M}$. The excitation band width was 1.9 nm , the emission was collected at 510 nm with 4.6 nm band width, and the spectra were automatically corrected for excitation lamp and monochromator characteristics using a thodamine B quantum corner [18].

The quantum yield of fluorescence of fluorescence for the 2 is about 0.5 with Ca^{2+} . This value is typical of dyes normally considered to be highly fluorescent. In all cases the calcium complex has quantum efficiency between 1.3- and 2.1-fold higher than the Ca^{2+} -free dye.

Dissociation constants for this indicator is about 140 nM at ionic strengths about 0.1. This values are close to the dissociation constant (110 nM) of the parent compound BAPTA [19]. The substituents that make up the rest of the chromophores must be only slighty electron-withdrawing, therefore moderately electron-withdrawing substituents such as halo, azo, and acyl cause larger increases in calcium dissociation constants [20]. Good complexation ability is caused by two carboxylic group on the "tail" of molecule, Figure 3, which can close cation in the form of pseudo ring.

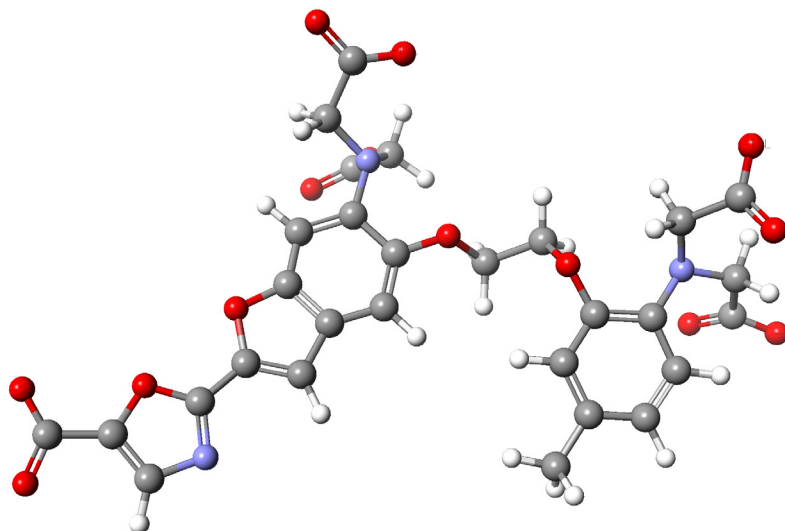
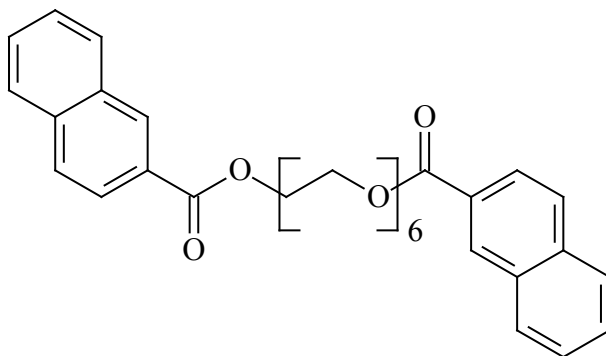


Figure 3. Structure of 3 calculated by PM5 semiempirical method [12].

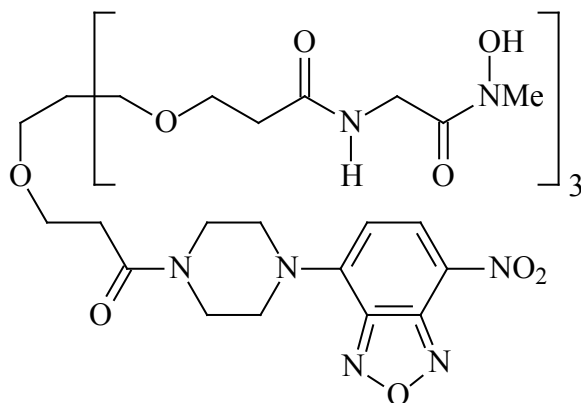
A fluorescent sensor for Ba²⁺



Kawakami and coworkers synthesized a new fluorescent ion sensor. Thanks to adjusting the length of the polyether chain binding two chromophores, they received an excellent fluorescent chemosensor for Ba²⁺ [21].

Fluorescent sensors for Fe³⁺

Siderophores are naturally good ligands to complex Fe³⁺ with excellent selectivity, [5] without which many microorganisms could not achieve their essential iron intake [22]. Some of these siderophores are also excellent at recognizing MoO₄⁻ [23]. These receptors were incorporated into fluorophore-spacer-receptor systems without compromising their coordination properties. The best sample of this receptor is 4 with a tris-hydroxamate motif in their structure [24].



They have tri-pendand-like arms (Fig. 4.) which can complex Fe³⁺ cations. The complexation of the cation causes significant fluorescence quenching.

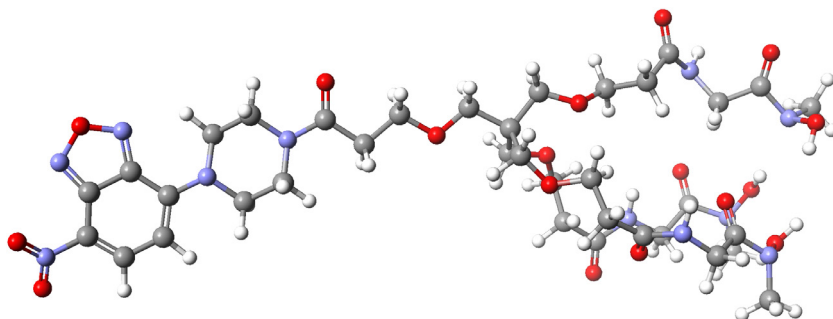
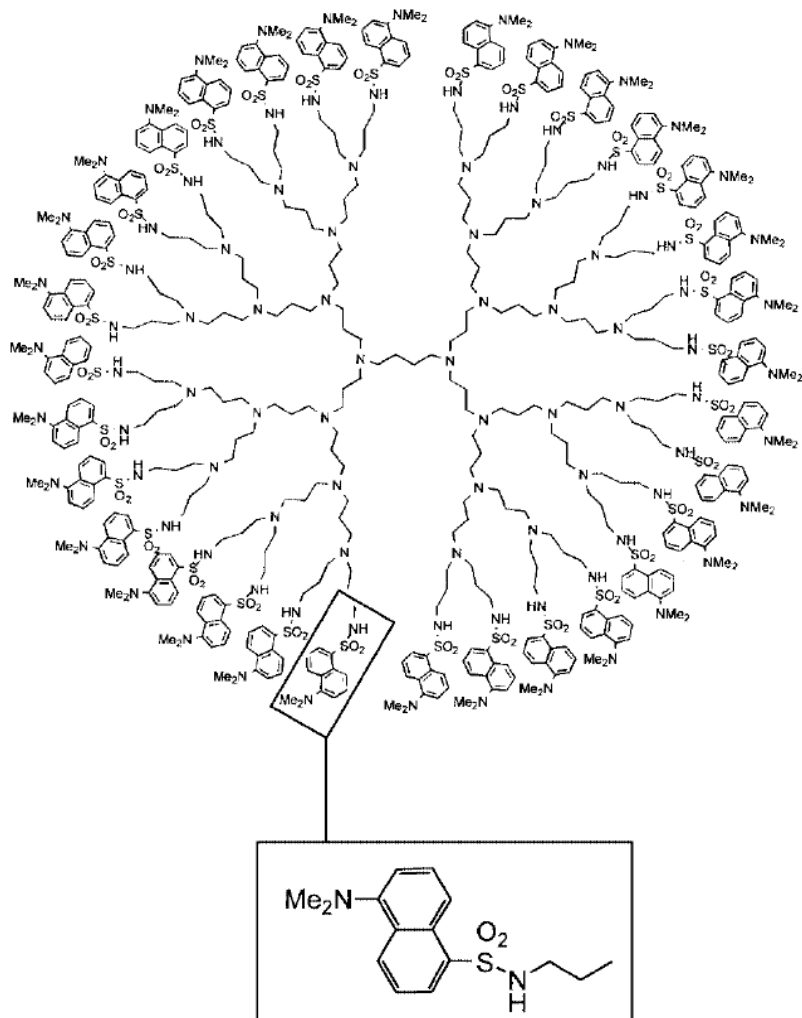


Figure 4. Structure of 4 calculated by PM5 semiempirical method [12].

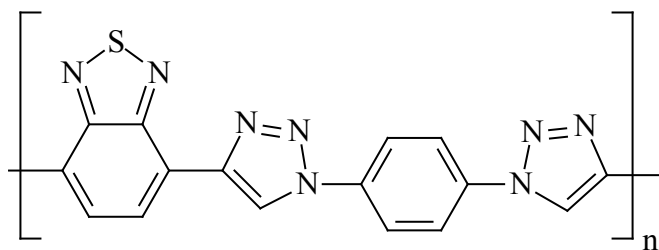
A fluorescent sensor for Co^{2+}



In a fourth generation poly(propylene amine) dendrimer decorated with 32 dansyl units at the periphery and containing 30 aliphatic amine units in the

interior, the strong fluorescence of all the dansyl units is quenched when a Co^{2+} ion is incorporated into the dendrimer. In acetonitrile–dichloromethane solution, dendrimer exhibits intense absorption bands in the near UV spectral region and a strong fluorescence band in the visible region ($\lambda_{\text{max}} = 514 \text{ nm}$). Addition of Co^{2+} solution caused a strong quenching on the fluorescence intensity of the dansyl units appended at the periphery of the dendrimer, without affecting the absorption spectrum [25].

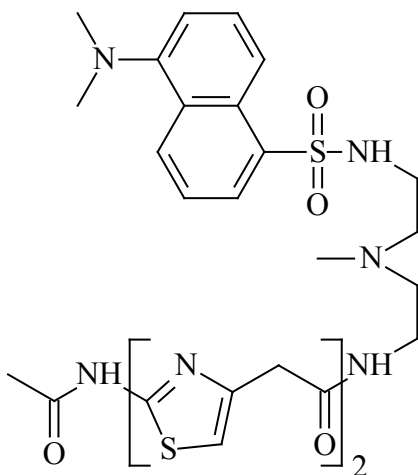
A fluorescent sensor for Ni^{2+}



A conjugated polymer was obtained by the polymerization of 4,7-diethynylbenzo[2,1,3]thiadiazole with 1,4-diazidobenzene via click reaction. The polymer shows strong blue-green fluorescence due to the extended p-electronic structure in the main chain backbone. The fluorescence intensities of the polymer were almost unaffected by the addition of Co^{2+} , Hg^{2+} , Ag^+ , Cd^{2+} , Zn^{2+} and Cu^{2+} , but strongly quenched by Ni^{2+} at 1:1 molar ratio. These results indicated that the polymer has highly specific recognition ability for Ni^{2+} ion. The good selectivity and high sensitivity of the polymer for Ni^{2+} recognition may be attributed to the building block receptor arisen from benzo[2,1,3]thiadiazole and triazole units in the main chain backbone that are well fit for the formation of a more stable Ni^{2+} -polymer complex as compared to other transition metal ions [26].

A fluorescent sensor for Cu^{2+}

Many of fluorescent receptors showing good Cu^{2+} selectivity is the presence of one or more primary amide moieties that appear to lose the amide proton during the complexation process [5]. Of course other ligating units are engaged in this chelating process. Sensor 5, synthesized by Bhattacharya and Thomas, contains a receptor unit that illustrates these generalities [1].



To study the nature of complex formed between 1 and copper cations in solution, Bhattacharya and Thomas examined the system by electrospray ionization mass spectrometry (ESI-MS). This studies shows that two independent co-ordination centers of similar nature as in 5 are present. Direct involvement of the central tertiary amino group and the dansyl group in metal-complexation is less probable. Autors propose a co-ordination scheme that explains the ESI-MS results. They suggested that copper cation are complexed by four nitrogen atoms, two for heterocyclic moieties and two deprotonated aliphatic nitrogen atoms [1]. This data are in good agreement with molecular modeling data Figure 5 [12].

In the emission fluorescence spectra recorded at excitation at 330 nm, a linear decrease in the fluorescence intensity was observed until one equiv. of Cu^{2+} was added, Figure 6. Continued addition of copper cation produced only a nominal decrease in fluorescence intensity.

The fluorescence quenching of 5 by Cu^{2+} was tested over a range of concentrations and was found to be linear with the added metal ion concentration.

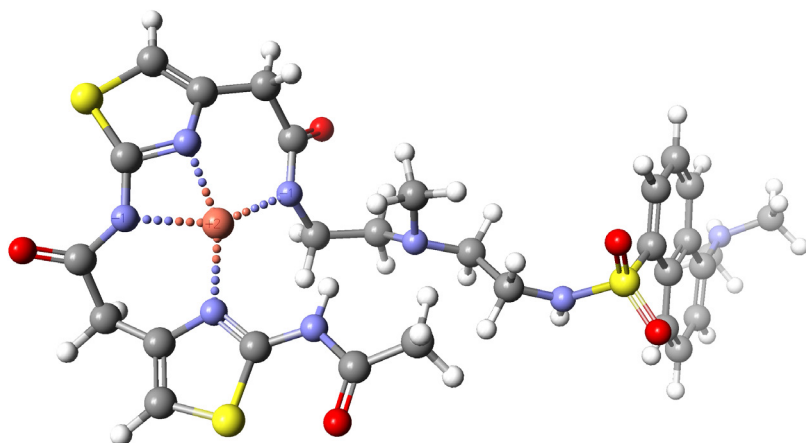


Figure 5. Structure of 5 with Cu^{2+} calculated by PM5 semiempirical method [12].

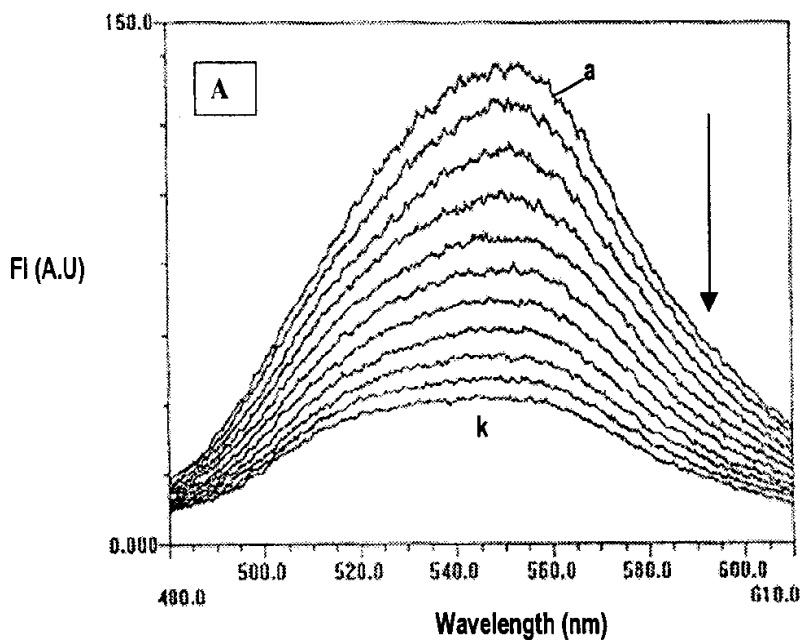
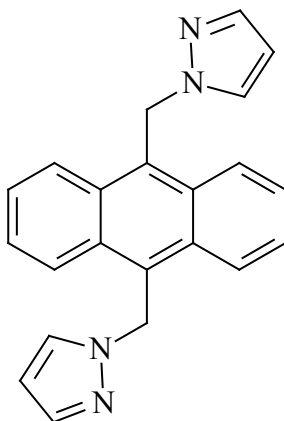


Figure 6. Effect of addition of Cu^{2+} on the emission spectra ($\lambda_{\text{ex}} = 330 \text{ nm}$) of 5 in 20 mM tris buffer containing 150 mM NaCl (pH 7.4). Curve "a", free probe (4.4 μM). 4.4 μM of Cu^{2+} was added in ten equal aliquots. Curve "k" corresponds to 4.4 μM of Cu^{2+} [1].

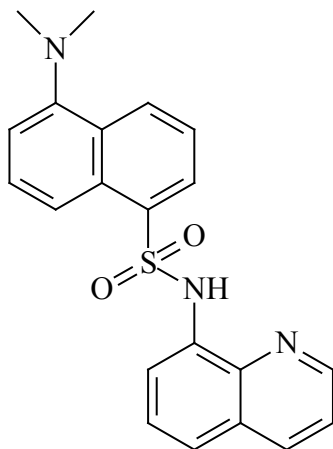
A fluorescent sensor for Ag^+



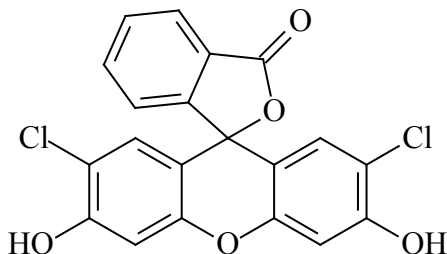
New fluorescent chemosensors, 1,8-bis(pyrazolylmethyl) anthracene and 9,10-bis(pyrazolylmethyl)anthracene, were synthesized by Kang and coworkers [27]. The 1,8-isomer showed selective fluorescent quenching effects with Ag^+ and Cu^+ . On the other hand, the 9,10-isomer (showed) displayed a selective fluorescent quenching effect only with Ag^+ . From the association constants obtained from fluorescent titrations and by extraction, we conclude that rigid immobilization of the ligands, 1,8-isomer, plays a more important role in the binding with Ag^+ than the additional δ -cation interaction offered by the 9,10-isomer.

A fluorescent sensor for Zn^{2+}

The novel ligand, [8-(5A-dimethylamino-1A-naphthalene)sulfonamidoquinoline] (L), was prepared. The fluorescence properties of L were also studied in a DMSO–H₂O mixture. The fluorescent experiment reveals that essential metal ions such as Cu^{2+} , Fe^{2+} , Fe^{3+} , Co^{3+} , Mn^{2+} and Ni^{2+} ions quenched the fluorescence of the ligand while Zn^{2+} ion enhanced the fluorescence. The maximum excitation band of L is at 357 nm with a shoulder at 381 nm. Whatever the excitation wavelength 300–450 nm is chosen, the maximum of the emission is always at 545 nm [28].



A fluorescent sensor for Cd²⁺

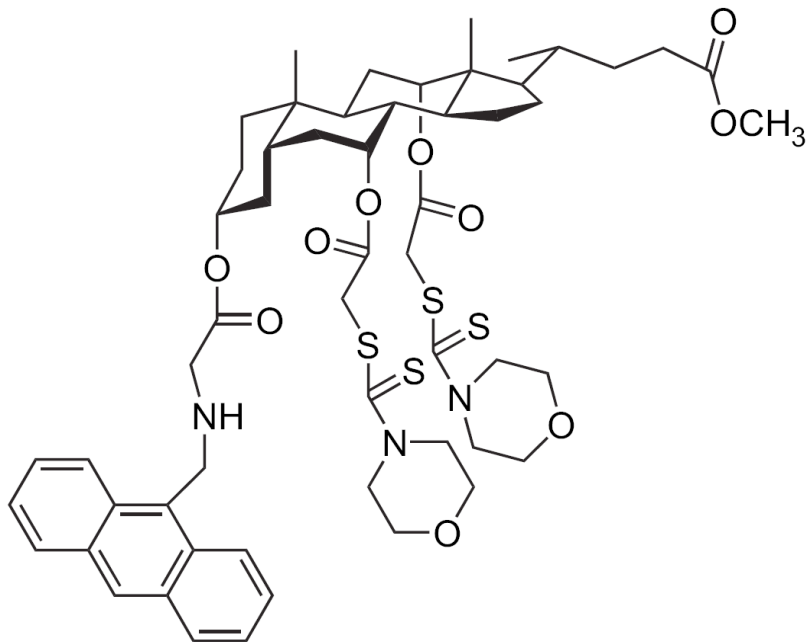


2,7-dichlorofluorescein exhibits a fluorescent peak At 540 nm when excited by 350 nm wavelength photons in 1:1 CH₃OH:H₂O. The intensity of fluorescent peak is found to increase on interaction with Cd²⁺ ion but not significant increase in the intensity was observed on interactions with the ions: Na⁺, K⁺, Ca²⁺, Cu²⁺, Ni²⁺ and Zn²⁺. These observations indicate that 2,7-dichlorofluorescein is good fluorescent sensor for Cd²⁺ ion [29].

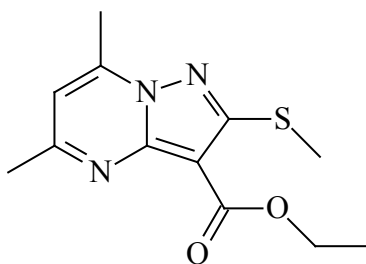
A fluorescent sensor for Hg²⁺

Wang and Chan [30] was synthesized cholic acid-based sensor and applied it as fluorescent sensor for the detection of both Hg²⁺ and MeHg⁺ in aqueous solutions. This sensor exhibits outstanding selectivity toward mercuric ion due to the complementary charge and size factor between the receptive site of the

host and the guest ion. A distinctive OFF–ON type signaling of up to 10-fold enhancement was observed for this new sensor probe.



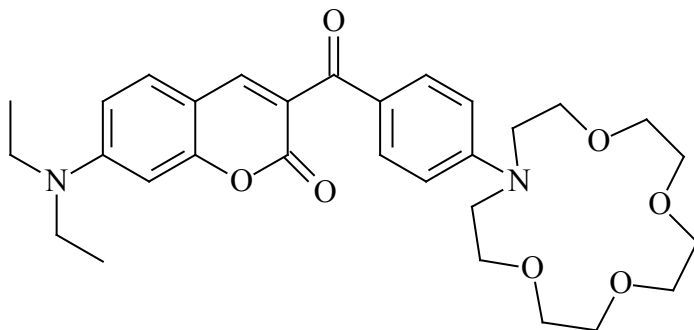
A fluorescent sensor for In^{3+}



Synthesized by Wu and coworkers [31] neutral fluorescent sensor based on pyrazolo[1,5-*a*]pyrimidine exhibited a unique selectivity for In^{3+} ion over

various other metal ions with dramatic fluorescence response in acetonitrile. This compound shows a relatively stable emission band around 412 nm. When the concentration of In^{3+} was increased up to 1.0 molar equivalent, 95% quenching of the initial fluorescence of pyrazolo[1,5-*a*]pyrimidine was observed.

A fluorescent sensor for Pb^{2+}

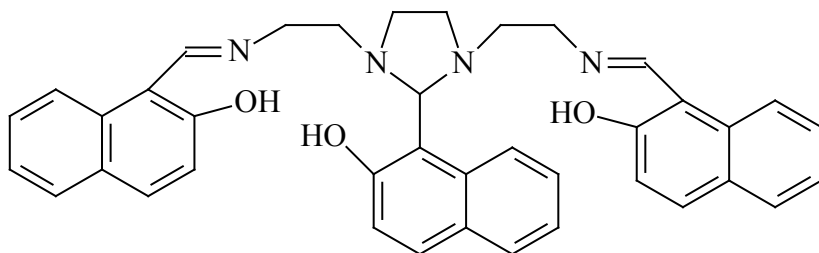


This Chemosensor (C) was prepared by the condensation of 4-(*N,N*diethylamino)salicylaldehyde with β -ketoester appended with 15-monoazacrown-5 ether in the presence of piperidine. To explore further the utility of C as an ion-selective fluorescent chemosensor for Pb^{2+} , the competition experiments are conducted in which C is first incubated with various metal ions at their saturation concentrations, and Pb^{2+} is added until the total concentration of Pb^{2+} reaches saturation concentration. Although absorption bands provide the most structurally relevant information about the binding, the absorption as well as fluorescence spectra are exploited to monitor the competition events. The absorption spectrum of C Mg^{2+} is consistent with the two carbonyl groups of the fluorophore taking part in the binding, regardless of the presence of the monoazacrown moiety. As the Pb^{2+} concentration increases, the characteristic absorption at 478 nm for CMg^{2+} complex gradually decreases, and a new characteristic absorption at 428 nm, responsible for CPb^{2+} complex, starts to appear with a concomitant fluorescence increase. Notably, Pb^{2+} ions do not simply replace Mg^{2+} in the same binding sites but form a new fluorescent complex [32].

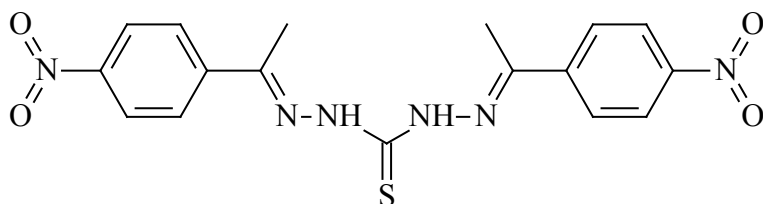
A fluorescent sensor for La^{3+}

Hosseini and coworkers [33] synthesized fluorescent sensor containing 1-[1-((2-[2-(2-hydroxy-1-naphthyl)-3-(2-((E)-1-(2-hydroxy-1-naphthyl)

methylidene]amino}ethyl)-1-imidazolidinyl[ethyl]-imino)methyl]-2-naphthol) (L) for detecting La^{3+} ratiometrically. Complexation between compound L and La^{3+} with high selectivity gives rise to a great red shift from 430 to 522 nm in the emission spectra. In acetonitrile, the red shift of fluorescent emission upon lanthanum binding is due to the formation of a 1:1 metal–ligand complex. The fluorescent probe exhibits high selectivity over other common metal ions and mono-, di-, and trivalent cations, which indicates good selectivity for La^{3+} ions over a large number of interfering cations.



A fluorescent sensor for F^-



Bisthiocarbonylhydrazones are found to be a class of sensitive, selective, ratiometric and colorimetric chemosensors for anions such as fluoride (F^-). The sensitivities or the binding constants of the sensors with anions, were found to be strongly dependent on the substituents appended on the π -conjugation framework, the delocalization bridge $\text{CH}=\text{N}$, the aromatic moiety and the hetero atom in the $\text{C}=\text{X}$ group of the sensors [34].

Acknowledgements

This work was supported by research funds in years 2009-2012 from the Polish Ministry of Science and Higher Education as scientific grants No. N 204

005536 and N 204 338237.

References

1. S. Bhattacharya, M. Thomas, *Tetrahedron Lett.* 41 (2000) 10313- 10317.
2. "Materiały supramolekularne" –"Fluorojonofory", T. Ossowski, P. Niedziałkowski, D. Zarzeczańska, M. Przyborowska, H. Sulowska; ISBN 978-83-89936-21-9, BETAGRAF P.U.H. Poznań 2008
3. L. Fabbrizzi, M. Licchelli, P. Pallavicini, L. Parodi, *Agew. Chem., Int. Ed. Engl.* 37 (1998) 800
4. R. Kraemer, *Agew. Chem., Int. Ed. Engl.* 37 (1998) 772
5. "Encyclopedia of Supramolecular Chemistry"-"Fluorescent Sensors" A.P. de Siilva, C.D. McClean, T.S. Moody; ISBN 0-8247-4723-2, Taylor & Francis Group Boca Raton 2004
6. "Luminescent Sensors" L. Fabbrizzi. Ed.: *Coord. Chem. Rev.* 205 (2000) 1-228.
7. C. IL Chenthamarakshan and A. Ajayaghosh, *Tetrahedron Letters* 39 (1998) 1795-1798
8. See "OPTI-CCA" and "OPTI-R" under <http://www.roche.com/diagnostics/products /prodlist.ht>
9. R.M. Izatt, K. Pawlak, J.S Bradshaw, R.L. Bruening, *Chem. Rev.* 95 (1995) 2529-2586
10. J.-M. Lehn "Supramolecular Chemistry"; VCH: Weinheim. 1995.
11. V. Balzani, F. Scandola "Supromolecular Photochemistry"; Ellis-Horwood: Chichester. 1991
12. R. Pankiewicz, G. Schroeder, unpublished results
13. A.P. de Silva, H.Q.N. Gunaratne, T. Gunnlaugsson, M. Nieuwenhuizen, *Chem. Commun.* (1996) 1967- 1968
14. J. Kim, D.T. McQuade, S.K. McHugh and T.M. Swager, *Angew. Chem. Int. Ed.* 21 (2000) 3868-3872
15. Xia Wen-Sheng, Schmehl Russell, H. Li Chao-Jun, *Chemical Communications (Cambridge)* 8 (2000) 695-696
16. Jian Pei, Ai-Lin Ding, Wang-Lin Yu, Yee-Hing Lai, *Macromolecular Rapid Communications* 1 (2002) 21-25
17. J.R Blinks, W.G. Wier, P. Hess and F.G. Prendergast, *Prog. Biophys. Mol. Biol.* 40 (1982) 1-114
18. G. Gryniewicz, M. Poenie, R.Y. Tsien, *J. Biol. Chem.* 260 (1985) 3440-3450
19. R.Y. Tsien, *Biochemistry* 19 (1980) 2396-2404
20. R.Y. Tsien, *Annu. Rev. Biophys. Bioeng.* 12 (1983) 91-116

21. J. Kawakami, Y. Komai, T. Sumori, A. Fukushi, K. Shimosaki, S. Ito, *Journal of Photochemistry and Photobiology A: Chemistry* 139 (2001) 71–78
22. J.B Neilands., *Ann. Rev. Biochem.* 50 (1981) 715-731
23. Hamilton A.D. Fluorescent Sensing of Anions. In *Encyclopedica of Supramolecular Chemistry*, Atwood J.L., Steed J.W., Eds.: Dekker, 2002
24. R. Nudelman, O. Ardon, Y. Hadar, Y.N. Chen. J. Libman, A. Shanzer, *J. Med. Chem.* 41 (1998) 1671 - 1678
25. V. Balzani, P. Ceroni, S. Gestermann, C. Kauffmann, M. Gorka and F. Vogtle, *Chemical Communications (Cambridge)* 10 (2000) 853-854
26. Xiaobo Huang, Yu Dong, Jie Meng, Yixiang Cheng, Chengjian Zhu, *Synlett* 12 (2010) 1841-1844
27. J. Kang, M. Choi, J. Young Kwon, E.. Lee and J. Yoon, *J. Org. Chem.* 67 (2002) 4384-4386
28. J. Pengju, C. Lizhen, L. Jun, L. Qin, D. Jun; G. Xiang, G. Zijian, *Chemical Communications (Cambridge)* 13 (2002) 1424-1425
29. P. Goswami, S. Baruah, D. Kumar Das, *Indian Journal of Chemistry*, 40a (2010) 1617-1620
30. H. Wang, W-H. Chan, *Tetrahedron* 63 (2007) 8825–8830
31. Y-C. Wu, H-J. Li, H-Z. Yang, *Org. Biomol. Chem.* 15 (2010) 3394-3397
32. C-T. Chen, W-P. Huang, *JACS* 22 (2002) 6246-6247
33. M. Hosseini, M. Reza Ganjali, B. Veismohammadi, S. Riahl, Parviz Norouzi, M. Salavati-Niasari, S. Dehghan Abkenar, *Analytical Letters* 7 (2009) 1029-1040
34. F. Han, Y. Bao, Z. Yang, T.M. Fyles, J. Zhao, X. Peng, J. Fan, Y. Wu, S. Sun, *Chem. Eur. J.* 13 (2007) 2880-2892

Видавниче підприємство “Східний видавничий дім”
Державне свідоцтво № ДК 697 від 30.11.2001
83086, м. Донецьк, вул. Артема, 45
тел./факс (062) 338-06-97, 337-04-80
e-mail: svd@stels.net

Publishing house „Schidnyj wydawnyczyj dim”

ISBN 978-966-317-076

